Étude de facteurs physiopathologiques et de nouvelles voies thérapeutiques du glaucome sur un modèle 3D original de trabéculum humain normal et pathologique

Juliette Buffault

Sorbonne Université

École doctorale 394 : Physiologie, Physiopathologie et Thérapeutique

Institut de la Vision

Équipe S12 « Chimiokines et physiopathologie du segment antérieur de l'œil »

Étude de facteurs physiopathologiques et de nouvelles voies thérapeutiques du glaucome sur un modèle 3D original de trabéculum humain normal et pathologique

Par Juliette Buffault

Thèse de doctorat de Physiologie, Physiopathologie et Thérapeutique

Codirection : Dr Françoise Brignole-Baudouin et Pr Christophe Baudouin

Présentée et soutenue publiquement le 22 mars 2024

Devant un jury composé de :

Pr Michel Paques, PU-PH	Président
Pr Alexandre Denoyer, PU-PH	Rapporteur
Pr Antoine Rousseau, PU-PH	Rapporteur
Pr Cédric Schweitzer, PU-PH	Examinateur
Pr Antoine Labbé, PU-PH	Membre invité
Pr Christophe Baudouin	Codirecteur
Dr Françoise Brignole-Baudouin	Codirecteur

À Igor, Agathe et Edgar

Remerciements

Au seuil de cette étape de ma vie académique, je tiens à exprimer ma profonde gratitude à toutes les personnes qui ont contribué à l'élaboration de ce travail de thèse, tant sur le plan professionnel que personnel.

Professeur Michel Paques**,** pour l'honneur qu'il me fait en présidant ce jury. Les travaux de votre équipe en imagerie clinique m'impressionnent. Soyez assuré de mon respect le plus sincère.

Docteur Françoise Brignole-Baudouin, depuis mon Master 2, vous avez été un pilier dans mon parcours. Travailler sous votre aile est un réel plaisir ; j'admire votre enthousiasme, votre dévouement, et votre intelligence. Chaque session de travail avec vous m'a toujours apporté un nouvel élan de motivation.

Professeur Christophe Baudouin, merci de m'avoir permis de réaliser ce travail, pour votre accompagnement, et vos conseils. Votre rôle déterminant dans l'impulsion de la recherche sur le glaucome au sein du laboratoire. Vous m'offrez des opportunités au-delà de mes espérances à New York, au sein des 15-20 et de l'IHU.

Professeur Antoine Labbé, pour ton précieux accompagnement, tes conseils avisés et ton amitié. Ton soutien constant et bienveillant contribue pour beaucoup au maintien de ma motivation pour poursuivre une carrière universitaire. Je t'en suis infiniment reconnaissante.

Professeur Antoine Rousseau, merci d'avoir accepté d'être rapporteur de ce travail. Je retiens de nos interactions ton don pour l'enseignement et ta grande sympathie. Je me réjouis de travailler à tes côtés.

Professeur Alexandre Denoyer, après avoir lu avec intérêt vos travaux menés à l'Institut de la Vision avant moi et en suivant certains de vos anciens patients qui ne tarissent pas d'éloges à votre égard, je mesure l'honneur de vous avoir comme rapporteur de ce travail.

Monsieur le Professeur Schweitzer, merci beaucoup d'avoir accepté de juger ce travail avec toute votre expertise.

Au Docteur Annabelle Réaux-Le Goazigo, cheffe de l'équipe S12 à l'Institut de la Vision et au Docteur Stéphane Melik Parsadaniantz pour leur accueil dans cette chaleureuse équipe de recherche et leurs précieux conseils.

À Élodie Reboussin pour ton accompagnement à chaque étape depuis mon Master 2, ta disponibilité et ta compétence qui ont su répondre à mes nombreuses questions techniques, merci infiniment.

À Karima Kessal, un grand merci pour ta volonté constante d'offrir ton aide. Ta disponibilité et ton engagement ont été des atouts majeurs dans mes projets, et je suis reconnaissante de pouvoir compter sur toi.

Xavier Guillonneau et Frédéric Blond, de l'équipe S14 pour leur disponibilité, leur efficacité et leur aide précieuse pour la préparation et le travail d'analyse des données de séquençage.

Romain Magny, Noémie Bonneau, Murat Akkurt, Tiffany Migeon, et au reste de l'équipe S12 de l'institut de la vision, merci pour vos partages de connaissances et d'expériences qui ont enrichi mon parcours.

À toute l'équipe du service 3 avec lequel c'est toujours un plaisir de travailler dans un environnement bienveillant. Particulièrement à Jade, Norman, Mathias, les Alexandres, Jean-Baptiste, Paul, Tristan et Hélène pour leur amitié.

À ma famille. Mes parents sur qui je peux toujours compter et qui sans pression encouragent mes ambitions. À Noémie et Joachim, sœur et frère parfaits, quel bonheur de continuer de grandir au milieu de cette fratrie.

À ma petite famille chérie, Igor mon amour synergique qui m'épaule et me soutient chaque jour et tous nos projets qui nous rassemblent. À Agathe dont je suis béate et Edgar ma pépite de bonheur qui grandit.

Résumé

Le glaucome est une neuropathie optique cécitante associée à une élévation de la pression intraoculaire (PIO). Le trabéculum, situé dans l'angle iridocornéen, constitue la voie principale de drainage de l'humeur aqueuse hors de l'œil et joue un rôle crucial dans le maintien de l'homéostasie de la PIO. Une dysfonction du trabéculum entraîne une résistance accrue et une élévation de la PIO dans le glaucome.

À mesure que le domaine de la recherche sur le glaucome évolue, avec des avancées dans les méthodes d'exploration telles que les approches -omiques, il devient de plus en plus nécessaire de trouver des modèles alternatifs à l'expérimentation animale pour tester les cibles thérapeutiques potentielles identifiées par ces méthodes.

Cette thèse se concentre sur l'étude de la dysfonction du trabéculum et de la rétine et l'exploration de nouvelles approches thérapeutiques à l'aide d'une part de modèles issus de cultures primaires en deux dimensions (2D) et trois dimensions (3D) du trabéculum humain et d'autres part de modèles d'explants de trabéculums et de rétine. Nous avons ainsi, sur les modèles 2D et 3D de trabéculum, examiné les effets du latanoprost et d'un inhibiteur de la Rho-kinase en présence du *transforming growth factor bêta*-2 (TGF-β2), principale cytokine impliquée dans la pathogenèse du glaucome, et démontré l'efficacité du latanoprost dans la réduction de l'accumulation de la matrice extracellulaire (MEC) induite par le TGF-β2 et celle de l'inhibiteur de la Rho-kinase sur la réorganisation de la MEC et du cytosquelette.

Puis grâce à la technique des explants de trabéculums humains permettant de préserver l'architecture complexe du trabéculum, nous avons caractérisé par séquençage complet de l'ARN les changements transcriptomiques induits par le TGF-β2 et le *Tumor necrosis factor alpha* (TNF-α). Ainsi, nous avons mis en évidence l'importance de l'équilibre entre ces deux cytokines dans l'homéostasie du trabéculum et envisagé de nouvelles cibles thérapeutiques potentielles. Pour étendre la compréhension de la physiopathologie du glaucome au niveau de la rétine, et évaluer des thérapies neuroprotectrices et anti-inflammatoires, nous avons utilisé un modèle d'explants rétiniens de rat après axotomie. Ce modèle maintient une architecture semblable à celle *in vivo*, avec des interactions cellulaires intactes. L'efficacité de cellules souches mésenchymateuses ainsi que celle d'inhibiteurs de la Rho-kinase ont pu être évaluées.

Ces modèles *ex vivo* innovants offrent des perspectives d'exploration précieuses sur la physiopathologie du glaucome, permettant une analyse complète de l'organisation matricielle, des interactions cellulaires et des altérations moléculaires. Ils constituent des alternatives convaincantes à l'expérimentation animale, comblant le fossé entre les études *in vitro* et *in vivo*. En établissant une plateforme robuste et cliniquement pertinente, cette recherche contribue de manière significative à la quête de nouvelles approches thérapeutiques dans le glaucome tout en promouvant des pratiques de recherche éthiques et en réduisant la dépendance à l'égard des modèles animaux.

Abstract

Glaucoma is a blinding optic neuropathy associated with an elevation of intraocular pressure (IOP). The trabecular meshwork (TM), located in the iridocorneal angle, constitutes the primary drainage pathway for aqueous humor outflow from the eye and plays a crucial role in maintaining IOP homeostasis. TM dysfunction leads to increased resistance and elevated IOP in glaucoma.

As the field of glaucoma research progresses, with advancements in investigative methods such as -omics approaches, there is an increasing need to find alternative models to animal experimentation to test potential therapeutic targets identified by these methods.

This thesis focuses on studying TM and retinal dysfunction and exploring novel therapeutic approaches using both two-dimensional (2D) and three-dimensional (3D) primary human TM culture models and TM and retinal explants. We have thus examined the effects of latanoprost and a Rho-kinase inhibitor on 2D and 3D trabecular models in the presence of transforming growth factor beta-2 (TGF-β2), the principal cytokine involved in glaucoma pathogenesis, and demonstrated the efficacy of latanoprost in reducing TGF-β2-induced extracellular matrix (ECM) accumulation and the Rho-kinase inhibitor on ECM and cytoskeletal remodeling.

Furthermore, using human TM explant technique to preserve the complex trabecular architecture, we characterized the transcriptomic changes induced by TGF-β2 and Tumor necrosis factor alpha (TNF-α) through complete RNA sequencing. Thus, we highlighted the importance of the balance between these two cytokines in TM homeostasis and envisaged new potential therapeutic targets.

To extend the understanding of glaucoma pathophysiology at the retinal level and evaluate neuroprotective and anti-inflammatory therapies, we used a rat retinal explant model after axotomy. This model maintains architecture similar to *in vivo*, with intact cellular interactions. The efficacy of mesenchymal stem cells as well as Rho-kinase inhibitors could be evaluated.

These innovative *ex vivo* models offer valuable insights into glaucoma pathophysiology, allowing comprehensive analysis of ECM organization, cellular interactions, and molecular alterations. They present compelling alternatives to animal experimentation, bridging the gap between *in vitro* and *in vivo* studies. By establishing a robust and clinically relevant platform, this research significantly contributes to the search for new therapeutic approaches in glaucoma while promoting ethical research practices and reducing reliance on animal models.

Abréviations

2D : deux dimensions

3D : trois dimensions

AC: *Anterior Chamber*

AH : *aqueous humor* (humeur aqueuse)

α-SMA : *alpha-smooth muscle actin*

ApoE : apolipoprotéine E

AQP1 : *Aquaporin 1*

ARG1 : Arginase 1

BAC/BAK : Chlorure de Benzalkonium

BAMBI : BMP and Activin Membrane-Bound Inhibitor

BDNF : *brain derived neurotrophic factor*

BF : Bulle de filtration

BMMSCs : *Bone Marrow Mesenchymal Stem Cells*

BMP : *Bone morphogentic protein*

Brn3a : *Brain-specific Homeobox/POU Domain Protein 3A*

BSA : *Bovine Serum Albumin*

CGR : cellules ganglionnaires rétiniennes

CHI3L1 : *Chitinase-3-Like Protein 1*

CLAN : *cross linked actin network*

CM : *Conditioned Medium*

CMH : complexes majeurs d'histocompatibilités

CNTF *: ciliary neurotrophic factor*

CS : canal de Schlemm

CTL : Contrôle

CXCL : Chemokine (C-X-C Motif) Ligand

DAC : *Displaced Amacrine Cells*

DAPI : 4',6-diamidino-2-phenylindole

DEG : Differentially Expressed Gene

DEV: *Day ex-vivo*

DEX/DXM : Dexaméthasone

DPBS : Dulbecco's Phosphate Buffered Saline

ECM : *Extracellular Matrix*

EFS : Établissement Français du Sang

ELP : *Elastin-Like Polypeptide*

ERK : *Extracellular signal-Regulated Kinases*

ERO : espèces réactives de l'oxygène

ESCs : Embryonic Stem Cells

ET-1 : Endothelin-1

FAK : Focal Adhesion Kinase

FCM : Flow Cytometry

FDR : False Discovery Rate

FGF : facteur de croissance des fibroblastes

FITC : Fluorescein Isothiocyanate

FN : Fibronectin

GAGs : *Glycosaminoglycans*

GALT : *Gonioscopy-assisted Transluminal Trabeculotomy*

GCC : couches des cellules ganglionnaires

GDNF : facteur de croissance dérivé des cellules gliales

GDP/GTP: Guanosine di/triphosphate

GFAP: *Glial Fibrillary Acidic Protein*

GO : *Gene Ontology*

GPAO : glaucome primitif à angle ouvert

H&E : *Hematoxylin and Eosin*

HA : humeur aqueuse

HTMC : cellules humaines trabéculaires

HTMEx : *Human Trabecular Meshwork Explants*

Iba1 : Ionized Calcium Binding Adaptor Molecule 1

ICM : Institut du Cerveau et de la Moelle Épinière

IGF : Insulin-like Growth Factor

IL: Interleukine

INL : Inner Nuclear Layer

IPL : Inner Plexiform Layer

iPSC : *Induced Pluripotent Stem Cell* (Cellule Souches Pluripotentes Induites)

IOP : *Intraocular Pressure* (Pression Intraoculaire)

ITGAM : Integrin Subunit Alpha M

JNK : protéine c-Jun N-terminale

KEGG : Kyoto Encyclopedia of Genes and Genomes

log2FC : Log2 Fold Change

LOXL1 : lysyl-oxydase de type 1

LT : Latanoprost

MAPK : Kinases des Protéines Activées par les Mitogènes

MEC : Matrice extracellulaire

MEW : *Melt Electrowriting*

MHC : *Major Histocompatibility Complex*

MIGS : Chirurgies Mini-Invasives du Glaucome

MLC(-P) : *Myosin Light Chain (Phosphorylated)*

MMP : Matrix métalloprotéase

MSCs : *Mesenchymal Stem Cells*

NeuN : *Neuronal Nuclei*

NF-kB : *Nuclear Factor kappa-light-chain-enhancer of activated B cells*

NOX : NADPH Oxydase

OCT : tomographie par cohérence optique

O.C.T. : *Optimal Cutting Temperature Compound*

OPL : Outer Plexiform Layer

ONL : Outer Nuclear Layer

OS : Outer Segments

Padj : Adjusted P-value

PBS : *Phosphate Buffered Saline*

PCA : Principal Component Analysis

PDGF : *Platelet-Derived Growth Factor*

PEUU : Poly(etherurethane)urea

PFA : Paraformaldehyde

PGA : *Prostaglandin Analogs* (analogues de prostaglandine)

PGF2α : Prostaglandine F2 alpha

PIO : Pression intraoculaire

POAG : *Primary Open-Angle Glaucoma* (Glaucome Primitif à Angle Ouvert)

RBPMS : *RNA Binding Protein with Multiple Splicing*

RGC : *Retinal Ganglion Cells* (Cellules Ganglionnaires de la Rétine)

RIN : RNA Integrity Number

RNA-Seq : *RNA Sequencing*

RNFL: couche des fibres nerveuses rétiniennes

ROCK : *Rho-associated coiled-coil protein kinase*

ROCK-i : *Rho-Kinase Inhibitor* (inhibiteur des Rho-kinases)

ROS : *Reactive Oxygen Species*

RPCs : *Retinal Progenitor Cells*

RR : risque relatif

RT : Room Temperature

RT-qPCR : *Reverse Transcription Quantitative Polymerase Chain Reaction*

SAP : synéchies antérieures périphériques

SC : *Schlemm's Canal* (Canal de Schlemm)

SDP : Syndrome de Dispersion Pigmentaire

SLT : Trabéculoplastie Sélective au Laser

SPNP : sclérectomie profonde non perforante

SU-8 : Epoxy-based negative photoresist

TGF-β : *transforming growth factor-beta*

TGF-βRI : Récepteur de Type I du TGF-β

TGF-βRII : Récepteur de Type II du TGF-β

TIGR : protéine de réponse trabéculaire aux glucocorticoïdes

TIMP: *Tissue Inhibitor of Metalloproteinases*

TM : *Trabecular Meshwork* (Trabéculum)

TMC : *Trabecular Meshwork Cells* (Cellules trabéculaire)

TNF-α: *Tumor Necrosis Factor-alpha*

tPA: activateur du plasminogène tissulaire

Liste des figures

Liste des tableaux

Table des matières

Avant-propos et objectifs de la thèse

Le glaucome est une neuropathie optique cécitante qui affecte environ 70 millions de personnes à travers le monde [1]. Son principal facteur de risque est l'augmentation de la pression intraoculaire (PIO) [2]. La pression intraoculaire (PIO) est déterminée par l'équilibre entre la production et le drainage de l'humeur aqueuse à l'intérieur de l'œil. L'humeur aqueuse, produite par les corps ciliaires, est évacuée principalement par deux voies : la voie trabéculaire et la voie uvéosclérale. Le trabéculum, au niveau de l'angle iridocornéen, constitue la principale voie de drainage et le lieu de régulation de la résistance à l'évacuation de l'humeur aqueuse hors de l'œil [3] et son dysfonctionnement est à l'origine de l'élévation de la PIO (figure 1). Dans le glaucome, la résistance à l'évacuation de l'humeur aqueuse au niveau du trabéculum est augmentée. Des études ont montré que cette augmentation de la résistance était liée à un mécanisme mixte associant une dégénérescence des cellules trabéculaires formant ce maillage et une accumulation de matrice extracellulaire (MEC) [4,5]. Des changements ont été aussi décrits au niveau des cellules trabéculaires qui acquièrent des caractéristiques contractiles [5,6]. Mais les mécanismes précis de la pathophysiologie de la dysfonction trabéculaire à l'origine du glaucome restent encore insuffisamment connus.

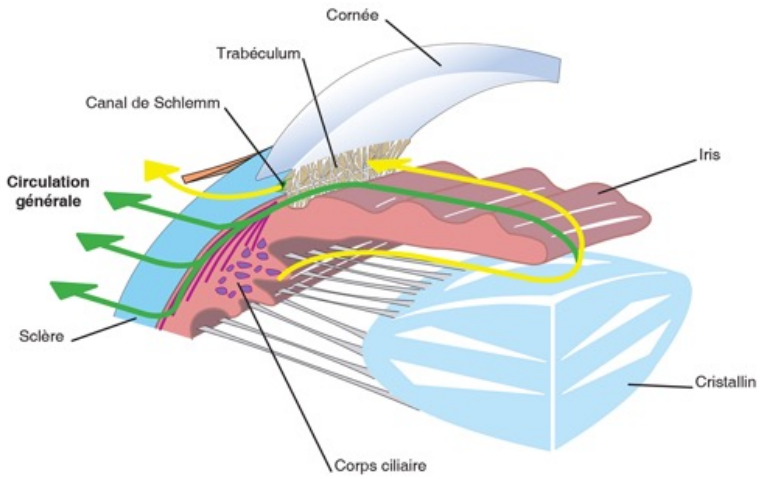

Figure 1 : Représentation schématique de la circulation de l'humeur aqueuse dans le segment antérieur de l'œil
en jaune est représentée la voie d'évacuation trabéculaire, et en vert, la voie d'évacuation uvéosclérale. (Source : Nahhale Y et al. Construction of Glaucoma Disease Ontology, 2021)

L'avènement des outils d'exploration dites "-omiques", tels que la génomique, la protéomique ou la métabolomique, a révolutionné notre capacité à identifier de nouvelles cibles thérapeutiques potentielles [7–10]. En utilisant ces approches, nous pouvons analyser de manière exhaustive les profils moléculaires et fonctionnels du trabéculum, permettant ainsi l'identification de marqueurs spécifiques et de voies de

signalisation altérées dans le contexte du glaucome ainsi que l'identification de potentielles cibles thérapeutiques. Celles-ci devront être cependant validées sur des modèles adaptés pour ouvrir de nouvelles perspectives pour le traitement du glaucome.

Par ailleurs, l'évolution sociétale et la réglementation en matière d'expérimentation animale, notamment la règle des trois R (remplacer, réduire, raffiner) nous pousse à réévaluer nos méthodes de recherche et à réduire autant que possible notre dépendance à l'expérimentation animale [11]. Bien que les modèles animaux aient été des outils indispensables pour la recherche dans le domaine du glaucome, leur transposition directe aux êtres humains comporte des limites inhérentes. Ainsi, nous sommes encouragés à développer activement des méthodes alternatives qui évitent ou minimisent l'utilisation d'animaux de laboratoire.

L'objectif de cette thèse est donc triple :

- Développer de nouveaux modèles 3D de trabéculum et de neurorétine normaux et pathologiques afin d'offrir une plateforme expérimentale plus représentative de la réalité histologique et physiologique humaine.
- Approfondir la compréhension de la physiopathologie de la maladie glaucomateuse à la fois sur la dysfonction trabéculaire et sur la souffrance des cellules ganglionnaire.
- Évaluer des stratégies thérapeutiques ciblées sur nos modèles.

Dans la première partie, nous présenterons, d'une part, la maladie glaucomateuse d'un point de vue clinique, son diagnostic, la surveillance ainsi que les options thérapeutiques, et d'autre part, les principales voies de recherches dans la physiopathologie, les biomarqueurs et le traitement de cette neuropathie optique.

Nous décrirons plus spécifiquement le trabéculum, sa structure, sa fonction ainsi que ses implications cliniques dans la pathologie glaucomateuse et en tant que tissu cible de thérapeutiques. Une partie de cette présentation a fait l'objet d'un article de revue de la littérature publiée en 2020 dans le *Journal Français d'Ophtalmologie* (article 1)[12].

Nous détaillerons aussi les différents modèles *in vitro* de trabéculum disponibles en alternatives aux expérimentations animales afin de placer notre modèle dans le paysage de la recherche actuelle. Cet état des lieux a été récemment publié dans la revue scientifique internationale *Current Eye Research* (article 2)[13].

Notre travail de recherche a, dans un premier temps, utilisé des cultures primaires de cellules trabéculaires humaines (HTMC) obtenues à partir de cellules trabéculaires isolées de collerettes

cornéosclérales obtenues après retrait du greffon cornéen au cours d'une chirurgie pour greffe de cornée. Nous avons ainsi voulu étudier l'effet des deux seules thérapeutiques anti-glaucomateuses qui modifient l'évacuation de l'HA au niveau trabéculaire : un ROCK-inhibiteur et un analogue des prostaglandines (latanoprost) sur des HTMC remaniées par du *transforming growth factor-beta 2 (*TGF-β2) en culture « classique » en 2D puis en culture 3D dans du Matrigel^{TM}. La culture cellulaire en 3D permet de recréer les conditions du microenvironnement rencontrées *in vivo*. L'objectif de la culture en 3D était de fournir aux cellules un environnement leur permettant d'interagir entre elles, ce qui nous a permis d'obtenir une organisation des cellules trabéculaires proche de la physiologie avec une organisation en mailles que nous ne retrouvions pas en 2D. Nous avons ainsi pu montrer sur ces deux modèles que le latanoprost avait une action sur l'accumulation de MEC induite par le TGF-β2 et que le ROCK inhibiteur (ROCK-i), en plus d'avoir une action sur la MEC, avait également une action sur le cytosquelette entrainant une réversibilité du remodelage induit par le TGF-β2. Cette étude a fait l'objet d'une publication dans le *Journal of Clinical Medicine* en 2022 (article 3)[14].

Afin d'aller plus loin dans notre objectif et d'être au plus près de l'architecture trabéculaire *in vivo*, nous avons ensuite utilisé la technique des explants. Celle-ci permet aux HTMC de subir le moins de manipulation possible et de les laisser dans leur matrice d'origine avec son architecture complexe qui peut être étudiée en particulier, en microscopie confocale. Une analyse en RNA-Seq a permis de caractériser de façon extensive les modulations transcriptomiques induite par le TGF-β2, de les comparer à un modèle utilisant des cellules trabéculaires humaines dissociées exposées au même agent et d'identifier de potentielles cibles thérapeutiques [15]. L'article qui découle de ce travail est soumis à la revue internationale *Experimental Eye Research* (article 4).

Nous disposons donc d'un modèle de trabéculum humain *ex vivo* permettant une analyse à triple niveau, sur l'organisation de la matrice et celle des cellules ainsi qu'au niveau moléculaire. Il ouvre un champ de recherche très large allant de l'étude de phénomènes toxiques, au criblage de molécules thérapeutiques. Ainsi, nous avons tout d'abord étudié sur ce modèle l'effet de la cytokine proinflammatoire *Tumor necrosis factor alpha* (TNF-α), connue pour contrebalancer les effets du TGF-β2. Nous avons pu mesurer leurs effets contradictoires sur l'organisation de la matrice, sur les cytokines relarguées par les cellules, et sur la modulation de la transcription des gènes impliqués dans la fibrose, l'inflammation, l'apoptose et la réponse au stress oxydant.

En parallèle de ce modèle d'explants trabéculaires humains, nous avons utilisé un modèle d'explants rétiniens de rat, afin d'évaluer des stratégies thérapeutiques de neuroprotection et d'immunomodulation. Ce modèle est présenté dans l'article 5 publié en 2022 dans le *Journal of Neuroinflammation* [16]. Dans la suite d'un précédent travail de l'équipe (Roubeix, 2015), nous avons utilisé les cellules souches mésenchymateuses et démontré leur pouvoir neuroprotecteur mais aussi mis en évidence un œdème de l'explant et le développement d'une membrane à leur surface, ce qui corrobore les cas de membrane

épirétinienne décrits en pratique clinique chez des patients ayant reçu ce traitement expérimental. Nous présenterons les résultats préliminaires de l'effet neuroprotecteur des ROCK-i sur ce modèle.

En conclusion, notre thèse est consacrée au développement de modèles 3D, qu'ils soient créés *de novo* par culture cellulaire ou *ex vivo* en utilisant des explants. Cette approche vise à approfondir la compréhension des facteurs inflammatoires et profibrotiques dans la physiopathologie du glaucome, tant au niveau de l'évacuation de l'humeur aqueuse par le trabéculum que de la souffrance des cellules ganglionnaires rétiniennes et nous permet d'évaluer des stratégies thérapeutiques ciblées.

Présentation de la pathologie glaucomateuse

Le glaucome est une maladie dégénérative du nerf optique qui affecte environ 70 millions de personnes à travers le monde [1]. Il se caractérise par des lésions progressives du nerf optique, généralement associées à une augmentation de la pression intraoculaire [17]. Son principal facteur de risque est l'augmentation de la pression intraoculaire (PIO) [17], elle-même consécutive à une maladie du trabéculum. Le trabéculum, au niveau de l'angle iridocornéen, constitue la principale voie de drainage de l'humeur aqueuse (HA) hors de l'œil. C'est une structure tridimensionnelle fenêtrée composée cellules trabéculaires au sein de multicouches de MEC [3]. Le trabéculum contrôle la PIO en régulant l'évacuation de l'HA de la chambre antérieure de l'œil vers le canal de Schlemm (CS) qui lui est adjacent, jusqu'aux canaux collecteurs des veines aqueuses puis vers le système veineux. Son dysfonctionnement est à l'origine de l'élévation de la PIO. Nous fournissons ici un état des lieux de la connaissance de cette structure complexe qui joue un rôle clé dans la physiopathologie du glaucome.

Glaucome

Diagnostic clinique et surveillance

Le glaucome est une pathologie oculaire chronique qui constitue la deuxième cause de cécité irréversible dans le monde [1]. Cette pathologie reste longtemps asymptomatique puisque la dégradation du champ visuel est d'abord périphérique avant d'occasionner une baisse de vision. En effet, la perte de la fonction visuelle est la conséquence de la mort des cellules ganglionnaires de la rétine périphérique, qui se propage ensuite vers le centre de la rétine. Le diagnostic clinique du glaucome repose sur une combinaison d'éléments cliniques et d'examens complémentaires.

L'anamnèse et les antécédents médicaux jouent un rôle essentiel dans le processus diagnostique. Les informations recueillies incluent les symptômes oculaires présents, les antécédents familiaux de glaucome, ainsi que les facteurs de risques (tableau 1) [18].

Tableau 1: principaux facteurs de risque de glaucome. RR : risque relatif

Hypertonie oculaire	>21mmHg RR 12,9 ≥30 mmHg RR 39
Âge	RR 2.1 par décennie
Ethnie	Prévalence du glaucome : mélanoderme 4,2% ; caucasien 2,1% ; asiatique 1,4%
Antécédents familiaux au premier degré	RR 2,9
Myopie	RR 1,6-3,3
Pression artérielle diastolique base	< 40 mmHg RR 2,1 < 30 mmHg RR 6,2

La mesure de la pression intraoculaire, principal facteur de risque de glaucome, est une étape cruciale dans le diagnostic du glaucome. Un tonomètre est utilisé pour évaluer la pression à l'intérieur de l'œil. Bien qu'une pression intraoculaire élevée soit souvent associée au glaucome, il convient de noter qu'un certain nombre de patients atteints de glaucome peuvent présenter une pression intraoculaire normale (glaucome à pression normale). La mesure de la PIO doit être accompagnée de celle de l'épaisseur cornéenne centrale (pachymétrie) puisqu'une pachymétrie fine est à l'origine d'une sous-estimation de la PIO réelle, et inversement.

L'examen du nerf optique au fond d'œil revêt une importance primordiale dans le diagnostic du glaucome. Il permet d'évaluer l'apparence du nerf optique et de détecter d'éventuelles altérations ou anomalies caractéristiques du glaucome, telles que l'excavation du disque optique, des encoches dans l'anneau neurorétinien ou encore des hémorragies péripapillaires. Il est désormais complété en routine par l'examen en tomographie par cohérence optique (OCT) du nerf optique en particulier de la couche de fibres nerveuses rétiniennes (RNFL). L'OCT permet également de mesurer l'épaisseur de la couche de cellules ganglionnaires (GCC), affectées par le glaucome. Une diminution de l'épaisseur de la RNFL ou de la GCC peut être un signe précoce de glaucome. L'OCT est également utilisé pour surveiller la progression du glaucome au fil du temps. Les examens réguliers par OCT permettent de détecter les changements de l'épaisseur de la RNFL et des cellules ganglionnaires, permettant ainsi une évaluation précise de la progression de la maladie.

Il est aussi primordial d'examiner l'angle iridocornéen à l'aide d'un verre de gonioscopie afin analyser son degré d'ouverture et évaluer un potentiel encombrement du trabéculum. Nous reviendrons plus en détail sur cette structure essentielle dans la suite de cette introduction.

En complément de ces examens cliniques, des tests de champs visuels automatisés sont utilisés pour évaluer les dommages causés au champ visuel. Ces tests permettent de détecter les altérations fonctionnelles précoces liées au glaucome, même en l'absence de symptômes perceptibles par le patient. Ils sont aussi indispensables au suivi de cette pathologie et doivent être répétés au moins deux fois par an pour s'assurer de l'efficacité des thérapeutiques qui doivent permettre d'obtenir une stabilité des examens.

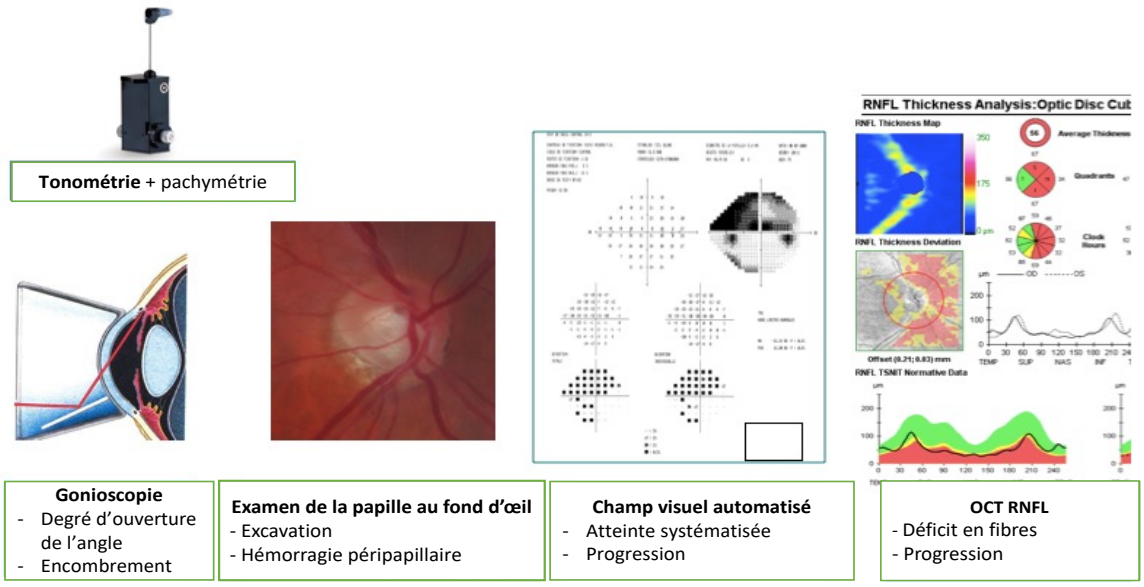

Figure 2: Les cinq examens essentiels dans le diagnostic du glaucome et les principales caractéristiques recherchées.

Prise en charge thérapeutique

Le glaucome à l'heure actuelle est traité exclusivement en contrôlant son facteur de risque principal, la PIO [17,19,20]. Tous les traitements actuels du glaucome, qu'ils soient médicaux, par laser ou chirurgicaux ont pour but de diminuer la PIO au-dessous du seuil de destruction des cellules ganglionnaires rétiniennes (CGR). Cette PIO cible est variable d'une personne à l'autre et ne peut être mesurée qu'*a posteriori* lorsque les preuves de la stabilisation des atteintes sont obtenues, sur les plans structurel (imagerie en OCT) et fonctionnel (champ visuel). Aucun traitement ne permet actuellement d'améliorer les atteintes liées au glaucome déjà survenues d'où l'importance d'un dépistage et d'un diagnostic précoce de cette maladie qui reste longtemps asymptomatique.

Les traitements médicaux, principalement topiques, agissent soit en augmentant l'évacuation de l'HA (collyres de dérivés de prostaglandine PGF2α (ex. latanoprost, travoprost), inhibiteur des rho-kinases (ROCK-i)) ; soit en diminuant la sécrétion d'HA (collyres bêtabloquants (ex. timolol) ou d'inhibiteurs de l'anhydrase carbonique (ex. brinzolamide ou acétazolamide) ou les deux à la fois avec des collyres d'agonistes des récepteurs α-adrénergiques (ex. brimonidine). Ces traitements peuvent être associés pour augmenter leur efficacité.

La trabéculoplastie au laser est une alternative ou un complément au traitement médical, elle agit aussi au facilitant l'écoulement de l'humeur aqueuse par photocoagulation sélective du trabéculum [21].

La prise en charge chirurgicale est variée. Elle peut être efficace en augmentant l'évacuation de l'HA par voie sous-conjonctivale : chirurgie filtrante (trabéculectomie, sclérectomie profonde non perforante), valve, Xen ™, Preserflo ™ (fistulisation sous-conjonctivale de l'HA) ; par voie trabéculaire (stent trabéculaire), ou par voie uvéo-sclérale (iStent Supra™). Le cyclo-affaiblissement au laser diode ou par ultrasons réduit la pression intraoculaire en détruisant les corps ciliaires responsables de la production d'HA dans l'œil. Il est généralement réservé aux cas de glaucome réfractaire, en raison des risques associés tels que l'hypotonie majeure, voire l'atrophie du globe (phtyse). Cette maladie nécessite un traitement à vie et une surveillance pluriannuelle.

Principaux axes de recherche dans le glaucome

La physiopathologie

La compréhension des mécanismes biologiques et moléculaires impliqués dans le développement et la progression du glaucome reste à ce jour un terrain de recherche. En effet, la physiopathologie et les mécanismes sous-jacents de la dégénérescence du CGR sont encore largement incompris. Cela comprend l'exploration de facteurs génétiques, d'anomalies de la circulation sanguine, d'inflammation, de stress oxydant, la dysfonction mitochondriale et d'autres processus cellulaires perturbés.

Les biomarqueurs

Les biomarqueurs jouent un rôle crucial dans la détection précoce, le suivi de la progression et l'évaluation de l'efficacité des traitements du glaucome. La PIO, les champs visuels automatisés et l'OCT du nerf optique et des cellules ganglionnaires sont déjà reconnus comme étant des indicateurs importants de progression. De nombreuses études se concentrent sur l'identification et la validation de nouveaux biomarqueurs qui peuvent fournir des indications précoces de la maladie, prédire la progression et évaluer la réponse au traitement, couvrant ainsi des domaines tels que l'analyse d'imagerie, la génétique et les marqueurs métaboliques. L'identification de biomarqueurs fiables facilitera le dépistage précoce et permettra une prise en charge plus personnalisée des patients atteints de glaucome [23]. De plus, l'intelligence artificielle offre également une perspective prometteuse pour la détection de la progression du glaucome, notamment par le biais de l'analyse des rétinographies, de l'imagerie (angio-)OCT, ou des champs visuels.

D'autre part, l'évolution du champ visuel est considérée comme le critère d'évaluation de référence pour les essais cliniques dans le glaucome, mais la PIO est souvent utilisée comme critère de substitution. Dans le glaucome, les médicaments actuellement disponibles ont été approuvés en fonction de leur capacité à réduire la PIO. Certaines découvertes récentes indiquent cependant qu'au même niveau de réduction de la PIO, tous les médicaments n'ont pas le même effet sur la progression du champ visuel.

Pour les essais de neuroprotection dans le glaucome, de nouveaux paramètres de substitution sont nécessaires, qui peuvent inclure des paramètres fonctionnels ou structurels ou une combinaison des deux. Des biomarqueurs fonctionnels et structurels pourraient ainsi être une alternative intéressante comme critère de jugement principal dans les essais cliniques dans le domaine du glaucome.

À ce jour, de nombreuses recherches ont concentré leur attention sur l'identification de nouveaux marqueurs moléculaires caractéristiques de la manifestation et de la progression du glaucome. Parmi ceux-ci, plusieurs métabolites et protéines ont été étudiés dans différents fluides biologiques, tels que le film lacrymal, le vitré, l'eau, le sérum et le plasma, car ils sont potentiellement impliqués dans les voies moléculaires et cellulaires causant des dommages aux cellules neuronales chez les personnes souffrant de glaucome [22,23].

Le traitement

Actuellement, la recherche dans le domaine du glaucome s'investit surtout dans une démarche de neuroprotection indépendante de la PIO [24]. En effet les traitements actuels visant à ralentir la progression de la maladie en diminuant la PIO ne sont pas toujours efficaces, notamment en cas de glaucome à pression normale. De plus, s'ils ralentissent ou bloquent sa progression, ils ne permettent pas une amélioration des atteintes de cette maladie.

Ces approches sont les suivantes :

La neuroprotection : elle vise à prévenir ou ralentir la dégénérescence des CGR en modifiant les CGR elles-mêmes ainsi que le microenvironnement des neurones pour favoriser la survie et la fonction des neurones. Les recherches se concentrent sur l'identification de substances ou de médicaments qui peuvent protéger les cellules nerveuses contre les dommages et la mort cellulaire. Certaines stratégies indépendantes de la PIO comprennent :

- L'usage des antioxydants : les antioxydants peuvent neutraliser les radicaux libres et réduire le stress oxydant, qui contribuent à la mort des cellules nerveuses. Des études examinent l'effet des antioxydants tels que la vitamine C, la vitamine E, les flavonoïdes et les caroténoïdes sur la protection du nerf optique [25,26]. D'autre part, l'inhibition ciblée des enzymes NOX pourrait permettre la régulation des espèces réactives de l'oxygène et des signaux redox [27].
- Le développement des facteurs de croissance nerveuse : les facteurs de croissance neuronale, tels que le FGF, le GDNF, le BDNF et le CNTF, peuvent favoriser la survie des cellules nerveuses et favoriser leur régénération [28].
- L'utilisation d'agents anti-apoptotiques : l'apoptose, ou mort cellulaire programmée, joue un rôle dans la dégénérescence du nerf optique. Les études sont en cours pour évaluer des agents qui peuvent inhiber les processus apoptotiques, tels que les inhibiteurs de caspases et les protéines anti-apoptotiques telles que la ghréline, la somatostatine ou la mélatonine [29–31].

Les stratégies anti-inflammatoires : l'inflammation chronique a été impliquée dans la progression du glaucome [32]. Les études visent à comprendre les mécanismes inflammatoires sous-jacents et à développer des traitements anti-inflammatoires pour atténuer les dommages au nerf optique. Elles incluent des inhibiteurs de cytokines impliquées dans la réponse inflammatoire tels que les anti-TNF-α et les inhibiteurs de l'IL-6 [33]. Elles incluent également les agents immunomodulateurs, modulant l'inflammation neuronale, tels que les neurostéroïdes, (stéroïdes neuroprotecteurs synthétisés de façon endogène dans le cerveau) [34,35].

Les thérapies géniques et cellulaires : ces thérapies sont des approches émergentes pour le traitement du glaucome. L'œil est un organe intéressant à cibler par la thérapie génique en raison de son accessibilité et de son privilège immunitaire. Plusieurs essais de thérapie génique sont en cours pour chercher à prévenir la progression des maladies neurodégénératives et protéger à la fois les CGR et les axones. Ces gènes peuvent être impliqués dans la protection cellulaire, la régénération ou la modulation de la réponse inflammatoire [36,37]. Différentes stratégies sont explorées, telles que l'utilisation de vecteurs viraux pour délivrer les gènes, ou encore la modulation de l'expression génique pour réduire l'inflammation ou favoriser la régénération cellulaire. En thérapie cellulaire, les cellules souches et les cellules progénitrices sont étudiées pour leur potentiel à régénérer les cellules nerveuses du nerf optique endommagé. Des essais cliniques évaluent l'efficacité et la sécurité de l'administration de cellules souches ou de cellules progénitrices dans le glaucome [16].

L'utilisation des nanoparticules à délivrance ciblée : Les nanoparticules sont utilisées pour délivrer des médicaments ou des gènes de manière ciblée dans les cellules du nerf optique. Ces approches pourraient permettre d'augmenter l'efficacité des traitements tout en minimisant les effets indésirables [38,39].

Trabéculum : structure et fonction

Le trabéculum joue donc un rôle important dans le maintien et le fonctionnement de la voie d'écoulement aqueuse, dans la suite de cette introduction nous allons détailler sa structure, sa fonction, ses implications cliniques et thérapeutiques ainsi que les axes de recherches fondamentales s'intéressant à cette structure clé.

Anatomie

Embryologiquement, le trabéculum dérive d'une origine mixte mésodermique et d'une vague de cellules mésenchymateuses issues de la crête neurale entre la 15ème et la 20ème semaine de développement [40,41].

C'est une structure en tamis qui joue un rôle de filtre entre la chambre antérieure et le canal de Schlemm (CS), canal circulaire qui collecte l'HA et l'évacue vers les émonctoires extraoculaires (figure 3a)[42].

Le trabéculum, qui passe en pont au-dessus du sulcus scléral, isolant ainsi le CS dans la gouttière sclérale, s'insère en avant à la cornée périphérique- au niveau de ligne de Schwalbe- tandis qu'en arrière, les lamelles trabéculaires sont connectées à la jonction entre le corps ciliaire, l'iris et l'éperon scléral.

On distingue deux parties fonctionnellement différentes: le trabéculum antérieur, ou non filtrant, qui n'est pas au contact du CS, et le trabéculum postérieur, ou filtrant, qui est au contact du CS [43].

Le trabéculum antérieur est une zone de transition entre l'anneau de Schwalbe et le trabéculum postérieur. Il est formé de 4 à 5 lamelles trabéculaires recouvertes de cellules trabéculaires. Au niveau de la zone de transition entre le trabéculum non filtrant et le trabéculum filtrant, on décrit en microscopie électronique des espaces organisés en petits canaux dont la signification est mal connue et qui pourraient servir au transport des fluides ou à l'accueil de cellules accessoires nécessaires à la régénération cellulaire.

Le trabéculum postérieur est dit filtrant car il est en contact avec le CS. Il représente le filtre trabéculaire proprement dit. Il comprend trois régions anatomiquement distinctes qui sont, de dedans en dehors: le trabéculum uvéal, le trabéculum cornéoscléral, et le trabéculum juxtacanalaire – ou trabéculum cribriforme- qui est en contact en dehors avec le CS [44,45] (figure 3b).

- Le trabéculum uvéal est en contact direct avec l'HA. Il s'organise en 2 à 4 couches de fins cordages ou lamelles qui s'entrecroisent de l'anneau de Schwalbe vers l'extrémité de l'éperon scléral, la bande ciliaire et la racine de l'iris. Ces lamelles sont composées de couches concentriques (fibres de collagène, fibres d'élastine, substance fondamentale) et sont recouvertes de cellules trabéculaires reposant sur une membrane basale, la face apicale des cellules étant recouverte de glycosaminoglycanes. L'entrecroisement des piliers ménage des orifices permettant l'écoulement de l'HA.
- Le trabéculum cornéoscléral, qui représente la majeure partie du trabéculum, est lui formé d'une superposition de lamelles conjonctives percées d'orifices, qui s'étendent et vont en nombre croissant de l'anneau de Schwalbe (de 3 à 4) à l'éperon scléral (une quinzaine). Ces lamelles ont la même ultrastructure que celles du trabéculum uvéal et sont recouvertes d'une monocouche de cellules trabéculaires unies entre elles par des desmosomes et des jonctions communicantes. Les espaces interlamellaires deviennent plus étroits à proximité du trabéculum juxtacanalaire mais ne constituent pas un obstacle à l'écoulement de l'HA.
- Le trabéculum juxtacanalaire, qui est la portion la plus externe du trabéculum filtrant postérieur, est histologiquement différent des deux autres parties du trabéculum. Il est formé d'un tissu conjonctif lâche, sans stratification, et de 2 à 5 couches de cellules trabéculaires dispersées au sein de la MEC dense et disposées en réseau grâce à leurs expansions cytoplasmiques [3]. Sa partie externe correspond à l'endothélium du mur interne du CS [46]. Cet endothélium est d'épaisseur irrégulière du fait de la taille des noyaux cellulaires, de la présence de vacuoles

géantes intracytoplasmiques et d'expansions cytoplasmiques en doigts de gant faisant saillie dans la lumière du canal. Les cellules endothéliales, séparées d'espaces de 15 à 20 nm, sont jointes par différents complexes jonctionnels. Des pores et vacuoles de 0,5 à 2 µm de diamètre réalisent des ouvertures dans la paroi interne du canal de Schlemm [47].

La porosité du trabéculum filtrant postérieur diminue de dedans en dehors [6], mais en conditions physiologiques, le trabéculum uvéal et cornéoscléral n'opposent pas de résistance à l'élimination de l'HA.

En terme d'innervation, le trabéculum reçoit des fibres postganglionnaires provenant des ganglions ptérygopalatins (parasympathique) et cervicaux supérieurs (sympathique) [48,49]. Le système nerveux autonome, comprenant les divisions sympathique et parasympathique, joue un rôle dans la régulation de la pression intraoculaire (PIO) en influant sur la dynamique de l'écoulement de l'humeur aqueuse à travers le trabéculum. Les mécanismes précis par lesquels cette innervation impacte la fonction de cette structure sont complexes et impliquent la modulation des réponses contractiles et de relaxation qui est encore mal compris [49,50].

a.

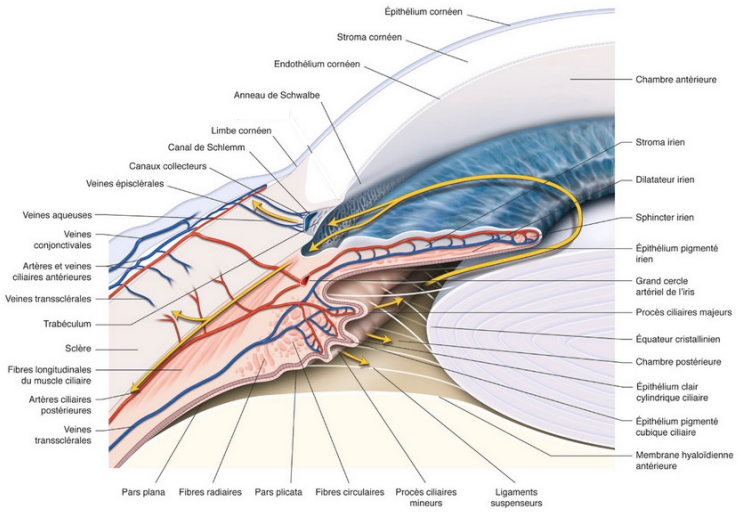

b.

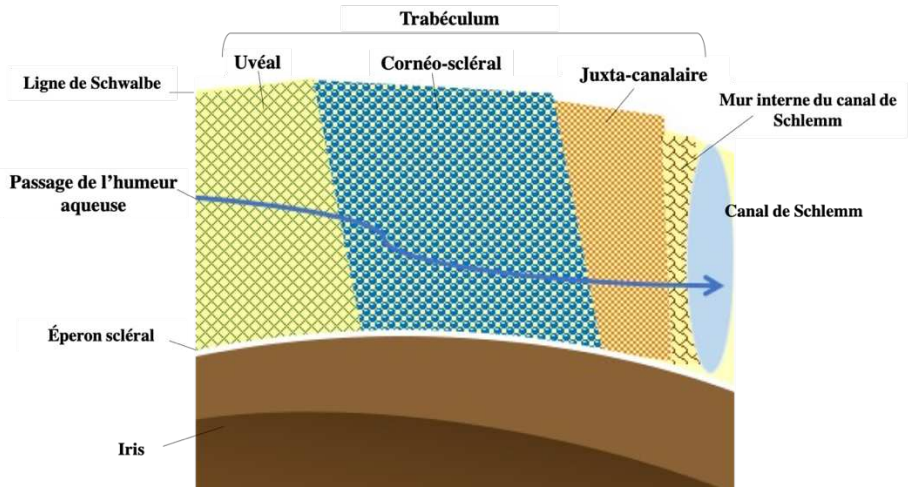

Figure 3: Anatomie du trabéculum
a. Représentation schématique de la circulation de l'HA détaillant les différentes structures histologiques impliquées (Source : Rapport SFO 2014 : Glaucome primitif à angle ouvert J-P Renard) b. Schéma de l'organisation histologique des différentes structures du trabéculum.

Cellules trabéculaires

Les cellules trabéculaires sont des cellules particulières alliant les propriétés de cellules endothéliales, de myofibroblastes et de macrophages (figure 4). Elles sont responsables de la régulation de la résistance à l'écoulement de l'HA. Les propriétés des cellules trabéculaires diffèrent selon leur localisation au sein du trabéculum et sont résumées dans le tableau 2.

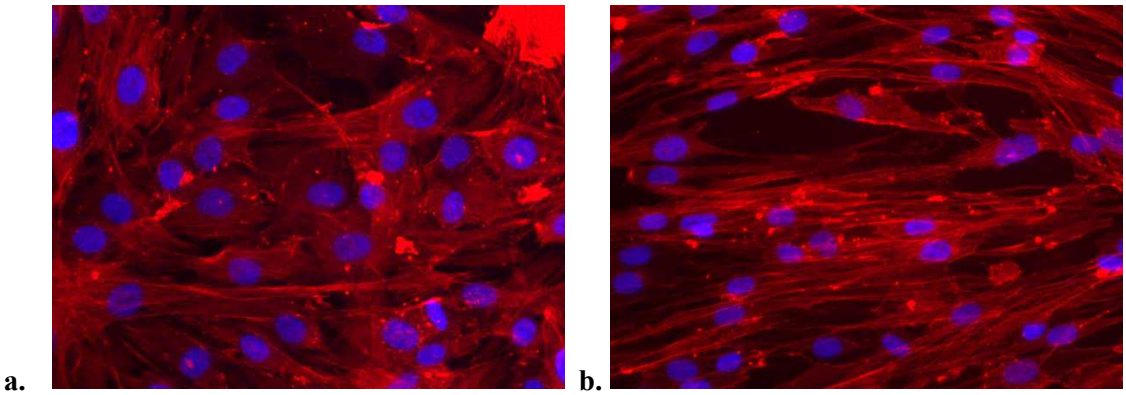

Figure 4 : Photographies au microscope à fluorescence de deux aspects de cellules trabéculaires humaines *in vitro*. a. morphologie étoilée b. Morphologie fusiforme (X200).
Le cytosquelette d'actine est marqué avec la phalloïdine (rouge) et le noyau au DAPI (bleu)

Tableau 2: Phénotypes et propriétés des cellules trabéculaires.

Phénotype	**Localisation**	**Comportement cellulaire**	**Responsabilité**
Endothélial Forme ronde à ovale,	Portion cornéosclérale et uvéale	Endothélium	Maintien de la perméabilité
			Neutralisation des espèces réactives de l'oxygène

large corps cellulaire		Macrophage	Filtre biologique/ phagocytose
			Médiation immunitaire
Fibroblastique Forme allongée	Juxtacanalaire	Fibroblaste	Renouvellement de la MEC/ Réparation tissulaire
		Cellule musculaire lisse	Contractilité
			Mécanotransduction

Fonctionnant comme les cellules d'un endothélium dans la portion cornéosclérale et uvéale, les cellules trabéculaires produisent de grandes quantités de substances antithrombotiques, telles que les héparanes sulfates et l'activateur du plasminogène tissulaire (tPA) [51]. De même que les cellules endothéliales, les cellules trabéculaires de la portion interne semblent participer à la médiation de l'inflammation. L'hypothèse que ces cellules joueraient un rôle dans la présentation de l'antigène a été proposée dans les années 1990 lorsque des complexes majeurs d'histocompatibilités (CMH) de classe I et II ont été détectés sur des coupes congelées de trabéculum et sur des cellules trabéculaires en culture [52–55]. Plus récemment des études ont montré que ces cellules pouvaient sécréter un certain nombre de facteurs, tels que des enzymes et des cytokines qui modulent les fonctions des cellules trabéculaires et de la MEC. Shifera et al. ont rapporté que des cellules trabéculaires humaines en culture sécrètent des quantités importantes de cytokines chimiotactiques CXCL8/IL-8, CXCL6/GCP-2 et CCL2/MCP1 en l'absence de toute stimulation [56]. La sécrétion de ces chimiokines augmentait sous l'effet des cytokines pro-inflammatoires TNF-α et IL-1β. Ils ont également pu montrer que des monocytes, vraisemblablement sous l'influence de ces signaux chimiotactiques, circulaient à travers le trabéculum [57]. Les cellules trabéculaires ont aussi une activité semblable à celle des macrophages pour éliminer les débris cellulaires présents dans l'HA [58,59].

Conformément à leur rôle de contrôle de la résistance à l'élimination de l'HA, les cellules trabéculaires de la région juxtacanalaire possèdent à la fois des propriétés fibroblastiques et contractiles. Leur phénotype est assez différent avec une morphologie en forme de fuseau. Elles sécrètent un certain nombre de protéines de la MEC (collagènes, fibronectine, élastine, fibrillines et protéoglycanes) et leurs enzymes de dégradation (métalloprotéases de la matrice (MMP-1, -2, -3, -9, -12, et -14)), afin de soutenir le remodelage continu de la MEC [60]. Elles sont contractiles, exprimant l'actine musculaire lisse et la myosine qui sont importantes dans la mécano-transduction [3]. La contraction des cellules trabéculaires augmente la facilité d'écoulement de l'humeur aqueuse. La noradrénaline semble faciliter l'écoulement par le trabéculum, mais le rôle du système nerveux autonome dans le contrôle direct de la résistance du trabéculum est encore peu clair [49].

Plusieurs auteurs ont émis l'hypothèse que la région non filtrante du trabéculum, proche de la ligne de Schwalbe, servirait de niche pour les cellules souches (ou progénitrices) capables de se diviser et de recoloniser le réseau trabéculaire après une lésion [61,62].

La matrice extracellulaire (MEC)

La MEC est faite de composants fibrillaires et d'une substance fondamentale amorphe composée de collagène de type IV, de hyaluronate, de glycosaminoglycanes et de protéoglycane [63]. Dans le trabéculum uvéal et cornéoscléral, des lamelles de tissu conjonctif sont recouvertes par des cellules trabéculaires. Dans la région juxtacanalaire, les cellules résident relativement librement et sont intégrées dans la MEC (figure 5) [64]. Le tissu juxtacanalaire est constitué de fibres de collagènes irrégulièrement orientées au sein de la matrice, et d'un réseau de fibres élastiques, le plexus cribriforme, qui s'étend entre le trabéculum cornéoscléral et la paroi interne du CS, de façon tangentielle à l'endothélium à celle-ci. Les fibres élastiques du plexus cribriforme sont constituées d'élastine, de décorine et de collagène de type VI[65]. Elles sont recouvertes d'une gaine de composants microfibrillaires contenant du collagène de type VI, de la laminine et de la fibronectine responsable de l'adhérence des cellules à leurs substrats [66].

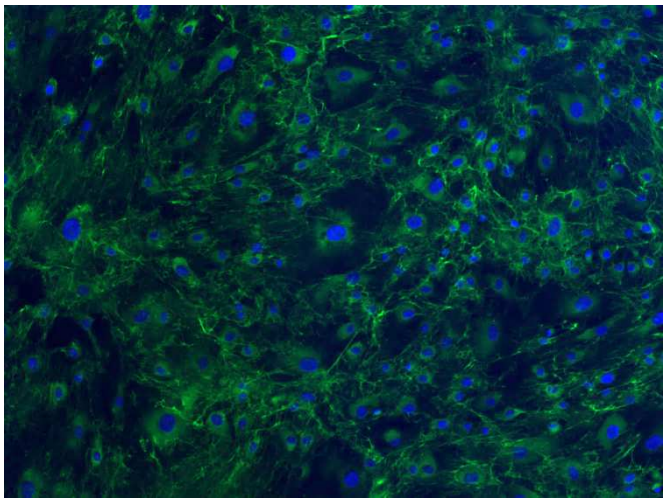

Figure 5 : Photographie au microscope à fluorescence de cellules trabéculaires humaines au sein de leur matrice extracellulaire
marquée avec un anticorps anti-fibronectine (vert) et les noyaux sont colorés au DAPI (bleu) (grossissement x100).

Évacuation de l'HA et régulation de la PIO

L'HA est évacuée hors de l'œil par deux voies : la voie principale, trabéculaire, dite aussi conventionnelle (40-96% du drainage [67,68]) et la voie secondaire dite uvéosclérale. Au niveau de la voie d'écoulement trabéculaire, le trabéculum contrôle la PIO en régulant l'évacuation de l'HA de la chambre antérieure vers le CS qui lui est adjacent, jusqu'aux canaux collecteurs des veines aqueuses

puis vers le système veineux (Figure 1). On peut l'imaginer comme un filtre biologique autonettoyant dont le maillage peut être plus ou moins serré en fonction de différents facteurs de régulation. Chez l'homme, 75% de la résistance à la sortie de l'HA se font au niveau du trabéculum, en particulier au niveau de sa partie juxtacanalaire, et 25% au niveau du CS [69].

La résistance est sous l'influence de deux systèmes contractiles, celui de la partie antérieure du muscle ciliaire via des extensions des tendons du muscle ciliaire qui traversent le trabéculum cribriforme et qui s'insèrent sur le mur du CS [70] et celui dû aux cellules contractiles de type myofibroblastique du trabéculum. Ainsi, la résistance est réduite par la contraction du muscle ciliaire ou par la relaxation des cellules trabéculaires. Le corps ciliaire est innervé par le système nerveux autonome sympathique et parasympathique[6]. Il est bien établi que la contraction du muscle ciliaire entraîne un changement conformationnel immédiat du réseau trabéculaire et possiblement une dilatation du canal de Schlemm conduisant à une diminution de la résistance à l'écoulement par cette voie. De plus, des études morphologiques ont démontré une innervation cholinergique et adrénergique du trabéculum lui-même et de la région de l'éperon scléral dans les yeux de divers mammifères, y compris les humains [48]. Des études sur des cellules trabéculaires en culture et dans des segments antérieurs perfusés ont démontré qu'elles sont contractiles et que leur relaxation augmente la facilité d'écoulement de l'humeur aqueuse. La régulation de la résistance se ferait en réponse à une détection cellulaire d'étirement ou de déformation dans la région juxtacanalaire du trabéculum sous l'effet des changements de PIO [71]. Les cellules trabéculaires de cette région sécrètent en même temps les protéines de la MEC et des enzymes de dégradation afin de soutenir le remodelage de la MEC. Sous la dépendance de récepteurs cellulaires à la tension, des ajustements de la résistance ont donc lieu par modification du turnover de la MEC : sécrétion et/ou activation de protéinases, clivage de la matrice, digestion des fragments et biosynthèse de ses composants [5].

Les cellules trabéculaires possèdent aussi des propriétés d'adaptation comme des mécanismes d'adhésion de cellule à cellule, des interactions cellule-matrice, une contractilité cellulaire liée à son cytosquelette d'actine, et l'expression de canaux hydriques pour faciliter les changements rapides du volume cellulaire [71].

La dégénérescence trabéculaire dans le glaucome

Le glaucome primitif à angle ouvert

Dans le glaucome primitif à angle ouvert (GPAO), la résistance à l'évacuation de l'HA au niveau du trabéculum est anormalement élevée [4]. Des études ont montré que cette augmentation de la résistance était liée à un mécanisme de rigidification du trabéculum associant une sénescence et une apoptose des cellules trabéculaires au remodelage de la MEC [3,4,6,40,72]. Ces changements sont similaires aux

altérations du trabéculum liées à l'âge mais semblent s'accélérer dans le glaucome [73]. Ainsi, Tektas *et al.* ont décrit une augmentation significative de l'épaisseur de la gaine des fibres élastiques par rapport à des trabéculums normaux de sujets du même âge. Celles-ci apparaissent en coupes transversales comme des « plaques » extracellulaires et ont donc été nommées « plaques dérivées de la gaine » [4]. Cette augmentation est due aux fibrilles et aux autres composants de la MEC qui adhèreraient aux gaines des fibres élastiques et à leurs connexions avec l'endothélium de la paroi interne. Dans les yeux atteints de GPAO, il y a également une perte marquée de cellules trabéculaires qui entraîne par endroits la fusion et l'épaississement des lamelles trabéculaires [4].

Une étude en microscopie confocale de Hamard *et al*. a ainsi montré une diminution très significative de la densité cellulaire au sein de la membrane trabéculaire externe retirée au décours de sclérectomies profondes non perforantes (SPNP) chez des sujets glaucomateux par rapport aux témoins (figure 6). Cette perte cellulaire intéressait aussi bien le trabéculum juxtacanalaire qu'une partie du trabéculum cornéoscléral adjacent [74].

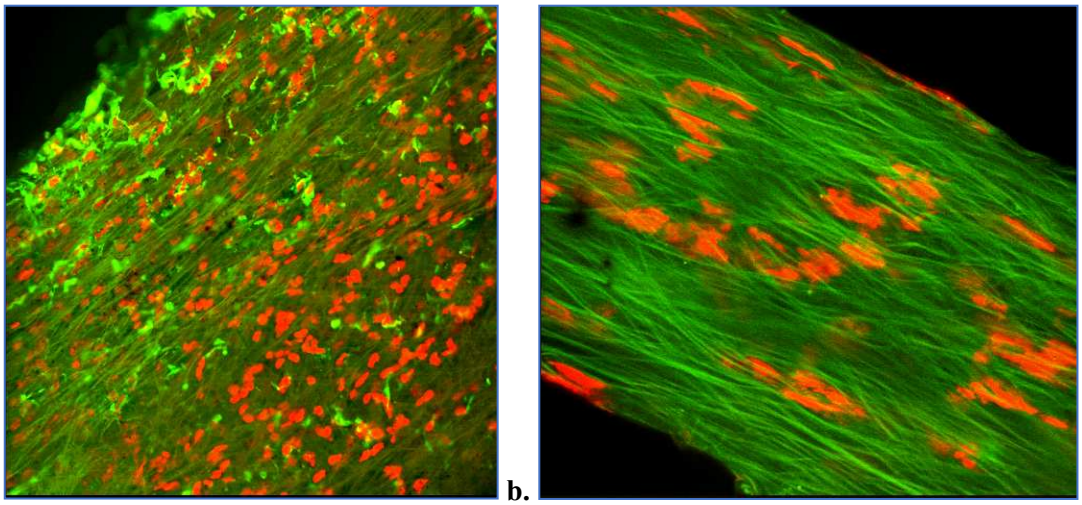

Figure 6 : Photographies en microscopie confocale d'un trabéculum normal (a) et d'un trabéculum glaucomateux (b). Les noyaux sont colorés en rouge avec du iodure de propidium, l'autofluorescence de l'élastine apparaît en vert permettant de visualiser la MEC. a. les cellules du trabéculum cribriforme ont un aspect dendritique et sont fortement fluorescentes après marquage avec un anticorps anti-vimentine. b. raréfaction majeure des cellules trabéculaires (rouge) et forte augmentation de la MEC (fibres vertes autofluorescentes) dans le trabéculum cornéoscléral.

Tamm *et al.* ont aussi décrit des changements au niveau des cellules du tissu conjonctif juxtacanalaire qui acquièrent des caractéristiques contractiles (5, 6). On observe ainsi une augmentation et une réorganisation de leur cytosquelette actinique et de la MEC aboutissant à un raidissement du mur interne du CS [75].

Sous l'influence du TGF-β2, on assisterait également à des modifications cellulaires du trabéculum lui-même. Le TGF-β2 semble ainsi jouer un rôle significatif dans la genèse du GPAO. C'est une cytokine profibrotique connue pour être en plus grande concentration dans l'HA des patients atteints de glaucome [76]. Le trabéculum est une source endogène de TGF-β2 [77,78]. Tripathi *et al.* ont pu montrer que le

TGF-β2 augmentait la PIO en induisant la synthèse par les cellules trabéculaires de certains composants matriciels moins facilement dégradables par les métalloprotéinases tels que le collagène de type IV, la fibronectine, la laminine et l'élastine [79–81]. Ces effets sont médiés par l'induction de cascades de signalisation du TGF-β2 conventionnelles (voies des Smad) ainsi que non-conventionnelles (voies des MAP kinases, et des Rho GTPases) [78] (figure 6). Les voies de signalisation conventionnelles Smad comprennent des protéines de signalisation omniprésentes avec de nombreux effecteurs en aval impliqués entre autres dans la cicatrisation des plaies cornéennes ou le maintien du privilège immunitaire oculaire. L'isoforme Smad 3 est plus systématiquement liée à l'expression de médiateurs impliqués dans l'hypertonie oculaire. Ceci implique qu'une inhibition ciblée de Smad3 serait une cible intéressante pour une thérapie contre le glaucome [78]. Une autre piste serait celle d'une modulation de Smad 7, un inhibiteur de Smad qui fonctionne comme un antagoniste intracellulaire de la signalisation du TGF-β.

Le TGF-β2 augmenterait aussi la rigidité cellulaire par la formation de *Cross-linked Actin Networks* (CLANs) *via* la voie Rho-GTPase (figure 8) [77]. Les CLANs sont des réarrangements du cytosquelette modifiant la forme et la rigidité des cellules et donc leur capacité à répondre à des signaux extérieurs. Les cellules des voies d'écoulement trabéculaires seraient donc stimulées par le TGF-β2 pour acquérir un phénotype plus rigide, impliquant à la fois une augmentation du cytosquelette d'actine et de la MEC fibrillaire environnante.

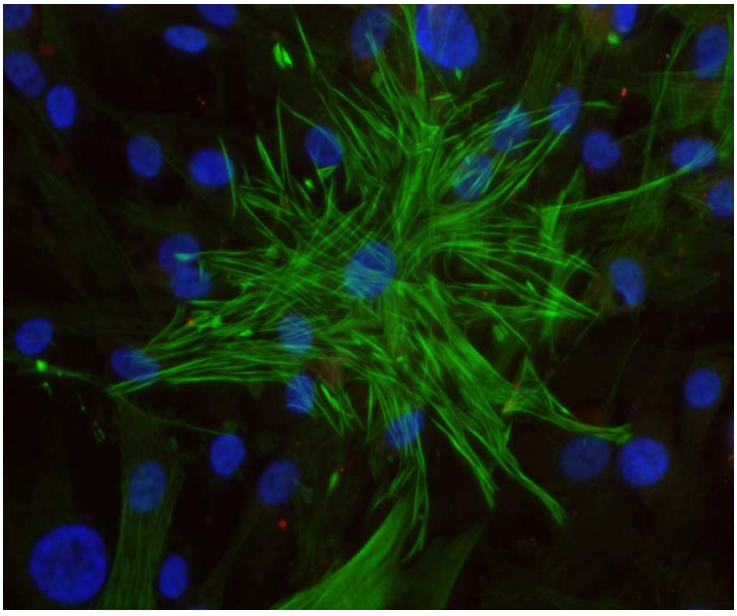

Figure 7 : Photographie au microscope à fluorescence des *Cross-linked Actin Networks* (CLANs) au sein de cellules trabéculaires humaines.
Réarrangement du cytosquelette avec interconnexion de fibres d'actine entrainant une modification de la forme et de la rigidité des cellules. Le cytosquelette d'actine est marqué avec un anticorps anti *alpha-smooth muscle actin* (vert) et le noyau au DAPI (bleu)(X20).

Les *Bone morphogentic proteins* (BMP) sont une famille de facteurs de croissance impliqués dans la régulation de la MEC et donc dans la régulation de la résistance à l'évacuation de l'HA. Les voies de signalisation BMP et TGF-β opposent leurs rôles antifibrotiques et profibrotiques. Les BMP peuvent ainsi dégrader les dépôts de matrice induits par le TGF-β2 [82]. Il a été montré que les antagonistes des BMP, *gremlin* et *noggin* étaient plus exprimés dans les cellules trabéculaires glaucomateuses et provoquaient une augmentation de la PIO dans des segments antérieurs perfusés [83–85]. *Gremlin* bloquerait aussi la répression de BMP4 sur la synthèse de fibronectine induite par le TGF-β [84,86]. La dérégulation de ce facteur, probablement sous l'effet de mutations ou de polymorphismes génétiquement induits pourrait donc expliquer la surexpression du TGF dans le glaucome primitif.

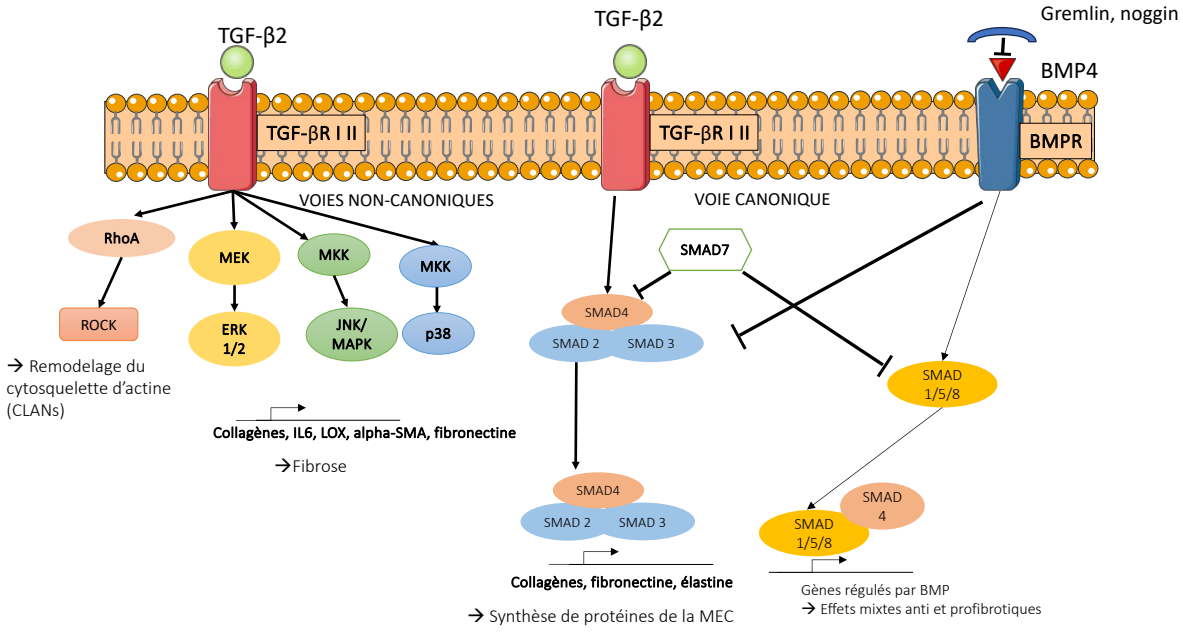

Figure 8 : Schéma représentant les voies de signalisation du TGF-β2 dans les cellules trabéculaires.

Le ligand TGF-β2 se lie aux récepteurs de type II du TGF-β (TGF-βRII) et phosphoryle le récepteur de type I du TGF-β (TGF-βRI), activant ainsi diverses cascades de signalisation intracellulaire. Les voies intracellulaires activées par le TGF-β2 comprennent la voie canonique SMAD2/3 et les voies non canoniques du TGF-β. La voie de signalisation canonique est utilisée à la fois par le TGF-β2 et les BMPs. En ce qui concerne le TGF-β2, l'activation du récepteur déclenche une signalisation en aval par l'intermédiaire des protéines Smad 2/3, suivie de l'hétérodimérisation avec Smad4 et de la translocation du complexe vers le noyau où il induit la transcription de gènes cibles spécifiques. La liaison des ligands BMP au complexe récepteur BMP entraîne la phosphorylation de Smad1, Smad5 ou Smad8 qui se lient avec Smad4, ce qui entraîne la translocation du complexe dans le noyau pour activer des gènes cibles spécifiques. *Gremlin* inhiberait la capacité de BMP4 à réprimer la synthèse de matrice extracellulaire (MEC) induite par le TGF-β.

Dans les voies non canoniques, les récepteurs activés du TGF-β utilisent des kinases MAP, notamment les kinases régulées par les signaux extracellulaires (ERK), les kinases des protéines activées par les mitogènes p38 (p38MAPK) ou les kinases de la protéine c-Jun N-terminale (JNK), pour activer les gènes cibles. Ceux-ci peuvent réguler l'organisation du cytosquelette des cellules (alpha-SMA, CLANs), et la synthèse de protéines de la MEC et de facteurs profibrotiques.

Le stress oxydant pourrait également jouer un rôle important dans la physiopathologie du glaucome. Une méta-analyse publiée en 2016 a ainsi rapporté que les marqueurs de stress oxydant étaient surexprimés dans le sérum et l'HA des patients glaucomateux [87]. La production d'espèces réactives

de l'oxygène (ERO) dans le trabéculum est à la fois d'origines endogène (générées par les mitochondries) et exogène. Elle peut augmenter sous l'effet de l'âge, de l'inflammation, de l'exposition aux radiations lumineuses, infrarouges ou ultraviolettes, ou de certains toxiques. Une perturbation de l'équilibre pro-oxydant / antioxydant dans l'HA provoque une augmentation de la production d'ERO à l'origine d'une altération du trabéculum [88]. Les ERO endommagent les protéines, les lipides et les molécules d'ADN ; ces processus sont associés au vieillissement cellulaire, à l'inflammation chronique, à l'apoptose et à la mort cellulaire libérant des radicaux libres à l'origine d'un cercle vicieux. Au niveau du trabéculum on assiste à un arrêt de la croissance des cellules, à une altération de la perméabilité des cellules, à des réarrangements du cytosquelette des cellules trabéculaires affectant leur fonction et les interactions de celles-ci avec la MEC et à une accumulation de la MEC [88,89]. Il a été ainsi montré que le TGF-β2 provoquait une augmentation du stress oxydant dans les cellules trabéculaires humaines. Le prétraitement des cellules trabéculaires avec des antioxydants ciblés sur les mitochondries (XJB-5-131 (10 μM) ou MitoQ (10 nM)) atténuait les changements médiés par le TGF-β2 dans l'activité transcriptionnelle dépendante de Smad, y compris des réductions marquées des fibres de stress et de l'expression des collagènes [90].

Le glaucome par fermeture de l'angle

Dans le glaucome par fermeture de l'angle, le mécanisme d'élévation de la PIO est expliqué par l'apposition de l'iris sur le trabéculum, ce qui bloque l'évacuation de l'HA. Cependant, dans certains cas, même après la levée du blocage trabéculaire, la PIO reste élevée. En gonioscopie, des synéchies antérieures périphériques ou des amas de pigments peuvent être observés au niveau trabéculaire.

Une étude histologique de Hamanaka *et al*. sur des échantillons de trabéculums de patients opérés de trabéculectomie dans un contexte d'angle iridocornéen fermé a permis de révéler des dommages au niveau du CS et du trabéculum postérieur [91]. En effet, le contact persistant du trabéculum avec l'iris ou les synéchies antérieures périphériques en bloquant l'évacuation de l'HA provoquait une atteinte du CS et son occlusion. Au niveau de la partie postérieure du trabéculum, il a également été observé une perte en cellules trabéculaires, une altération de leur fonction mitochondriale avec un élargissement et une fusion des faisceaux trabéculaires [91,92]. Ces mécanismes permettent d'expliquer l'élévation persistante de la PIO même lorsque l'angle a été rouvert chez un patient ayant un glaucome chronique par fermeture de l'angle.

Le glaucome induit par les corticoïdes

La principale découverte dans le glaucome cortico-induit est une accumulation de collagène de type IV et de fibronectine dans la portion externe du trabéculum [93]. On trouve également une augmentation

d’un matériel mixte associant des replis de membrane basale arrangés en empreinte digitale et de dépôts de fines fibrilles non-identifiées arrangées en bandes dans la région sous-endothéliale du CS [4]. Les glucocorticoïdes comme la dexaméthasone (DEX) sont connus pour modifier l’architecture du trabéculum en augmentant la rigidité des cellules trabéculaires. La matrice déposée par les cellules trabéculaires sous l’effet de la DEX serait environ 4 fois plus rigide, plus organisée et présenterait une expression élevée des protéines de la MEC généralement impliquées dans le glaucome (décorine, myociline et fibrilline) [94,95]. Des études biochimiques et génétiques ont suggéré qu’une augmentation au niveau du trabéculum de l'expression de la myociline, encore appelée protéine de réponse trabéculaire aux glucocorticoïdes (TIGR), pourrait jouer un rôle dans le développement du glaucome cortico-induit [96,97]. Il est intéressant de noter que l’expression de ce gène induite par une exposition aux corticoïdes aurait un effet pro-apoptotique [98,99]. Par conséquent, la capacité phagocytaire de la population cellulaire restante dans le trabéculum serait insuffisante pour un nettoyage efficace de l'HA, augmentant ainsi la résistance à l’évacuation de l’HA. Dans ce cas également, existerait donc un mécanisme mixte, à la fois mécanique et dégénératif pouvant expliquer que la PIO ne se normalise pas systématiquement à l’arrêt des corticoïdes en cas de glaucome cortico-induit.

Le glaucome pigmentaire

Le syndrome de dispersion pigmentaire (SDP) résulterait d’un contact mécanique entre les fibres zonulaires du cristallin et la partie postérieure de l'iris, responsable d’un relargage de pigments iriens dans l'œil [100]. Chez les patients qui présentent un SDP, l’encombrement progressif du trabéculum par les pigments iriens peut entraîner un dysfonctionnement de ce dernier et une élévation de la PIO. Ainsi, entre 25 et 50% des patients avec un SDP risqueraient de développer une hypertonie oculaire [101].

Dans cette maladie, on constate au niveau du trabéculum une perte des cellules trabéculaires, plus importante que dans le GPAO, et probablement liée à la toxicité de la surcharge en granules de pigments [4]. L'exposition des cellules trabéculaires aux pigments entrainerait aussi une réduction des capacités de phagocytose et de migration cellulaires, ainsi qu'une augmentation de la formation de fibres de stress et de la contraction cellulaire [102,103]. Du fait de son rôle dans la régulation du mouvement et de la forme des cellules, la voie de signalisation Rho-ROCK joue un rôle central dans la formation et la contraction des fibres de stress, l'adhésion cellulaire, la migration, la phagocytose et l'apoptose. Dans un modèle porcin de glaucome pigmentaire, l’utilisation d’un ROCK-inhibiteur diminuait ainsi la PIO et augmentait la phagocytose [104,105].

Le glaucome pseudoexfoliatif

Le syndrome pseudoexfoliatif correspond à des dépôts de matériel exfoliatif sur certains organes comme le cœur, les vaisseaux, les poumons ou les méninges mais aussi dans le segment antérieur de l'œil. Cette fibrillopathie dégénérative généralisée est multifactorielle. Ses facteurs de risque sont génétiques et environnementaux (âge, exposition aux ultraviolets) [106]. Le glaucome pseudoexfoliatif résulte de l'accumulation de matériel fibrillaire extracellulaire et de pigments dans le maillage trabéculaire et le CS conduisant à une augmentation de la PIO. Des analyses immunohistochimiques et en spectrométrie de masse ont révélé que ce matériel pseudoexfoliatif était un complexe protéique hautement glycosylé extrêmement résistant à la dégradation. Ce complexe protéique regroupe des protéines de la membrane basale, des fibres élastiques, du TGF-β, des métalloprotéinases, des protéines chaperonnes, des protéines du complément, de la lysyl-oxydase de type 1 (LOXL1) et de l'apolipoprotéine E (ApoE) [107].

Le glaucome secondaire aux uvéites

Chez les patients atteints d'uvéites, l'hypertonie constatée peut être due à l'uvéite elle-même ou être un effet secondaire de la corticothérapie locale. En effet, selon les études 45% à 62% des patients atteints d'uvéites sont répondeurs aux corticoïdes [108]. Il a été démontré que des niveaux élevés de protéines trabéculaires réduisaient l'écoulement trabéculaire. Les cellules inflammatoires, les radicaux libres, les enzymes sont également susceptibles de contribuer à l'élévation de la PIO [109]. Les principales étiologies des uvéites hypertensives sont l'hétérochromie de Fuchs, l'herpès, le syndrome de Posner–Schlossman et l'arthrite juvénile idiopathique. Tektas *et al.* ont analysé le trabéculum de patients atteints de glaucome uvéitique recueilli après trabéculectomie [110]. Ils ont constaté qu'il y avait une augmentation de la MEC au niveau de trabéculum cribriforme et un épaississement des lamelles trabéculaires contribuant vraisemblablement aux élévations de la PIO. Chez les patients atteints de cyclite hétérochromique de Fuchs, la plupart des faisceaux trabéculaires étaient épaissis par un matériel fibrillaire déposé entre les cellules trabéculaires et les membranes basales. Sous l'endothélium de la paroi interne, il y avait une augmentation des "plaques" morphologiquement comparables à celles observées chez les patients atteints de GPAO. Le trabéculum de patients atteints d'arthrite juvénile idiopathique montrait également des accumulations de "plaques" sur la paroi interne et un épaississement des faisceaux trabéculaires, mais ce dernier était dû à un épaississement de la membrane basale elle-même avec des inclusions de collagène. Le trabéculum en cas d'herpès montrait des replis de membrane basale entre les lamelles trabéculaires. La région sous-endothéliale révélait aussi une augmentation de plaques et de matériel fibrillaire. Par ailleurs, une fermeture secondaire de l'angle iridocornéen au cours d'une uvéite peut survenir par différents mécanismes: synéchies postérieures avec blocage pupillaire, synéchies antérieures périphériques, rotation vers l'avant du corps ciliaire [111]. Près de 11% des patients développent des synéchies antérieures périphériques (SAP) secondaires à l'inflammation [108]. Les facteurs de risques de développer des SAP sont un angle iridocornéen étroit, l'usage des

mydriatiques et la présence de synéchies postérieures. Le mécanisme sous-jacent serait une accumulation de cellules inflammatoires et de débris au niveau de l'angle iridocornéen entraînant la formation de ponts entre la périphérie de l'iris et la sclère, aboutissant à la constitution de synéchies.

La toxicité trabéculaire des traitements antiglaucomateux

Le glaucome étant une pathologie chronique, il est important de prendre en compte les conséquences de l'exposition aux collyres et à leurs conservateurs qui sont administrés au long cours chez les patients, en particulier, le chlorure de benzalkonium (BAC), qui est le conservateur le plus couramment utilisé dans les collyres antiglaucomateux multidoses, et qui a montré des effets toxiques, pro-oxydants et pro-inflammatoires au niveau de la surface oculaire mais aussi à l'intérieur de l'œil et notamment au niveau du trabéculum [112]. En effet, Brignole-Baudouin *et al.* ont démontré, chez le lapin, grâce à l'imagerie en spectrométrie de masse que le BAC pouvait pénétrer dans le trabéculum après des instillations oculaires répétées [113]. Baudouin *et al.* ont aussi montré que le BAC induisait une apoptose, un stress oxydant et l'expression de la chimiokine fractalkine. En outre, le BAC participe au clivage de SDF1 (CXCL12) en une forme tronquée SDF-1(5-67); SDF1 a des effets protecteurs *via* son récepteur classique de type GPCR, le CXCR4 et sa forme tronquée serait responsable de mort cellulaire par l'intermédiaire d'un autre GPCR, le CXCR3.

Dans la même équipe, un effet pro-apoptotique du BAC avec une inhibition de Bcl2 a été également démontré sur des cellules trabéculaires humaines en culture [114–116].

Le BAC induit aussi un effet pro-inflammatoire avec une augmentation de l'expression des cytokines pro-inflammatoires interleukine-6 (IL-6) et IL-8 (CXCL8) dans un modèle de trabéculum en trois dimensions [117]. Ces travaux suggèrent donc que le BAC aggrave toutes les caractéristiques de la dégénérescence trabéculaire décrites dans le glaucome : apoptose des cellules trabéculaires, stress oxydant et induction de chimiokines inflammatoires.

Le trabéculum comme cible thérapeutique

La seule stratégie thérapeutique démontrée visant à ralentir la progression de la neuropathie glaucomateuse consiste aujourd'hui à réduire la PIO [2,20,118]. Elle s'appuie sur des moyens médicaux, physiques comme les lasers, ou chirurgicaux. Le trabéculum, comme lieu principal de résistance à l'élimination de l'HA, est donc largement impliqué dans les traitements du glaucome.

Stratégie médicamenteuse

Même si la dégénérescence trabéculaire semble être à l'origine de la maladie glaucomateuse, rares sont les traitements qui ont une action directement trabéculaire. Parmi les traitements médicaux du glaucome, les analogues des prostaglandines sont les traitements les plus utilisés, les plus efficaces et les mieux tolérés. Le mécanisme de l'action hypotonisante des prostaglandines est encore aujourd'hui imparfaitement compris. Il serait principalement dû à une augmentation de l'évacuation de l'HA par la voie uvéosclérale. Mais des résultats plus récents suggèreraient une action directe des prostaglandines sur le trabéculum avec un remodelage de la MEC trabéculaire [60,68,119]. Kalouche *et al.* ont ainsi montré que le latanoprost, un analogue de la prostaglandine F2α, diminuait l'accumulation de collagène de la MEC trabéculaire mais favorisait un phénotype contractile de ses cellules. En revanche, le butaprost, un agoniste des récepteurs prostanoïdes EP2 atténuait à la fois la contraction des cellules trabéculaires et le dépôt de collagène, inhibant ainsi la transition myofibroblastique des cellules [120]. Le concept de traitements agissant directement sur le cytosquelette trabéculaire a ainsi vu le jour.

Les inhibiteurs des Rho-kinases (ROCK-i) constituent un exemple particulièrement intéressant puisqu'ils ciblent justement la voie profibrotique en cause dans la modification de la MEC trabéculaire. La voie de signalisation Rho/ROCK joue en effet un rôle important dans la modulation du cytosquelette des cellules et de la synthèse de la MEC [121]. La famille Rho comprend de petites protéines liant la guanosine triphosphate (GTP), qui régulent la forme, la motilité, la prolifération et l'apoptose des cellules dans tout le corps. Comme le montre le schéma de la figure 9, après la fixation du TGF-β2 à son récepteur, Rho-GTP active ses molécules effectrices (Rho-kinase ROCK1 et 2). Les ROCK inhibent ainsi la phosphatase des chaînes légères de la myosine en phosphorylant la sous-unité de liaison à la myosine, induisant ainsi des modifications du cytosquelette d'actine. Les ROCK activent les kinases LIM via la phosphorylation, ce qui stabilise l'actine filamenteuse et réduit la migration cellulaire. L'activation de cette voie entraîne une augmentation de la résistance à l'évacuation d'HA alors que son inhibition diminue la PIO [104,122]. Les ROCK-i représentent une nouvelle stratégie thérapeutique dans le glaucome ciblant la voie de TGF-β en cause dans la modification de la MEC [123]. Un ROCK-i, le Ripasudil a été approuvé par les autorités de santé japonaises pour le traitement du glaucome ou de l'hypertonie oculaire, en seconde intention après les antiglaucomateux de référence. La première étude publiée sur l'efficacité du Ripasudil montrait une efficacité modérée sur la PIO qui passe de 15,1 ± 4,6 mmHg avant traitement à 13,3 ± 3,0 mmHg à 24 mois ($p<0,05$) [124]. Une autre molécule de la même famille, le Nétarsudil 0,02% (Rhopressa®, Aerie Pharmaceuticals, Inc., USA) a reçu l'autorisation de la FDA en décembre 2017 pour la baisse de la PIO chez les patients atteints de GPAO [125] et fin 2019 une AMM européenne. Dans trois essais de phase III de patients avec une PIO élevée, l'efficacité hypotensive oculaire du Nétarsudil 0,02% instillé une fois par jour répondait aux critères de non-infériorité par rapport au timolol 0,5% instillé deux fois par jour, produit de référence accepté par la FDA [126]. On peut toutefois déplorer des effets indésirables fréquents : blépharite, hyperhémie conjonctivale, hémorragies sous-conjonctivales, des opacités cornéennes de type *cornea verticillata*

[124,127,128]. L'association d'un ROCK-i à une prostaglandine a été proposée et semble obtenir des résultats synergiques sur la baisse de la PIO avec des réductions de la PIO de 30% ou plus observées chez 59 à 65% des sujets traités par l'association de nétarsudil et latanoprost, contre 29 à 37% des sujets traités par latanoprost seul et 21 à 29% des sujets traités par nétarsudil seul ($p<0.0001$) [129,130].

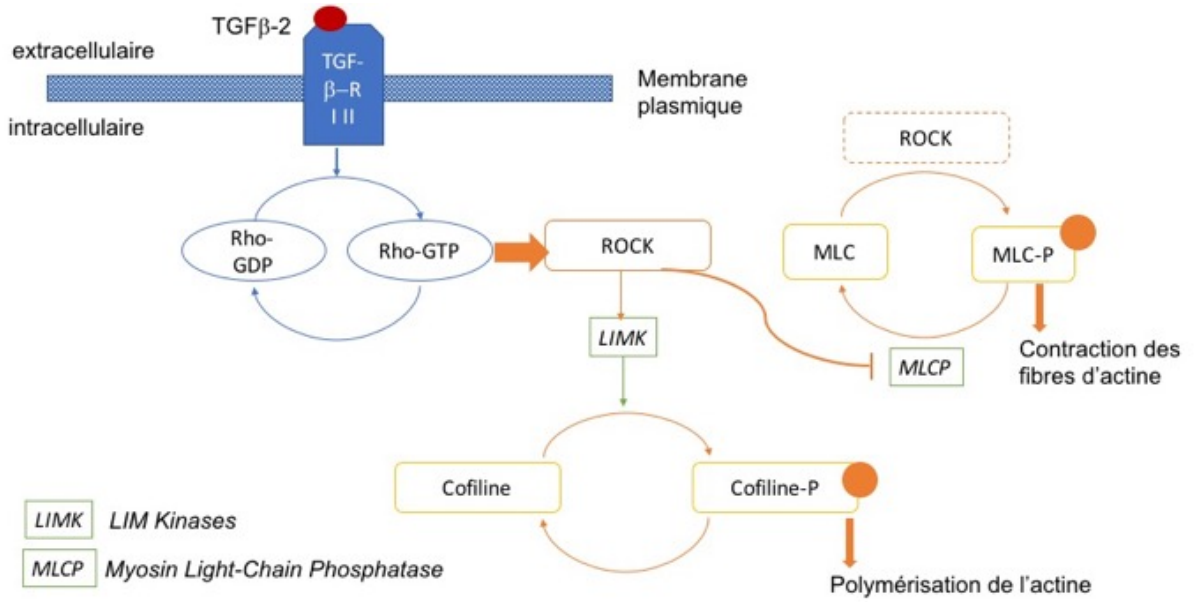

Figure 9 : Voie de signalisation des Rho-kinases.
Le récepteur du TGF β activé (TRF- β RI-II) lie la guanosine triphosphate (GTP) à la protéine Rho. Rho-GTP active ses molécules effectrices, les ROCK (Rho-kinases ROCK1 et 2). Les ROCK inhibent la phosphatase des chaînes légères de la myosine (MLCP). La phosphorylation de la sous-unité de liaison à la myosine, induit la contraction des fibres d'actine. Les ROCK activent aussi les kinases LIM qui phosphorylent la cofiline ce qui stabilise l'actine.

Traitement au Laser

La trabéculoplastie sélective au laser (SLT), décrite par Latina et Park en 1995 [131], est réalisée avec un laser Nd : YAG à impulsions courtes doublé en fréquence (Q-switch). Elle a été qualifiée de « sélective » pour son ciblage des cellules trabéculaires pigmentées tout en laissant le réseau trabéculaire intact. L'augmentation de l'évacuation de l'HA hors de l'œil après une SLT peut être expliquée par plusieurs mécanismes, notamment la rétraction mécanique du maillage trabéculaire uvéoscléral et du CS, les mécanismes cellulaires qui stimulent la division cellulaire, et les mécanismes biochimiques qui altèrent les cytokines et stimulent les propriétés macrophagiques des cellules trabéculaires [132]. Une étude histologique sur des yeux ayant reçu un SLT ne montrait ainsi que des dommages mécaniques minimes [133]. L'effet d'abaissement de la PIO par le SLT pourrait donc s'expliquer avant tout par des changements biochimiques et cellulaires, plutôt que par des effets mécaniques [21].

Traitement chirurgical

Étant donné que l'élévation de la PIO se produit à la suite d'une altération de l'écoulement de l'HA, les traitements chirurgicaux du glaucome visent à améliorer le drainage par les voies d'écoulement physiologiques existantes ou à détourner l'HA vers de nouvelles voies non physiologiques (telles que le drainage sous-conjonctival).

Chirurgies filtrantes

En France, les chirurgies du glaucome les plus pratiquées sont la trabéculectomie [134] et la sclérectomie profonde non perforante (SPNP) [135]. Ce sont deux chirurgies filtrantes dont le principe est d'abaisser la PIO en créant une voie d'évacuation de l'HA à partir de la chambre antérieure de l'œil jusqu'à un espace sous-conjonctival nouvellement formé : la bulle de filtration (BF) en court-circuitant tout ou partie du trabéculum. La trabéculectomie consiste au retrait en bloc de toute l'épaisseur du trabéculum. Elle permet une baisse de la PIO d'environ 46 à 51% à 2 ans selon les études [136–138]. La technique de SPNP a été mise au point pour minimiser les complications de la trabéculectomie. Elle consiste au retrait sélectif de la membrane trabéculaire externe (trabéculum juxtacanalaire et mur interne du CS) au niveau de laquelle se situe la majeure partie de l'élévation de la résistance à l'écoulement de l'HA. Cillino et al. [138] ont comparé la baisse de la PIO après trabéculectomie ou SPNP, et retrouvaient une diminution de 51 % pour la trabéculectomie et de 42,5% pour la SPNP. Les taux de complications telles que l'hypotonie (38,1 % vs 0%) et l'hypothalamie (33,3% vs 5,2%) étaient significativement moindres dans le groupe SPNP.

MIGS trabéculaires

Ces dernières années, les options de prise en charge chirurgicale du glaucome se sont multipliées, en particulier avec l'apparition des MIGS ou chirurgies mini-invasives du glaucome. Avec ces techniques, l'objectif de baisse de la PIO est plus modeste qu'avec une chirurgie filtrante classique mais avec moins de risque de complications et une récupération visuelle plus rapide. Ils sont le plus souvent associés à une chirurgie de la cataracte. Les MIGS utilisent différentes voies afin de favoriser l'écoulement de l'HA : trabéculaire, suprachoroïdienne ou sous-conjonctivale.

Les dispositifs trabéculaires ont pour objectif de rétablir la voie naturelle d'écoulement de l'HA de la chambre antérieure vers le CS. Ces procédures sont basées sur le fait que la portion juxtacanalaire est le site de la plus grande résistance à l'écoulement de l'HA chez la plupart des patients atteints de glaucome à angle ouvert. Les MIGS trabéculaires augmentent l'évacuation trabéculaire par un ou plusieurs des

quatre mécanismes suivants : 1. Bypass du trabéculum et mise en communication directe de la chambre antérieur et du CS par stent ; 2. Maintien de la lumière du CS ; 3. Dilatation des canaux collecteurs ; 4. Ouverture chirurgicale de la paroi interne du canal [139].

L'iStent® et l'iStent Inject (Glaukos Corp., San Clemente, CA) sont des stents trabéculaires qui agissent en shuntant localement le trabéculum pour aboutir dans le CS [140,141]. Une limite de cette approche réside dans le fait que le stent n'est pas nécessairement positionné près d'un des 25 à 30 canaux collecteurs du CS. De plus, certains canaux collecteurs peuvent être plus actifs que d'autres. L'Hydrus Microstent® (Iventis Inc., Irvine, CA) est un stent de 8mm de long qui est implanté dans la portion nasale du CS. Il agit en ouvrant le trabéculum mais aussi en l'étirant. Il maintient aussi la lumière du CS ouverte [142]. L'Excimer Laser Trabeculotomy® (ELT) permet de réaliser des ouvertures dans toute l'épaisseur du trabéculum et du mur interne du CS afin de diminuer la résistance trabéculaire [139]. Le Kahook Dual Blade® (New World Medical Inc, Cucamonga, CA) consiste à inciser le trabéculum et le mur interne du CS pour ouvrir 90° de trabéculum [143]. Le Trabectome® (NeoMedix Corp., Tustin, CA) est une pièce à main qui permet de réaliser une trabéculotomie circonférentielle électrochirurgicale de 60 à 120° du trabéculum et de la paroi interne du CS [139]. La canaloplastie *ab interno* a pour but de dilater le CS en injectant du produit viscoélastique par le biais d'un micro-cathéter introduit *ab interno* par goniotomie. Il crée aussi des microperforation dans le trabéculum qui pourraient augmenter sa perméabilité [144]. La *Gonioscopy-assisted Transluminal Trabeculotomy* (GALT) prévoit d'insérer dans le CS le même cathéter illuminé utilisé pour la canaloplastie *ab interno* mais, une fois complété le tour du CS sur 360°, les deux extrémités du cathéter sont externalisées pour réaliser un trabéculotomie complète *ab interno* [145]. Le succès de ces MIGS trabéculaires peut également être limité par des cicatrices postopératoires sur le site du CS. Enfin, ces procédures réduisent la résistance juxtacanalaire mais ne réduisent pas les sites distaux plus résistants à l'écoulement, comme une pression veineuse épisclérale élevée, qui peut être plus importante chez certains patients. Le résultat postopératoire de la PIO après ces procédures ne diminuera pas en dessous de la pression veineuse épisclérale. C'est la raison pour laquelle l'efficacité des techniques trabéculaires est généralement moindre que les techniques de filtration sous-conjonctivales qui créent une voie non physiologique pour l'écoulement de l'HA [146].

Perspectives

Nouvelles techniques d'exploration

En pratique clinique, l'examen du trabéculum repose sur la gonioscopie. Le trabéculum a un aspect translucide et est souvent d'aspect gris terne ou brun (figure 10a). La partie antérieure du réseau trabéculaire est généralement moins pigmentée et est considérée comme la partie non filtrante du réseau. La partie postérieure est plus importante en taille et recouvre le CS. Le réseau trabéculaire est pigmenté

et peut accumuler des pigments avec l'âge et lors de maladies oculaires spécifiques telles que la dispersion pigmentaire et le syndrome pseudoexfoliatif. Les traumatismes, les uvéites et la chirurgie, y compris les lasers (iridotomie en particulier) sont également des causes de dépôts de pigments dans l'angle. La gonioscopie clinique permet de se rendre compte du degré d'ouverture de l'angle, de la quantité de pigmentation, et des caractéristiques anatomiques telles que les processus iriens. De nouvelles techniques d'exploration clinique du trabéculum se développent pour imager plus précisément cette structure clé. En effet, une meilleure résolution de l'ordre du micron aiderait à comprendre les changements provoqués par le vieillissement sur le trabéculum et permettrait d'évaluer les médicaments antiglaucomateux ciblant le trabéculum afin d'améliorer l'évaluation des résultats et les causes d'échec des chirurgies classiques ou mini-invasives du glaucome (MIGS). La tomographie par cohérence optique (OCT) du segment antérieur fournit certains détails mais ne représente qu'une approche encore grossière du trabéculum et du CS (figure 10b). L'OCT couplé à la gonioscopie offre une résolution supérieure à la goniophotographie et permet aussi une meilleure exploration en profondeur [147,148]. Ainsi King *et al.* ont mis au point un système d'imagerie haute résolution basée sur un système d'optique adaptative à balayage laser ophtalmoscopique (AOSLO), conçu à l'origine pour l'imagerie rétinienne et couplé à une lentille gonioscopique. Celui-ci fournit une imagerie du trabéculum à l'échelle du micron *in vivo* chez l'homme. Les images obtenues montrent les faisceaux et les cellules endothéliales du trabéculum (figure 10c) [149]. Le développement de cette technique pourrait permettre des mesures directes à l'échelle micrométrique *in vivo* des changements qui se produisent dans le maillage trabéculaire humain au cours du glaucome ainsi qu'après intervention thérapeutique.

a.

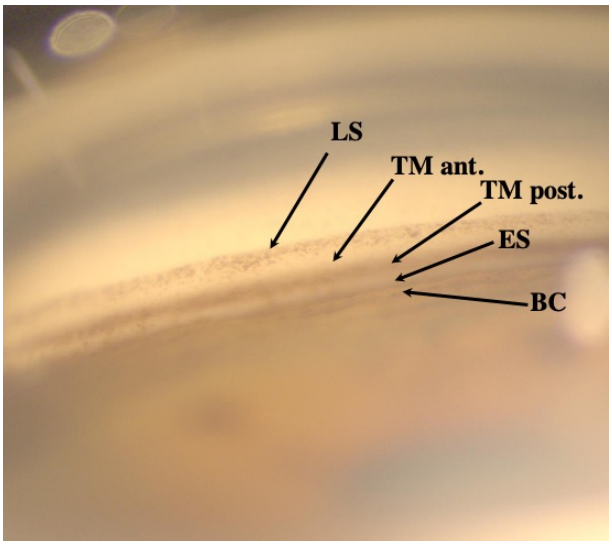

b.

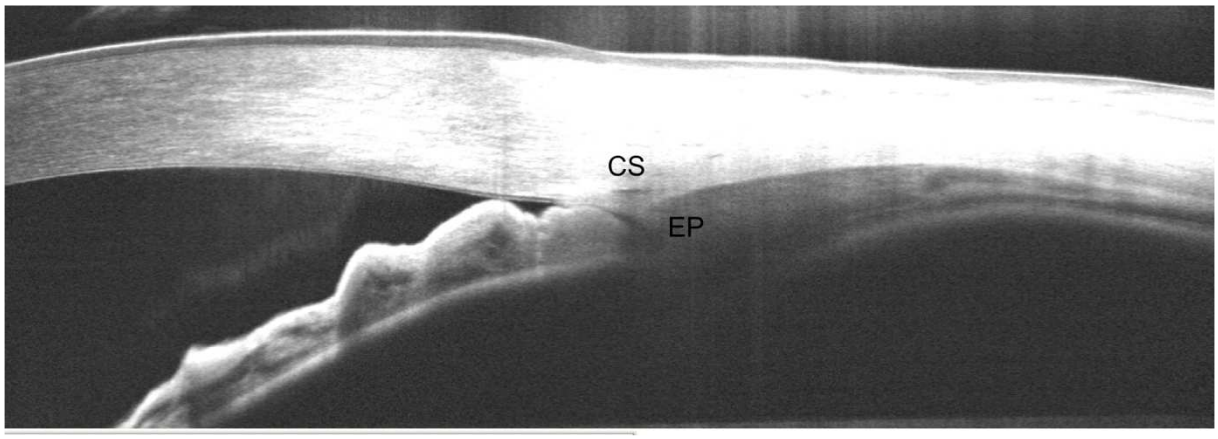

c.

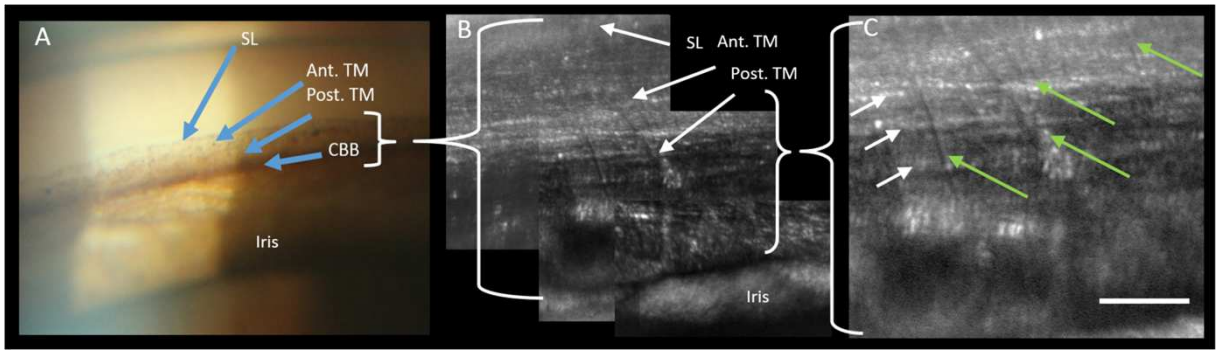

Figure 10 : Imagerie de l'angle iridocornéen
a. Goniophotographie de l'angle iridocornéen. La partie antérieure du réseau trabéculaire (TM ant.) est généralement moins pigmentée, la partie postérieure (TM post.) est plus importante en taille et recouvre le canal de Schlemm. Les structures ne sont visibles que comme des bandes délimitées par la pigmentation et aucune structure anatomique fine n'est évidente. LS : ligne de Schwalbe ; ES : éperon scléral ; BC : bande ciliaire. b. Visualisation de l'angle iridocornéen en OCT swept source de segment antérieur. CS : canal de Schlemm; ES : éperon scléral. c. Gonioscopie clinique et en optique adaptative d'après King et al .[150]. (A) Image au biomicroscope montrant la ligne de Schwalbe (SL), le trabéculum antérieur (Ant. TM) et postérieur (Post. TM), et le corps ciliaire (CBB). (B) Image en optique adaptative de la même région chez le même participant (C) Image acquise de la même région que (B), avec la magnification maximale du système d'imagerie AOG, mise au point sur le trabéculum postérieur. Ici, nous pouvons distinguer à la fois les faisceaux uvéaux (flèches vertes) et les faisceaux cornéoscléraux plus profonds (flèches blanches). Barre d'échelle, 50 µm

Stratégie de protection du trabéculum

Le stress oxydant induit des dommages sur le trabéculum et intervient dans les mécanismes physiopathologiques à l'origine du glaucome [88]. La régulation de la balance redox (oxydation/réduction) constitue donc une piste thérapeutique comme protection du trabéculum et pour prévenir le glaucome [90,150]. Kalouche *et al*. ont montré que l'activation des récepteurs prostanoïdes E de sous-type 2 (EP2) protégeait de l'apoptose induite par le stress du réticulum endoplasmique par le biais d'une régulation négative de p53 [151]. Une autre piste thérapeutique a été suggérée par Denoyer et al. [116] : le blocage de l'interaction entre la forme tronquée de CXCL12/SDF1, SDF1(5-67), sous l'effet de métalloprotéinases, notamment, avec le CXCR3 à l'origine d'une apoptose des cellules trabéculaires. Le traitement par un antagoniste de CXCR3 dans un modèle de rat présentant une

hypertonie oculaire réduisait la PIO. L'inhibition de cette voie pourrait constituer une approche thérapeutique innovante pour restaurer la fonction trabéculaire chez les patients atteints de GPAO.

Thérapie cellulaire

La diminution du nombre de cellules trabéculaires liée à l'âge et à la maladie, l'apoptose et la sénescence accélérées, sont associées à une résistance accrue à l'écoulement de l'HA et donc à une augmentation de la PIO [72]. En effet, les cellules trabéculaires grâce à leurs propriétés de phagocytose ont la capacité d'éliminer les débris obstruant potentiellement le filtre trabéculaire, tandis qu'elles ont un rôle dans la synthèse et la dégradation des éléments constitutifs de la MEC [3]. La réduction de la densité cellulaire trabéculaire affecte donc le renouvellement de la MEC et provoque l'accumulation de débris, d'où une augmentation de la résistance à l'écoulement dans les yeux glaucomateux. Théoriquement, la recolonisation du trabéculum à partir de cellules souches pourrait compenser la perte en cellules des yeux glaucomateux et permettre au trabéculum de retrouver sa fonctionnalité, réduisant ainsi la PIO [61,152,153].

Les thérapies cellulaires à partir de cellules souches pour la régénération du trabéculum fournissent des perspectives prometteuses de traitements. Les cellules souches trabéculaires sont localisées au niveau de la région d'insertion du trabéculum sur l'anneau de Schwalbe [154]. Elles peuvent être isolées par tri cellulaire, culture de clones ou de sphères. Les cellules souches trabéculaires sont multipotentes avec la capacité de coloniser la région trabéculaire et de se différencier en cellules trabéculaires *in vivo*. D'autres types de cellules souches, comme les cellules souches dérivées des adipocytes, les cellules souches mésenchymateuses et les cellules souches pluripotentes induites ont été découverts pour la différenciation et la régénération des cellules trabéculaires [62]. Roubeix *et al.* ont montré que, chez le rat, l'injection en chambre antérieure de cellules souches mésenchymateuses isolées de la moelle osseuse de fémurs, diminuait la PIO dans un modèle d'hypertonie oculaire par cautérisation des veines épisclérales, et démontrait un effet protecteur sur le trabéculum. On observait en effet une augmentation de la survie des cellules trabéculaires avec une activation de la voie anti-apoptotique AKT, une relaxation des cellules trabéculaires ainsi qu'une inhibition du phénotype profibrotique induit par le TGF-β2 [155].

Une autre piste thérapeutique est celle du guidage des cellules souches pluripotentes induites (iPSC). Ding et al. ont ainsi réussi à obtenir des cellules iPSC avec un phénotype proche de celui des cellules trabéculaires humaines après les avoir mises en coculture avec des cellules trabéculaires humaines [156]. La transplantation de ces cellules dans des segments antérieurs humains perfusés ou dans des modèles animaux stimulaient la prolifération des cellules trabéculaires endogènes [157] et restaurait l'évacuation de l'HA et donc abaissait la PIO [158]. Ce type de thérapie à base d'iPSC est une stratégie prometteuse pour réguler la PIO chez des patients atteints de glaucome [159].

Modèles disponibles pour la recherche sur le trabéculum

Le dysfonctionnement du trabéculum est la cause de l'élévation de la PIO et représente le *primum movens* du GPAO mais les mécanismes précis à l'origine ne sont pas encore clairs. Le développement de modèles robustes de trabéculums physiologiques et pathologiques est nécessaire pour étudier les différents mécanismes à l'origine de cette dérégulation mais aussi pour développer et tester des traitements ciblant le trabéculum lui-même qui sont actuellement rares. Plusieurs types de modèles expérimentaux ont été décrits avec leurs avantages et leurs inconvénients, des modèles animaux ou segments antérieurs en culture de perfusion aux modèles de culture cellulaire.

In vivo

Des modèles de glaucome existent chez la souris, le rat, le chien, le chat et les primates [160]. Chacun présente ses propres défis, notamment en termes de disponibilité des ressources génétiques et de difficulté de manipulation génétique, de considérations éthiques, de coût et d'entretien. Le primate est l'animal dont l'anatomie du trabéculum se rapproche le plus de celle de l'humain, mais l'utilisation de primates est limitée en raison de leur prix élevé, de l'inaccessibilité des souches transgéniques et des préoccupations éthiques. La plupart des études précliniques dans le domaine du glaucome utilisent des souris, car leur anatomie des voies d'écoulement est comparable à celle des humains. Elle est décrite comme suit : trabéculum, tissu juxtacanalaire, canal de Schlemm, canaux collecteurs et veines épisclérales. Cependant, la principale différence anatomique est que la structure du trabéculum humain est constituée de 9 à 18 faisceaux trabéculaires, tandis que dans le trabéculum de la souris, il n'y a que 2 à 5 couches de lamelles, ce qui diminue la résistance générée par le trabéculum par rapport à celle de l'humain. Ces différences de structure du trabéculum animal ainsi que de régulation de l'excrétion de l'humeur aqueuse constituent une limitation sérieuse à l'utilisation de modèles animaux. Les résultats obtenus avec des modèles animaux ne sont donc pas toujours transposables à l'homme, bien que la majorité des médicaments hypotenseurs de la PIO dans le glaucome humain soient également efficaces sur les yeux des souris. De plus, le manque de coopération des animaux et donc l'utilisation d'anesthésie pour effectuer les expérimentations affectent les résultats. Les valeurs de la PIO varient en fonction de l'espèce animale, de la méthode de sédation et de mesure. En général, une contention excessive, un positionnement inadéquat ou un manque d'expérience dans l'utilisation de l'équipement peuvent augmenter la PIO. Enfin, ils sont remis en question d'un point de vue éthique.

Pour étudier la physiopathologie du trabéculum ou ses modifications sous l'effet des traitements, tous les modèles qui augmentent artificiellement la PIO en bloquant ou en sclérosant les voies d'écoulement ne sont pas appropriés, par exemple en utilisant la photocoagulation au laser, la cautérisation des veines épisclérales, l'injection de microbilles ou d'acide hyaluronique dans la chambre antérieure ou l'injection de solution saline hypertonique dans les veines épisclérales, car ils ne reproduisent pas le processus

naturel des lésions glaucomateuses de la voie d'écoulement de l'humeur aqueuse [161]. En effet, il convient de distinguer entre les modèles animaux d'hypertonie oculaire utilisés pour étudier la perte des cellules ganglionnaires rétiniennes et ceux spécifiquement développés pour l'étude du trabéculum.

Récemment, une recommandation consensuelle pour les modèles murins d'étude de l'écoulement de l'humeur aqueuse a été publiée en 2022 afin d'établir des pratiques standard dans ce domaine [162]. Les modèles génétiques sont les plus utiles, car ils permettent de provoquer une hypertension oculaire grâce à la transduction du trabéculum avec des gènes liés au glaucome (par exemple, MYOC, TGFβ2, GREM1, CTGF, DKK1, SFRP1, CD44, Cre). Pour répondre aux attentes de cette recommandation consensuelle, les modèles animaux utilisés pour étudier la physiologie de l'écoulement doivent [162] :

- avoir un angle iridocornéen ouvert
- présenter une diminution de la facilité d'écoulement
- présenter une élévation de la PIO
- inclure des descriptions morphologiques des voies d'écoulement conventionnelles (trabéculum, canal de Schlemm, canaux collecteurs et régions intrasclérales et épisclérales), de préférence par microscopie électronique, afin de pouvoir analyser l'organisation de la MEC
- et une évaluation du nombre de cellules du trabéculum.

La souris MyocY437H, responsable d'un glaucome juvénile, est la plus connue et la plus utilisée. Elle présente une élévation de la PIO dès l'âge de 3 mois et une dégénérescence progressive du CGR et du nerf optique [163]. Les souris génétiquement modifiées expriment des niveaux élevés de myociline mutante dans le trabéculum et la sclère, ce qui entraîne une diminution de la facilité d'écoulement de l'humeur aqueuse et une augmentation secondaire de la PIO. Des changements morphologiques peuvent être observés dans le trabéculum : diminution des espaces intertrabéculaires et perte progressive des cellules trabéculaires. Cependant, le niveau de la PIO peut varier en fonction de l'origine génétique de la souche de souris sélectionnée pour induire la mutation MYOCY437H.

La souris DBA/2J est également largement utilisée, elle présente des mutations dans les gènes Tyrp1b et GpnmbR150X responsables d'un glaucome par dispersion de pigment. L'apparition des premières anomalies oculaires a lieu entre trois et quatre mois et l'élévation de la PIO est présente à six mois.

In vitro

Les modèles animaux sont utilisés depuis longtemps malgré leurs nombreuses limites. En effet, l'utilisation d'animaux dans la recherche a des implications éthiques, ainsi que des limites en termes de translation à humain. Ainsi, il y a eu un intérêt croissant pour le développement de modèles alternatifs pour étudier le trabéculum *in vitro*. Ces dernières années, les progrès de la culture cellulaire

tridimensionnelle et de la fabrication par génie tissulaire ont offert des approches prometteuses pour réduire l'expérimentation animale [11]. Nous détaillons les modèles *in vitro* alternatifs aux modèles animaux qui ont été développés pour étudier le trabéculum dans la revue de la littérature intitulée *An Overview of Current Glaucomatous Trabecular Meshwork Models* publiée en 2023 dans la revue internationale *Current Eye Research*.

Article 1 : An Overview of Current Glaucomatous Trabecular Meshwork Models

Taylor & Francis
Taylor & Francis Group

Current Eye Research

ISSN: (Print) (Online) Journal homepage: https://www.tandfonline.com/loi/icey20

An Overview of Current Glaucomatous Trabecular Meshwork Models

Juliette Buffault, Françoise Brignole-Baudouin, Antoine Labbé & Christophe Baudouin

Abstract: The trabecular meshwork (TM) is a complex tissue that regulates aqueous humor outflow from the eye. Dysfunction of the TM is a major contributor to the pathogenesis of open-angle glaucoma, a leading cause of irreversible blindness worldwide. The TM is a porous structure composed of trabecular meshwork cells (TMC) within a multi-layered extracellular matrix (ECM). Although dysregulation of the outflow throughout the TM represents the first step in the disease process, the underlying mechanisms of TM degeneration associate cell loss and accumulation of ECM, but remain incompletely understood, and drugs targeting the TM are limited. Therefore, experimental models of glaucomatous trabeculopathy are necessary for preclinical screening, to advance research on this disease's pathophysiology, and to develop new therapeutic strategies targeting the TM. Traditional animal models have been used extensively, albeit with inherent limitations, including ethical concerns and limited translatability to humans. Consequently, there has been an increasing focus on developing alternative in vitro models to study the TM. Recent advancements in three-dimensional cell culture and tissue engineering are still in their early stages and do not yet fully reflect the complexity of the outflow pathway. However, they have shown promise in reducing reliance on animal experimentation in certain aspects of glaucoma research. *This review provides an overview of the existing alternative models for studying TM and their potential for advancing research on the pathophysiology of open-angle glaucoma and developing new therapeutic strategies.*

Keywords: glaucoma model, trabecular meshwork, 3D culture, in vitro model, tissue engineering, outflow

Introduction

Glaucoma is a blinding optic neuropathy affecting over 70 million people worldwide [164]. Its most important risk factor is elevated intraocular pressure (IOP). The trabecular meshwork (TM) plays a key role in the pathophysiology of glaucoma. This filter is located within the iridocorneal angle and constitutes the main outflow pathway for the aqueous humor. It is a fenestrated triangle-form structure in which trabecular meshwork cells (TMC) populate a multi-layered extracellular matrix. The TM tissue is not a rigid structure, but a highly dynamic, avascular filtration system that has a multitude of roles, including filtering aqueous humor of waste material, sensing and regulating IOP through the mechanical stretch, and altering ECM composition and deposition [12,165,166]. The TM contributes to the regulation of IOP by regulating the outflow of aqueous humor from the eye's anterior chamber, primarily through the juxtacanalicular tissue and the endothelium of Schlemm's canal (SC) [12,167]. The juxtacanalicular tissue, located adjacent to the inner wall of SC, plays a crucial role in the regulation of outflow resistance. It consists of specialized cells and extracellular matrix (ECM) components that modulate the flow of aqueous humor [168]. Dysfunction of the TM and the inner wall of SC is the cause of IOP elevation and represents the *primum movens* of primary open-angle glaucoma (POAG) but the

precise mechanisms at the origin are still unclear. It is known that abnormal TMC function and excess of ECM deposit contribute to TM stiffening in POAG[169]. Alterations in the structure and composition of the TM ECM generate aqueous humor outflow resistance. Cell-ECM interactions within the TM and SC play a role in regulating outflow resistance. Cellular responses to ECM components and their remodeling can influence the contractility and overall functionality of the tissue[168,170,171]. The endothelial cells lining the inner wall of SC exhibit contractile properties. Contraction and relaxation of these cells regulate the diameter of the canal and thereby influence outflow resistance[172,173]. Tight junctions between endothelial cells of SC also contribute to the formation of a barrier that controls the paracellular movement of aqueous humor[174]. A second 'unconventional' outflow pathways exists in the human eye, but it only accounts for less than 10% of the total outflow, and thus does not significantly contribute to the regulation of IOP in the normal eye[175].

The development of robust models of physiologic and pathologic TM is necessary to study the different mechanisms at the origin of this deregulation but also to develop and test treatments targeting TM, which are currently rare. Several experimental models have been described with advantages and disadvantages, from animal models or perfusion-cultured anterior segments to cell culture models.

To study the pathophysiology of the TM or its changes under the effects of treatments, all models that artificially increase the IOP by blocking or sclerosing the outflow pathways, for example using laser photocoagulation, episcleral vein cauterization, injection of microbeads or hyaluronic acid into the anterior chamber or hypertonic saline injection into the episcleral veins are not appropriate as they do not mimic the natural course of glaucomatous dysfunction to the aqueous outflow pathway[161]. Indeed, a distinction must be made between animal models of ocular hypertension made to study RGC loss and those specifically developed for the study of TM.

Models of glaucoma exist in mice, rats, dogs, cats, and primates[160]. Each has its challenges, including the availability of genetic resources and difficulty of genetic manipulation, ethical considerations, cost, and maintenance. Translational research in glaucoma is faced with numerous challenges. One significant factor is the divergence in eye anatomy between animals and humans. Furthermore, the etiology of the disease differs between glaucoma animal models and human patients. Additionally, there are notable disparities in study design and statistical analysis methods employed in preclinical and clinical investigations. Moreover, significant differences exist in terms of dosage, scale, timing of intervention, methodologies, endpoints, age groups studied, and the presence or absence of IOP-lowering treatment, which further complicates the comparison between preclinical and clinical studies in glaucoma[176]. The animal whose TM anatomy is the closest to humans is the primate, but their use is limited because of their expensive price, the inaccessibility of transgenic strains and the rise of ethical concern. Most preclinical studies in the field of glaucoma used mice as their outflow tract anatomy is comparable to

humans. It is described as follows: TM, juxtacanalicular tissue, Schlemm canal, collector channels, and episcleral veins[160]. However, the main anatomical difference is that the human TM structure consists of 9 to 18 trabecular beams whereas in the mouse TM, there are only 2 to 5 layers of lamellae. This difference in the structure of the animal TM as well as the regulation of aqueous humor excretion constitutes a limitation to use of animal models. The results obtained with animal models are therefore not always transposable to humans although the majority of IOP lowering glaucoma medications in human are also effective in mouse eyes[176]. Moreover, the lack of cooperation of animals and the use of anesthesia to perform experimentation affects the results. The IOP values vary by animal breed, method of sedation, and measure. In general, excessive restraint, inadequate positioning, or lack of experience in the use of equipment can increase IOP. Last but not least, they are questioned from an ethical point of view. Recently, a consensus recommendation for mouse models to study the aqueous humor outflow was published in 2022 to set standard practice in this field [162]. The most useful models are genetic models that allow OHT by transduction of the TM with glaucoma-related genes[177] (e.g., *MYOC*[178,179], *TGFβ*[180–182], *GREM1*[183], *CTGF*[184], *DKK1*[185], *SFRP1*[186], *CD44*[187]). To meet the expectations of this consensus recommendation animal models used to study outflow physiology must[162]:

- have an open iridocorneal angle
- present decreased outflow facility
- present elevated IOP
- include morphologic descriptions of the conventional outflow tract (TM, Schlemm's canal, collector channels, and intrascleral and episcleral regions) preferably by electronic microscopy to be able to analyze the organization of the ECM
- and assessment of TMC numbers.

The Myoc^{Y437H} mouse, responsible for a juvenile glaucoma, is the best-known and most used[179]. The genetically modified mice express high levels of mutant myocilin in the TM and sclera resulting in a decline of AH outflow facility and a secondary increase of IOP. Morphological changes can be observed in the TM: decreased intertrabecular spaces and a progressive loss of TMC. However, the level of IOP can vary based on the genetic background of the mouse strain selected for inducing the MYOCY437H mutation[188].

In recent years, progress in three-dimensional cell cultures and tissue engineering fabrication has offered promising approaches to reduce the use of animal models, partly encouraged by the three Rs rule (Reduce the number of animals used; Replace the living animal with alternative experimental techniques; and Refine the techniques to minimize animal suffering) [11,189]. While conventional 2D cell culture models represent an attractive alternative to animal models for analyzing the TM and allow for more accurate assessment at the cellular scale, they are limited by the absence of differentiation, polarization, or relationship with an extracellular matrix, making them insufficient in reflecting the actual porous

architecture of the TM [190,191]. However, this deficient architecture is precisely the cause of its dysfunction [192]. *Ex vivo* models such as organ perfusion chambers, whole tissue explants, and decellularized tissues are commonly used natural sources; however, their limited availability restricts their use in perfusion studies and drug testing[193,194]. This is why a three-dimensional (3D) cellular model of the TM would be an interesting tool to advance research on this pathology by considering the biomechanics, which is a key element in the pathophysiology of glaucoma[166]. 3D cell culture would enable the recreation of the microenvironment encountered *in vivo* and provide cells with an environment allowing them to interact with each other[191]. This, in turn, would lead to a better understanding of the physiological functioning of the TM, its behavior under conditions of stress or toxicity, and the effect of treatments[195]. Additionally, *in vitro* models provide a more precise analysis of cell behavior and molecular mechanisms involved in the pathology than do animal experiments[196]. This approach allows to investigate specific biological phenomena in isolated cells, eliminating potential confounding factors present in whole organisms. However, it is crucial to acknowledge that while in vitro systems provide controlled environments, they cannot fully replicate the complex conditions and interactions that occur within a living organism. Technological advances in TM *in vitro* models can help fill the gap in considering the mechanistic modifications involved in glaucoma, such as changes in porosity resulting from alterations in morphology and the mechanical properties of the interaction between TMC and ECM.

In this literature review, we will provide an overview of existing alternative TM models to animal experimentation. We will detail the different cell types used, culture modes, and means to obtain a pathological model. Finally, we will focus on the potential applications of these different models.

Available cell types

Primary cell cultures:

TM is composed of three regions, from the anterior chamber to the Schlemm canal: the uveal meshwork, the corneoscleral meshwork, and the juxtacanalicular tissue, the location of greatest resistance to AH outflow. TMC have a different organization in these three regions, but it is complex to isolate cells from only one of these three regions. Thus, TMC cultures are generally a mixture of cells from all three regions [190].

Cultures of primary human TMC (HTMC) are sampled from donor eye tissue commonly from a corneal rim discarded from corneal transplant[197]. Whole globe or anterior segment from normal subjects, developing fetuses, or patients with glaucoma can also be purchased.

Cultures of TMC from patients with glaucoma are more difficult due to the accelerated loss of these cells. Nevertheless, they retain their glaucomatous characteristics after culture[198].

TMC change their morphology after 6 to 8 passages, thus it is recommended to use TMC from human eyes before the 7th passages. Methods used to validate that cells are TMC is required for publications including at least responsiveness of myocilin expression by cells to dexamethasone [190].TMC cultures can also come from animal eyes with the limitations that this brings.

Immortalized human TM cells

Immortalized TMC lines can be generated with TMC transfected with an original defective mutant of the SV40 virus[199,200]. However, during the immortalization process, some properties of the TMC can be lost, for example the myocilin expression. It is recommended that cell line findings be replicated with non-immortalized TMC[190].

Induced pluripotent stem cell-derived trabecular meshwork (iPSC-TM)

The reproducibility of primary cell cultures is a challenge and immortalized cell lines are considered poorly relevant to TMC physiology and disease patterns. The experimental transplantation of iPSC-derived TM (iPSC-TM) highlighted the huge therapeutic potential of these new human cell models, offering perspectives for toxicological or therapeutic evaluations[201,202]. Moreover, the pathogenesis of the glaucomatous disease is explained by a TMC loss greater than the physiological age-related cell loss. This loss has been suggested to affect the ability of the human TM to regulate aqueous humor outflow and to lead to IOP elevation. In addition to providing a source of reproducible and valuable cells for the constitution of an *in vitro* model iPSC-TM cells are promising autologous cell sources that can be used to regenerate the declining TMC population and function of IOP regulation[203,204].

TM progenitor cells

A population of progenitor cells has been identified in Schwalbe's Ring, which is located at the junction between the corneal endothelium and the anterior portion of the TM[205]. These progenitors can be isolated and expanded, and studies have shown that they have the ability to differentiate into both keratocytes and TMC. Zhang et al. developed an optimized method to expand multipotent progenitors from human TMC in a two-dimensional (2D) culture followed by three-dimensional (3D) culture in Matrigel using a modified embryonic stem cell medium[206]. The expanded cells expressed TM markers, embryonic stem cell (ESC) markers, and neural crest (NC) markers. Although some markers were lost after passage, the cells regained the markers when seeded on 3D Matrigel via activation of the canonical BMP signaling[206]. These cells can be used in an *in vitro* model system to help better understand how TM is affected in glaucoma and whether TM progenitor cells may have potential therapeutic applications for glaucoma.

Generation of Pathological Models:

As discussed earlier, obtaining cells from the glaucomatous TM is a challenging task for researchers, which is why different molecules are used to induce a diseased phenotype.

Applying mechanical stress to the TM can induce changes similar to those observed in glaucoma. This can be done by stretching or compressing the tissue using a variety of devices. In a previous study, Schlunck et al. demonstrated that the stiffness of the ECM could alter the structure of the cytoskeleton of trabecular cells as well as the profiles of certain protein expressions [170].

Various chemicals can be used to induce glaucomatous changes in the TM, such as transforming growth factor β2 (TGF-β2), and have been shown to contribute to the changes in the ECM of the TM.

TGF-β2 is a profibrotic cytokine known to be elevated in the aqueous humor of patients with glaucoma[207,208]. It has been used in many studies as a model of pathological TM [199,200,209,210,14]. Studies have revealed that TGF-β2 can increase intraocular pressure (IOP) by promoting the synthesis of certain ECM components by trabecular cells (collagens, fibronectin) through epithelial-mesenchymal transition in TMC [211,212]. Furthermore, TGF-β2 can increase cell rigidity by triggering the formation of Cross-linked Actin Networks (CLANs) via the Rho-GTPase pathway[14,213].

Hydrogen peroxide (H2O2), another molecule used to induce a glaucomatous phenotype, is a chemical compound with powerful oxidizing properties and has been shown to promote cellular senescence, rearrange cytoskeletal structure, and increase proinflammatory mediators such as IL-6, IL-8, and endothelial–leukocyte adhesion molecule 1 (ELAM-1) in the TM[214].

Endothelin-1 (ET-1) is another biomarker found in the aqueous humor of patients with POAG[215,216]. It has been shown that ET-1 can induce TMC contraction in culture and that it can affect the outflow facility[217,218]. Wang et al. showed that in a cultured HTMC model, treatment with ET-1 increased the expressions of fibronectin and collagen IV, and that in an ex-vivo model, IOP increased after ET-1 administration[219]. Zhou et al. also used ET-1 in a whole eye perfusion system and found a decreased outflow after ET-1 exposition and successfully tested several pretreatments to reverse this effect[220].

Benzalkonium chloride (BAK) *in vitro* induced apoptosis, oxidative stress, and also an IOP increase, with reduction of aqueous outflow *in vivo*. BAK enhances all characteristics of TM degeneration typical of glaucoma and causes degeneration in acute experimental conditions, potentially mimicking TM degeneration[221]. In an *in vitro* 3D TM model, Bouchemi et al. showed that BAK disorganized the TMC and decreased their number resulting in an enlargement of spaces between cells [222].

Available 3D models:

3D scaffolds culture

The first successful scaffold was a micro-fabricated SU-8 porous structure, where TMC were cultured to study steroid-induced glaucoma. Scaffolds with pores of approximately 20 micrometers in thickness, which were seeded with primary HTM cells, were able to imitate some of the normal tissue functions *in vivo*. This included being able to induce or reverse glaucomatous conditions using medication [223,210,224]. A follow-up study showed that applying a hyaluronic acid-containing hydrogel coating to the SU-8 scaffold improved cell proliferation. Over time, various technologies and materials have been explored, including traditional polymeric filters, SU-8 membranes, electrospun nanofibers, and other methods. These methods offer precise control over morphological characteristics such as porosity and beam thickness in both 2D and 3D environments. However, the stiffness of the scaffold cannot be directly controlled using most of these methods. Despite these limitations, 3D cultures have the potential to create an in vivo-like microenvironment for HTM cell growth. Tissue engineering aims to produce functional biomimetic replicas of tissues of interest, but only a limited number of studies have been reported on bioengineered 3D HTM *in vitro* models. These models partially mimic normal tissue function and provide a platform for drug testing and evaluating the effectiveness of different treatment options. Wlodarczyk-Biegun et al. studied the biofabrication technique of melt electrowriting (MEW), a marriage between electrospinning and 3D printing, as a means of producing fibrillar and porous scaffolds with thermoplastic polymers that replicate the multilayer and gradient structure of the natural HTM [225]. HTMC cultured on these scaffolds maintained the phenotype of native HTMC and infiltrated the scaffolds. However, some may argue that these models are more comparable to a 2D cell culture system rather than a true 3D model, as they cannot fully replicate the 3D cell-ECM interface apart from the ECM secreted by the HTM cells grown on top of the synthetic polymer scaffold.

Hydrogel-based TM scaffolds

Recent research has focused on using hydrogels as scaffolds to study the behavior of HTMC in response to environmental changes and disease conditions[226,227]. Hydrogels are networks of crosslinked, hydrophilic polymers used to recapitulate the 3D architecture of organ systems in tissue engineered models. These materials are so useful in cell culture because they provide a biocompatible, degradable, hydrated microenvironment that mimics the cell–ECM interactions of natural tissues. Hydrogel scaffolds offer higher control over the morphology, stiffness, and 3D environment compared to photolithography and electrospinning, while also maintaining structural integrity.

Ideally, 3D cell culture matrices can reproduce the features of the ECM to closely resemble the *in vivo* environment. The interaction between cells and ECM is essential for a range of biophysical and biochemical functions, such as the transportation of signaling molecules, nutrients, and waste metabolites, as well as mechanical integrity. Thus, these matrices need to reflect the specific ECM characteristics of each tissue for a given application. Moreover, the mechanical properties of 3D matrices

are also significant, as they can directly influence cell adhesion, thereby affecting both the shape and response of cells [228]. The utilization of degradable scaffolds presents an opportunity for more molecular research, as opposed to permanent ones. Hydrogels can be created using various synthetic or natural components. In tissue engineering, natural polymers are the most commonly used approach to developing hydrogels [229]. Collagen, fibrin, and elastin, which are components of the ECM of the TM, have been used as attachment factors for HTMC to study specific functions and interactions [222]. 3D Corning® Matrigel® Matrix (Corning Life Sciences, Tewksbury, MA, United States) contents several proteins found in extracellular matrix (ECM) such as laminin, collagen IV, heparin sulfate proteoglycan, and entactin/nidogen [230,231]. Several studies demonstrated that unlike cells cultured on traditional 2D planar surfaces, cells in 3D scaffolds are more physiologically relevant concerning in vivo characteristics exhibited by in-vivo surrogates[232] (figure 11). Vernazza et al. conducted a study to compare the response of HTMC in 2D and 3D *in vitro* models following chronic stress exposure. Their results revealed that 3D TMC cultured on Matrigel exhibited a higher sensitivity to the production of intracellular reactive oxygen species induced by hydrogen peroxide treatment compared to 2D cultures. Furthermore, the 3D models demonstrated a more precise regulation of apoptosis triggers and cell adaptation mechanisms than the 2D models [191]. Another scaffold-based approach by Osmond and colleagues utilized HTMC cultured on various collagen scaffolds containing different glycosaminoglycans (GAGs) and different pore architectures to better understand how HTMC respond to changes in their extracellular environment. The cellular response was assessed by quantifying cellular proliferation and the expression of fibronectin, an important extracellular matrix (ECM) protein. Fibronectin plays a crucial role in organizing ECM proteins both among themselves and with trabecular cells, thereby contributing to the resistance of outflow [233–235]. The pore architecture of the scaffolds was altered using the freeze-casting technique to make both large and small pores that are aligned or with a non-aligned random structure. The composition of the scaffolds was altered with the addition of chondroitin sulfate and/or hyaluronic acid. It was found that HTMC grown on large pore scaffolds proliferate more than those grown on small pores. There was an increase in the fibronectin expression with the incorporation of GAGs, and its morphology was changed by the underlying pore architecture. These works offer a better understanding of how human TMC behave in response to alterations in their microenvironment and highlight the importance of the mimicry of the 3D structure [236–238]. However, the study did not explore how the constructs would react under conditions that induce glaucoma. Furthermore, if the accumulation of extracellular matrix (ECM) proteins is a characteristic feature of the pathogenic process in glaucoma, it is important to highlight that cell proliferation is not[234,239]. Therefore, it is crucial to determine whether cells can survive under normal conditions on these new substrates. However, it should be noted that the ability to proliferate does not necessarily indicate an appropriate glaucoma model.

3D bioprinting can produce a variety of architectural patterns on a wide array of biomaterials. Li and colleagues developed a hydrogel using a tissue-engineering approach for HTM. The hydrogel consisted of ECM biopolymers and normal HTMC obtained from a donor. By mixing HTMC with collagen type I, hyaluronic acid, and elastin-like polypeptide (ELP) - each containing photoactive functional groups - researchers were able to create HTM hydrogels in various sizes and shapes. Short UV cross-linking, mediated by photo-initiators, was used to solidify the hydrogels. To induce glaucomatous changes, dexamethasone (DEX) was administered, and the therapeutic effects of the ROCK inhibitor Y27632 were evaluated[240].

To create an *in vitro* 3D TM scaffold for potential use as a tissue scaffold in glaucoma patients after trabeculectomy, Waduthanthri et al. developed a hydrogel peptide called MAX8B which partly mimics the motif of cellular integrins and enables interactions with ECM components [241]. The scaffold material demonstrated the ability to undergo shear-thinning and exhibited biocompatibility, facilitating appropriate growth and proliferation of TMC in tightly packed cell monolayers resembling typical TMC morphology. Moreover, the MAX8B scaffold was utilized in an in vitro perfusion system to investigate the impact of Dexamethasone on the outflow facility of the trabecular meshwork proving the effectiveness of this three-dimensional (3D) model as a platform for drug testing[241].

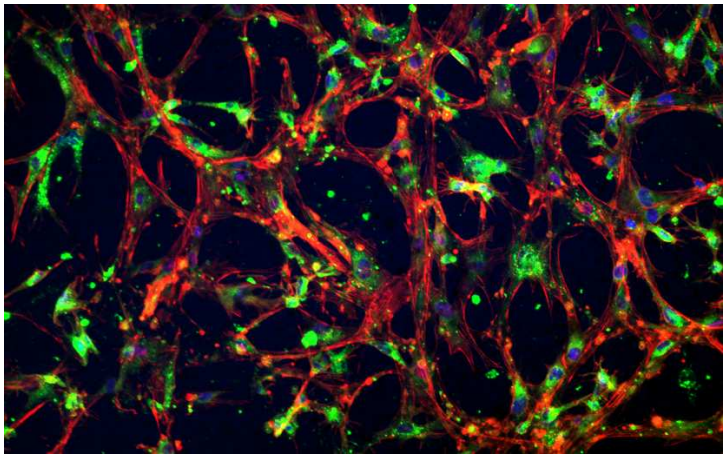

Figure 11 : Confocal microscopy image of the 3D cultured pHTMCs in Matrigel.
The pHTMC organized in a mesh conformation with interconnections and the formation of intercellular spaces. Actin fibers are stained in red by phalloidin, membranes with DiO (green) and nuclei with DAPI (blue). Magnification 200X

Spheroids

Although 3D culture techniques have gained popularity for their ability to better mimic *in vivo* environments, there are some limitations when it comes to replicating physiological and pathological conditions of human TM. This is because the use of scaffolds in 3D cultures is not reflective of the absence of such structures in human TM. However, 3D spheroid cell cultures have recently emerged as a promising alternative to conventional 2D cell cultures, particularly as *in vivo* models for various diseases. These spheroids allow for more intercellular interactions in a 3D space, potentially resulting

in protein networks that resemble those found in real tissues. This makes it possible for 3D spheroids to replicate biological features associated with real tissues.

The spheroid model of TM refers to a 3D culture system that mimics the structural and functional properties of the TM in the eye. HTMC have been cultured as spheroids *in vitro* to study their role in glaucoma. These spheroids have been shown to exhibit features of the TM *in vivo*, such as the presence of ECM components and cytoskeletal proteins. These spheroids have been shown to respond to mechanical stress and exhibit physiological responses similar to those observed *in vivo*. These spheroids have been shown to be structurally and functionally similar to the TM *in vivo* and have been used to study the effects of various drugs on TMC behavior. 3D HTM spheroids became significantly and differently smaller and stiffer in response to TGF-β2 or dexamethasone stimulation[199,242]. Watanabe et al. successfully obtained 3D HTM spheroids and found that TGFβ2 significantly induced the down-sizing and stiffness of 3D spheroids from human orbital fibroblasts, and those effects were substantially inhibited by a ROCK-inhibitor.[200,243]

Outflow studies

Perfusion studies of outflow in HTMC began in the late 1980s and have since evolved to include a range of techniques and models. One of the earliest studies involved the use of filters to culture HTMC and measure hydraulic conductivity using a pressure/flow circuit[244]. This study led to further investigations into the biomechanics of HTMC. The perfusion system developed by Yubing Xie's group enabled continuous pressure monitoring at different flow rates to investigate the effects of drugs such as Lat-B, ROCK inhibitors, or TGFβ2[210,223,224]. As previously mentioned, 3D culture models of TMC are superior to 2D models due to the ability to enable cell-cell and cell-ECM interactions. However, these 3D models fail to reproduce the dynamic continuous supply of nutrients, oxygen, and removal of metabolic waste products. Recent advances propose models that combine the benefits of 3D culture with milli-fluidic techniques to improve the physiological relevance of the culture and address the issues related to cell responses under static culture conditions. Microfluidic systems allow for the creation of a 3D microenvironment that mimics the *in vivo* conditions of the TM, including the presence of shear stress and fluid flow. Recently, the MAX8 peptide-hydrogel scaffold and a 3D Matrigel® model have been tested in perfusion chambers to evaluate their use as artificial TM scaffolds[197,241].

In their closed-circuit *in vitro* model developed by Tirendi et al., 3D-HTMCs cultured in Matrigel were provided with a continuous medium supply. This was achieved by connecting single-flow bioreactor culture chambers to a peristaltic pump. The milli-fluidic technology as well as the 3D culture model mimicked cell responses found *in vivo* as a result of the increase in outflow resistance [214]. This type of model can be used to investigate the effects of various factors on TM function, such as mechanical stress and changes in ECM composition.

Ex vivo models

Ex vivo models, specifically perfusion studies, utilizing animal eyes such as pigs, cows, and primates, have been instrumental in advancing our understanding of glaucoma [245–248]. These models offer valuable insights into the dynamics of aqueous humor outflow and provide a platform to investigate the effects of various experimental interventions on the disease. By perfusing the enucleated eyes with a controlled flow of fluid, researchers can mimic physiological conditions and measure parameters such as intraocular pressure and outflow facility. These models have helped elucidate the mechanisms underlying glaucoma and evaluate potential treatments[220,246]. For example, Zhou et al. developed a platform to simultaneously evaluate outflow facility and its time- and dose-dependent responses to treatments of 20 eyes. They used whole porcine and bovine eyes to develop a perfusion system and studied the regulation of outflow facility by endothelin-1, nitric oxide donor, and sphigosine1-phosphate [220].

However, it is important to acknowledge the limitations of ex vivo models. They do not fully replicate the complex in vivo environment of the eye, including interactions with surrounding tissues and systemic factors. Additionally, the use of animal eyes may introduce species-specific differences that may not fully reflect human physiology. Given these limitations and the fact that they do not represent an alternative to the reliance on animal experimentation, we will primarily focus on human models.

The human anterior segment perfusion culture model is a valuable tool for studying the TM and aqueous humor outflow in glaucoma[246,249,250]. *Ex vivo* models possess several significant benefits compared to other models, including their ability to maintain the structure of pathways and their capacity to facilitate analysis in nearly ideal physiological conditions[251]. Outflow facility measurements can be performed *ex vivo* or *in vivo*, with *ex vivo* measurements offering a simpler approach by avoiding confounding factors that are difficult to control. However, *in vivo* measurements are more representative of real-life conditions.

Bahler et al. used perfusion organ culture of human anterior segments to study the effect of prostaglandin on the trabecular outflow. Since this human anterior segment culture model lacks a choroid or functional ciliary body, the uveoscleral pathway is absent. This simplification facilitates the analysis by directly assessing the sclera's impact on outflow facility[250].

Peng et al. have created an *ex vivo* model of human corneal rim for perfusion culture experiments as an alternative to the human anterior segment perfusion culture model. This model can be used to study the TM and aqueous humor outflow in glaucoma while improving cost and availability. The corneal rims were affixed to 3D-printed perfusion culture plates and perfused in constant flow mode. Pressure changes were recorded using a computerized system. TM stiffness of corneal rims treated with dexamethasone was significantly higher than in the control group[252]. Additionally, the model allows histology or immunohistochemistry of the TM to investigate biomechanical changes or treatments.

Baudouin et al. examined TM specimens using immunohistology and reverse transcriptase–polymerase chain reaction. Trabecular specimens of glaucomatous patients showed extremely low densities of trabecular cells and the presence of cells expressing fractalkine and fractalkine receptor and their respective mRNAs [221]. These explants methods have the advantages to retain tissue architecture and cellular interactions closer to in vivo conditions as opposed to traditional cell culture methods. They are suitable for studying tissue responses and drug effects at the cellular level[16]. The low cell count of TMC in TM explants from glaucomatous patients can be circumvented by using TM from healthy donors and exposing them to TGF-β2. The addition of TGF-β2 to healthy TM permits reproduction of the changes in TM cell cytoskeletal organization and ECM compaction, while providing sufficient material for a transcriptomic study[12,239,253].

Discussion

This article discusses the importance of developing models of TM, a structure within the eye that plays a crucial role in regulating IOP, to study the pathophysiology of glaucoma. The TM is a dynamic filtration system that helps regulate IOP by controlling the outflow of aqueous humor.

Developing new 3D in vitro models is crucial to studying TM pathophysiology in glaucoma. They mimic the physiological microenvironment of the TM, providing a more physiologically relevant model than traditional 2D cell culture methods[254].

One of the key advantages of these 3D models is that they reduce the need for animal studies, which can be costly, time-consuming, and ethically challenging[11,160]. *In vitro* models can be used as a complementary tool to animal studies, as they can provide useful data on mechanisms and drug efficacy before moving to animal models or clinical trials.

While *in vitro* models offer several advantages, they also have limitations that need to be considered. One of the main challenges is that *in vitro* models may not fully recapitulate the complexity of the TM *in vivo*, such as interactions with other tissues and the influence of systemic factors. To address this limitation, researchers often use a multiplicity of models to collect data for a particular question. For example, to study the modification of ECM, a natural hydrogel medium that closely resembles the components of TM ECM is more interesting than a synthetic one. As it provides a more physiologically relevant environment that can better mimic the ECM interactions in the TM. Similarly, a microfluidic bioreactor can be used to study the effect of sheer stress or biomechanical impact on TMC[223,255]. This type of model allows researchers to control the flow of fluids and apply mechanical forces to the cells, providing more accurate simulations of the TM microenvironment. A comparison of innovative 3D TM models and measured outcomes is presented in table 3.

Furthermore, biomimetic 3D in vitro models, in addition to enhancing our understanding of TM tissue biology and outflow pathology, have the potential to be used therapeutically for restoring

compromised TM function[256]. Promising research has demonstrated the effectiveness of stem cell therapy in repairing TM tissue and preserving vision in glaucoma patients [204]. Moreover, the presence of TM progenitor cells capable of differentiating into functional TM cells further supports the potential for tissue repair[257,258]. Advanced biofabrication techniques allow for the creation of scaffolds that closely mimic the native ECM and provide cues for stem or progenitor cell differentiation, replicating cellular responses observed in vivo[259]. By incorporating biomaterials alongside TM progenitor cells, the development of a delivery system for effective stem cell therapy can be facilitated.

In conclusion, the use of multiple models that can better replicate the different aspects of the TM *in vivo* can provide more robust and accurate data. By using a combination of *in vitro*, *ex vivo*, and *in vivo* models, researchers can gain a more comprehensive understanding of glaucoma pathology and develop better treatments for this disease.

However, it is important to consider the limitations of non-animal. The progress made in the alternative models presented in this study does not imply that we can completely eliminate the need for animal experimentation at present. In vivo experiments enable a substantial prediction of the effect of hypotonic treatment on IOP, even if the organization of their outflow system is not totally similar to that of humans[176]. These alternative models are still in their early stages and may not fully replicate the complexity of the TM or its interactions within the eye. They may not provide the same comprehensive data as animal models, particularly in terms of assessing IOP, estimating natural flow rate, accessing the outflow facility, evaluating cellularity, tissue integrity, and capturing natural expression profiles as it would be in a living in vivo system. Additionally, organ culture has a significant limitation whereby the regulation of IOP relies solely on external manipulative regulations, lacking intrinsic regulation in enucleated eyes. Nonetheless, despite these current limitations, the progress made in developing these alternative models is encouraging. While they may not completely replace the need for animal models, they do hold the potential to significantly reduce their utilization, provided of course that the trabecular cells used are not derived from animals.

Overall, this progress in *in vitro* and *ex vivo* models offer a promising tool for studying the TM in glaucoma and reducing the need for animal studies. While it has limitations, it provides a more physiologically relevant model than traditional 2D cell culture methods, and its potential applications in drug discovery and testing make it a valuable addition to glaucoma research.

Tableau 3 : Comparison of innovative 3D TM models and measured outcomes

Article	Model	Cells	Glaucoma induction	Measured outcomes
3D scaffolds culture				
Schlunk[260] (2008)	Collagen-coated tissue culture	HTMC	Increased subtract rigidity (plastic or polyacrylamide gels of different rigidity)	Immunofluorescence microscopy: α-SMA and fibronectin Western blot: focal adhesion kinase (FAK), α-SMA, tubulin, α-B-crystallin, phosphorylation of focal adhesion kinase and serum-induced activation of ERK
Kim [261] (2011)	Poly(etheruret hane)urea (PEUU) microstructure d electrospun micro/nanofib ers	Primary HTMC	Topographic parameters of scaffolds	Quantification of myocilin expression
Torrejon [223,224,262] (2016)	Gelatin-coated SU-8-based scaffolds fabricated using standard photolithograp hic techniques.	primary HTM cells from various healthy donors isolated from discarded donor tissue rings	TGF-β2, 2.5 ng/mL for six days	Optical and Scanning Electron Microscopy Immunocytochemistry: α-SMA, fibronectin Western blot: myocilin, Cytoskeleton analysis (phalloidin + DAPI staining) Perfusion study
Tian [263] (2020)	SU-8 scaffolds (Torrejon)	iPSC-derived TM cells	Dexamethasone 100nM 7 days	Optical and Scanning Electron Microscopy Immunocytochemistry: α-SMA, fibronectin, myocilin, OCT3/4 Western blot: myocilin, OCT3/4, and β-actin Cytoskeleton analysis (phalloidin + DAPI staining) Perfusion study
Włodarczyk-Biegun (2022)[225]	Melt electrowriting thermoplastic polymers printed scaffold	primary HTMC (P10879, Innoprot, Spain)	Scaffold design	Morphological characterization of the scaffolds: stereo microscope and scanning electron microscopy Mechanical properties of the scaffolds: static compression and uniaxial tensile tests Immunocytochemistry: α-B-crystallin, Phalloidin

Hydrogel-based TM scaffolds				
Bouchemi [222] (2017)	Matrigel® Matrix (Corning Life Sciences, Tewksbury, MA, United States)	HTM3 cells (immortalized)	DEX (10^{-6} M) TGF-β2 (5 ng/ml) BAK (10^{-4} %) 48 h	Confocal microscopy cytoskeleton analysis (phalloidin +DAPI staining) RT-qPCR: IL6, IL8, MMP9
Waduthanthri [241] (2019)	MAX8B (Shear thinning peptide hydrogel) 3D model fluid flow system	Primary HTMC	DEX	Cytoskeletal and ECM protein expression, cell viability, biomaterial stiffness and permeability rheology analysis
Vernazza[191,264,265] Tirendi [214] Saccà [255] (2019-2020)	Combination of 3D Matrigel® Matrix and a millifluidic bioreactor system	HTMC (Cell Applications Inc., San Diego, CA, United States)	hydrogen peroxide (H_2O_2) 500 μM 2 hours/ day up to 72 hours pressure fluctuations from base-line pressure	Confocal analysis To-Pro™-3 Iodide 642/64 + phalloidin staining. Outflow resistance measurement RT-qPCR assays: MMPs profibrotic markers, NF-kB, IL1-α,-β, IL6, TN α, TGF-β2 Apoptosis protein array Western blot: PARP1, phospho-NF-κB p65 and Ser 536 DCF assays: reactive oxygen species (ROS) production
Li [240] 2021	hydrogels (collagen type I, elastin-like polypeptide and hyaluronic acid) followed by UV crosslinking	Normal Donor HTMC and glaucomatous HTMC	DEX 100 nM 5 days TGF-β2 2.5 ng/ml 5 days Glaucomatous cells	RT-qPCR: myocilin Immunocytochemistry: myocilin, α-B-crystallin, α-SMA, fibronectin, collagen 4 Cell morphology and cytoskeleton analysis (phalloidin + DAPI staining) rheology analysis and hydrogel contractility
Buffault[14] (2022)	Matrigel® Matrix	Primary HTMC from various healthy donors isolated from discarded donor tissue rings	TGF-β2 5ng/ml 48 hours	Optical and confocal microscopy Immunocytochemistry: α-SMA, fibronectin Western blot: myocilin, fibronectin Cell morphology and cytoskeleton analysis (phalloidin + DiO + DAPI staining)

Osmond (2017, 2020) Adikhari (2022) [236–238]	Highly porous matrix of collagen-chondroitin sulfate scaffold	Porcine TMC Human TMC	DEX exogeneous glycosaminoglycans (GAGs)	Scaffold characterization: scanning electron microscopy, dynamic mechanical analysis, and chondroitin sulfate quantification assay RT-qPCR: fibronectin, elastin, laminin, and MMP-2 Immunocytochemistry: fibronectin, elastin, laminin, and MMP-2
Spheroid				
Watanabe, Ota [199,200,242] (2020-2022)	2D ou Spheroid 3D	immortalized HTM cells	TGF-β2 5ng/ml 6 days DEX 250 nM 6 days	Transendothelial electrical resistance (2D) measurements, FITC dextran permeability (2D), Scanning electron microscopy RT-qPCR and Immunocytochemistry: collagen 1, 4 and 6, fibronectin, α-SMA, TIMP1–4, and MMP2, 9 and 14 (2D and 3D) Solidity and size of 3D spheroids measured using a micro-squeezer

Conclusion

Le trabéculum est une structure complexe au centre de la physiopathologie du glaucome. Une connaissance plus approfondie des mécanismes à l'origine de sa dégénérescence et une meilleure visualisation de ses modifications architecturales pourraient modifier la prise en charge médicale mais aussi chirurgicale du glaucome.

Les travaux de recherche et les publications

Développement du modèle expérimental de trabéculum glaucomateux induit par le TGF-β2 et évaluation de l'effet des analogues de prostaglandines et des inhibiteurs des Rho-kinases

Contexte et objectif

L'introduction de cette thèse nous a permis d'appréhender la complexité du trabéculum et sa fonction essentielle au cœur de la pathologie glaucomateuse. Malgré les efforts constants déployés dans la recherche pour élaborer de nouveaux modèles permettant l'étude approfondie de cette structure, il est indéniable que, jusqu'à présent, aucun modèle n'est encore idéal. À l'heure actuelle, pour étudier le trabéculum, la plupart des études sont menées sur des modèles animaux et de cultures cellulaires *in vitro* en deux dimensions (2D). Les modèles de culture cellulaire en 2D représentent une alternative intéressante aux modèles animaux pour l'analyse du trabéculum car ils permettent des investigations précises au niveau cellulaires. Mais ils ne reflètent malheureusement pas l'architecture réelle du trabéculum. Il semblerait cependant que cette architecture déficiente soit justement à l'origine de son dysfonctionnement. C'est pourquoi un modèle cellulaire de trabéculum en trois dimensions (3D) est un outil novateur particulièrement intéressant pour poursuivre la recherche sur cette pathologie en prenant en compte l'architecture de ce tissu qui est un élément clé dans la physiopathologie du glaucome [254,266]. Comme nous l'avons rapporté dans la revue de la littérature présentée en introduction, quelques modèles tridimensionnels ont été expérimentés. La culture de cellules trabéculaires humaines dans une matrice de Matrigel® (Corning Life Sciences, Tewksbury, MA USA) dont la composition est proche de la MEC humaine permet d'obtenir une organisation spontanée des cellules trabéculaires humaines (HTMC) en un réseau à mailles semblable à celui du trabéculum humain. Dans notre laboratoire, Bouchemi et al. ont publié un article sur l'effet du chlorure de benzalkonium dans un modèle 3D de trabéculum obtenu en cultivant des HTMC dans le Matrigel [117]. Vernazza et al. ont montré que ce modèle 3D mimait mieux la réponse cellulaire au stress oxydant que le modèle en 2D [254]. Pour modéliser le glaucome primitif à angle ouvert (GPAO), nous avons préféré utiliser le TGF-β2 car cette cytokine profibrotique est connue pour être augmentée dans l'humeur aqueuse des sujets atteints de glaucome. Tripathi *et al.* ont ainsi pu montrer que le TGF-β2 augmentait la PIO en induisant la synthèse par les cellules trabéculaires de certains composants de la MEC non dégradables par les métalloprotéinases [79,80]. Le TGF-β2 augmenterait aussi la rigidité cellulaire par la formation de

Cross-linked Actin Networks (CLANs) via la voie Rho-GTPase [267]. Ces réarrangements du cytosquelette modifient la forme de la cellule et donc la structure fenêtrée du trabéculum.

Bien que la dysfonction trabéculaire soit le *primum movens* de la pathologie glaucomateuse, elle est encore rarement la cible des traitements. Les analogues des prostaglandines sont la classe thérapeutique la plus couramment utilisée et la plus efficace pour traiter le glaucome. Ils augmentent l'évacuation de l'humeur aqueuse principalement par la voie uvéosclérale. Cependant, des recherches récentes suggèrent également une influence directe des prostaglandines sur le trabéculum en remodelant la MEC [250,268]. Récemment, le concept de médicaments agissant directement sur le cytosquelette trabéculaire a conduit au développement de ROCK-i, qui ciblent précisément une voie impliquée dans les modifications observées au niveau du trabéculum. La voie de signalisation Rho/ROCK joue en effet un rôle important dans la modulation du cytosquelette des cellules et de la synthèse de la MEC [269]. L'activation de cette voie entraîne une augmentation de la résistance à l'évacuation d'HA alors que son inhibition diminue la PIO (cf. le trabéculum comme cible thérapeutique)[267].

L'objectif de cette première partie consistait à développer des modèles 2D et 3D de trabéculum pathologique *in vitro* induit par le TGF-β2 à partir de cultures primaires de cellules trabéculaires humaines (HTMC) puis de comparer sur ceux-ci les effets sur le cytosquelette et sur la MEC du latanoprost, le composé principal de la famille des analogues des prostaglandines, et du ROCK-i Y-27632, qui inhibe à la fois ROCK1 et ROCK2 par compétition avec l'ATP dans leur domaine kinase.

L'essentiel des développements réalisés et des résultats obtenus sont rapportés dans l'article suivant, publié dans le *Journal of Clinical Medicine* en 2021.

Article 2 : The Dual Effect of Rho-Kinase Inhibition on Trabecular Meshwork Cells Cytoskeleton and Extracellular Matrix in an In Vitro Model of Glaucoma

Journal of
Clinical Medicine

MDPI

Article

The Dual Effect of Rho-Kinase Inhibition on Trabecular Meshwork Cells Cytoskeleton and Extracellular Matrix in an In Vitro Model of Glaucoma

Juliette Buffault [1,2,3,*], Françoise Brignole-Baudouin [2,4], Élodie Reboussin [2], Karima Kessal [2], Antoine Labbé [1,2,3], Stéphane Mélik Parsadaniantz [2] and Christophe Baudouin [1,2,3]

Abstract: The trabecular meshwork (TM) is the main site of drainage of the aqueous humor, and its dysfunction leads to intraocular pressure elevation, which is one of the main risk factors of glaucoma. We aimed to compare the effects on cytoskeleton organization and extracellular matrix (ECM) of latanoprost (LT) and a Rho-kinase inhibitor (ROCK-i) on a transforming growth factor beta2 (TGF-β2)-induced glaucoma-like model developed from primary culture of human TM cells (pHTMC). The TGF-β2 stimulated pHTMC were grown and incubated with LT or a ROCK-i (Y-27632) for 24 hours. The expression of alpha-smooth muscle actin (αSMA) and fibronectin (FN), and phosphorylation of the myosin light chain (MLC-P) and Cofilin (Cofilin-P), were evaluated using immunofluorescence and western blot. The architectural modifications were studied in a Matrigel™ 3D culture. TGF-β2 increased the expression of αSMA and FN in pHTMC and modified the cytoskeleton, with cross-linked actin network formation. LT did not alter the expression of αSMA but decreased FN deposition. The ROCK-i, decreased TGF-β2-induced αSMA and FN expression, as well as MLC-P and Cofilin-P, and stimulated the cells to recover a basal cytoskeletal arrangement. In the preliminary 3D study, pHTMC organized in a mesh conformation showed the widening of the TM under the effect of Y-27632. By simultaneously modifying the organization of the cytoskeleton and the ECM, with fibronectin deposition and overexpression, TGF-β2 reproduced the trabecular degeneration described in glaucoma. The ROCK-i was able to reverse the TGF-β2-induced cytoskeletal and ECM rearrangements. LT loosened the extracellular matrix but had no action on the stress fibers.

Keywords: glaucoma; trabecular meshwork; Matrigel; 3D culture; intraocular pressure; outflow; cytoskeleton; Rho-kinase inhibitor; prostaglandin analog

1. Introduction

Primary open-angle glaucoma (POAG) is a leading cause of irreversible blindness. This optic neuropathy affects more than 50 million people worldwide in 2020 [270]. Its main risk factor is elevated intraocular pressure (IOP) [2]. The trabecular meshwork (TM), in the iridocorneal angle, is the main site of drainage of the aqueous humor, and its dysfunction results in IOP elevation. The TM is a complex, three-dimensional structure composed of multiple layers of extracellular matrix (ECM) covered with trabecular meshwork cells (TMC) [3].

In POAG, anormal resistance is generated in the outflow pathway including the juxtacanalicular TM, the inner wall of Schlemm's canal, and its basement membrane [4]. In the TM increase in resistance is linked to a mixed mechanism, including loss of TMC and changes in their architecture and remodeling of the ECM [4–6,72]. Changes in the morphology and stiffness of juxtacanalicular TM cells have been described. [6]. TGF-β2 is a profibrotic cytokine known to be involved in glaucoma pathophysiology. It is significantly elevated in the aqueous humor of patients with POAG [271]. TM exposure to TGFβ 2 has been used to induce ocular hypertension in animal models and cultured human anterior segments perfusion studies [209,272] . *In vitro* studies have shown that TGF-β induced the synthesis by TM cells of components of the ECM not degradable by metalloproteinases which could lead to increased outflow resistance [273]. TGF-β2 also increases cell stiffness by the formation of cross-linked actin networks (CLANs) *via* the Rho-ROCK pathway [122].

However, this *primum movens* of the glaucomatous pathology is still rarely targeted by glaucoma treatments. The only demonstrated therapeutic strategy to stop the progression of the visual field deterioration in glaucoma is to reduce IOP [2,20]. Among the medical treatments, prostaglandin analogs (PGA) are the most effective. PGAs increase the aqueous humor outflow. The mechanism of the hypotonic action of PGA is still imperfectly understood. It is mainly due to a promotion of the aqueous humor outflow through the uveoscleral route. However, an action of PGA on the TM, acting by remodeling the ECM was described [68,119]. In recent years, studies in the field aimed to develop medication that act directly on the trabecular cytoskeleton. ROCK-i represent a new therapeutic strategy in glaucoma which precisely target a major pathway involved in the modifications observed in the TM [274].

The Rho GTPase / Rho kinase (ROCK) signaling pathway plays a important role in the modulation of the cytoskeleton of cells and the synthesis of ECM [121,274]. Rho GTPase activates its effector molecules, Rho-kinase ROCK1 and ROCK2. ROCK1 and 2 inhibit the myosin light chain phosphatase complex of Type 1 (MYPT1), thereby modifying the actin cytoskeleton. ROCK1 and 2 also activate LIM kinases (LIMKs) leading to the inhibition of Cofilin. This results in actin polymerization [275,276] (Figure 12). Activation of this pathway increases resistance to outflow, while its inhibition reduces IOP [104,122]. ROCK-i were recently approved for clinical use [127,277–281].

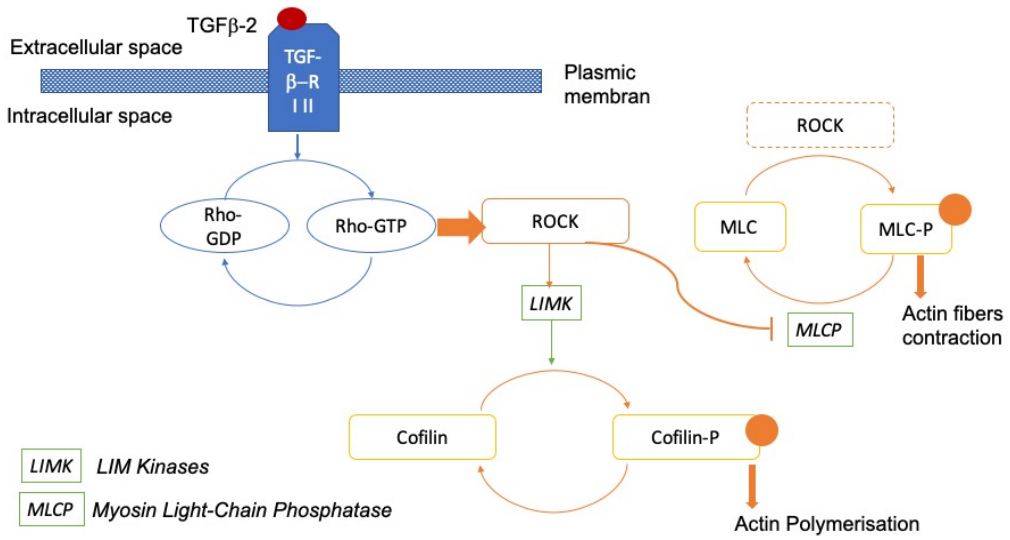

Figure 12 :Rho-kinase signaling pathway.
The TGF-β receptor (TRF-β RI-II) activates its effector molecules, ROCK (Rho-kinases ROCK1 and 2). ROCK inhibits myosin light chain phosphatase (MLCP). Phosphorylation of the myosin light chain induces actin fibers' contraction. ROCK activates LIM kinases, which phosphorylate cofilin, leading to actin stabilization [282]

We aimed to study the effect of a ROCK-i on two major targets in glaucoma pathophysiology: the organization of both the trabecular ECM and TM cytoskeleton. We used a pathological TM model induced by TGF-β2 on 2D and 3D primary cultures of human TMC (pHTMC). Indeed 2D cell culture models may not fully reflect the actual architecture of the TM. Cell culture in 3D could allow to better mimic the microenvironmental conditions encountered *in vivo*. We compared the effects of ROCK-i Y-27632 on the cytoskeleton of pHTMC and the TM ECM, with LT, the lead compound of the PGA family.

2. Materials and Methods

2.1. Primary Human Trabecular Meshwork Cell Isolation and Culture

Primary human TMC (pHTMC) were isolated from non-glaucomatous donor tissue rings. All donor tissues were obtained and managed following the guidelines of the Declaration of Helsinki for research involving human tissue. The human tissues used in our study came from corneoscleral rings discarded after the corneal graft. Human tissues were provided by the French eye bank which ensured complete anonymization. The TM was carefully dissected under a microscope from a corneoscleral ring and transported in an Optisol-GS conservation medium (Bausch and Lomb Surgical, Inc.; Irvine, CA, USA) at room temperature (RT). The TM samples were digested with collagenase (Gibco^{TM} Collagenase, Type IV, Fisher Scientific, Cat. # 17-104-019) diluted to 10 mg/ml in culture medium for TMC (Trabecular Meshwork Cell Medium (TMCM), ScienCell Cat. # 6591, composition: basic medium, 2% fetal calf serum (FBS), 1% trabecular cell growth supplement, and 1% penicillin and streptomycin solution (penicillin 10,000 U/ml, streptomycin 10,000 µg/ml) for 30 minutes at 37°C and then stirred at RT for 30 minutes. After digestion, the cells were centrifuged at 1500 G for 5 minutes before being suspended in 250 µl of TMCM and seeded into a 24-well plate. Cells were seeded at 100.000 cells/ml (25.000 cells

per well). The cultured cells were incubated at 37°C in a humid atmosphere with 5% carbon dioxide. At 48 hours, we added 250 µl of TMCM. Fresh culture medium was supplied every 3 to 4 days. Cells were maintained at 37°C in a humidified atmosphere until 80–90% confluence was achieved, at which point cells were trypsinized using 0.05% Trypsin/0.5mM EDTA (Gibco^{TM}, Cat . #25300062, Grand Island, NY) and subcultured at 1.8×10^5 cells/ml in 25 cm^2 or 75 cm^2 cell culture flasks with TMCM. At each passage (P), a part of the pHTMC was seeded in 48-well plates for immunofluorescence analysis. Before use in experiments, all pHTMC strains were characterized by immunohistochemistry. All studies were conducted using cells before the 7th passage, and at least three different donors' human primary cell cultures were used for each experiment. Information about pHTMC lines is available in supplementary data (Table 6).

2.2. Trabecular Meshwork Cell Characterization

Before use in experiments, all pHTMC strains were characterized by immunohistochemistry for expression of α-smooth muscle actin (alpha-SMA), aquaporin 1 (AQP1), chitinase-3-like 1 (CHI3L1), and CD44. Characterization was performed between the 1st and 4th passages. The induction of alpha-SMA in response to dexamethasone (DXM) at 100 nM for 7 days was also used. It represents a reliable marker for characterizing trabecular cells. The pHTMC were fixed with 4% paraformaldehyde for 15 min. Then, a saturation/permeation solution containing 0.1% Triton X-100 and 5% NGS in PBS was employed for 1 hour at RT before incubation with specific primary antibodies overnight at 4°C. Primary antibodies and dilutions used are listed in Table 4. After washing with PBS, the cells were incubated with the corresponding secondary antibodies (Thermo Fisher, donkey anti-mouse conjugated with Alexa fluor 594 (A21203), and donkey anti-rabbit conjugated to Alexa fluor 488 (A21206)), at a dilution of 1/1000 for 1 hour at RT. The nuclei were stained with DAPI (1/1000 dilution).

Tableau 4 : Primary antibodies used in immunofluorescence for the characterization of cells

Antibody	Dilution	Host	Supplier	Reference
Alpha-SMA	1/100	Rabbit polyclonal	Abcam	ab 5694
CD44	1/125	Rabbit monoclonal	Abcam	ab 189524
Aquaporin 1 (AQP1)	1/100	Mouse monoclonal	Santa Cruz	sc 25287
Chitinase-3like 1 (CHI3L1)	1/125	Rabbit polyclonal	Thermo Fisher	PAS-43746

Western immunoblot analysis of the myocilin induction in response to DXM was also used to characterize the pHTMC in accordance with the consensus recommendations [190]. The analysis of myocilin induction by DXM compared two conditions: 1 / TMCM + 2.10^{-3}% ethanol (control) for 6 days and 2 / TMCM + 100 nM DXM (Sigma D8893, stock solution 20µg/ml) dissolved in ethanol for 6 days. Mouse anti-myocilin (Santa Cruz sc-137233, dilution 1/100), anti-β-actin (Cell signaling 3700, 1/5000) primary antibodies, and HRP-linked anti-mouse secondary antibody (Invitrogen) were used. Protein expression was analyzed using Quantity One software and normalized with β – actin protein.

2.3. Exposure to TGF-β2 and therapeutic molecules

pHTMC were seeded at 100.000 cells/ml in 48-well plates (100µl/well;10.000 cells/well); At subconfluence, TGF-β2 (5ng/ml) was introduced in the TMCM and let incubated for 24 hours [117]. Then, the pHTMC were incubated for 24h with TGF-β2 (5ng/ml) combined either with the ROCK-i Y -27632 (Santa Cruz Biotechnology) at 25nM [283,284] or with Monoprost® (LT) at 1/100 (i.e. 1.15µM) (latanoprost 50µg/ml, Laboratoires Théa, France). We used Y-27632 (25 nM), a ROCK-i, which acts upstream of the phosphorylation of MYPT1 and Cofilin. The controls were vehicle (TMCM only) or TGF-β2 (5ng/ml) for 48h.

2.4. Immunocytochemistry

The effects on the organization of the cytoskeleton and of the ECM were characterized in immunocytochemistry using the anti-alpha-SMA and the anti-fibronectin (FN) antibodies, respectively. Involvement of the Rho-kinase pathway was studied using the anti-Phospho-Myosin Light Chain 2 (Ser19) (MLC-P) and anti-Phospho-Cofilin (Ser3) (Cofilin-P). The pHTMC were fixed with 4% paraformaldehyde for 15 min. Primary antibodies and dilution used are listed in Table 5. After washing with PBS, the cells were incubated with the corresponding secondary antibodies (donkey anti-rabbit, conjugated to Alexa fluor 488 (Thermo Fisher, A21206)), at a dilution of 1/1000 for 1h at RT. The nuclei were stained with DAPI (1/1000). Phalloidin (Alexa 546 (A22283) 1/200) was used to label actin filaments in the cytoplasm.

Tableau 5 : Primary antibodies used in immunofluorescence staining

Antibody	Dilution	Host	Supplier	Reference
Alpha-SMA	1/100	Rabbit	Abcam	ab5694
Fibronectin	1/100	Rabbit	Abcam	ab2413
Phospho-Myosin Light Chain 2 (Ser19)	1/100	Rabbit	Cell signaling	3671S
Phospho-Cofilin (Ser3)	1/100	Rabbit	Cell signaling	3313S

The immunofluorescence images were taken using a Nikon ECLIPSE Ti fluorescence inverted microscope; the images were acquired with 100X and 200X magnifications and then processed using ImageJ software (NIH, Bethesda, MD, USA).

The quantification was carried out using the Cellomics ArrayScanVTI (Thermo Fisher Scientific, France), an imaging system that detects, analyzes, and quantifies immunofluorescence staining on adherent cells. In each well, a central zone of 16mm^2 was analyzed. Using the HCS Studio Cellomics Scan software (Thermo Scientific, version 6.6.0), we measured the total area of positive labeling, which we related to the number of nuclei. An annular analysis pattern around each nucleus was drawn. The positive labeling area was measured in each of these rings. This area was then related to the number of nuclei

2.5. Protein Extraction and Western Blot Analysis

The protein levels of fibronectin (FN) were quantified by western blotting. Cellular proteins were extracted with ice-cold radioimmunoprecipitation assay (RIPA) buffer (RIPA Buffer, Sigma-Aldrich R0278) containing protease inhibitors (Complete Protease Inhibitor, Roche, Manheim, Germany) on ice. Proteins were quantified using a bicinchoninic acid assay (Thermo Fischer Scientific). Proteins from each sample (1 µg) were separated by electrophoresis on a NuPAGE™ 3-8% Tris-Acetate Protein Gel (Invitrogen EA03752PK2) in SDS running buffer (Invitrogen). The proteins were then transferred onto a polyvinylidene fluoride (PVDF) membrane and probed with the following primary antibodies: rabbit anti-fibronectin (Abcam ab2413, 1/500) and anti-β-actin (Cell signaling 3700, 1/1000). HRP-linked anti-rabbit secondary antibodies (Invitrogen) were used. Bound antibody was detected using Pierce™ ECL Plus Western Blotting Substrate (Thermo Scientific). Protein expression was analyzed by densitometry using ImageJ and normalized to the housekeeping proteins β–actin.

2.6. 3-Dimensional (3D) Trabecular Meshwork Cell Culture

For the 3D pHTMC culture, we used Matrigel® (Corning Inc, Tewksbury, MA), a basement membrane matrix secreted by Engelbreth-Holm-Swarm (EHS) mouse sarcoma cells [285]. Its composition is close to that of trabecular ECM, as it contains laminin-11, collagen IV, heparin sulfate proteoglycans, entactin/nidogen, and growth factors (FGF, EGF, TGF beta, IGF, and PDGF) [286]. The pHTMC stained with DiO (Vybrant™ DiO Cell-Labeling Solution, Invitrogen, V-22886) were gently mixed at a concentration of 10^5 cells/ml in Matrigel® diluted 1/2 in the TMCM culture medium and then sewn onto inserts in a 12-well plate (Greiner Bio-One ThinCert cell culture insert for 12 well plates, sterile, polyethylene terephthalate (PET) transparent membrane, pore diameter: 0.4 µm. Cat. N° 665641). The cells were incubated at 37°C for 30 minutes, then 800 µl of TMCM medium were added to the bottom of the well, and 200 µl in the inserts. The cells were then let incubate at 37°C in a humid atmosphere with 5% CO2. Fresh culture medium was supplied every 3 to 4 days. The cells were exposed to TGF-β2 (5ng/ml) for 48h and LT and Y-27632 for 24h, according to the same protocol as for the two-dimensional model. At 7 days, the 3D cultures obtained were fixed with 4% paraformaldehyde for one hour. Actin was stained with phalloidin (1/100), and the nuclei were stained with DAPI (1/1000) before analysis in confocal microscopy. Confocal laser scanning microscopy was performed using an Olympus IX81 confocal microscope coupled to Fluoview software (Olympus, Ver 4.2), and the images were acquired at 200X magnification. Confocal 3D images were processed using Imaris3D® software (Bitplane AG, Zurich, Switzerland). All confocal images from the same experiment were captured using the same laser intensity and gain settings so that the intensities of different samples could be compared.

2.7. Statistical Analysis

At least three different donors' human primary cell cultures were used for each experiment. Data are expressed as mean ± standard deviation. The differences between vehicle-treated (controls), TGF-β2-treated, and TGF-β2/LT- or TGF-β2/Y27632-treated pHTMC were analyzed using ANOVA followed by

Tukey's multiple comparisons test (GraphPad Prism 9, LLC). P values < 0.05 were considered significant.

3. Results

3.1. Trabecular Meshwork Cell Characterization

Experiments conducted to validate our pHTMC culture are available in supplementary data. (Figure S1). There are no specific markers for trabecular cells, so we used a set of molecules known to be expressed by trabecular cells. pHTMC expressed alpha-SMA in relation to their important contractile property in the mechanotransduction process [3]. As expected, the AQP1 and CD44 antigens were located at the pHTMC plasma membrane. Nuclear localization of the protein CHI3L1 was found, compatible with the macrophagic activity of trabecular cells [287] (Figure S1b). Then, we used dexamethasone (DXM) exposure (100 nM) for 7 days to further characterize the pHTMC through alpha-SMA induction of and actin skeleton reorganization (Figure S1c).

Western immunoblot analysis of the myocilin induction in response to DXM confirmed the TMC characterization in accordance with the consensus recommendations [190] (Figure S1d).

3.2. Exposure to TGF-β2

Unlike the untreated primary trabecular cells, which displayed aligned actin fibers, after 48 hours of exposure to TGF-β2 at 5ng/ml, pHTMC exhibited rearrangements of the actin cytoskeleton, appearing disorganized and more extended. While labeling of alpha-SMA was more diffuse in the cytosol of untreated cells, there was a reorganization of fibers under the effect of TGF-β2. An increase in cell stress fibers was thus observed accompanied by the formation of CLANs (Figure 13 and 14). These CLANs were present in 38.7% (± 12%) of cells exposed to TGF-β2 and were not present in the control. Quantification of the alpha-SMA expression was also greater after treatment with TGF-β2 compared with the control (1.8-fold, *P*=0.0116) (Figure 3b, alpha-SMA).

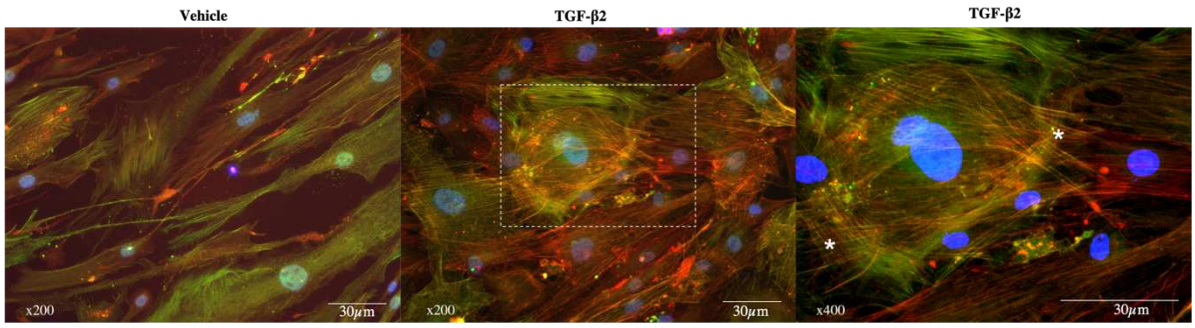

Figure 13 :Cytoskeletal remodeling after TGF-β2 exposure.
pHTMC were treated for 48h with TMCM only (Vehicle) or with TGF-β2 (5ng/ml). F-actin filaments were visualized by phalloidin staining (red), alpha-SMA antibody (green), and nuclei were counterstained with DAPI (blue). Right: enlarged images from corresponding areas. Asterisks indicate CLANs.

The Rho-ROCK downstream signaling pathway for TGF-β2 induces phosphorylation of MYPT1, which inhibits the dephosphorylation of MLC and the phosphorylation of the intracellular protein Cofilin. After 48 hours of exposure to TGF-β2 at 5 ng/ml, there was an activation of the ROCK pathway, with increased expressions of MLC-P and Cofilin-P compared the the vehicle treated pHTMC (Figure 14b, MLC-P and Cofilin-P) (respectively 1.5 and 2.0-fold, $P<0.05$). MLC-P immunofluorescence labeling presented the same distribution as actin: rather diffuse in the cytosol of untreated cells and organized into fibers after exposure to TGF-β2 (Figure 14a, MLC-P). Cofilin-P was located in the cytosol of pHTMC, and the staining was more intense after TGF-β2 exposure (Figure 14a, Cofilin-P).

Regarding the ECM, immunofluorescence analysis showed that the following exposure to TGF-β2 at 5 ng/ml, fibronectin organized differently, with multiple joint fibrils forming a network that appeared thicker and denser than that found in the controls (Figure 14a, fibronectin). Quantification of the fibronectin expression was also greater after treatment with TGF-β2 *vs.* control (1.8-fold, $P=0.0119$) (Figure 14b, fibronectin).

Western blot analysis confirmed the induction of fibronectin expression in pHTMC cultures after TGFβ2 treatment compared with the control (Figure 15 a and b).

3.3. Effects of therapeutic molecules on TGF-β2-induced pathological trabecular meshwork model

Cytoskeletal rearrangements induced by TGF-β2 persisted under the effect of LT (Figure 14a, alpha-SMA). The expression of alpha-SMA remained more intense than in vehicle-treated pHTMC, which was confirmed after quantification using Arrayscan (Figure 14b, alpha-SMA) (ANOVA, P<0,0001, TGFβ2 vs. TGFβ2/LT ns). CLANs were also present, and the expression profile of MLC-P and Cofilin-P did not differ qualitatively from TGFβ2 exposed cells in immunofluorescence images even though the quantification showed a significant decrease in the total positive labeling area (figure 14a and b).

a.

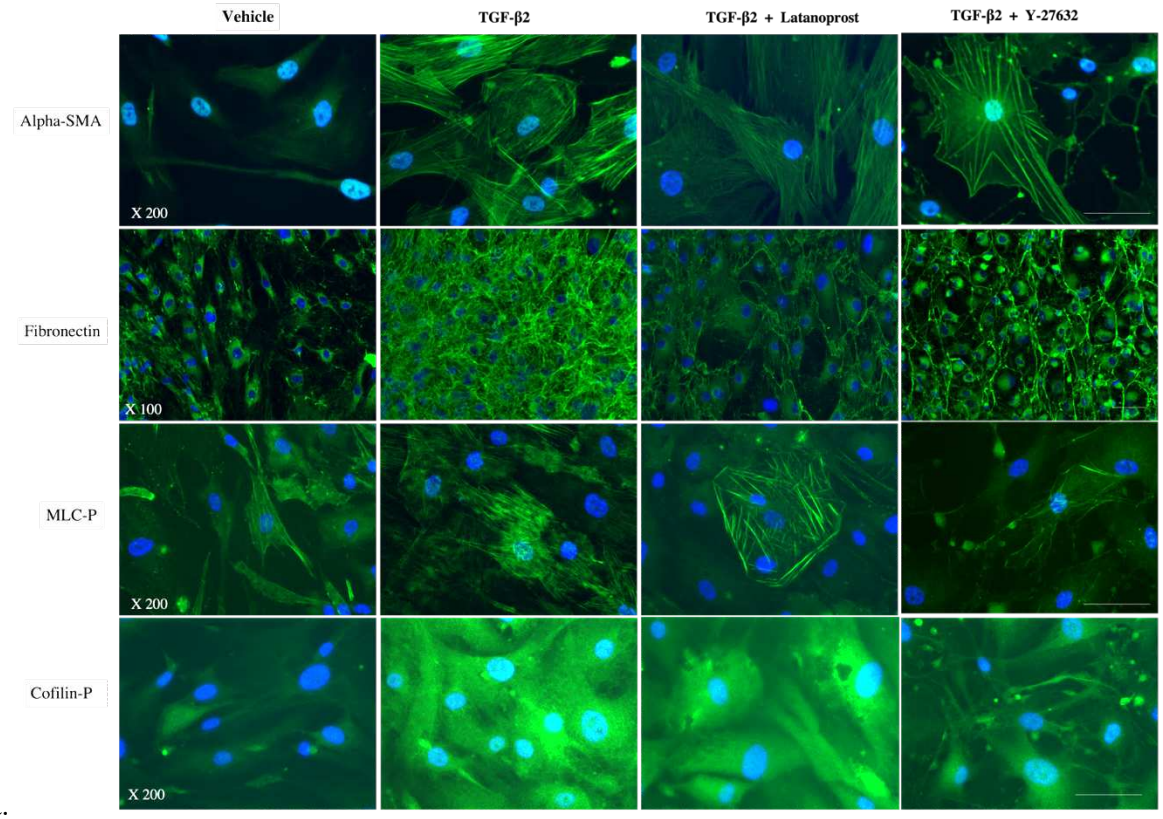

b.

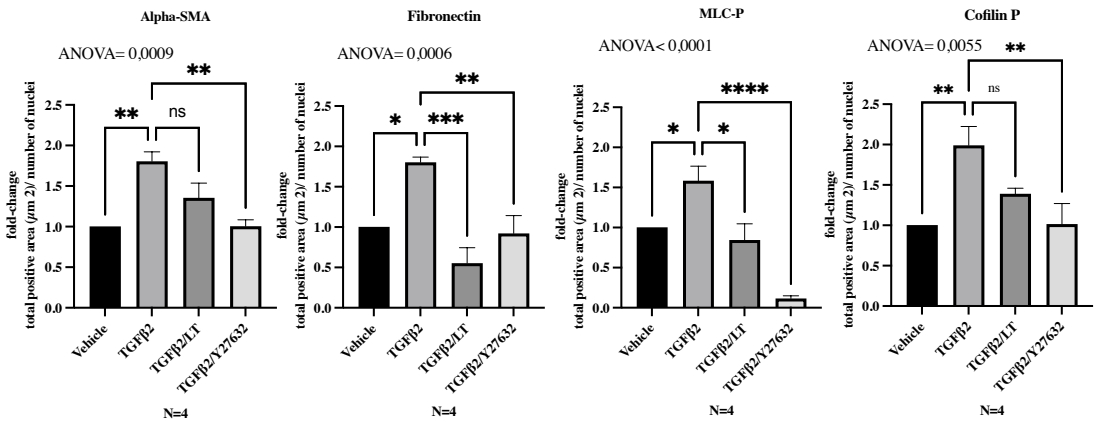

Figure 14 : Immunofluorescence analysis of the effect of LT 0.5 µg/ml or the ROCK-i Y-27632 25 nM for 24h on pHTMC
a. Immunofluorescence analysis of the effect of LT 0.5 µg/ml or the ROCK-i Y-27632 25 nM for 24h on pHTMC. pHTMC were treated for 48h with TMCM only (Vehicle) or with TGF-β2 5ng/ml or with 24h of TGF-β2 5ng/ml followed by 24h of TGF-β2 5ng/ml along with LT 0.5µg/ml or Y-27632 25 nM. Nuclei are stained with DAPI (blue). The green staining corresponds to the antibodies indicated. Scale bar = 30 µm. This figure shows the major effect of LT on the density of ECM with no effect on the cytoskeleton itself. The ROCK-i modified both the cytoskeleton and the ECM relaxation. **b.** Quantification, with Arrayscan, of the total positive labeling area related to the number of cells (µm²) in fold-change (mean ± SEM). *P<0.05, **P<0.01, ***P<0.001, ****P<0.0001.

Regarding the ECM, following exposure to TGF-β2 at 5 ng/ml, fibronectin increased in density compared to that of the controls. LT greatly reduced the expression of fibronectin, resulting in the formation of a much looser mesh compared with TGF-β2-exposed pHTMCs (Figure 14a, fibronectin). The total positive area related to the number of nuclei was reduced (0.55-fold) when treating the TGF-

β2-exposed pHTMC with LT (*P*=0.0004) compared with TGF-β2-exposed pHTMC (Figure 14b, fibronectin). While non-significant, western blot analysis revealed that the TGF-β2-exposed pHTMC with LT (0.5µg/ml) seems to decrease the TGF-β2-stimulated expression of fibronectin (ANOVA, *P*= 0,0548) (Figure 15 a and b).

The cytoskeletal rearrangements induced by TGF-β2 were modified by Y-27632. The intensity of α-SMA labeling was reduced compared to TGF-β2-exposed pHTMC (*P*= 0.017) (figure 3b, alpha-SMA). Inhibition of ROCK was associated with relaxation of the cells and disassembly of stress fibers and CLANs . A new distribution of actin fibers in the periphery was observed in response to the alteration of the actin cytoskeleton (Figure 14a, alpha-SMA). TGF-β2-induced MLC-P and Cofilin-P overexpression was also inhibited by Y-27632 (*P*<0.01) (Figure 14 a and b, MLC-P and Cofilin-P).

Regarding the ECM, the ROCK-I Y-27632 decreased fibronectin expression, with a looser mesh and enlarged intercellular spaces compared with TGF-β2-exposed pHTMC (Figure 14a, fibronectin). The labeling quantification revealed a reduction in fibronectin expression compared to TGF-β2-exposed pHTMC (*P*=0.0062) (Figure 14b, fibronectin). Western blot analysis showed that treating the TGF-β2-exposed pHTMC with the ROCK-I Y-27632 (25 nM) for 24h decreased the TGF-β2-induced overexpression of fibronectin (Figure 15a and b).

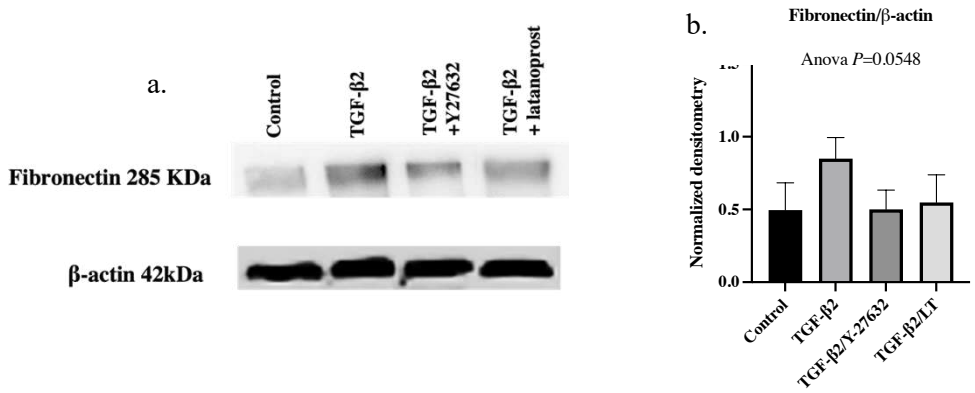

Figure 15 : Protein expressions in pHTMC cultures after treatment with 5ng/mL TGFβ2 for 48h in the absence or presence of 25nM Y27632 or 0.5µg/ml LT for 24h
a. Representative western blots of fibronectin and β-actin (mean ± SEM). b. Densitometry of western blot analysis of fibronectin normalized to β-actin.

3.4. 3-Dimensional trabecular meshwork cell cultures

Figure 16 shows the 3D organization of pHTMC in Matrigel™. The pHTMC organized in a mesh conformation with interconnections and the formation of intercellular spaces. Visual observations show that TGF-β2 induced rearrangements of the cytoskeleton with an organization of actin into more extensive fibers and decreased intercellular space. There was no modification of the actin disposition nor of the intercellular spaces after exposure to LT. However, the changes induced by TGF-β2 were modified under the effect of Y-27632. Actin fibers were less extensive resulting in the widening of spaces between cells (Figure 16).

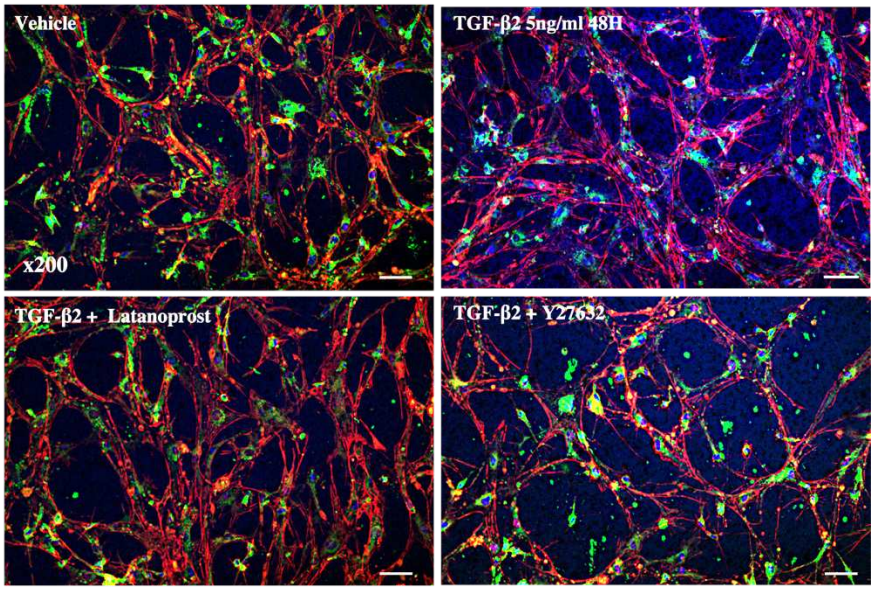

Figure 16 : Confocal microscopy images of the 3D cultured pHTMC
Analysis of the effect of the ROCK-I Y27632 at 25nM for 24h and the effect of LT at 0.5µg/ml on primary human pHTMC treated with TGF-β2 at 5ng/ml for 48h. The cells were treated with TMCM alone (vehicle), 5ng/ml of TGF-β2 for 48h or with TGF-β2 (5ng/ml) for 24h followed by a combination of TGF-β2 at 5ng/ml and with Y-27632 (25nM) or LT (0.5µg/ml) for 24h. Actin fibers are stained in red by phalloidin, membranes with DiO (green), and nuclei with DAPI (blue). Magnification 200X. Scale bar = 30 µm.

4. Discussion

In the present study, we used an *in vitro* TGF-β-induced pathological TM model from primary cultures of human trabecular cells. We first showed an effect of TGF-β2 on the organization of the cytoskeleton, with the formation of CLANs, and an increase in its contractibility, as well as an effect on the ECM, with an increase in fibronectin deposits. We also demonstrated activation of the ROCK pathway. We then showed that ROCK-i has a dual effect on pHTMC with action on both the fibronectin deposition and the cytoskeleton whereas latanoprost only acts on ECM degradation.

The family of TGF-β cytokines is known to be associated with impairment of several cellular functions, including differentiation, proliferation, and remodeling of the ECM [288]. The profibrotic role of TGF-β2 and its presence in the aqueous humor of patients with glaucoma implicates its potential role in the pathogenesis of ocular hypertension through TM degeneration/dysfunction [289]. In our study, we showed that TGF-β2 activated the Rho-ROCK pathway in TMC and induced Actin fiber rearrangement and co-localization of alpha-SMA to stress fibers. TGF-β2 also induced fibronectin deposition. By simultaneously modifying the organization of the cytoskeleton and the ECM, with fibronectin deposition and overexpression, TGF-β2 allows the trabecular degeneration described in glaucoma to develop. TGF-β2 was also used in a TM model by Torrejon *et al.*, who described the production of ECM and increased resistance to the aqueous humor outflow *in vitro* [123]. Ota *et al.*, also showed that TGF-β2 enhances transendothelial electrical resistance in a culture of HTM [200]. Glucocorticoids like dexamethasone are often used to model trabecular degeneration because they modify the cytoskeleton of TMC and the ECM. However, this corresponds more to the modifications obtained in corticosteroid-induced iatrogenic

glaucoma, which constitutes a subtype of open-angle glaucoma [290]. This constitutes an advantage of the TGF-β2-induced model of TM alteration compared to the use of glucocorticoids. One of the limitations of our study is that we did not study the effect of therapeutic molecules in the absence of TGF-β2. Torrejon *et al.* studied the effect of Y-27632 alone on fibronectin expression of TMC and found no difference with the control. However, they have demonstrated that Y-27632 in combination with TGF-β2 substantially decreased the expression of fibronectin compared to samples treated with TGF-β2 alone. Compared to vehicle control, TGF beta2/Y-27632 combined treatment increased fibronectin, demonstrating that the ROCK-i counteracts the otherwise fibrotic effect of TGF-β2, effectively lowering ECM accumulation [123]**.**

We highlighted an action of latanoprost on the fibronectin deposition without action on the cytoskeleton. This is consistent with the literature. Kalouche *et al.* showed that latanoprost decreased the accumulation of collagen onto cultured human trabecular cells [120]. Bahler *et al.* studied the effect of latanoprost on histologic sections of the anterior segment of the eye and observed focal losses of ECM in the juxtacanalicular region of the TM [119].

Moreover, in our study, we enriched our result on a three-dimensional (3D) TM cellular model. Our preliminary results presented an interesting tool to advance research on this pathology by taking into account biomechanics, which is a key element in the pathophysiology of glaucoma [71]. Nevertheless, for the moment the results provided are only qualitative, which constitutes a limitation of the study. Quantification work is in progress. The 3-Dimensional cell cultures in Matrigel^{TM} allowed us to obtain a meshed organization of trabecular cells with interconnections and the formation of intercellular spaces, that we did not find in 2D, and which better reflects the real anatomy of the TM. We were able to show with this model that the ROCK-i Y-27632 widened the meshes between the cells by modifying the cytoskeleton of pHTMC. Cell culture in 3D recreates the conditions of the microenvironment encountered *in vivo* and provides cells with an environment allowing them to interact with each other and with the ECM. It would also help to better understand not only the physiological function of the TM but also its behavior under conditions of stress or toxicity, as well as the effect of medications [291]. This 3D TM model was first used by Bouchemi *et al*. to study the effect of benzalkonium chloride (BAK), a preservative commonly used in eye drops [117]. They showed that BAK induced inflammatory chemokines and inhibited the activity of MMPs, which play a crucial role in ECM degradation and increase outflow facility. Further research will be necessary to better exploit all the information provided by this model. Indeed, main biomechanical cues experienced by TMC are not investigated in this article. For example, TMC *in vivo* are subjected to a significant pressure change, shear stress and mechanical stretch. Rigidity and outflow measurement systems using this model might also be implemented to improve the relevance of the model. Analysis and understanding of the pathophysiology of the TM are essential for understanding and treating glaucoma.

We also showed the involvement of the ROCK signaling pathway in the stiffening of the TM and that the inhibitor Y-27632 modified the TGF-β2-induced cytoskeletal rearrangements. Previous studies have demonstrated the changes in pHTMC cytoskeleton organization with a modification of cell shape and actomyosin organization [292]. A new distribution of actin fibers in the periphery was observed in response to the alteration of the actin cytoskeleton. This redistribution was first described by Murphy *et al.* and qualified as cortical actin arrays (CAA)[293]. In our study, there was also reversibility of ECM deposition induced by TGF-β2 after treatment with ROCK-i. Indeed, the ROCK-i Y-27632 decreased TGF-β2-induced fibronectin deposition. A recent study by Li et al. also demonstrated the antifibrotic activity of a ROCK-i on an *in vivo* glucocorticoid-induced ocular hypertension model [290]. Our work confirmed the anti-fibrotic action of ROCK-i to prevent cell contractility and accumulation of ECM, consistent with studies by Torrejon *et al.,* Pattabiraman *et al.,* and Ota *et al.* [122,123,200].

Although it is known that the mechanism of action of PGA relies on increased expression of MMP in the TM, few studies have investigated the remodeling of the ECM by MMPs under the effect of ROCK-i [294]. Torrejon et al. showed that after 3 and 5 days, TMC exposed to MMP2 mRNA-level in TMC was enhanced after a 3-days co-treatment with Y27632 and TGF-β2[123]. Watanabe *et al.* showed that the addition of a pan-ROCK-i (ripasudil 10nM) to TGF-β2 (5ng/ml) exposed TMC induced significant up-regulation of MMP2, MMP9, and MMP14 at Day 6[243]. Further studies exploring MMP and TIMP expression in TMC after PGA and ROCK-i exposure would be of interest.

A ROCK-i, 0.02% netarsudil (Rhopressa® (US)/ Rhokiinsa® (EU), Aerie Pharmaceuticals, Inc., NC) received Food and Drug Administration approval in December 2017 and marketing authorization to the European Medicines Agency in November 2019 for lowering IOP in patients with POAG [125]. Another molecule from the same family, ripasudil (Glanatec®, Kowa Pharmaceuticals, Japan) was approved by the Japanese health authorities in 2014 for the treatment of glaucoma, or ocular hypertension, as a second line after prostaglandin therapy[295]. In addition, the combination of netarsudil with latanoprost was clinically developed and led to a new formulation (Rocklatan® (US)/Roclanda® (EU), Aerie Pharmaceuticals, Inc., NC), which had a greater effect on the reduction of IOP than either of its two components, by reducing IOP by an additional 1.8 mmHg on average compared to netarsudil, and 2.7 mmHg compared to latanoprost [296,297]. Although we have not tested the combination of the two molecules, our work suggests that the significant effect of latanoprost on fibronectin deposition associated with the remodeling of the ROCK-i cytoskeleton could effectively lead to a significant decrease in resistance to the aqueous humor outflow.

5. Conclusion

We used an in vitro TGF-β2-induced TM remodeling mimicking glaucomatous trabeculopathy to confirm the effects of both a ROCK-i and a PGA on the TM. We showed that ROCK inhibition had an

action on the TM cells' cytoskeleton by reducing actin stress fibers, as well as on ECM release. In our model, we also demonstrated that latanoprost loosened the ECM.

Supplementary Materials

Tableau 6 (supplementary) : HTMC lines information P: passage, IF: immunofluorescence, WB: Western blot

HTMC line number	Age of the donor (years)	Characterization at passage	Used in experimental set (passage)
1	60	P1	IF (P3)
2	83	P1	IF (P3)
3	86	P1	IF (P4) WB (P6) Matrigel (P5)
4	62	P3	IF (P4, P6)
5	60	P3	WB (P6)
6	51	P2	IF (P3) Matrigel (P5)
7	50	P2	IF (P3)
8	76	P2	IF (P6) Matrigel (P6)
9	71	P2	IF (P6) WB (P6)
10	49	P4	WB (P5)
11	74	P4	IF (P5) WB (P5) Matrigel (P6)

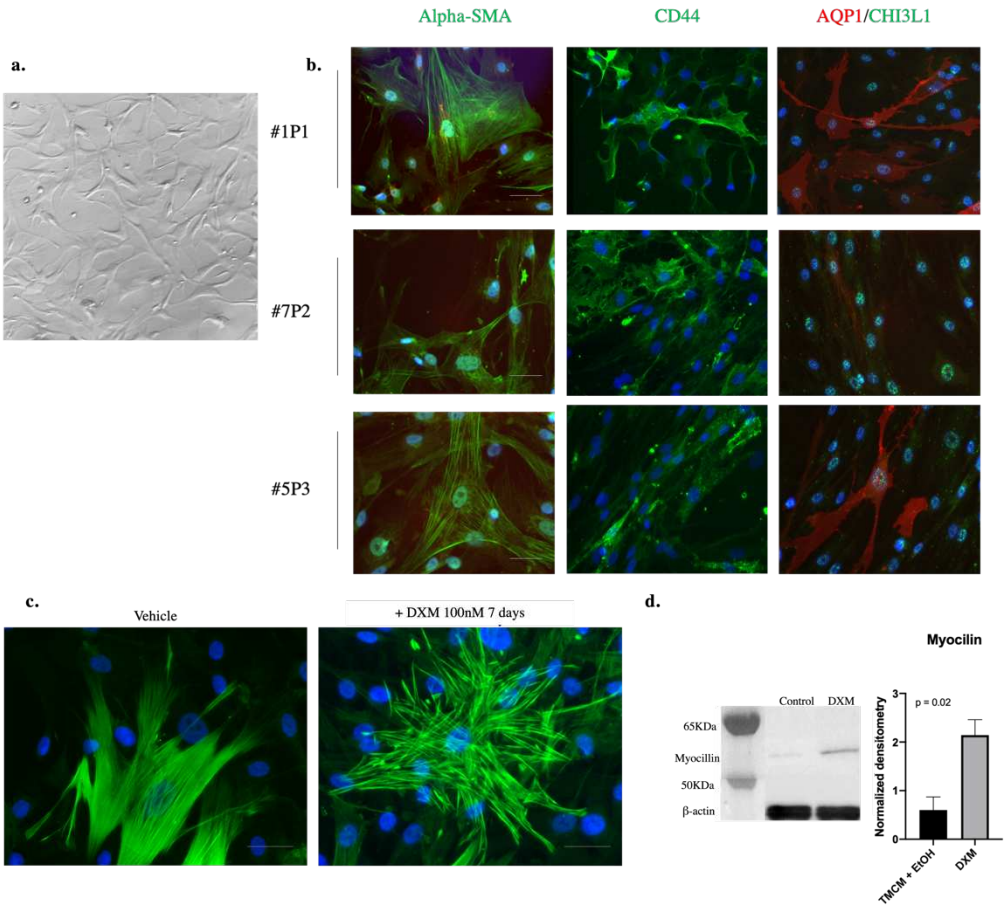

Figure S1: Characterization of the normal human trabecular meshwork cells a. Representative phase-contrast images of pHTMC on confluent phase (x20), TMC culture presented a cobblestone-like pattern with some overlapping processes. b. pHTMC from different donors (1 P1, 7 P2, 5 P3) were stained for markers expressed by TMC: alpha-SMA (green), CD44 (green), CHI3L1 (green), AQP1 (red) c. Immunolabeling of alpha-SMA (green), and nuclei (DAPI in blue) with or without exposure to dexamethasone (DXM, 100nM) for 7 days on pHTMC. The actin cytoskeleton is rearranged and there is an increase in the expression of alpha-SMA after exposure to dexamethasone. Magnification 200X, scale bar = 30 µm. d. Representative western blot of myocilin and β-actin and the densitometry analysis of myocilin normalized to β-actin showing dexamethasone (DXM)-induction of myocilin.

Étude transcriptomique de l'effet du TGF-β2 sur des explants de trabéculums humains.

Contexte et objectif

Si l'étude précédente nous a permis de décrire et de confirmer les effets du TGFB2 sur l'organisation du cytosquelette des HTMC en 2D et en 3D, notre seconde étude élargit notre champ d'investigation en employant des techniques d'analyses transcriptomiques pour analyser l'impact du TGF-β2 sur des explants de trabéculums humains. Cette approche permet de mettre en lumière les altérations géniques survenues en réponse à cette cytokine, délivrant ainsi des données cruciales sur les mécanismes cellulaires impliqués dans le glaucome. En effet, le TGF-β2 a été utilisé dans des modèles de GPAO *in vitro* et *in vivo* [207,209,262,272]. Cependant, les mécanismes moléculaires impliqués dans la pathogenèse du glaucome sont encore mal connus et, par conséquent, peu de thérapies sont disponibles pour agir sur eux.

Plusieurs études ont indiqué que les conditions de culture des TMC peuvent altérer leur expression génique, comme les méthodes de culture 2D ou 3D, ou la rigidité du substrat [191,228,260].

Ces dernières années, la recherche sur des modèles de glaucome *in vitro* s'est concentrée sur l'importance de l'organisation 3D pour mieux modéliser la physiopathologie du dysfonctionnement du trabéculum [227,240]. Considérant donc que les conditions de culture des cellules TM humaines (HTMC) influencent l'expression des gènes, nous avons utilisé des explants de trabéculums humains (HTMEx) pour étudier le transcriptome des HTMC au plus proche des conditions physiologiques. Cette approche nous a permis de garder les HTMC dans leur propre MEC et de préserver leur interconnectivité.

Afin de mieux caractériser le rôle du TGF-β2 dans la pathologie moléculaire du glaucome, nous avons utilisé le séquençage complet de l'ARN (RNA-Seq) pour décrire les modifications du transcriptome du HTMEx exposé au TGF-β2.

Notre étude nous a conduit à l'identification des gènes surexprimés, qui se sont révélés participer principalement à la régulation de la MEC et à la voie de signalisation profibrotique du TGF-β. Les méthodes d'analyse d'enrichissement des ensembles de gènes (GO, Reactome) permettent d'identifier les voies biologiques, les fonctions moléculaires ou les composants cellulaires sur- ou sous-exprimés. Elles ont ici révélé une modulation de l'expression génique liée à l'organisation du cytosquelette et à l'activation des voies BMP et Wnt en réponse au TGF-β2.

Cette caractérisation des modifications transcriptomiques et de l'activation des voies de signalisation sur un modèle d'explant innovant de TM obtenu sous l'effet de cette cytokine profibrotique impliquée dans le glaucome est cruciale afin de développer et tester de nouvelles molécules capables de bloquer leurs voies de signalisation.

L'essentiel des résultats obtenus sont rapportés dans l'article suivant, en cours de soumission dans une revue internationale.

Article 3 : RNA-Seq Transcriptomic Profiling of TGF-β2-Exposed Human Trabecular Meshwork Explants: Advancing Insights Beyond Conventional Cell Culture Models

Article soumis à Experimental Eye Research

J. Buffault[1-3*], E. Reboussin[2], K. Kessal1[2], M. Akkurt Arslan[2], F. Blond[2], X. Guillonneau[2,] S. Melik-Parsadaniantz[2], A. Réaux-le Goazigo[2], A. Labbé[1-3], F. Brignole-Baudouin[2,4c], C. Baudouin[1-2*c]

[1-] Department of Ophthalmology III, Quinze-Vingts National Ophthalmology Hospital, IHU Foresight, Paris, France.

[2-] Sorbonne Université, INSERM, CNRS, IHU Foresight, Institut de la Vision, Paris, France

[3-] Department of Ophthalmology, Ambroise Paré Hospital, APHP, Université de Paris Saclay, Boulogne-Billancourt, France.

[4-] Department of Biology, CHNO des Quinze-Vingts, IHU Foresight, Paris, France

[c] Co-last authors

[*] Corresponding authors

Juliette Buffault

jbuffault@15-20.fr

Christophe Baudouin

cbaudouin@15-20.fr

Abstract

Glaucoma is a progressive optic neuropathy that can lead to irreversible blindness. Its main risk factor is elevated intraocular pressure (IOP). The trabecular meshwork (TM) acts as a filter between the anterior chamber of the eye and the aqueous humor collecting ducts, and dysfunction of this meshwork is responsible for the increased IOP in primary open-angle glaucoma (POAG). Considering that the culture conditions of human TM cells (HTMC) influence gene expression, we used human TM explants (HTMEx), which most closely mimic physiological conditions, to study the transcriptome of HTMC. The transforming growth factor-beta 2 (TGF-β2) signaling pathway has been implicated in the pathophysiology of POAG. To better characterize the role of TGF-β2 in this pathophysiology, we used bulk RNA sequencing and immunohistological analyses to establish gene signatures of TGF-β2-exposed HTMEx and correlate them with morphological alterations. We confirmed differentially upregulated genes primarily involved in ECM regulation, as well as profibrotic TGF-β signaling pathways, confirmed using confocal microscopy to highlight changes in trabecular architecture, TGFβ2-induced F-actin rearrangements, and extracellular matrix (ECM) deposition. Enrichment analysis also revealed modulations of gene expression related to cytoskeletal organization, as well as activation of the bone morphogenic protein (BMP) and Wnt signaling pathways in response to TGF-β2.

Introduction

Glaucoma is a progressive neurodegenerative disease resulting in irreversible loss of retinal ganglion cells and eventually leading to blindness if left untreated. Its main risk factor is elevated intraocular pressure (IOP), the only modifiable factor currently shown to slow the progression of the disease[298]. Primary open-angle glaucoma (POAG) is the most common form of glaucoma, affecting over 65.5 million people worldwide [270].

The trabecular meshwork (TM), located within the iridocorneal angle, acts as a filter between the anterior chamber of the eye and the aqueous humor collecting ducts. In POAG, dysfunction of the TM is responsible for increased IOP. This complex, fenestrated, three-dimensional structure is composed of trabecular meshwork cells (TMCs) organized into a meshwork of extracellular matrix (ECM)[12]. In POAG, increased outflow resistance throughout the TM is multifactorial, including loss of TMCs, changes in their cytoskeletal organization, and extracellular matrix remodeling [192].

The transforming growth factor-beta2 (TGF-β2) signaling pathway has been widely implicated in the pathophysiology of POAG. Indeed, TGF-β2 signaling is increased in the aqueous humor of POAG patients, and it has also been used as an inducer of TM degeneration in *in vitro* and *in vivo* models of POAG [5-8]. *In vitro* studies have shown that TGF-β2 induces the synthesis of ECM components by TMCs (collagens, elastic fiber components, proteoglycans, glycosaminoglycans, fibronectin, matricellular proteins[235]), leading to increased resistance to outflow[273]. TGF-β2 also increases cellular stiffness

through the formation of cross-linked actin networks (CLANs) via the Rho-ROCK signaling pathway[14,299]. However, the molecular mechanisms involved in the pathogenesis of glaucoma are still poorly understood, and few therapies are available to address them[300].

Several studies have indicated that the culture conditions, such as two-dimensional (2D) or three-dimensional (3D) culture methods for TMCs, can alter their gene expression or substrate rigidity[191,228,260]. In recent years, research on *in vitro* glaucoma models has focused on the importance of 3D organization to better model the pathophysiology of TM dysfunction[227,240]. We used the explant method to closely mimic the *in vivo* conditions of the TMC.

In fact, it is widely accepted that primary cells are physiologically more relevant than immortalized cells, and it is recommended to replicate cell line findings with non-immortalized TMCs[190]. Our human TM explant (HTMEx) approach expands upon this concept, as it allows us to keep the primary human TMCs (HTMC) in their extracellular matrix (ECM) environment and preserve their interconnectivity.

A previous study by Callaghan *et al*. used dissociated HTMCs from cadaver eyes, cultured between passage 5 and 7 and exposed to TGF-β2 to investigate gene modulations with deep RNA sequencing (RNA-Seq) analysis[301]. RNA-Seq analysis has revolutionized our ability to study gene expression and identify novel transcripts. By using high-throughput sequencing, RNA-Seq enables comprehensive mapping of the transcriptome. This technology has greatly advanced our understanding of biological processes, including disease mechanisms, developmental processes, and gene regulation[9,302,303].

To gain a better understanding of the role of TGF-β2 in the molecular pathology of glaucoma, we used bulk RNA-Seq to analyze changes in the transcriptome of HTMEx exposed to TGF-β2.

Materials and methods

Trabecular meshwork sample collection and exposure to TGF-β2

Human TM specimens were meticulously dissected in the aseptic environment of an operating room from corneoscleral rings of non-glaucomatous donor tissue after they were used for corneal transplantation. The dissection involves separating the trabecular meshwork from the sclera using Bonn forceps and Vannas scissors, under an operating microscope. A photography showing the dissection and an image of the untreated specimen were included (supplementary figure 1). Subsequently, the dissected trabecular meshwork is carefully partitioned into 8 mm segments. All donor tissue was obtained and managed in accordance with the guidelines of the Declaration of Helsinki for research involving human tissue. Human tissues were provided by the biotissue bank of the *Etablissement Français du Sang* (EFS), which ensured complete anonymization. Consequently, data regarding the donors from whom the TM were obtained is limited. The age, sex, cause of death, and the date of harvesting and TM dissection are specified in the supplementary table 12. The donors were between 56 and 86 years of age. After

dissection, the TM was transported in Cornea Jet preservation medium (Eurobio Scientific, Les Ulis, France) at room temperature (RT). The HTMEx were stimulated with recombinant human TGF-β2 (PeproTech Inc., 100-35B, Thermo Fisher Scientific, MA, USA) at a concentration of 5 ng/mL for 48 h in complete culture medium [DMEM/F12 (Gibco, 11320) supplemented with 1% penicillin and streptomycin solution (penicillin 10,000 U/mL, streptomycin 10,000 µg/mL) and 0.001% bovine serum albumin (BSA) (Sigma-Aldrich, A2153)]. Vehicle control explants from the same donors were incubated with equal volumes of complete culture medium [DMEM/F12 (Gibco, 11320) supplemented with 1% penicillin and streptomycin solution (penicillin 10,000 U/mL, streptomycin 10,000 µg/mL) and 0.001% bovine serum albumin (BSA) (Sigma-Aldrich, A2153)]. Each corneoscleral ring provided a sample of vehicle control trabecular meshwork (CTL) and a TGF-β2 treated sample (TGF).

Immunohistochemistry

Four pieces HTMEx were fixed with 4% paraformaldehyde overnight at 4°C and rinsed in 1x PBS before the immunofluorescence procedure. The effects on the organization of both the cytoskeleton and the ECM were characterized by immunohistochemistry using anti-alpha-SMA (Abcam, ab5694, 1/100 dilution) and anti-fibronectin (R&D Systems, MAB19181, 1/100 dilution) antibodies. HTMEx were incubated for 2h at RT in a blocking buffer (5% BSA, 2% Triton X-100, and 0.5% Tween20, in 1x PBS) and left to incubate overnight at 4°C in the incubation buffer (2.5% BSA, 1% Triton X-100 and 0.25% Tween20, in 1x PBS) with the same primary antibodies. The HTMEx were then rinsed three times in 1x PBS and incubated with the corresponding secondary antibodies (anti-rabbit conjugated to Alexa fluor 488 (Thermo Fisher, A21206), and anti-mouse conjugated to Alexa Fluor 594 (Thermo Fisher, A21203), at a dilution of 1/500 for 1h at RT. The nuclei were stained with DAPI (ThermoFisher, D1306, dilution 1/1000). Finally, HTMEx were deposited in fluorescent mounting medium and coverslipped (Sigma Aldrich, ref. F4680). Confocal laser scanning microscopy was performed using an Olympus IX81 confocal microscope coupled to Fluoview software (Olympus, Ver 4.2), and the images were acquired at 200x and 400x magnification. Confocal 3D images were processed using Imaris3D® software (Bitplane AG, Zurich, Switzerland). All confocal images from the same experiment were captured using the same laser intensity and gain settings.

Bulk RNA-seq of TGF-β2-stimulated TM explants

For whole transcriptome analysis, HTMEx from 14 donors were exposed for 48 h to either vehicle [control (CTL), complete culture medium)] or TGF-β2 (TGF) (5ng/ml). After tissue lysis, total RNA was extracted from the HTMEx using the Nucleo Spin RNA XS kit (Macherey-Nagel, 740902.50) according to the manufacturer's specifications. Total RNA for each sample was quantified, and its quality was determined using a BioAnalyser 2100 with the RNA 6000 pico Kit (Agilent Technologies, Leuven, Belgium). RNA samples with a RNA intergrity number (RIN) greater than 8 were selected for

RNA-seq analysis, corresponding to 15 samples from 8 donors. Fifteen mRNA libraries could be prepared: 8 CTL and 7 TGF. Amplification and RNA sequencing experiments from 3.5 ng of total RNA were conducted using SmartSeq (Takara), Nextera XT (Illumina), and NovaSeq 6000 SP Reagent Kit (200 cycles) (Illumina) at iGenSeq (Institut du Cerveau (ICM), Paris, France).

RNA-Seq data analysis, Bioinformatic analysis of biological process and pathways

Fastq files obtained from the sequencing facility were aligned using STAR (v2.7.9a) against the Human reference genome from Ensembl v106 (based on assembly GRCh38, generated 2022/06/21), with option "--quantMode GeneCounts" to extract the raw counts for each gene, and all count files were concatenated into a single file. A sample file was created with the sample data including the conditions (CTL, TGF) and the replicate numbers.

Control and treated libraries were not paired for the analysis. Nevertheless, we conducted an additional analysis by applying a donor effect correction (Bioconductor package 'sva').

The count file and the sample file were loaded in our in-house R Shiny application EYE DV seq (plateforme Phénotypage Cellulaire et Tissulaire, Institut de la Vision, Paris, France). We added 1 to all counts in the count file to avoid any 0 read count errors. We then removed the genes having a total count < 10 across all samples. Finally the DESeq2 (v1.40.2) analysis was performed comparing the groups defined in the 'condition' column, with 'CTL' as control group and 'TGF' as condition. The plots were obtained using ggplot2 or an appropriate library ('EnhancedVolcano', 'ComplexHeatmap').

The results were then filtered for significant genes using the adjusted p-values (< 0,05). An enrichment analysis was performed to study the implicated pathways, using the Reactome database (using the Bioconductor package 'ReactomePA' (v1.44.0) and the GO database (using the Bioconductor packages 'org.Hs.eg.db' (v 3.17.0) and 'clusterProfiler' (v 4.8.1)).

Pathcards (Weizmann Institute of Science, Tel Aviv) was used to explore human biological pathways.

The raw RNA-Seq data was deposited and released in the GEO database (ID GSE236302, https://www.ncbi.nlm.nih.gov/geo/query/acc.cgi?acc=GSE236302).

Transcriptomic trabecular meshwork characterization

TM characterization was carried out using a typical panel of HTMC identification markers reported by Keller et al.[190], and Stamer et al.[304] and enriched by the most highly expressed genes reported by

Carnes *et al*.[305] in their RNA-Seq transcriptome analysis of adult TM and by van Zyl's Cell atlas of the human ocular anterior segment[306,307].

Results

F-actin rearrangements and ECM deposition in the 3D explant model of TM exposed to TGF-β2

Confocal microscopy of the explants allowed us to demonstrate the characteristic organization of the TM, which showed a progressively tighter mesh from the anterior chamber (AC) to the outer wall of Schlemm's canal (SC). In contrast to the untreated HTMEx, wherein alpha(α)-SMA labeling was diffuse in the cytosol, exposure to TGF-β2 at 5 ng/ml for 48 h resulted in rearrangements of the actin cytoskeleton, with cells appearing more elongated, and fibers appearing sharper and more extensive (figure 17).

Immunofluorescence analysis of the ECM revealed that exposure to TGF-β2 at 5 ng/ml led to a different organization of fibronectin, wherein multiple joint fibrils formed a network that appeared denser than in the control group (figure 17).

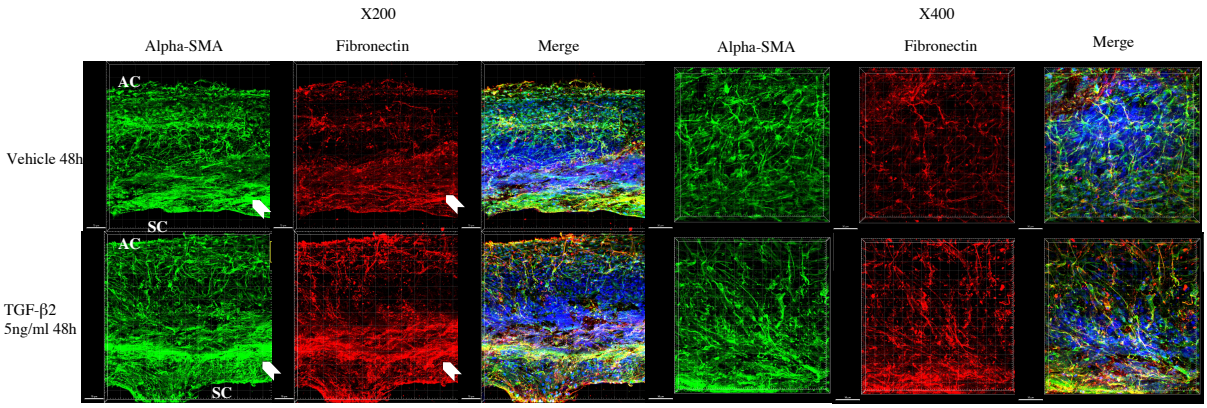

Figure 17 : Representative confocal microscopy images of HTMEx showing cytoskeletal and ECM remodeling after TGF-β2 exposure
at 200x (scale bar 70 µm) and 400x (scale bar 50 µm) magnifications. The explants were incubated for 48 h with Vehicle or with TGF-β2 (5 ng/ml). F-actin filaments were visualized with anti-alpha-SMA antibody (green), ECM with anti-fibronectin antibody (red), and nuclei were counterstained with DAPI (blue). For each image, the side of the less compact TM in contact with the anterior chamber (AC) is at the top, and the more compact side in contact with Schlemm's canal (SC) at the bottom. The juxtacanalicular region of the TM exhibits a higher labeling intensity of fibronectin and alpha-SMA, with more intense labeling seen in explants exposed to TGF-β2 (arrow head).

Transcriptomic trabecular meshwork characterization

The 15 most highly expressed genes in our samples are: Metastasis Associated Lung Adenocarcinoma Transcript 1 (MALAT1) , Mitochondrially Encoded 16S RRNA (MT-RNR2), Ferritin Light Chain (FTL), Actin Beta (ACTB), Mitochondrially Encoded Cytochrome C Oxidase I (MT-CO1), beta-2-

microglobulin (B2M), TIMP Metallopeptidase Inhibitor 1 (TIMP1), Prosaposin (PSAP), Enolase 1 (ENO1), matrix GLA protein (MGP), Insulin Like Growth Factor Binding Protein 7 (IGFBP7), Lactate Dehydrogenase A (LDHA), Actin Gamma 1 (ACTG1), Cathepsin B (CTSB), and Ferritin Heavy Chain 1 (FTH1).

As shown in Table 7, RNAs of the main markers of TM [165,190,305–307] were present in high quantity in HTMEx. They exhibited markers of both the uveal portion and the juxta canalar portion of the TM [306,307].

Tableau 7 : The 20 most highly expressed gene markers of trabecular meshwork
ranked by mean normalized read count. For each gene, the articles that refer to it are indicated.

Gene ID	Gene Name	Read count	Source
B2M	Beta-2-Microglobulin	103019	Carnes et al.[305]
MGP	Matrix Gla Protein	73409	Carnes et al.[165], Keller et al.[190] , Stamer et al.27.04.2024 12.49.00[165]
FTH1	Ferritin Heavy Chain 1	42853	Carnes et al.[306], van Zyl et al.[306]27/04/2024 12:49:00
CLU	Clusterin	38780	Carnes et al.[305]
TMSB4X	Thymosin Beta 4 X-Linked	33889	Carnes et al.[305]
IFITM3	Interferon Induced Transmembrane Protein 3	31605	Carnes et al.[305]
EEF1A1	Eukaryotic Translation Elongation Factor 1 Alpha 1	29513	Carnes et al.[305]
S100A6	S100 Calcium Binding Protein A6	27444	Carnes et al.[305]
CHI3L1	Chitinase 3 Like 1	22686	Carnes et al.[165], van Zyl et al.[306], Stamer et al.[165], 27-04-2024 12:49:00 Keller et al.[190]
CRYAB	Crystallin Alpha B	19791	Keller et al.[165], , van Zyl et al.[306], Stamer et al.[165] 27/04/2024 12:49:00
CEMIP	Cell Migration Inducing Hyaluronidase 1	14829	van Zyl et al.[306]
CYP1B1	Cytochrome P450 Family 1 Subfamily B Member 1	12919	van Zyl et al.[306]
DCN	Decorin	10660	van Zyl et al.[306]
MYOC	Myocilin	10238	Keller et al.[165] , van Zyl et al.[306], Stamer et al.[165] 27/04/2024 12:49:00
IGFBP5	Insulin Like Growth Factor Binding Protein 5	8561	van Zyl et al.[306]
PRRX1	Paired Related Homeobox 1	8451	van Zyl et al.[306]
APOD	Apolipoprotein D	7867	Carnes et al.[305] , van Zyl et al.[306]
AQP1	Aquaporin 1	6601	Keller et al.[165] , van Zyl et al.[306], Stamer et al. [165] 27/04/2024 12:49:00
TPT1	Tumor Protein, Translationally-Controlled 1	5218	Carnes et al.[305]
CDH11	Cadherin 11	4496	van Zyl et al.[306]

Differential Gene Expressions in HTMEx following TGF-β2 treatment

To determine changes in gene expressions in a TGF-β2 induced model of glaucomatous TM, control HTMEx (CTL) and HTMEx exposed to 5 ng/ml TGF-β2 for 48 hours (TGF) were analyzed using an RNA-Seq. Principal Component Analysis (PCA) plot, which illustrates the distribution of samples across the two conditions and is shown in supplementary figure 18.

Features with a count number less than 10 were filtered out. A total of 61,552 genes were detected in the samples. The expression of 481 genes was found to be significantly different between the two groups (adjusted p-value, padj < 0.05). Figure 18a

shows a volcano plot of all genes with thresholds set at false discovery rate (FDR) = 0.10, and statistical significance of padj < 0.05 and |log2FC| = 1.5. The heat map (Figure 18B) shows the individual donor responses to TGF-β2 and the variability for the top 50 DEGs.

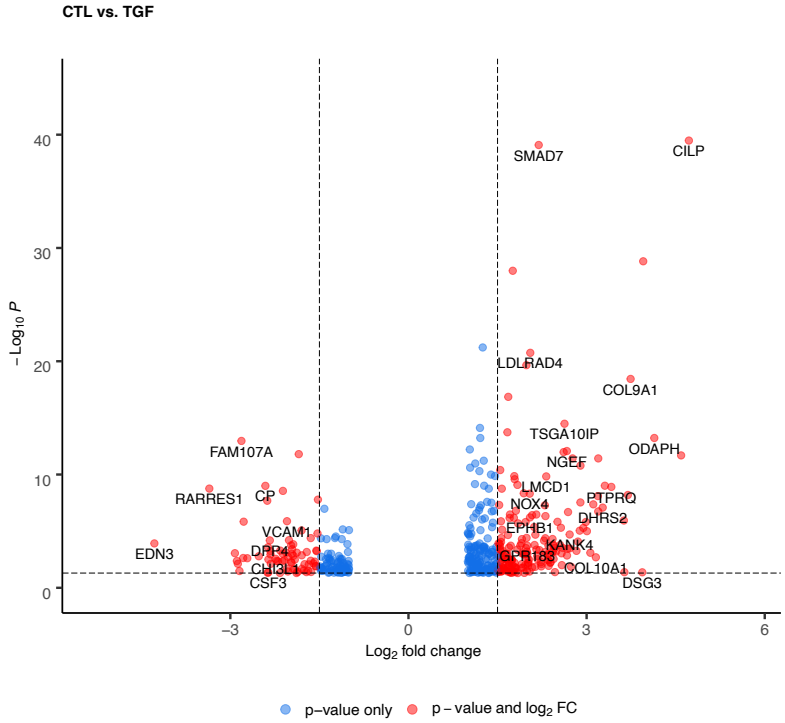

a.

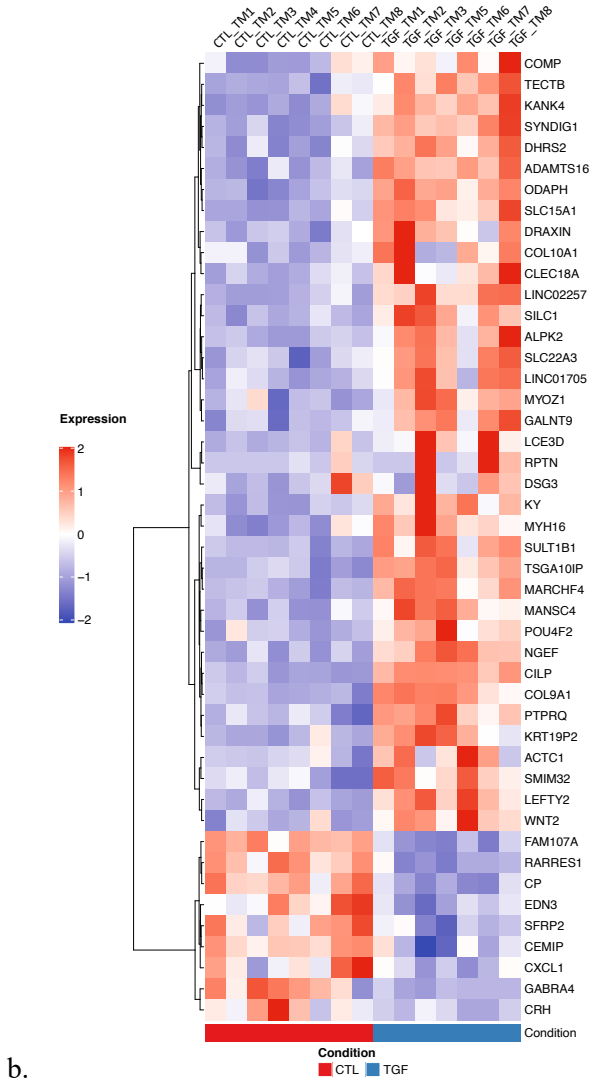

b.

Figure 18 : Differential Gene Expressions in HTMEx following TGF-β2 treatment
a. Volcano plot identifying the genes differentially expressed in response to TGF-β2. Red dots represent the 194 genes that were significantly expressed (padj < 0.05) and showed a high fold-change (|log2FC| > 1.5), among which 140 genes were upregulated, and 54 genes were downregulated. Blue dots represent genes with padj < 0.05 and |log2FC| ≤ 1.5. b. Heatmap showing the expression of the top 50 differentially expressed genes (DEGs). Expression of the 50 top DEGs in log2cpm. Clustering was performed using the Ward D1 method. This heatmap shows correct clustering of up- and downregulated genes and the biological variability between the donors.

The 50 most up- and downregulated genes were ranked by log Fold Change and are shown in Tables 8 and 9, respectively (padj < 0.05, and base mean>50). Among the most expressed genes, 10 coded for components of the ECM (COL7A1, COL9A1, COL10A1, PRG4, ELN, VCAN, HS3ST3A1), its synthesis, degradation, or organization (SERPINE1, ADAM12, BMP2). Understandably, the genes involved in TGF-β signaling were also represented (SMAD7, BMP2, FSTL3, PTK7, LBH, SERPINE1). With regard to the most downregulated genes, they were mainly involved in the regulation of inflammation and response to cytokines (CXCL1, CXCL6, IL6, IL1RL1, CSF3, CHI3L1, VCAM1, CD38, SELE), apoptosis (GAS1, G0S2), metalloprotease inhibitor activity (LXN, RARRES1), or cellular response to corticosteroid stimulus (FAM107A, STC1, CRH, PCK1). When we apply a donor

effect correction, the most up- and down-regulated genes remain the same (supplementary data figure 3 and table 15 and 16).

Tableau 8 : Top 50 upregulated genes (TGF versus CTL)
ranked by binary logarithm of fold change (log2FC). For each gene identifier, name, log2FC, and adjusted p-value (padj) are presented.

Gene ID	Gene Name	log2FC	padj
CILP	Cartilage Intermediate Layer Protein	4.722	3.3E-40
LEFTY2	Left-Right Determination Factor 2	4.592	2.1E-12
ODAPH	Odontogenesis-Associated Phosphoprotein	4.140	6.0E-14
DSG3	Desmoglein 3	3.937	4.3E-02
COL9A1	Collagen Type IX Alpha 1 Chain	3.741	3.7E-19
PTPRQ	Protein-Tyrosine Phosphatase, Receptor-Type	3.417	1.2E-09
DHRS2	Dehydrogenase/Reductase 2	3.271	8.3E-08
SYNDIG1	Synapse Differentiation-Induced Gene 1	3.196	3.8E-12
LINC01705	Long Intergenic Non-Protein Coding RNA 1705	3.196	1.8E-07
TECTB	Tectorin Beta	3.190	8.0E-09
COL10A1	Collagen Type X Alpha-1 Chain	3.156	2.0E-03
SULT1B1	Sulfotransferase Family 1b, Member 1	2.764	3.8E-12
ACTC1	Actin Alpha Cardiac Muscle	2.715	3.4E-04
KANK4	Kn Motif- And Ankyrin Repeat Domain-Containing Protein 4	2.714	2.0E-05
NGEF	Neuronal Guanine Nucleotide Exchange Factor	2.667	8.4E-13
TSGA10IP	Testis Specific 10 Interacting Protein	2.628	3.3E-15
GALNT9	Polypeptide N-Acetylgalactosaminyltransferase 9	2.568	5.0E-06
SLC22A3	Solute Carrier Family 22 (Extraneuronal Monoamine Transporter), Member 3	2.510	1.5E-06
DRAXIN	Dorsal Inhibitory Axon Guidance Protein	2.426	4.9E-05
FOXS1	Forkhead Box S1	2.349	3.5E-03
LMCD1	Lim And Cysteine-Rich Domains 1	2.320	1.5E-10
POSTN	Periostin	2.307	4.7E-07
PRG4	Proteoglycan 4	2.305	4.2E-05
LINC01614	Long Intergenic Non-Protein Coding RNA 1614	2.300	6.9E-04
ENSG00000286013	Novel Transcript	2.297	5.2E-08
SMAD7	Smad Family Member 7	2.193	8.1E-40

LPO	Lactoperoxidase	2.082	3.9E-07
LDLRAD4	Low Density Lipoprotein Receptor Class A Domain-Containing Protein 4; Ldlrad4 [*606571]	2.052	1.8E-21
EPHB1	Ephrin Receptor Ephb1	2.046	6.2E-07
NOX4	NAPDH Oxidase 4	2.042	4.9E-09
GPR183	G Protein-Coupled Receptor 183	2.000	1.9E-04
TSPAN2	Tetraspanin 2	1.989	3.9E-05
GPAM	Glycerol-3-Phosphate Acyltransferase, Mitochondrial	1.986	2.2E-20
SERPINE1	Serpin Family E Member 1 (Plasminogen Activator Inhibitor Type 1)	1.941	4.5E-09
EGR2	Early Growth Response 2	1.846	2.0E-06
ADAM12	ADAM Metallopeptidase Domain 12	1.836	8.3E-10
ENSG00000227619	Novel Transcript	1.810	1.6E-07
APCDD1L	APC Downregulated 1 Like	1.805	4.2E-02
GPR68	G Protein-Coupled Receptor 68	1.788	6.2E-03
LINC01943	Long Intergenic Non-Protein Coding RNA 1943	1.782	1.4E-10
HAS1	Hyaluronan Synthase 1	1.782	1.4E-02
FSTL3	Follistatin-Like 3	1.756	1.0E-28
H1-9P	H1.9 Linker Histone, Pseudogene	1.729	3.7E-03
GXYLT2	Glucoside Xylosyltransferase 2	1.704	6.9E-07
CHAC1	Chac Glutathione-Specific Gamma-Glutamylcyclotransferase 1	1.697	5.4E-03
ZNF365	Zinc Finger Protein 365	1.693	2.8E-04
LBH	Lbh Regulator of Wnt Signaling Pathway	1.681	1.4E-17
PLPP4	Phospholipid Phosphatase 4	1.666	1.9E-14
PLEK2	Pleckstrin 2	1.608	1.9E-02
ASB2	Ankyrin Repeat- And Socs Box-Containing Protein 2	1.594	1.9E-02
COL7A1	Collagen Type VII Alpha 1 Chain	1.558	9.0E-05

Tableau 9 : Top 50 downregulated genes (TGF versus CTL)
ranked by binary logarithm of fold change (log2FC). For each gene identifier, name, log2FC, and adjusted p-value (padj) are shown.

Gene ID	Gene Name	log2FC	padj
EDN3	Endothelin 3	-4.279	1.2E-04
RARRES1	Retinoic Acid Receptor Responder 1	-3.354	1.7E-09
SFRP2	Secreted Frizzled Related Protein 2	-2.889	4.3E-03
CXCL1	C-X-C Motif Chemokine Ligand 1	-2.873	7.6E-03
FAM107A	Family With Sequence Similarity 107 Member A	-2.813	1.1E-13

GABRA4	Gamma-Aminobutyric Acid Type A Receptor Subunit Alpha4	-2.776	1.5E-06
CRH	Corticotropin Releasing Hormone	-2.714	2.4E-03
CEMIP	Cell Migration Inducing Hyaluronidase 1	-2.521	1.6E-03
CP	Ceruloplasmin	-2.410	1.0E-09
LYVE1	Lymphatic Vessel Endothelial Hyaluronan Receptor 1	-2.378	2.1E-08
ADH1B	Alcohol Dehydrogenase 1B (Class I), Beta Polypeptide	-2.366	2.6E-04
CSF3	Colony Stimulating Factor 3	-2.360	4.5E-02
VMO1	Vitelline Membrane Outer Layer 1 Homolog	-2.359	3.1E-03
DPP4	Dipeptidyl Peptidase 4	-2.335	6.5E-05
LINC01235	Long Intergenic Non-Protein Coding RNA 1235	-2.322	1.1E-03
CD38	CD38 Molecule	-2.318	7.6E-03
CHI3L1	Chitinase 3 Like 1	-2.237	2.8E-03
PCK1	Phosphoenolpyruvate Carboxykinase 1	-2.222	4.2E-03
HIGD1B	HIG1 Hypoxia Inducible Domain Family Member 1B	-2.197	4.6E-03
COL14A1	Collagen Type XIV Alpha 1 Chain	-2.160	5.2E-04
ANXA10	Annexin A10	-2.123	4.6E-03
ERP27	Endoplasmic Reticulum Protein 27	-2.119	9.6E-04
STC1	Stanniocalcin 1	-2.114	2.8E-09
GALNT16	Polypeptide N-Acetylgalactosaminyl transferase 16	-2.061	8.1E-04
KIF19	Kinesin Family Member 19	-2.050	2.0E-02
VCAM1	Vascular Cell Adhesion Molecule 1	-2.046	1.3E-06
GABRB1	Gamma-Aminobutyric Acid Type A Receptor Subunit Beta1	-2.012	6.3E-05
MLIP	Muscular LMNA Interacting Protein	-1.980	5.2E-03
SELE	Selectin E	-1.976	1.8E-04
PLA1A	Phospholipase A1 Member A	-1.968	6.1E-03
BMPER	BMP Binding Endothelial Regulator	-1.962	1.0E-03
C2CD4A	C2 Calcium Dependent Domain Containing 4A	-1.960	3.9E-04
IL1RL1	Interleukin 1 Receptor Like 1	-1.941	1.4E-04
BMP5	Bone Morphogenetic Protein 5	-1.938	1.5E-03
LGR5	Leucine Rich Repeat Containing G Protein-Coupled Receptor 5	-1.917	2.3E-02
BANCR	BRAF-Activated Non-Protein Coding RNA	-1.914	3.3E-03
CAMK1G	Calcium/Calmodulin Dependent Protein Kinase IG	-1.881	8.0E-04
LXN	Latexin	-1.847	1.6E-12
TSPAN19	Tetraspanin 19	-1.800	8.6E-06
LINC02289	Long Intergenic Non-Protein Coding RNA 2289	-1.798	1.4E-03
COX4I2	Cytochrome C Oxidase Subunit 4I2	-1.795	2.1E-02
ZCCHC12	Zinc Finger CCHC-Type Containing 12	-1.750	8.3E-03
PIP5K1B	Phosphatidylinositol-4-Phosphate 5-Kinase Type 1 Beta [Source:HGNC Symbol;Acc:HGNC:8995]	-1.713	6.9E-04

SOX1-OT	SOX1 Overlapping Transcript	-1.679	8.6E-03
LINC02432	Long Intergenic Non-Protein Coding RNA 2432	-1.646	4.1E-03
G0S2	G0/G1 Switch 2	-1.646	4.1E-05
AIM2	Absent In Melanoma 2	-1.640	4.0E-02
GALNT15	Polypeptide N-Acetylgalactosaminyltransferase 15	-1.577	4.9E-03
WDR86	WD Repeat Domain 86	-1.552	5.2E-04
GAS1	Growth Arrest Specific 1	-1.545	5.8E-04
ABHD17C	Abhydrolase Domain Containing 17C, Depalmitoylase	-1.532	1.6E-05

Functional Enrichment and Pathway analysis of upregulated genes

Using Reactome enrichment settings on the top 50 DEGs (Figure 19), 14 pathways were found, most related to matrix organization, and TGF and BMP-signaling, and interestingly, there were also pathways involved in ephrin signaling (EPHB2, EPHB1, NGEF).

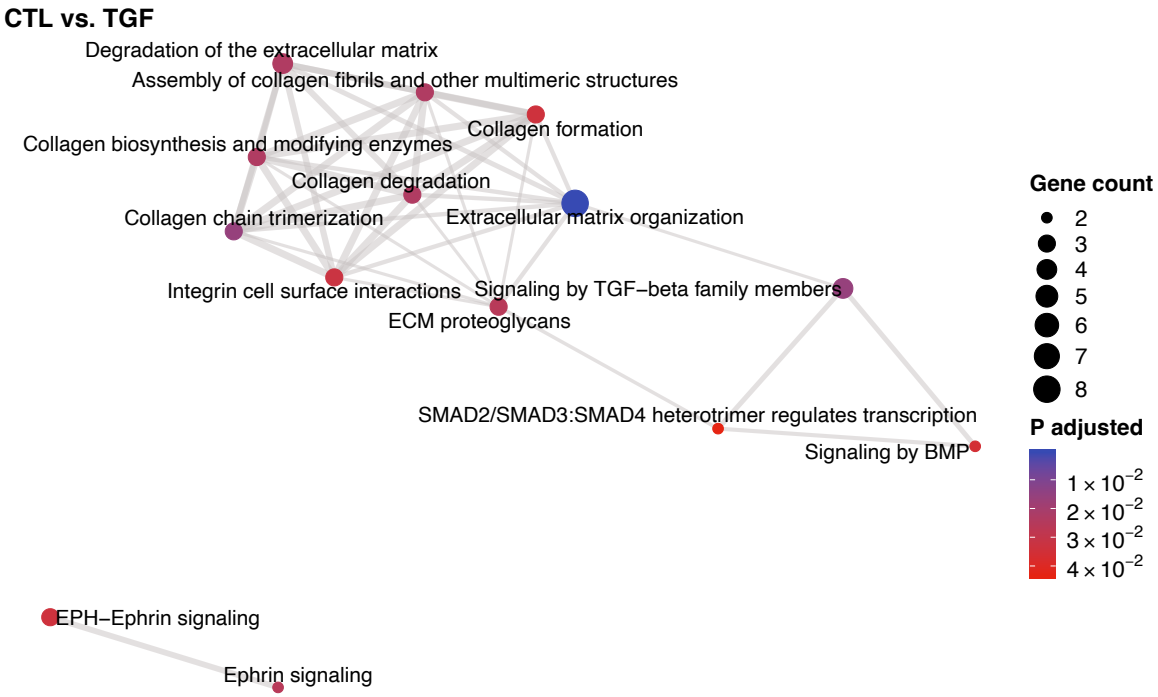

Figure 19 : Reactome enrichment map showing the 14 pathways involved in ECM, TGF-beta, BMP and ephrin signaling.

Using the Cytoscape software (Cytoscape 2.8.3 (http://www.cytoscape.org)[308] overexpression analysis was performed on the list of 109 significantly differentially expressed genes to identify significantly altered pathways in KEGG, Reactome, and enriched biological processes (BP) and molecular functions (MF) in Gene Ontology (GO) and WikiPathway after removing redundant terms. Enrichment results were assumed to be significant when p value < 0.01 and FDR < 0.1. This analysis resulted in a total of 20 enrichment terms containing the majority of DEGs presented in the enrichment

map (Figure 20). This subset of all enriched terms points mainly to ECM organization, ephrin receptor activity, canonical TGF-β pathway and regulation via SMADs, regulation of actin filament-based movement and cellular response to corticosteroid stimulus.

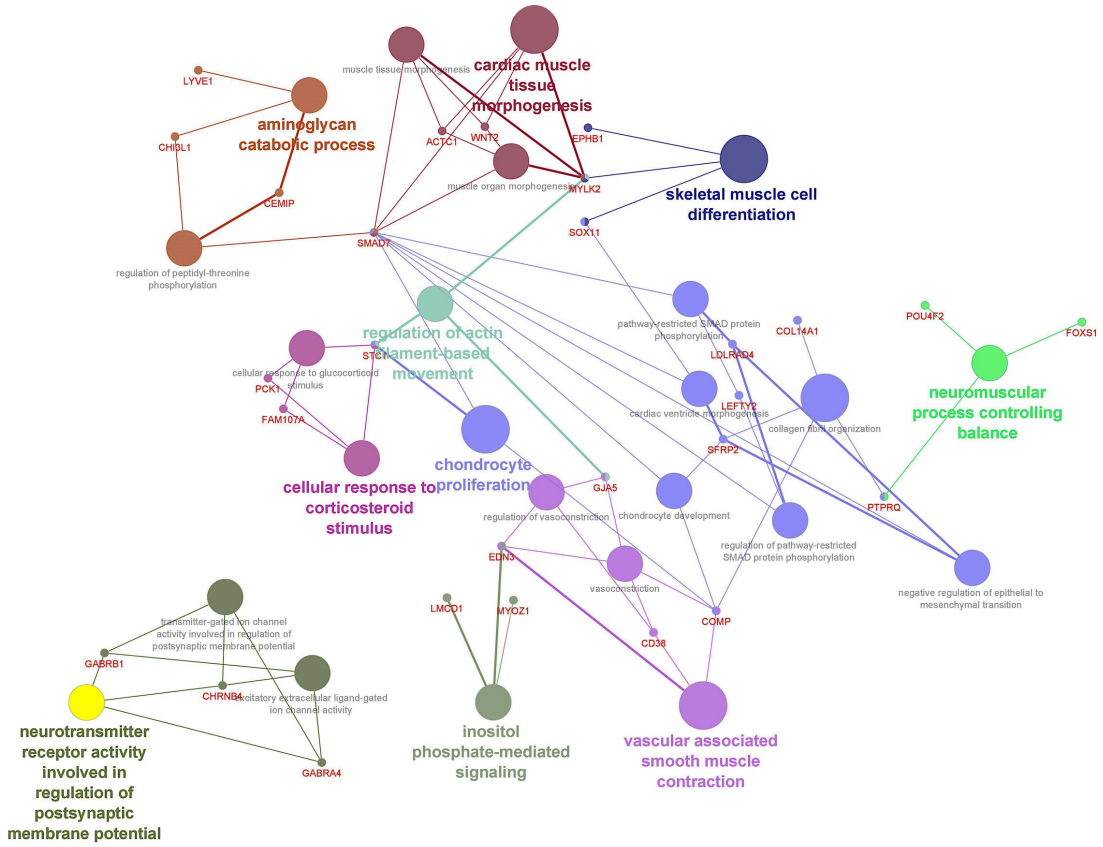

Figure 20 : Cytoscape GO Biological Process enrichment map of the top 109 significantly differentially expressed genes. This analysis found mainly genes related to ECM organization, ephrin receptor activity, canonical TGF-β pathway and regulation via SMADs, regulation of actin filament-based movement, and cellular response to corticosteroid stimulus.

Functional Enrichment and Pathway analysis of downregulated genes

GO BP enrichment analysis shows that genes involved in cellular response to corticosteroid stimulus (FAM107A, STC1, CRH, PCK1) and regulation of cell population proliferation (CSF3, CD38, RARRES1, CRH, VCAM1, DPP4, CXCL1) were significantly downregulated (FDR= 0.008, and 0.037 respectively).

Interestingly, KEGG enrichment analysis of the 50 most downregulated genes revealed the TNF signaling pathway (VCAM1, SELE, CXCL1; FDR=0.0039), which is known to counter-regulate the TGFβ pathway.

Analysis of the genes involved in the organization of the actin cytoskeleton

Since TGF-β2 is known to reorganize the cytoskeleton of TMCs, we were interested in the genes involved in actin and microtubule polymerization, stabilization and organization. Using Pathcards, we identified 186 genes involved in the regulation of the actin cytoskeleton. From these, we identified 19 significantly upregulated genes. The modulation of these genes by TGF-β2 is shown in table 10.

Tableau 10 : DEGs implicated in cytoskeletal organization
listed alphabetically (TGF versus CTL). For each gene identifier (ID), gene name, binary logarithm of fold change (log2FC), and adjusted p-value (padj) are shown.

GeneID	Gene Name	log2FC	padj
ACTC1	Actin alpha cardiac muscle 1	2.71	3.3E-04
ASB2	Ankyrin repeat and SOCS box containing 2	1.59	0.02
FGF1	Fibroblast Growth Factor 1	0.99	5.4E-03
FGF2	Fibroblast Growth Factor 2	0.73	4.8E-03
FGF18	Fibroblast Growth Factor 18	2.00	0.03
GNA13	G Protein Subunit Alpha 13	0.67	8.5E-05
MAPK6	MAP Kinase 6	0.36	0.04
MRAS	Muscle RAS Oncogen Homolog	0.53	0.01
MYH16	Myosin heavy chain 16	2.42	6.9E-04
MYH9	Myosin heavy chain 9	0.76	1.3E-03
MYLK2	Myosin light chain kinase 2	2.21	4.7E-04
NCKAP1	NCK Associated Protein 1	0.41	0.02
NEDD9	Neural precursor cell expressed, developmentally downregulated 9	0.94	1.7E-04
NOTCH2	Notch receptor 2	0.81	2.6E-03
PIK3CD	Phosphatidylinositol-4,5-Bisphosphate 3-Kinase Catalytic Subunit Delta	0.85	0.02
PLEK2	Pleckstrin 2	1.61	0.02
PXN	Paxillin	0.79	1.4E-05
RALA	Ras homolog family member A	0.78	0.01
SLC9A1	Solute Carrier Family 9 Member A1	0.79	4.2E-04

Analysis of genes involved in the TGF-β2, Wnt and BMP signaling pathways

These pathways are interconnected and synergistically or antagonistically participate in multiple cellular processes, including fibrosis [309–311]. TGF-β is predominantly profibrotic, whereas BMP is primarily antifibrotic. The Wnt pathway is another pathway involved in fibrosis that is present in the human TM[185,312]. We analyzed the genes involved in these pathways: transcription factors, activators, repressors and target genes. Figure 21 and table 11 summarize our results.

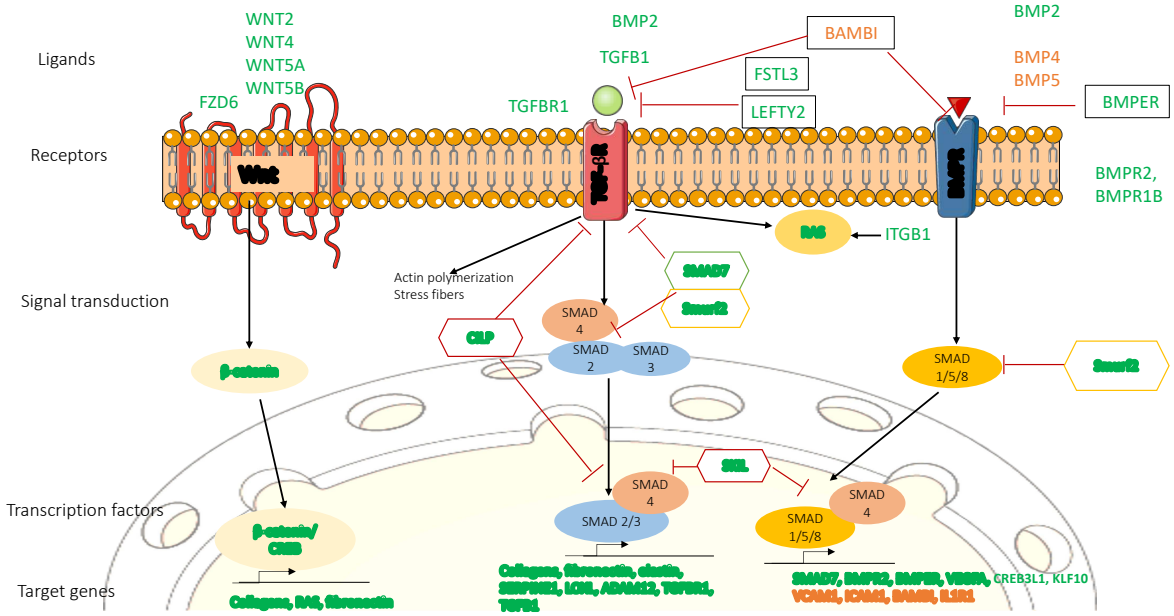

Figure 21 : Schematic representation of DEGs involved in the TGF-β, Wnt, and BMP signaling pathways and their actions.
Green font indicates upregulated genes, and orange font indicates downregulated genes.

Tableau 11 : DEGs implicated in the TGF-β, Wnt, and BMP pathways
listed alphabetically. For each gene identifier (ID), description, binary logarithm of fold change (log2FC), p-value, and adjusted p-value (padj) are shown.

Gene ID	Description	log2FC	padj
ADAM12	ADAM metallopeptidase domain 12	1.84	8.3E-10
ADAMTS10	ADAM metallopeptidase with thrombospondin type 1 motif 10	1.41	6.4E-04
ADAMTS16	ADAM metallopeptidase with thrombospondin type 1 motif 16	2.90	1.6E-11
ADAMTS16-DT	ADAMTS16 divergent transcript	2.03	3.2E-03
ADAMTS3	ADAM metallopeptidase with thrombospondin type 1 motif 3	1.19	8.2E-03
ADAMTS6	ADAM metallopeptidase with thrombospondin type 1 motif 6	1.53	4.9E-08
BAMBI	BMP and activin membrane bound inhibitor	-0.98	4.2E-04
BMP2	bone morphogenetic protein 2	1.55	4.0E-11
BMP4	bone morphogenetic protein 4	-1.26	4.6E-02
BMP5	bone morphogenetic protein 5	-1.94	1.5E-03
BMPER	BMP binding endothelial regulator	-1.96	1.0E-03
BMPR1B	bone morphogenetic protein receptor type 1B	0.76	1.0E-02
BMPR2	bone morphogenetic protein receptor type 2	0.57	2.4E-02
CILP	Cartilage Intermediate Layer Protein	4.72	3.3E-40
COL10A1	collagen type X alpha 1 chain	3.16	2.0E-03
COL1A2	collagen type I alpha 2 chain	0.86	1.8E-02
COL7A1	collagen type VII alpha 1 chain	1.56	9.0E-05
COL9A1	collagen type IX alpha 1 chain	3.74	3.7E-19
CREB3L1	cAMP responsive element binding protein 3 like 1	1.25	1.3E-02
CTNNB1	catenin beta 1	0.59	1.7E-02
ELN	elastin	1.57	3.4E-02
FSTL3	follistatin like 3	1.76	1.0E-28
FZD6	frizzled class receptor 6	0.52	3.9E-02
ICAM1	intercellular adhesion molecule 1	-0.87	1.6E-02
ITGB1	integrin subunit beta 1	1.12	6.9E-10
ITGB1-DT	integrin subunit beta - divergent transcipt	1.52	3.7E-02
ITGB1P1	None	1.06	4.1E-08
KLF10	Kruppel like factor 10	0.91	8.9E-07

LEFTY2	left-right determination factor 2	4.59	2.1E-12
MRAS	muscle RAS oncogene homolog	0.53	1.4E-02
RALA	RAS like proto-oncogene A	0.78	1.0E-02
RASA1	RAS p21 protein activator 1	0.62	8.3E-04
RASA2	RAS p21 protein activator 2	0.40	4.5E-02
RASD1	ras related dexamethasone induced 1	-0.94	1.1E-02
RASGEF1B	RasGEF domain family member 1B	0.91	5.8E-04
RASL11B	RAS like family 11 member B	1.56	6.3E-04
SERPINE1	Serpin family E member 1	1.94	4.5E-09
SKIL	SKI like proto-oncogene	1.13	1.1E-11
SMAD7	SMAD family member 7	2.19	8.1E-40
SMURF2	SMAD specific E3 ubiquitin protein ligase 2	0.64	6.4E-03
TGFB1	transforming growth factor beta 1	0.64	4.1E-02
TGFBR1	transforming growth factor beta receptor 1	0.91	8.6E-04
TGFBR2	transforming growth factor beta receptor 2	-0.67	1.4E-02
VCAM1	vascular cell adhesion molecule 1	-2.05	1.3E-06
VEGFA	vascular endothelial growth factor A	1.24	9.4E-07
WNT2	Wnt family member 2	2.44	1.6E-04
WNT4	Wnt family member 4	1.48	4.6E-02
WNT5A	Wnt family member 5A	1.17	1.1E-02
WNT5B	Wnt family member 5B	1.29	7.4E-07

Discussion

Glaucoma is a disease which stems from increased resistance to outflow at the level of the TM[192]. It is therefore essential to have available a model of this structure that accurately reflects its filtering architecture. Thus, we used the profibrotic, TGF-β2, to mimic the disease on human TM explants. TGF-β2 induced F-actin rearrangements and ECM deposition, modifying the filtering structure of the HTMEx. In this study, we aimed to characterize the transcriptomic differences induced by TGF-β2 in this *in vitro* explant model of pathologic TM. As expected, our results showed that the many differentially expressed genes (DEG) are involved in ECM composition and organization, as well as in the TGF-β, BMP, and Wnt pathways[312,313].

The TGF-β cytokine family is known to be associated with impairments of several cellular functions, including differentiation, proliferation, and accumulation of the ECM. TGF-β2 has a profibrotic effect, and elevated levels of this cytokine have been found in the aqueous humor of patients with glaucoma[207], suggesting that it may play a role in the pathogenesis of ocular hypertension by impairing TM function[207]. TGF-β2 has been used in several studies to replicate the changes seen in the TM of glaucoma patients, as it simultaneously alters the cytoskeleton and the ECM [14,200,262]. The alterations in the trabecular architecture induced by TGF-β2 had already been demonstrated through electron microscopy in perfused human eyes [209]. In this study, we confirmed that TGF-β2 induces expression of ECM proteins, such as collagens, fibronectin, elastin, inhibitors of extracellular matrix degradation such as SERPINE1, cross-linking proteins such as lysyl oxidase (LOX), and LOX-like enzymes.

Recent advances in deep sequencing technology have made it possible to investigate in depth the molecular mechanisms induced by TGF-β. Callaghan *et al.* performed an RNA-Seq analysis of the effect of TGF-β1 and TGF-β2 on primary cultures of HTMC [196,301]. All the DEGs listed by Callaghan *et al.* were also upregulated in our model. Among these DEGs induced by TGF-β2, we found in common SMAD7, LEFTY2 and FSTL3, which inhibit the TGF pathway. We also found NOX4, involved in oxidative stress, as well as LIM and cysteine-rich domains 1 (LMCD1), which is known to induce fibrosis by promoting TGF-β [314].

Furthermore, leveraging the publicly available gene expression profiling datasets, we extended our analysis beyond comparing the most Differentially Expressed Genes (DEGs) between the two methods (HTMEx versus HTM cells culture). We went a step further to compare the gene expression profiles of Callaghan's dissociated HTMC culture model with our HTMEx model, both subjected to TGF-β2 treatment. This allowed us to highlight the genes most modulated based on the respective methodologies employed[301]. In our HTMEx model, using Reactome pathway analysis, we found greater expressions of genes involved in ECM organization (ITGA10, SPP1, ITGB8, CTSV, A2M, ITGB4, PECAM1, BMP2, MMP9, COL9A3), cell junction organization (CLDN4, KRT5, ITGB4, KRT14, CLDN5), integrin cell surface interactions (ITGA10, SPP1, ITGB8, PECAM1, COL9A3), MHC class II antigen presentation (CD74, HLA-DRA, HLA-DPB1, HLA-DPA1, HLA-DRB1, CTSV), and post-translational protein phosphorylation implicated in regulation of Insulin-like Growth Factor (IGF) (VWA1, SPARCL1, SPP1, CHGB, APOE) (Supplementary tables 13 and 14). Thus, we observed that maintaining cells within their original tissue appears to enhance the detection of genes involved in intercellular communication, compared to cultures of dissociated cells. The higher expression of MHC class II molecules in HTMEx compared to dissociated HTMC is probably due to the tissue structure, which potentially includes immune cells, as reported by Patel *et al.* in their single-cell transcriptomics analysis of human outflow tissues[315]. Indeed, there is an increased expression of macrophage gene markers CD14, CD33, LYVE1, C1QB, and TYROBP compared to Callaghan[301].

Progress has been made in the attempt to obtain *in vitro* models that are similar in physiology to the TM. 2D TM cell cultures do not reflect the architecture and the whole cellular environment of the tissue and its ECM, which is essential to its regulation of aqueous humor outflow. Indeed, changes in porosity are a consequence of alterations in morphology and mechanical properties of the interaction between HTMC and the ECM. The rigidity of the culture support also modifies the behavior of the cells[260]. In recent years, partly encouraged by the 3Rs rules (Reduce the number of animals used; Replace the living animal with alternative experimental techniques; and Refine the techniques to minimize animal suffering), advances in 3D cell culture and tissue engineering offer promising approaches to reducing the use of animal models [191,222,227,255]. In fact, conventional 2D cell culture, while allowing the study of biological responses, does not take into account the biomechanical and architectural changes that occur in glaucoma. This gap might be filled by technological advances in *in vitro* TM models[13]. Another

such approach is the use of *ex vivo* HTMEx, which preserves the physiological architecture and the cell-to-cell and cell-to-matrix interactions of the tissue[16]. Indeed, the HTMEx model is a simple and effective way to obtain a 3D model of TM. This model allows the study of the effect of drugs, growth factors, and other molecules on TM function and its role in the pathogenesis of glaucoma. Furthermore, we were able to subdivide the TM from a single donor and study how it changed under different conditions. In addition, although we used TGF-β2 to mimic POAG in this study, other molecules could be utilized to develop models for secondary glaucoma. For example, exposure of the HTMEx to dexamethasone may provide an effective method to study corticosteroid-induced glaucoma, and using TGF-β1 may provide insight into pseudoexfoliative glaucoma[196,199]. The use of benzalkonium chloride or hydrogen peroxide would also be valuable to study the effects of oxidative stress and xenobiotics on HTMEx[222,316].

However, the use of *ex vivo* HTMEx has its own limitations, such as difficulty in obtaining fresh tissue, variability between donors, and limited availability of tissue from glaucoma patients. The availability of corneoscleral rim discarded after corneal transplantation is a valuable source of whole TM tissue. Since TM from glaucoma patients often has a low cell count, the addition of TGF-β2 to healthy TM permits reproduction of the changes in TM cell cytoskeletal organization and ECM compaction, while providing sufficient material for a transcriptomic study[12,239]. However, before conducting RNA-seq analysis on HTMEx, the RNA integrity needs to be assessed.

An important consideration in our study is that control and treated samples were derived from the same donors, but the RNA seq was performed without donor matching to evaluate transcriptional responses to treatment within each sample. We acknowledge the potential for bias due to interindividual variability. To address this limitation, we undertook a complementary analysis by applying a patient effect correction. Upon re-analysis with this correction, we identified a similar set of differentially expressed genes, thereby reinforcing the robustness of our results and underscoring the relevance of our observations beyond the inherent individual variability in samples from the same donors. Furthermore, one limitation of this study is the restricted availability of donor data, particularly pertaining to their medical history, treatments, and medication usage at the time of death. Nevertheless, the absence of alterations in the most differentially expressed genes after correction for donor effects allows us to posit that donor variability does not significantly impact the primary findings.

One of the key advantages of RNA-Seq is its ability to detect low-abundance transcripts that may be missed by traditional microarray-based methods[15]. In the case of TM tissue, the low RNA content makes it difficult to obtain enough material for analysis, but amplification techniques can help to overcome this difficulty by generating enough material for deep sequencing analysis. This approach allows researchers to study the gene expression patterns directly within the TM tissue without the need to manipulate and culture the cells away from their natural environment, providing valuable insights into the molecular mechanisms involved in glaucoma pathology. To go further, and get even closer to

the physiology of the aqueous humor outflow pathways, RNA extraction on HTMEx could be used on the ex vivo model of human corneal rim perfusion organ culture developed by Peng et al[252].

In addition, although we used TGF-β2 to mimic POAG in this study, other molecules could be utilized to develop models for secondary glaucoma. For example, exposure of the HTMEx to dexamethasone may provide an effective method to study corticosteroid-induced glaucoma, and using TGF-β1 may provide insight into pseudoexfoliative glaucoma[196,199]. The use of benzalkonium chloride or hydrogen peroxide would also be valuable to study the effects of oxidative stress and xenobiotics on HTMEx[222,316].

The pathological HTMEx model exposed to TGF-β2 might also be used to study therapeutic molecules. It would be interesting to study the changes achieved with the only therapeutics on the market that specifically target the TM to reduce intraocular pressure (IOP) – ROCK-i [127,277–281]. The Rho GTPase / Rho kinase (ROCK) signaling pathway plays an important role in the modulation of the cytoskeleton of HTMC and synthesis of the ECM[121,274]. Activation of this pathway increases resistance to outflow, while inhibition of it reduces IOP[104,122]. In a previous study using a primary culture of HTMC in 2D and 3D, we demonstrated that the ROCK-i, Y-27632, was able to reverse TGF-β2-induced cytoskeletal and ECM rearrangements[14]. By further exploring the potential of ROCK-i in this HTMEx model, we may gain a deeper understanding of glaucoma pathology and improve treatment options for patients.

In addition, this study highlights that the interrelated Wnt, TGF-β, and bone morphogenic proteins (BMP) pathways, which play critical roles in regulating IOP homeostasis, are modulated in HTMEx exposed to TGF-β2 [313,317,318]. Due to their structural similarity and shared signaling modalities, BMPs are likely to function interactively with TGF-β to participate in various cellular processes such as fibrosis[309–311]. The balance between the activation of TGFβ-dependent SMADs (SMAD2/3) and BMP-dependent SMADs (SMAD1/5/8) is regulated by competition for assembly with SMAD4 and inhibitory action by SMAD7, which downregulates TGFβ1R and SMAD2. It is also worth noting that BMP ligands can bind to and activate TGFβ receptors, allowing BMP2 to induce SMAD2 and SMAD3 phosphorylation[309].

These pathways represent potential therapeutic targets for treating the glaucomatous trabecular meshwork. For instance, BAMBI has been shown to negatively regulate TGFβ signaling, and inhibition of it altered ECM expression in TM and reduced aqueous humor outflow in mice, indicating its potential for regulating IOP and treating glaucoma[319]. Similarly, Smad7 is a key molecular switch that inhibits TGF-β2 signaling, and therapeutic modulation of Smad7 may be a promising approach to influencing ECM turnover in the TM and treating POAG[311].

Wnt/β-catenin signaling in the TM is necessary for maintaining normal IOP, and its inhibition leads to ocular hypertension[320]. The Wnt/β-catenin signaling inhibitor, secreted frizzled-related protein 1 (sFRP1), is increased in glaucomatous TMC as well as in the aqueous humor of glaucoma patients[312]. Cross-inhibition mediated by Smad4 and β-catenin has been described between the TGFβ/Smad and canonical Wnt pathways in the TM[312]. Interestingly, we report herein that TGF-β2 treatment of HTMEx increases the expression of β-catenin and several Wnt ligands (Wnt2, 4, 5) and receptor (FZD6). [301]

The most significant DEG we identified was Cartilage Intermediate Layer Protein (CILP). This protein is a matrix protein of human articular cartilage and has been associated with several cartilage-related diseases[321]. CILP has also been recognized as a significant mediator of cardiac remodeling and heart failure through its role in regulating extracellular matrix (ECM) metabolism. Recent research has shown that CILP-1 may have antifibrotic properties in pressure overload-induced fibrotic remodeling by interfering with TGF-β1 signaling[322–325]. This suggests that CILP could be a promising therapeutic agent to reverse the TM remodeling in glaucoma. However, additional studies are necessary to determine the effect of CILP blockade on ECM protein expression in the TM.

Finally, among the top 50 DEGs after TGF-β2 treatment, we identified genes involved in the ephrin signaling pathway (EPHB2, EPHB1, NGEF). Ephrin signaling has been reported to play a role in axonal survival in a mouse model of glaucoma. A genome-wide expression profiling on leukocytes of patients with POAG reported ephrin receptor signaling among the most significantly altered canonical pathways in POAG [326,327]. There has been limited research on the ephrin signaling pathway in the TM, but a study conducted by Vittal *et al.* reported that ephrin-B2 was upregulated in the TM in response to mechanical stretching[328]. The authors suggested that upregulation of ephrin-B2 could be important for maintaining the ECM of the TM and could be involved in modulating the Rho A-cytoskeletal changes that occur during mechanical stretching of TM cells[328].

This study thoroughly characterizes the genes that are differentially expressed in response to TGF-β2 in human TM tissue. Identification and characterization of TGF-β2-induced differentially expressed genes and pathways in the human TM are crucial for understanding the pathophysiology of glaucoma and developing or testing new therapeutics.

Data Availability

The raw RNA-Seq data was deposited and released in the publicly available GEO database (ID GSE236302, https://www.ncbi.nlm.nih.gov/geo/query/acc.cgi?acc=GSE236302).

Acknowledgments

This work benefited from equipment and services from the iGenSeq core facility, at the Paris Brain Institute (ICM).

Author Contribution statement

J.B and F.B.B and C.B. designed the study. J.B. and F.B.-B. and C.B. wrote the main manuscript text.

S.M.P., A.R.-L.G. A.L. F.B.-B. and C.B contributed to funding acquisition and study design and supervision.

J.B., E.R., K.K., M.A.A., F.B., X.G, S.M.P., A.R.-L.G. A.L. F.B.-B. and C.B. contributed to the acquisition, analysis and interpretation of the data.

J.B. and E.R. did the experiments.

All authors reviewed and approved the submitted version.

Additional information

Competing interests: The authors declare no competing interests.

Supplementary information:

A.

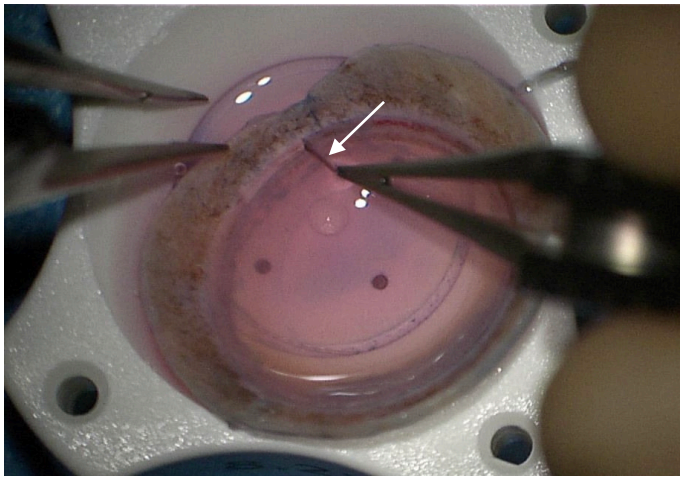

B.

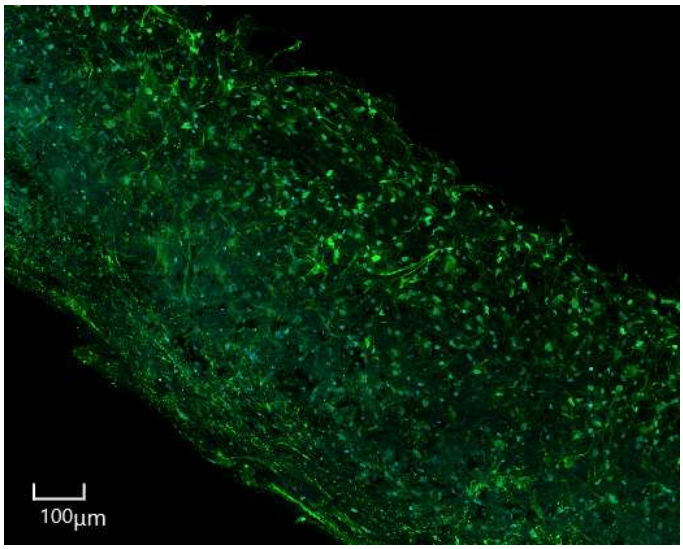

Supplementary figure 1: A. Microscopic photograph showing trabecular meshwork dissection on a human donor corneoscleral ring. The detached trabecular meshwork is indicated by the white arrow. B. Untreated specimen of HTMEx imaged by CellVoyager™ CQ1 (scale bar 100µm). Actin filaments are visualized using the alpha-SMA antibody (green), and nuclei are counterstained with DAPI (blue).

Tableau 12 (supplementary) : donors description.
na: not available, F: female, M: male, date format : dd/mm/yyyy.

Donor	Gender	Age (years)	Cause of death	Date of harvest	Date of dissection
TM1	na	67	respiratory accident	05/05/2022	20/05/2022
TM2	F	86	malignant tumor	31/05/2022	17/06/2022
TM3	M	76	respiratory accident	21/05/2022	15/07/2022
TM4	na	65	heart attack	29/06/2022	21/07/2022
TM5	M	56	malignant tumor	01/07/2022	21/07/2022
TM6	F	78	heart attack	25/05/2022	18/05/2022
TM7	M	79	malignant tumor	29/04/2022	19/05/2022
TM8	M	79	malignant tumor	29/04/2022	19/05/2022

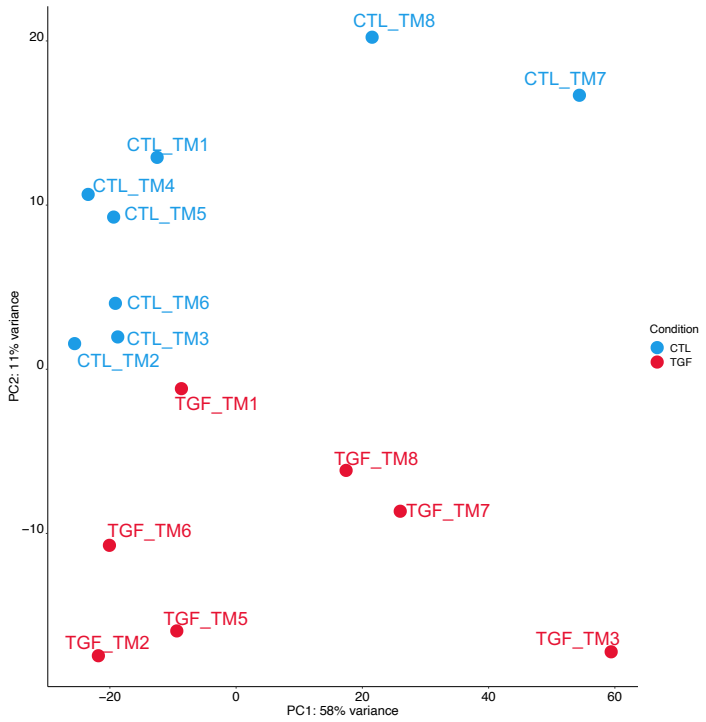

Supplementary figure 2: Principal Component Analysis (PCA) plot showing the distribution of samples across the two conditions (TGF-β2 (TGF) versus vehicle (CTL).

Tableau 13 (supplementary) : Comparison of the gene expression of Callaghan's HTM cell culture model with our HTMEx model, both of which were treated with TGF-β2.
Top 50 upregulated genes (HTMEx vs HTM cells culture), ranked by binary logarithm of fold change (log2FC). For each gene identifier, name, log2FC, and adjusted p-value (padj) are shown.

GeneID	Description	baseMean	log2FC	padj
CDH19	cadherin 19	3836.17	12.68	4.4E-62
KRT6A	keratin 6A	3781.83	12.66	1.6E-18
NPNT	nephronectin	3927.42	12.04	7.4E-48
PCP4	Purkinje cell protein 4	7737.83	11.85	3.0E-66
PTPRZ1	protein tyrosine phosphatase receptor type Z1	1379.00	11.20	5.2E-48
KRT5	keratin 5	1484.33	11.05	1.9E-15
H4C3	H4 clustered histone 3	1924.00	10.68	1.6E-82
S100B	S100 calcium binding protein B	828.42	10.21	5.5E-43
DSG3	desmoglein 3	639.92	10.10	6.0E-11
CLDN5	claudin 5	633.25	10.08	1.4E-37
TYRP1	tyrosinase related protein 1	5970.26	9.91	1.2E-54
PMP2	peripheral myelin protein 2	530.08	9.82	1.5E-39
RNASE1	ribonuclease A family member 1, pancreatic	503.08	9.75	2.3E-36
PLVAP	plasmalemma vesicle associated protein	564.75	9.65	4.0E-34
TYR	tyrosinase	842.50	9.64	3.7E-58
HLA-DRB1	major histocompatibility complex, class II, DR beta 1	1555.00	9.38	1.3E-41
CASQ2	calsequestrin 2	547.92	9.19	1.4E-43
ALKAL2	ALK and LTK ligand 2	1141.00	9.00	2.3E-67
MMP9	matrix metallopeptidase 9	692.92	8.95	2.1E-38
SLC35F1	solute carrier family 35 member F1	512.09	8.92	1.2E-37
TMEM176B	transmembrane protein 176B	2081.34	8.76	5.7E-38

HLA-DRA	major histocompatibility complex, class II, DR alpha	2460.93	8.53	5.2E-45
CCN3	cellular communication network factor 3	2088.11	8.21	4.7E-41
PECAM1	platelet and endothelial cell adhesion molecule 1	904.84	8.16	6.2E-69
KRT14	keratin 14	2734.68	7.87	4.7E-10
PDK4	pyruvate dehydrogenase kinase 4	951.17	7.78	1.0E-60
SMOC2	SPARC related modular calcium binding 2	1152.50	7.74	1.9E-17
TMEM176A	transmembrane protein 176A	942.67	7.73	6.5E-26
ASPA	aspartoacylase	591.59	7.71	1.8E-43
PMEL	premelanosome protein	2020.51	7.58	5.3E-65
COL9A3	collagen type IX alpha 3 chain	878.09	7.55	1.0E-72
CTSV	cathepsin V	928.10	7.39	1.2E-09
ITGB4	integrin subunit beta 4	839.93	7.28	2.9E-67
DES	desmin	2878.21	7.27	1.0E-22
TREM1	triggering receptor expressed on myeloid cells 1	1786.93	7.15	3.6E-33
MT1G	metallothionein 1G	696.84	7.11	3.7E-23
APOE	apolipoprotein E	2698.11	6.98	2.8E-80
ESAM	endothelial cell adhesion molecule	571.25	6.96	5.1E-47
CSF3	colony stimulating factor 3	752.51	6.94	6.5E-19
SBSPON	somatomedin B and thrombospondin type 1 domain containing	968.67	6.86	1.7E-30
IL1RN	interleukin 1 receptor antagonist	649.25	6.82	7.4E-14
PLP1	proteolipid protein 1	1747.18	6.82	1.9E-30
SPARCL1	SPARC like 1	1263.00	6.61	1.5E-25
SPP1	secreted phosphoprotein 1	6442.62	6.57	2.0E-25
CLDN4	claudin 4	703.09	6.57	6.1E-17
CHL1	cell adhesion molecule L1 like	635.77	6.56	5.8E-26
RGS16	regulator of G protein signaling 16	1279.61	6.56	9.0E-138
CXCR4	C-X-C motif chemokine receptor 4	579.09	6.51	3.1E-29
CBLN2	cerebellin 2 precursor	853.08	6.45	2.6E-14
BEX2	brain expressed X-linked 2	527.67	6.40	3.0E-29

Tableau 14 (suppplementary) : Reactome Pathway enrichment results for the top 137 upregulated genes in HTMEx compared to Callaghan's dissociated HTMC culture model.

Description	pvalue	padj	Count	GeneID
Extracellular matrix organization	7.98E-05	0.006	10	ITGA10, SPP1, ITGB8, CTSV, A2M, ITGB4, PECAM1, BMP2, MMP9, COL9A3
MHC class II antigen presentation	0.0003	0.016	6	CD74, HLA-DRA, HLA-DPB1, HLA-DPA1, HLA-DRB1, CTSV
Formation of the cornified envelope	0.0004	0.017	6	KRT5, KRT6A, KRT14, KRT16, KRT17, DSG3
Integrin cell surface interactions	0.0004	0.017	5	ITGA10, SPP1, ITGB8, PECAM1, COL9A3
Cell junction organization	0.0006	0.021	5	CLDN4, KRT5, ITGB4, KRT14, CLDN5
Post-translational protein phosphorylation	0.0013	0.037	5	VWA1, SPARCL1, SPP1, CHGB, APOE
Regulation of Insulin-like Growth Factor (IGF) transport and uptake by Insulin-like	0.0024	0.050	5	VWA1, SPARCL1, SPP1, CHGB, APOE

Growth Factor Binding Proteins (IGFBPs)				
Translocation of ZAP-70 to Immunological synapse	1.05E-05	0.003	4	HLA-DRA, HLA-DPB1, HLA-DPA1, HLA-DRB1
Assembly of collagen fibrils and other multimeric structures	0.0011	0.035	4	CTSV, ITGB4, MMP9, COL9A3
Plasma lipoprotein assembly, remodeling, and clearance	0.0018	0.043	4	A2M, ANGPTL4, APOE, ABCG1
Type I hemidesmosome assembly	6.44E-05	0.006	3	KRT5, ITGB4, KRT14
Plasma lipoprotein remodeling	0.0014	0.038	3	ANGPTL4, APOE, ABCG1
HDL remodeling	0.0024	0.050	2	APOE, ABCG1

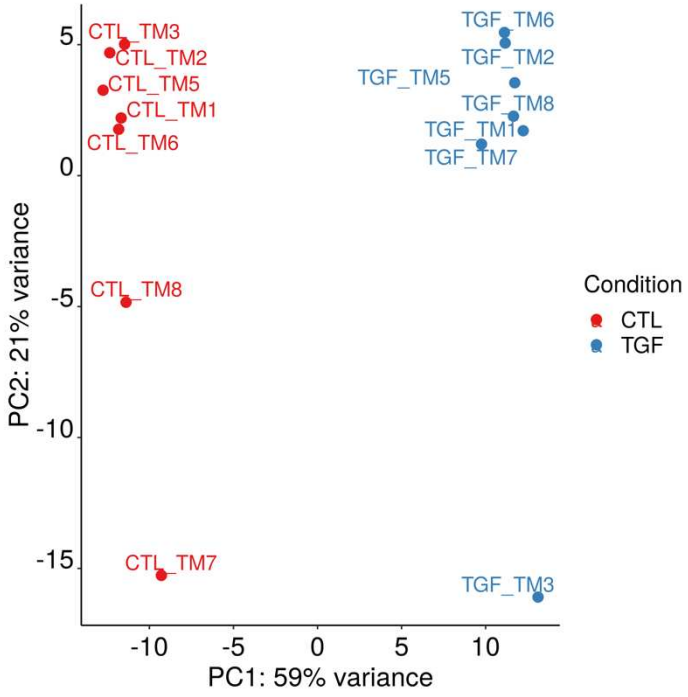

Supplementary figure 3: Principal Component Analysis (PCA) plot showing the distribution of samples across the two conditions (TGF-β2 (TGF) versus vehicle (CTL) after the application of a donor effect correction.

Tableau 15 (supplementary) : Top 50 upregulated genes (TGF versus CTL), ranked by binary logarithm of fold change (log2FC) after we apply a donor effect correction.
For each gene identifier, name, log2FC, and adjusted p-value (padj) are presented.

GeneID	Description	baseMean	log2FC	padj
LEFTY2	Left-right determination factor 2	65.16	5.15	5.55E-59
CILP	Cartilage intermediate layer protein	392.33	4.72	9.55E-291
ODAPH	Odontogenesis associated phosphoprotein	215.39	4.58	1.13E-142
COL9A1	Collagen type IX alpha 1 chain	142.92	3.67	1.06E-122
PTPRQ	Protein tyrosine phosphatase receptor type Q	648.30	3.46	5.70E-242
TECTB	Tectorin beta	53.72	3.43	1.59E-50

DHRS2	Dehydrogenase/reductase 2	170.08	3.38	4.34E-134
SYNDIG1	Synapse differentiation inducing 1	91.49	3.12	7.77E-80
KANK4	KN motif and ankyrin repeat domains 4	122.59	3.07	1.06E-88
TSGA10IP	Testis specific 10 interacting protein	125.20	2.76	3.73E-88
LINC01705	Long intergenic non-protein coding RNA 1705	72.74	2.75	1.65E-40
PRG4	Proteoglycan 4	2234.21	2.63	1.65E-181
SULT1B1	Sulfotransferase family 1B member 1	105.13	2.62	1.52E-69
NGEF	Neuronal guanine nucleotide exchange factor	126.99	2.55	6.88E-82
SLC22A3	Solute carrier family 22 member 3	236.89	2.52	3.32E-119
COL10A1	Collagen type X alpha 1 chain	79.57	2.40	7.03E-50
POSTN	Periostin	469.57	2.31	9.56E-130
GPR183	G protein-coupled receptor 183	436.13	2.30	9.60E-135
GALNT9	Polypeptide N-acetylgalactosaminyltransferase 9	100.83	2.28	1.52E-57
LINC01614	Long intergenic non-protein coding RNA 1614	59.37	2.28	6.52E-37
TSPAN2	Tetraspanin 2	2296.27	2.26	3.29E-193
LMCD1	LIM and cysteine rich domains 1	379.38	2.25	1.08E-115
HAS1	Hyaluronan synthase 1	189.34	2.24	5.94E-76
SMAD7	SMAD family member 7	670.68	2.20	1.55E-151
FOXS1	Forkhead box S1	81.40	2.20	6.44E-46
LPO	Lactoperoxidase	72.93	2.18	1.69E-43
ENSG00000286013	Novel transcript	59.07	2.17	1.21E-36
NOX4	NADPH oxidase 4	1782.80	2.03	4.74E-153
LDLRAD4	Low density lipoprotein receptor class A domain containing 4	532.53	1.99	3.29E-118
SERPINE1	Serpin family E member 1	12978.57	1.99	7.73E-158
ENSG00000227619	Novel transcript	1317.74	1.97	1.54E-134
H1-9P	H1.9 linker histone. pseudogene	75.58	1.95	6.63E-38
ACTC1	Actin alpha cardiac muscle 1	117.98	1.94	2.06E-19
ZNF365	Zinc finger protein 365	308.98	1.93	5.08E-94
GPAM	Glycerol-3-phosphate acyltransferase. mitochondrial	558.50	1.92	4.36E-115
EPHB1	EPH receptor B1	126.42	1.91	7.29E-51
EGR2	Early growth response 2	325.45	1.91	9.76E-94
ALKAL2	ALK and LTK ligand 2	1135.18	1.86	1.12E-104
GPR68	G protein-coupled receptor 68	149.45	1.85	8.98E-37
APCDD1L	APC down-regulated 1 like	88.42	1.81	3.77E-39
LINC01943	Long intergenic non-protein coding RNA 1943	52.89	1.81	5.31E-25
ELN	Elastin	618.11	1.80	1.04E-87
DNAI3	Dynein axonemal intermediate chain 3	497.23	1.79	6.76E-93
ADAM12	ADAM metallopeptidase domain 12	534.74	1.78	6.22E-92
CHAC1	Chac glutathione specific gamma-glutamylcyclotransferase 1	329.52	1.78	5.94E-76

FSTL3	Follistatin like 3	5067.65	1.76	1.38E-129
SH2D2A	SH2 domain containing 2A	56.34	1.74	1.45E-25
GRB14	Growth factor receptor bound protein 14	384.19	1.72	1.51E-80
PLPP4	Phospholipid phosphatase 4	409.79	1.70	3.96E-82
ASB2	Ankyrin repeat and SOCS box containing 2	298.34	1.68	2.13E-72

Tableau 16 (supplementary) : Top 50 downregulated genes (TGF versus CTL), ranked by binary logarithm of fold change (log2FC) after we apply a donor effect correction.
For each gene identifier, name, log2FC, and adjusted p-value (padj) are presented.

GeneID	description	baseMean	log2FoldChange	padj
EDN3	endothelin 3	253,26	-4,12	1,47E-41
SFRP2	secreted frizzled related protein 2	125,38	-3,46	2,87E-74
CEMIP	cell migration inducing hyaluronidase 1	7373,62	-3,27	6,11E-272
RARRES1	retinoic acid receptor responder 1	800,73	-3,23	0,00E+00
ETNPPL	ethanolamine-phosphate phospho-lyase	218,35	-3,14	3,70E-132
FAM107A	family with sequence similarity 107 member A	396,59	-3,09	3,54E-205
PCK1	phosphoenolpyruvate carboxykinase 1	221,74	-2,85	1,22E-118
SCARA5	scavenger receptor class A member 5	462,24	-2,71	1,40E-145
CSF3	colony stimulating factor 3	2611,87	-2,42	2,86E-188
CHI3L1	chitinase 3 like 1	9981,64	-2,41	6,82E-175
CP	ceruloplasmin	438,70	-2,38	8,80E-148
COL14A1	collagen type XIV alpha 1 chain	70,88	-2,25	2,46E-45
HAPLN1	hyaluronan and proteoglycan link protein 1	90,11	-2,25	1,42E-03
STC1	stanniocalcin 1	30126,07	-2,22	1,12E-163
VMO1	vitelline membrane outer layer 1 homolog	1073,45	-2,21	1,54E-181
CXCL1	C-X-C motif chemokine ligand 1	1609,37	-2,21	8,90E-174
VCAM1	vascular cell adhesion molecule 1	2879,62	-2,20	2,95E-153
C2CD4A	C2 calcium dependent domain containing 4A	322,86	-2,20	9,78E-103
DPP4	dipeptidyl peptidase 4	208,57	-2,18	2,52E-93
BMPER	BMP binding endothelial regulator	105,72	-2,17	1,77E-58
CAMK1G	calcium/calmodulin dependent protein kinase IG	85,20	-1,99	3,37E-43
IL1RL1	interleukin 1 receptor like 1	372,21	-1,94	1,41E-93
GPR88	G protein-coupled receptor 88	73,12	-1,83	6,74E-32
SECTM1	secreted and transmembrane 1	103,09	-1,81	9,98E-41
BMP5	bone morphogenetic protein 5	259,91	-1,78	8,12E-78
TMC5	transmembrane channel like 5	187,09	-1,77	1,33E-58

LXN	latexin	1538,74	-1,75	1,12E-108
WFDC1	WAP four-disulfide core domain 1	1141,84	-1,72	4,33E-14
LMLN2	None	102,98	-1,71	6,79E-03
PDE7B	phosphodiesterase 7B	301,00	-1,70	5,34E-68
LINC02432	long intergenic non-protein coding RNA 2432	58,24	-1,68	4,47E-24
LRRN3	leucine rich repeat neuronal 3	148,47	-1,66	3,20E-50
GAS1	growth arrest specific 1	866,51	-1,65	8,64E-83
CD36	CD36 molecule	63,04	-1,64	1,10E-22
MMP3	matrix metallopeptidase 3	3908,43	-1,64	1,54E-93
WDR86	WD repeat domain 86	85,93	-1,62	5,76E-31
ABHD17C	abhydrolase domain containing 17C, depalmitoylase	920,67	-1,61	5,61E-90
G0S2	G0/G1 switch 2	1125,23	-1,58	1,80E-89
SSTR2	somatostatin receptor 2	113,12	-1,57	1,99E-36
CXCL6	C-X-C motif chemokine ligand 6	1288,69	-1,57	2,59E-74
GALNT15	polypeptide N-acetylgalactosaminyltransferase 15	232,20	-1,54	1,23E-55
FGF7	fibroblast growth factor 7	2396,08	-1,54	9,49E-83
BMP4	bone morphogenetic protein 4	509,47	-1,54	1,57E-65
HSD11B1	hydroxysteroid 11-beta dehydrogenase 1	2468,84	-1,53	1,91E-86
CSGALNACT1	chondroitin sulfate N-acetylgalactosaminyltransferase 1	601,01	-1,51	1,28E-66
GABRB1	gamma-aminobutyric acid type A receptor subunit beta1	82,77	-1,50	3,80E-04
IGFBP6	insulin like growth factor binding protein 6	4434,65	-1,49	8,89E-79
ARHGAP29	Rho GTPase activating protein 29	1343,07	-1,49	5,45E-81
S100A8	S100 calcium binding protein A8	299,75	-1,49	7,61E-06
OGN	osteoglycin	88,45	-1,47	1,73E-27

Rôle du TNF-α dans la physiopathologie de la dégénérescence trabéculaire dans le glaucome et équilibre avec le TGF-β2

Contexte et objectif

Nous disposons donc d'un modèle de trabéculum humain *ex vivo* permettant une analyse au niveau de l'organisation de la matrice et des cellules ainsi qu'au niveau moléculaire. Il ouvre un champ de recherche très large couvrant la physiopathologie, la toxicologie, et le criblage de molécules thérapeutiques. Nous avons tout d'abord étudié sur ce modèle l'effet de la cytokine pro-inflammatoire TNF-α, connue pour contrebalancer le TGF-β2. Nous avons pu mesurer leur effet contradictoire sur l'organisation de la matrice, sur les cytokines relarguées par les cellules, et sur la modulation de la transcription des gènes impliqués dans la fibrose, l'inflammation, l'apoptose et la réponse au stress oxydant.

Dans cette étude, nous avons utilisé la technique de RNA-seq pour comparer l'effet du TGF-β2 et du TNF-α, individuellement et combinés, sur des explants de trabéculum humain (HTMEx) en termes de fibrose, d'inflammation, d'apoptose et de réponse au stress oxydant. En menant ces analyses, nous visons à acquérir une compréhension plus complète de la réponse inflammatoire et du remodelage de la MEC dans le trabéculum, ce qui pourrait éventuellement conduire au développement de nouvelles stratégies thérapeutiques pour le glaucome.

Article 4 : Analysis of the TNF-α/TGF-β2 balance in glaucomatous trabecular dysfunction in an ex vivo human trabecular meshwork explant model.

J Buffault, E Reboussin, L Riancho, F Blond, C Baudouin, F Brignole-Baudouin

Introduction

Glaucoma is a leading cause of irreversible blindness worldwide, and elevated intraocular pressure (IOP) is the most significant risk factor for the disease. The trabecular meshwork (TM) is a crucial structure in regulating IOP, and dysfunction of this tissue is strongly associated with glaucoma.

The importance of the balance between transforming growth factor-beta (TGF-β) and tumor necrosis factor-alpha (TNF-α) TNF-α is well known in numerous chronic inflammatory pathologies (Crohn's, sarcoidosis, rheumatoid arthritis)[329,330]. Some anti-TNFs treatments act by increasing the production of TGF-β [331]. The interplay between TGF-β and TNF-α has shown to regulate non-tumorigenic processes such as fibrosis, senescence and autophagy as well [332,333].

TNF-α and TGF-β2 are two cytokines known to be involved in the regulation of the TM. TNF-α is a pro-inflammatory and pro-apoptotic cytokine that plays a major role in glaucomatous optic neuropathy by causing oxidative stress and apoptosis of RGCs [334]. TNF-α has been shown to reduce TM cell viability, while TGF-β2 is known to promote TM cell cytoskeleton reorganizations and ECM synthesis. TGF-β is involved in the physiopathology of tissue repair and fibrosis [262,335]. In contrast, TNF-α has an opposite matrix-remodeling function [336].

In this study, we used a multi-pronged approach, utilizing RNA-seq, quantitative analysis of soluble proteins via multiplex assay, and immunohistochemistry. Our objective was to assess and compare the impact of TGF-β2 and TNF-α, both individually and in combination, on human trabecular meshwork explants (HTMEx). We focused our investigation on key factors including fibrosis, inflammation, apoptosis, and the oxidative stress response within the TM.

Material and methods

Trabecular meshwork sample collection and exposure to TGF-β2 and TNF-α

Human TM were carefully dissected from non-glaucomatous donor tissue corneoscleral rings after corneal graft. All donor tissues were obtained and managed following the guidelines of the Declaration of Helsinki for research involving human tissue. Human tissues were provided by tissue biobank of the *Etablissement Français du Sang* (EFS), which ensured complete anonymization. All donors were aged between 56 and 86 years of age. After dissection, the TM was transported in Cornea Jet conservation medium (Eurobio Scientific, Les Ulis, France) at room temperature (RT). The TM samples were placed in a 12-well plat and stimulated with recombinant human TGF-β2 (PeproTech Inc., cat number 100-35B, Thermo Fisher Scientific, MA, USA) at a concentration of 5 ng/mL or with recombinant human TNF-α (R&D Systems, cat number 210-TA-020, Bio-Techne, MN, USA) at 40ng/ml or both combined for 48 hours in DMEM/F12 (Gibco, cat number 11320), 1% penicillin and streptomycin solution (penicillin 10,000 U/mL, streptomycin 10,000 µg/mL), and 0.001% BSA. Vehicle control explants were incubated with equal volumes of DMEM/F12, 1% penicillin and streptomycin solution (penicillin 10,000 U/mL, streptomycin 10,000 µg/mL), and 0.001% BSA (Sigma, UK).

Immunocytochemistry

The HTMEx were fixed with 4% paraformaldehyde overnight at 4°C and rinsed in 1x PBS before the immunofluorescence procedure. The effects on the organization of both the cytoskeleton and the ECM were characterized in immunocytochemistry using antibodies, anti-alpha-SMA (Rabbit, Abcam ab5694, 1/100 dilution) and anti-fibronectin (Mouse, R&D Systems MAB19181, 1/100 dilution). HTMEx were incubated for 2h at RT in a blocking buffer (5% BSA, 2% Triton X-100, and 0.5% Tween20, in 1x PBS) and left to incubate overnight at 4°C in the incubation buffer (2.5% BSA, 1% Triton X-100 and 0.25% Tween20, in 1x PBS) with the aforesaid antibodies. The HTMEx were then rinsed in 1x PBS and

incubated with the corresponding secondary antibodies (Donkey anti-rabbit, conjugated to Alexa fluor 488 (Thermo Fisher, A21206)), at a dilution of 1/1000 for 1h at RT. The nuclei were stained with DAPI (1/1000). Finally, HTMEx were washed and mounted in Fluoromount (Sigma Aldrich, ref. F4680-25ML). Confocal laser scanning microscopy was performed using an Olympus IX81 confocal microscope coupled to Fluoview software (Olympus, Ver 4.2), and the images were acquired at 200× magnification. Confocal 3D images were processed using Imaris3D® software (Bitplane AG, Zurich, Switzerland). All confocal images from the same experiment were captured using the same laser intensity and gain settings, so that the intensities of different samples could be compared.

Determination of the serum levels of soluble proteins by multiplex Luminex Assay

Supernatants of the HTMEx exposed to various conditions were collected and stored at -80˚C until use. Levels of the following soluble proteins: TNF-α, IFN-γ, IL-6, IL-1β, IL-8, IL-10, CCL2 and matrix metalloproteinase (MMP)-1, -3, -9, and -12 were assayed using the multiplex Human Magnetic Luminex Assay (cat. no. LXSAHM-11; R&D Systems, Inc.) according to the manufacturer's instructions. Quantification of proteins were determined using the Bio-Rad analyzer Bio-Plex 200 System and its software (Bio-Rad Laboratories Inc.). All samples were tested at least in duplicate. The concentration of each soluble protein was normalized to the total amount of protein in each sample quantified with BCA Protein assay (Thermo Scientific Kit Pierce BCA Protein Assay Kit 23227).

RNA-seq of stimulated HTMEx

For whole transcriptome analysis, 15 human HTMEx exposed for 48h to vehicle or TGF-β2 (5ng/ml), or TNF-α (40ng/ml), or both combined were prepared. After tissue lysis, total RNA from HTMEx was extracted using the Nucleo Spin RNA XS kit (Macherey-Nagel ref. 740902.50, Fisher Scientific) according to manufacturer’s specifications. Total RNA was quantified, and its quality was determined using a BioAnalyser 2100 with the RNA 6000 pico Kit (Agilent Technologies, Leuven, Belgium). RNA samples with a RNA intergrity number (RIN) greater than 8 were selected for RNA-seq analysis. 22 mRNA libraries were prepared: 8 control, 7 TGF-β2 treated, 3 TNF-α treated and 4 TGF-β2 and TNF-α combined. Amplification and RNA sequencing experiments were conducted at iGenSeq (Institut du Cerveau (ICM), Paris, France) using SmartSeq (Takara), Nextera XT (Illumina), and NovaSeq 6000 SP Reagent Kit (200 cycles) (Illumina) from 3.5 ng of total RNA per sample.

Normalization and differential expression values were computed with Internet-baseD tool for the Visualization and exploration of RNA-Seq data (EYE DVseq, Institut de la Vision, Paris, France).

Reactome enrichment analysis was carried out to investigate relationships between the significantly expressed genes.

Characterization

TM characterization was carried out as previously reported (article 4).

Results

TGFβ2 and TNF-α induced F-actin rearrangements and ECM deposition in the HTMEx

In contrast to the untreated HTMEx, where alpha-SMA labeling was diffuse in the cytosol, exposure to TGF-β2 at 5ng/ml for 48 hours resulted in rearrangements of actin cytoskeleton, with cells appearing more elongated, and fiber visualization becoming sharper and more extensive (figure 22). Exposure to TNF-α at 40 ng/ml for 48h disrupted actin cytoskeleton and and drastically reduced fibronectin deposits compared to TGF-β2 but also to the control group. When the two treatments were combined, the aspect of the organization of the explant resembled that of TNF-α alone, with cells with a disrupted cytoskeleton and less intense fibronectin labeling (figure 22).

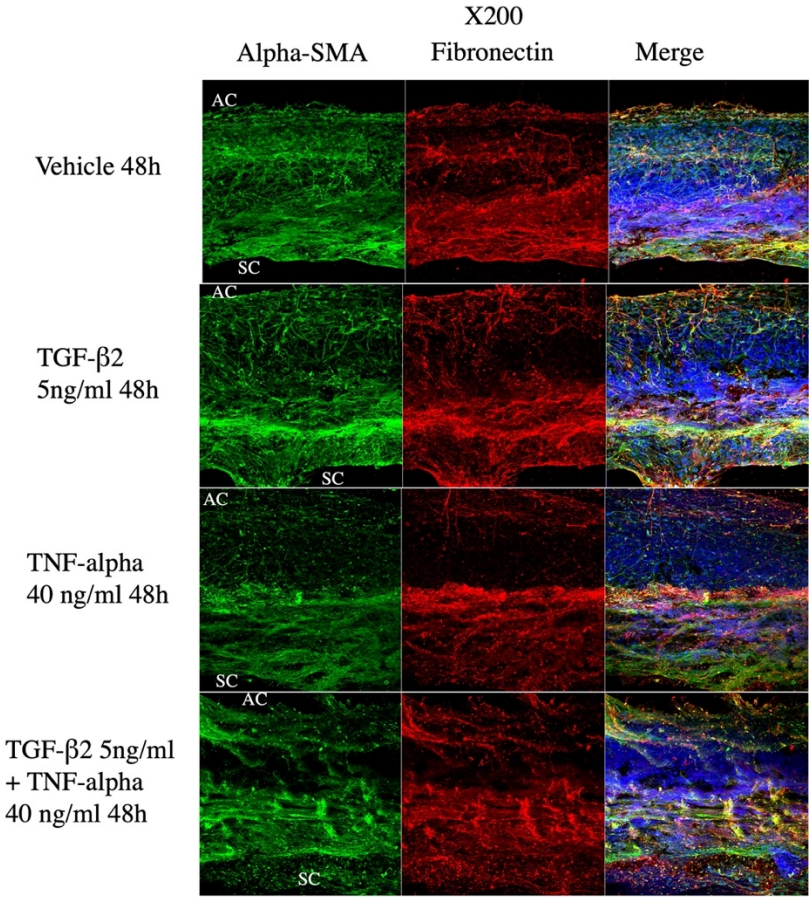

Figure 22 : Representative confocal microscopy images of HTMEx showing cytoskeletal and ECM remodeling after TGF-β2 (5ng/ml), TNF-α (40ng/ml) or both treatments exposure for 48 hours at x200 magnification
F-actin filaments were visualized with anti-alpha-SMA antibody (green), ECM with anti-fibronectin antibody (red) and nuclei were counterstained with DAPI (blue). For each image, the side of the looser TM in relation to the anterior chamber (AC) is at the top and the tighter side in relation with Schlemm's canal (SC) at the bottom. The juxtacanalar region of the TM exhibits a higher labeling intensity of fibronectin and alpha-SMA, with a more intense labeling seen in explants exposed to TGF-β2. TNF-α decreases alpha-SMA and fibronectin labeling in the HTMEx.

Differential Gene Expressions in HTMEx following TNF-α treatments compared to TGF-β2 treatment

To determine changes in gene expressions induced by TNF-α compared to a model reproducing the POAG-associated TM induced by TGF-β2. HTMEx were exposed to 5 ng/ml TGF-β2 for 48 hours or to 40 ng/ml TNF-α for 48h or both treatments for 48 hours and analyzed using RNA-Seq. The top 50 most up- and downregulated genes (TNF-α versus TGF-β2) were ranked by log Fold Change and are shown in Tables 17 and 18, respectively.

Among the most differentially expressed genes (TNF-α versus TGF-β2), eleven coded for chemokines or cytokines (CXCL10, CXCL11, IL1B, CCL20, CCL5, CXCL8, CCL2, IL32, CXCL1, CXCL5, CXCL6) confirming the pro-inflammatory action of TNF alpha. We also observed an effect on the degradation of the ECM with five genes coding for MMPs (MMP12, MMP13, MMP3, MMP1, MMP9), which counteracts the profibrotic action of TGF-β2.

This is consistent with the most downregulated genes (TNF-α versus TGF-β2), that were mainly coding for ECM components (COL9A1, COL10A1, ELN, VCAN, PRG4, COL6A3, COL15A1, SGCD).

Tableau 17 : Top 50 upregulated genes (TNF-α versus TGF-β2)
ranked by binary logarithm of fold change (log2FC). For each gene identifiers, description, base mean, log2FC, and adjusted p-value (padj) are shown.

Gene ID	Description	Base Mean	log2FC	padj
CXCL10	C-X-C motif chemokine ligand 10	617.61	6.85	4.28E-29
OR2I1P	olfactory receptor family 2 subfamily I member 1 pseudogene	480.59	6.33	9.46E-15
PI3	peptidase inhibitor 3	6391.94	6.31	1.30E-08
CXCL11	C-X-C motif chemokine ligand 11	116.70	5.86	6.59E-17
FDCSP	follicular dendritic cell secreted protein	5079.81	5.70	4.24E-16
CLDN1	claudin 1	984.08	5.50	1.02E-04
SELE	selectin E	159.85	5.08	7.26E-19
IDO1	indoleamine 2,3-dioxygenase 1	406.70	5.02	8.95E-23
LCE3E	late cornified envelope 3E	128.49	4.98	2.17E-02
MMP12	matrix metallopeptidase 12	615.86	4.94	1.26E-06
SERPINB2	serpin family B member 2	1347.53	4.94	1.45E-04
IL1B	interleukin 1 beta	521.06	4.61	1.37E-12
MMP13	matrix metallopeptidase 13	112.98	4.56	1.24E-16
CCL20	C-C motif chemokine ligand 20	736.88	4.47	1.75E-17
BIRC3	baculoviral IAP repeat containing 3	4080.23	4.43	1.27E-21
MMP3	matrix metallopeptidase 3	12008.52	4.42	6.16E-14
CSTA	cystatin A	1225.45	4.33	2.97E-02
WFDC2	WAP four-disulfide core domain 2	263.66	4.30	2.18E-07
CCL5	C-C motif chemokine ligand 5	334.09	4.28	4.58E-04
NT	Novel transcript	134.36	4.25	1.89E-14
MRGPRX3	MAS related GPR family member X3	177.35	4.25	2.97E-07
C15orf48	chromosom 15 open reading frame 48	515.23	3.97	7.84E-04

LCE3D	late cornified envelope 3D	361.66	3.96	4.66E-02
CXCL8	C-X-C motif chemokine ligand 8	43716.65	3.94	2.35E-15
MT1G	metallothionein 1G	4850.81	3.85	9.56E-06
CCL2	C-C motif chemokine ligand 2	16788.10	3.79	2.31E-25
CFB	complement factor B	165.68	3.78	3.97E-09
MMP1	matrix metallopeptidase 1	3096.26	3.72	2.13E-13
PNLIPRP3	pancreatic lipase related protein 3	150.55	3.72	1.05E-05
IL32	interleukin 32	1529.96	3.68	1.04E-15
TSLP	thymic stromal lymphopoietin	701.01	3.64	7.63E-12
NT	Novel transcript	108.47	3.62	1.09E-13
MMP9	matrix metallopeptidase 9	4129.18	3.56	1.11E-02
CXCL1	C-X-C motif chemokine ligand 1	3582.41	3.53	2.94E-03
RHBDL2	rhomboid like 2	100.59	3.48	2.88E-02
LRRN3	leucine rich repeat neuronal 3	340.42	3.44	1.54E-10
LINC02732	long intergenic non-protein coding RNA 2732	937.96	3.43	2.91E-06
TNFAIP6	TNF alpha induced protein 6	7123.94	3.32	6.54E-11
TNFAIP3	TNF alpha induced protein 3	2014.08	3.30	9.80E-12
MT1H	metallothionein 1H	955.60	3.30	2.61E-02
VCAM1	vascular cell adhesion molecule 1	4073.91	3.25	1.59E-07
FAM177B	family with sequence similarity 177 member B	285.14	3.21	1.38E-08
SOD2	superoxide dismutase 2	83870.68	3.17	3.16E-11
NOD2	nucleotide binding oligomerization domain containing 2	141.43	3.15	1.09E-09
PTX3	pentraxin 3	931.79	3.14	9.87E-06
GNA15	G protein subunit alpha 15	140.38	3.14	3.67E-02
ICAM1	intercellular adhesion molecule 1	3656.79	3.12	2.66E-12
CXCL5	C-X-C motif chemokine ligand 5	4610.17	3.11	2.19E-07
CXCL6	C-X-C motif chemokine ligand 6	3008.28	3.10	2.01E-04
GCH1	GTP cyclohydrolase 1	394.80	3.09	5.76E-10

Tableau 18 : Top 50 downregulated genes (TNF-α versus TGF-β2)
ranked by binary logarithm of fold change (log2FC). For each gene identifiers, description, base mean, log2FC, and adjusted p-value (padj) are shown.

GeneID	Description	baseMean	log2FC	padj
CILP	cartilage intermediate layer protein	310.10	-6.46	6.75E-21
COL9A1	collagen type IX alpha 1 chain	115.11	-5.45	6.71E-15
COL10A1	collagen type X alpha 1 chain	115.48	-5.23	4.25E-05
WNT16	Wnt family member 16	150.30	-5.03	1.32E-11
DCT	dopachrome tautomerase	491.31	-4.77	1.02E-07
TRPM1	transient receptor potential cation channel subfamily M member 1	158.52	-4.17	1.84E-03
APLNR	apelin receptor	197.07	-4.06	1.53E-02

ELN	elastin	473.74	-3.87	4.82E-07
KANK4	KN motif and ankyrin repeat domains 4	118.93	-3.86	7.40E-06
ACE	angiotensin I converting enzyme	144.89	-3.82	9.13E-06
NOX4	NADPH oxidase 4	1331.63	-3.79	1.03E-12
LINC02192	long intergenic non-protein coding RNA 2192	117.48	-3.77	1.57E-06
AQP7P2	aquaporin 7 pseudogene 2	134.00	-3.60	4.35E-03
PMP2	peripheral myelin protein 2	794.83	-3.55	6.28E-09
PLVAP	plasmalemma vesicle associated protein	696.29	-3.50	4.12E-05
ANGPTL7	angiopoietin like 7	273.06	-3.48	1.48E-06
ADRA2A	adrenoceptor alpha 2A	104.42	-3.47	1.05E-07
VCAN	versican	570.65	-3.41	4.31E-07
PRG4	proteoglycan 4	1961.04	-3.36	5.75E-05
POSTN	periostin	381.57	-3.31	7.03E-08
SCARA3	scavenger receptor class A member 3	3241.88	-3.22	2.31E-07
COL6A3	collagen type VI alpha 3 chain	735.53	-3.15	9.83E-06
PTPRQ	protein tyrosine phosphatase receptor type Q	632.11	-3.14	1.18E-02
CRLF1	cytokine receptor like factor 1	241.37	-3.13	1.69E-04
PMEL	premelanosome protein	2838.29	-3.03	1.77E-02
MFAP4	microfibril associated protein 4	1357.07	-3.01	4.24E-11
ALK	ALK receptor tyrosine kinase	179.27	-2.97	9.46E-07
COL15A1	collagen type XV alpha 1 chain	586.76	-2.97	3.53E-04
GFRA3	GDNF family receptor alpha 3	189.19	-2.96	1.73E-03
SPOCK1	SPARC (osteonectin), cwcv and kazal like domains proteoglycan 1	3636.48	-2.96	3.79E-13
LZTS1	leucine zipper tumor suppressor 1	305.96	-2.92	1.18E-05
SGCD	sarcoglycan delta	314.72	-2.90	1.55E-05
SCG2	secretogranin II	1246.04	-2.88	2.45E-07
LHFPL3-AS1	LHFPL3 antisense RNA 1	142.83	-2.83	1.61E-03
CHST6	carbohydrate sulfotransferase 6	198.82	-2.81	4.97E-04
ITGA11	integrin subunit alpha 11	483.74	-2.80	3.95E-05
FCGR3A	Fc gamma receptor IIIa	175.43	-2.80	1.71E-03
OLFM2	olfactomedin 2	209.83	-2.74	1.05E-07
AEBP1	AE binding protein 1	5609.43	-2.73	8.30E-09
AQP7P1	aquaporin 7 pseudogene 1	190.83	-2.72	5.36E-03
HMCN1	hemicentin 1	743.84	-2.69	4.82E-07
HTRA3	HtrA serine peptidase 3	521.43	-2.67	1.94E-06
NCALD	neurocalcin delta	203.88	-2.66	5.27E-07
DNAI3	dynein axonemal intermediate chain 3	399.73	-2.65	2.91E-05
LRP4	LDL receptor related protein 4	144.66	-2.65	1.15E-06
HEYL	hes related family bHLH transcription factor with YRPW motif like	187.32	-2.65	1.99E-03
ODAPH	odontogenesis associated phosphoprotein	244.47	-2.64	1.11E-02

TYR	tyrosinase	1191.83	-2.64	1.75E-03
NRXN1	neurexin 1	540.28	-2.62	7.40E-03

Functional Enrichment and Pathway analysis of differencially expressed genes

Using Reactome enrichment settings on the top 163 upregulated genes of HTMEx treated with TNF-α vs HTMEx treated with TGF-β2 after applying the following filters: log fold change >1,5 padj <0,05, base mean > 100, 42 pathways were found statistically significant. The main pathways involved were chemokine activity, IL-1 -4 -10 and -13 signaling, IFN-alpha, -beta, gamma signaling, Toll like receptor 2, 3, 4, 6 cascades, NF-kB signaling. The ECM organization, collagen formation and degradation, and MMP activation were also found (figure 23 and table 19).

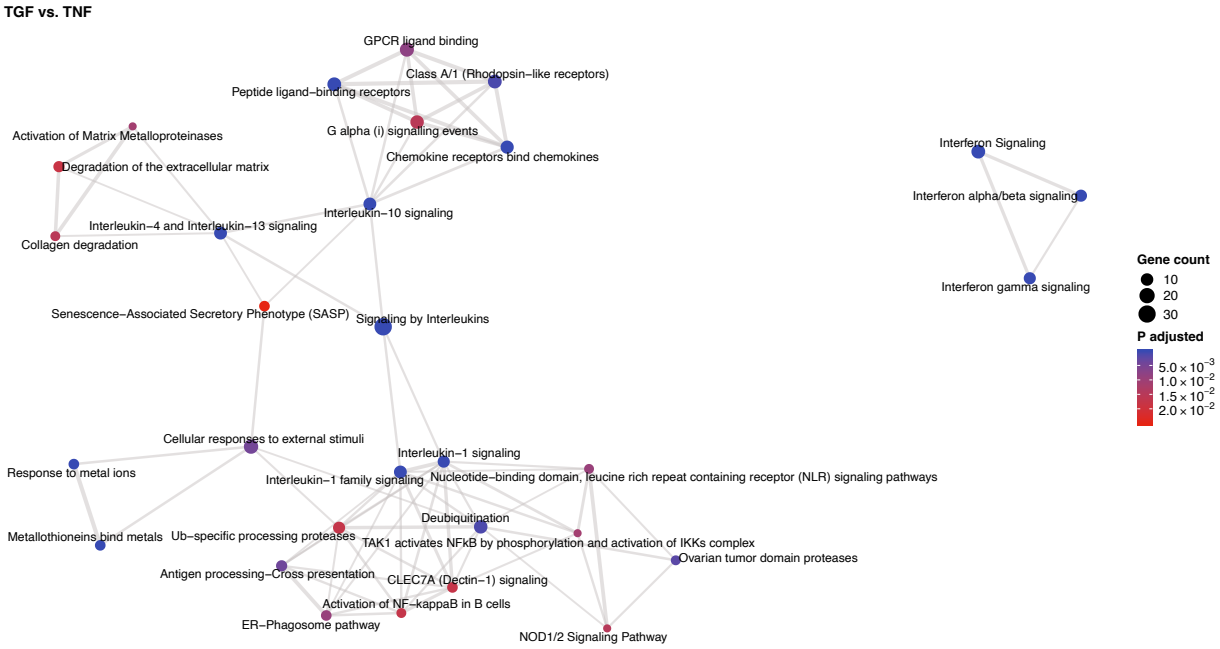

Figure 23 : Reactome enrichment map showing the 42 pathways involved in interleukins signaling, ECM degradation, NF-kB signaling and NOD1/2 signaling.

Tableau 19 : Reactome pathway enrichment table of the most upregulated genes in HTMEx exposed to TNF-α compared with HTMEx exposed to TGF-β2 ranked by gene ratio.

Description	Gene ratio	P adj	Gene id
Chemokine receptors bind chemokines	12/123	5.19E-10	CCL20, CXCL6, CXCL2, CXCL10, CXCL11, CXCL1, CXCL5, CXCL3, CXCL8, CCL5, CCL7, CCL2
Interleukin-10 signaling	11/123	5.69E-10	IL1B, IL1A, CCL20, CXCL2, CXCL10, CXCL1, CXCL8, IL6, CCL5, CCL2, ICAM1
Metallothioneins bind metals	6/123	1.04E-07	MT1M, MT1A, MT1F, MT1X, MT1H, MT1G
Response to metal ions	6/123	5.26E-07	MT1M, MT1A, MT1F, MT1X, MT1H, MT1G
Interleukin-4 and interleukin-13 signaling	11/123	3.12E-06	VCAM1, IL1B, IL1A, CXCL8, IL6, MMP1, MMP3, CCL2, MMP9, ICAM1, JAK3
Interferon signaling	14/123	4.12E-06	VCAM1, GBP3, GBP1, GBP4, IFI6, RSAD2, IRF1, HLA-F, IFIT1, OAS1, OAS3, IFI27, ISG20, ICAM1

Peptide ligand-binding receptors	14/123	4.12E-06	CCL20, CXCL6, CXCL2, CXCL10, CXCL11, CXCL1, CXCL5, CXCL3, CXCL8, BDKRB1, CCL5, CCL7, CCL2, C3
Interferon alpha/beta signaling	9/123	4.30E-06	IFI6, RSAD2, IRF1, HLA-F, IFIT1, OAS1, OAS3, IFI27, ISG20
Interleukin-1 family signaling	11/123	2.69E-05	IL1B, IL1A, IRAK2, PSMB9, IL33, IL18BP, NFKB2, PSME2, NFKBIA, NOD2, PSMB10
Interferon gamma signaling	9/123	4.32E-05	VCAM1, GBP3, GBP1, GBP4, IRF1, HLA-F, OAS1, OAS3, ICAM1
Interleukin-1 signaling	9/123	1.03E-04	IL1B, IL1A, IRAK2, PSMB9, NFKB2, PSME2, NFKBIA, NOD2, PSMB10
Class a/1 (rhodopsin-like receptors)	14/123	1.06E-03	CCL20, CXCL6, CXCL2, CXCL10, CXCL11, CXCL1, CXCL5, CXCL3, CXCL8, BDKRB1, CCL5, CCL7, CCL2, C3
Deubiquitination	13/123	1.20E-03	IFIH1, TNIP3, TNIP1, PSMB9, TNFAIP3, H2BC4, H2BC5, IL33, BIRC3, PSME2, NFKBIA, NOD2, PSMB10
Ovarian tumor domain proteases	5/123	2.10E-03	IFIH1, TNIP3, TNIP1, TNFAIP3, NOD2
Antigen processing-cross presentation	7/123	4.01E-03	CTSS, VAMP8, TLR2, HLA-F, PSMB9, PSME2, PSMB10
Cellular responses to external stimuli	16/123	4.46E-03	IL1A, CXCL8, SOD2, PSMB9, H2BC4, H2BC5, CDK6, IL6, PSME2, MT1M, MT1A, MT1F, MT1X, MT1H, MT1G, PSMB10
Gpcr ligand binding	15/123	7.80E-03	CCL20, CXCL6, CXCL2, CXCL10, CXCL11, CXCL1, CXCL5, CXCL3, CXCL8, ADM, BDKRB1, CCL5, CCL7, CCL2, C3
Er-phagosome pathway	6/123	9.09E-03	VAMP8, TLR2, HLA-F, PSMB9, PSME2, PSMB10
Nucleotide-binding domain, leucine rich repeat containing receptor (nlr) signaling pathways	5/123	9.35E-03	IRAK2, TNFAIP3, BIRC3, NFKB2, NOD2
Activation of matrix metalloproteinases	4/123	1.10E-02	MMP1, MMP3, MMP13, MMP9
Tak1 activates nfkb by phosphorylation and activation of ikks complex	4/123	1.10E-02	IRAK2, NFKB2, NFKBIA, NOD2
Nod1/2 signaling pathway	4/123	1.47E-02	IRAK2, TNFAIP3, BIRC3, NOD2
G alpha (i) signalling events	13/123	1.51E-02	CCL20, CXCL6, CXCL2, CXCL10, CXCL11, CXCL1, CXCL5, CXCL3, CXCL8, RGS10, BDKRB1, CCL5, C3
Collagen degradation	5/123	1.51E-02	MMP1, MMP3, MMP12, MMP13, MMP9
Ub-specific processing proteases	9/123	1.72E-02	IFIH1, PSMB9, H2BC4, H2BC5, IL33, BIRC3, PSME2, NFKBIA, PSMB10
Activation of nf-kappab in b cells	5/123	1.72E-02	NFKBIE, PSMB9, PSME2, NFKBIA, PSMB10
Clec7a (dectin-1) signaling	6/123	1.75E-02	IL1B, PSMB9, NFKB2, PSME2, NFKBIA, PSMB10
Degradation of the extracellular matrix	7/123	1.81E-02	CTSS, ADAMTS9, MMP1, MMP3, MMP12, MMP13, MMP9
Senescence-associated secretory phenotype (sasp)	6/123	2.50E-02	IL1A, CXCL8, H2BC4, H2BC5, CDK6, IL6
Zbp1(dai) mediated induction of type i ifns	3/123	2.50E-02	DTX4, NFKB2, NFKBIA
Toll-like receptor cascades	7/123	2.95E-02	CTSS, IRAK2, TLR2, BIRC3, NFKB2, NFKBIA, NOD2
Extracellular matrix organization	10/123	3.19E-02	VCAM1, CTSS, ADAMTS9, COL22A1, MMP1, MMP3, MMP12, MMP13, MMP9, ICAM1
Diseases of immune system	3/123	3.19E-02	TLR2, NFKB2, NFKBIA

Diseases associated with the tlr signaling cascade	3/123	3.19E-02	TLR2, NFKB2, NFKBIA
Traf6 mediated nf-kb activation	3/123	3.19E-02	IFIH1, NFKB2, NFKBIA
Downstream signaling events of b cell receptor (bcr)	5/123	3.26E-02	NFKBIE, PSMB9, PSME2, NFKBIA, PSMB10
Toll like receptor 4 (tlr4) cascade	6/123	4.40E-02	IRAK2, TLR2, BIRC3, NFKB2, NFKBIA, NOD2
Collagen formation	5/123	4.40E-02	CTSS, COL22A1, MMP3, MMP13, MMP9
Toll like receptor 3 (tlr3) cascade	5/123	4.98E-02	IRAK2, BIRC3, NFKB2, NFKBIA, NOD2
Nik-->noncanonical nf-kb signaling	4/123	4.98E-02	PSMB9, NFKB2, PSME2, PSMB10
Myd88:mal(tirap) cascade initiated on plasma membrane	5/123	4.98E-02	IRAK2, TLR2, NFKB2, NFKBIA, NOD2
Toll like receptor tlr6:tlr2 cascade	5/123	4.98E-02	IRAK2, TLR2, NFKB2, NFKBIA, NOD2

Regarding the 184 downregulated genes of HTMEx treated with TNF-α vs HTMEx treated with TGF-β2 after applying the following filters: log fold change <-1, 5, p adj <0, 05, base mean > 100, 24 pathways were found statistically significant. They were mostly involved in ECM components formation or assembly (table 20).

Tableau 20 : Reactome pathway enrichment table of the most downregulated genes in HTMEx exposed to TNF-α compared with HTMEx exposed to TGF-β2 ranked by gene ratio

Description	Gene Ratio	P adj	Gene ID
ECM proteoglycans	13/116	2.29E-10	FMOD, COL6A3, VCAN, SPARC, COL9A1, SERPINE1, COL1A2, BGN, COL5A1, LRP4, COL4A2, COL1A1, TGFB1
Assembly of collagen fibrils and other multimeric structures	12/116	2.29E-10	LOXL3, COL6A3, COL8A1, COL10A1, COL9A1, PCOLCE, COL1A2, COL15A1, COL5A1, COL4A2, LOXL1, COL1A1
Collagen formation	12/116	2.07E-08	LOXL3, COL6A3, COL8A1, COL10A1, COL9A1, PCOLCE, COL1A2, COL15A1, COL5A1, COL4A2, LOXL1, COL1A1
Collagen chain trimerization	9/116	6.41E-08	COL6A3, COL8A1, COL10A1, COL9A1, COL1A2, COL15A1, COL5A1, COL4A2, COL1A1
Collagen biosynthesis and modifying enzymes	10/116	1.54E-07	COL6A3, COL8A1, COL10A1, COL9A1, PCOLCE, COL1A2, COL15A1, COL5A1, COL4A2, COL1A1
Crosslinking of collagen fibrils	6/116	1.30E-06	LOXL3, PCOLCE, COL1A2, COL4A2, LOXL1, COL1A1
Collagen degradation	9/116	1.30E-06	COL6A3, COL8A1, COL10A1, COL9A1, COL1A2, COL15A1, COL5A1, COL4A2, COL1A1
Integrin cell surface interactions	9/116	1.30E-05	COL6A3, COL8A1, COL10A1, COL9A1, COL1A2, COL5A1, COL4A2, ITGA11, COL1A1
Degradation of the extracellular matrix	11/116	1.30E-05	COL6A3, COL8A1, COL10A1, COL9A1, COL1A2, ELN, COL15A1, COL5A1, A2M, COL4A2, COL1A1
Elastic fibre formation	7/116	1.75E-05	LTBP1, LOXL3, ELN, LTBP2, LOXL1, MFAP4, TGFB1
Non-integrin membrane-ECM interactions	7/116	1.07E-04	NRXN1, COL10A1, COL1A2, COL5A1, COL4A2, COL1A1, TGFB1

Binding and Uptake of Ligands by Scavenger Receptors	6/116	1.70E-04	STAB1, SPARC, COL1A2, CD163, COL4A2, COL1A1
Signaling by Receptor Tyrosine Kinases	17/116	3.75E-04	NGF, COL6A3, PDGFRB, MEF2C, SPARC, COL9A1, VEGFA, TNS3, COL1A2, COL5A1, DNM1, PDGFD, ADAM12, FLT1, COL4A2, CILP, COL1A1
Signaling by PDGF	6/116	9.86E-04	COL6A3, PDGFRB, COL9A1, COL5A1, PDGFD, COL4A2
Molecules associated with elastic fibres	5/116	1.31E-03	LTBP1, ELN, LTBP2, MFAP4, TGFB1
Platelet activation, signaling and aggregation	11/116	3.01E-03	SPARC, F2R, VEGFA, SERPINE1, COL1A2, CLU, ADRA2A, A2M, COL1A1, TGFB1, TIMP3
Syndecan interactions	4/116	4.25E-03	COL1A2, COL5A1, COL1A1, TGFB1
Platelet degranulation	7/116	1.03E-02	SPARC, VEGFA, SERPINE1, CLU, A2M, TGFB1, TIMP3
Anchoring fibril formation	3/116	1.03E-02	COL1A2, COL4A2, COL1A1
Response to elevated platelet cytosolic Ca2+	7/116	1.20E-02	SPARC, VEGFA, SERPINE1, CLU, A2M, TGFB1, TIMP3
Diseases associated with glycosaminoglycan metabolism	4/116	1.70E-02	FMOD, VCAN, BGN, CHST6
MET promotes cell motility	4/116	1.70E-02	TNS3, COL1A2, COL5A1, COL1A1
Scavenging by Class A Receptors	3/116	1.72E-02	COL1A2, COL4A2, COL1A1
NCAM1 interactions	4/116	1.72E-02	COL6A3, COL9A1, COL5A1, COL4A2

Exploration of the genes expression and cytokines release involving M1 and M2 states of inflammation.

To investigate the immunomodulatory influence of TGF-β2 and TNF-α exposures on the HTMEx model, we analyzed inflammation polarization markers through the mRNA expression and cytokine release in the supernatant of HTMEx of type M1 *classically activated*, namely TNF, IL1β, IL6, IL8 (CXCL8), CCL2 and CD38 and M2 *alternatively activated*, namely TGFB1, TGFB2, IL4, IL10, PPARG, HMOX1, SLC40A1 and CD163 [337–339]. Our data showed that mRNA expression of M1 phenotype markers IL8 (CXCL8) and CCL2 levels were significantly higher in in presence of TNF-α 40ng/ml (alone or combined with TGF) compared to the control group ($P<0.05$). mRNA expression of the M1 marker IL8 (CXCL8), and CCL2 were significantly lower in the TGF-β2 group compared to the control group ($P<0.05$) (figure 24 a.). The mRNA expression levels of the markers of M2 state of inflammation, TGFB1, PPARG, SLC40A1, and CD163 were significantly lower after TNF-α stimulation compared to the control group ($P<0.05$). mRNA expression of the M2 marker IL4, TGFB2, and SLC40A1 were significantly lower in the combined group compared to the control group ($P<0.05$). Only mRNA expression of the M2 marker HMOX1 was significantly upregulated in presence of TGF-β2 compared to the control group (figure 24 b.). To complete gene expression analysis by RNA seq, we measured the levels of these cytokines in HTMEx supernatants exposed to TGF-β2 and TNF-α, either individually or in combination using a multiplex assay. The results were not statistically significant, but a trend was nevertheless observed that corroborated the results obtained by RNAseq (figure 24 c.). TGF-β2 and

TNF-α have an opposite effect on immunomodulation in HTMEx. TNF-α enhanced the expression of M1 and reduced the expression of M2 inflammatory markers.

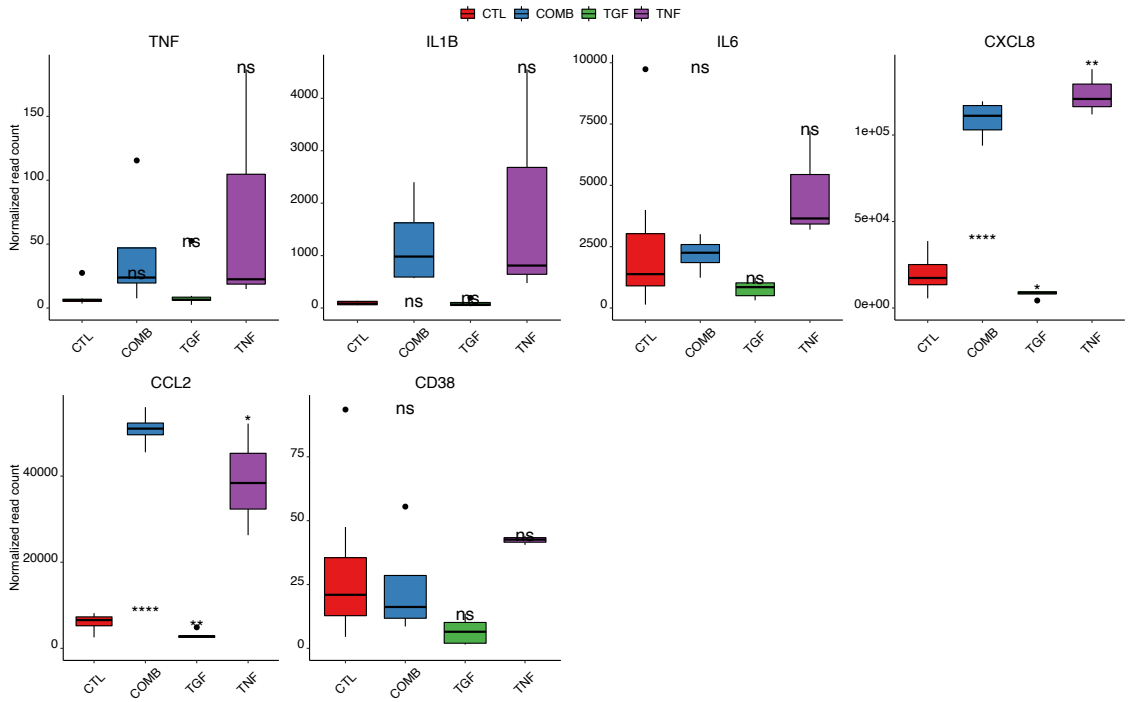

a.

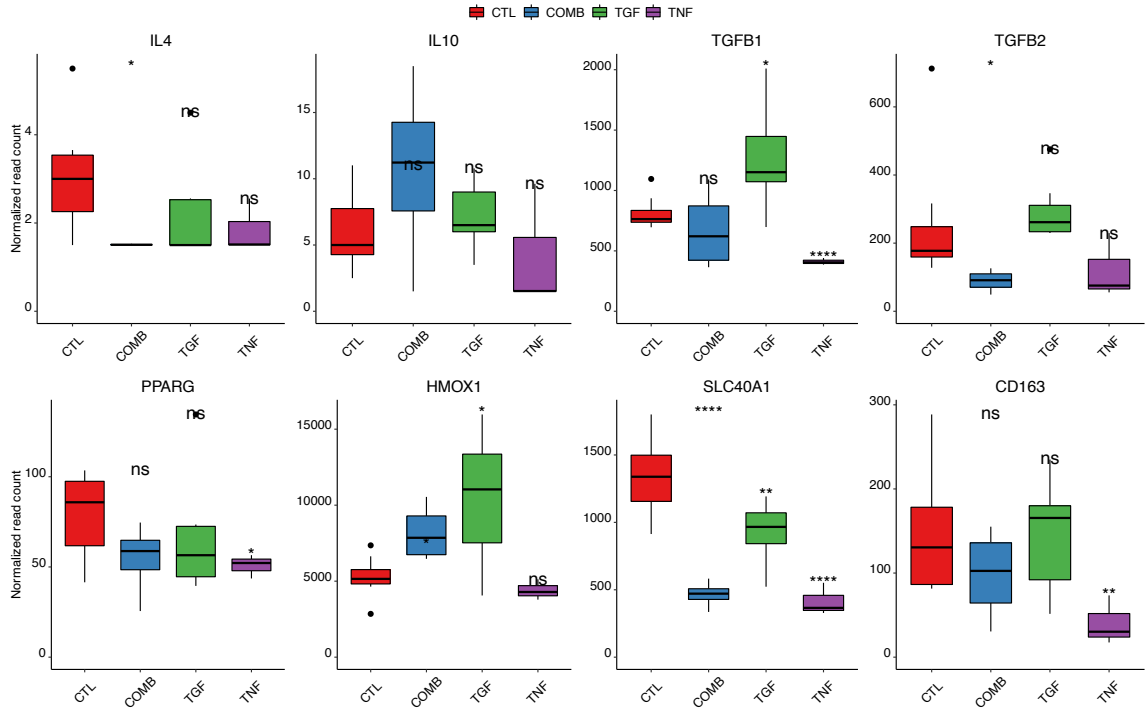

b.

c.

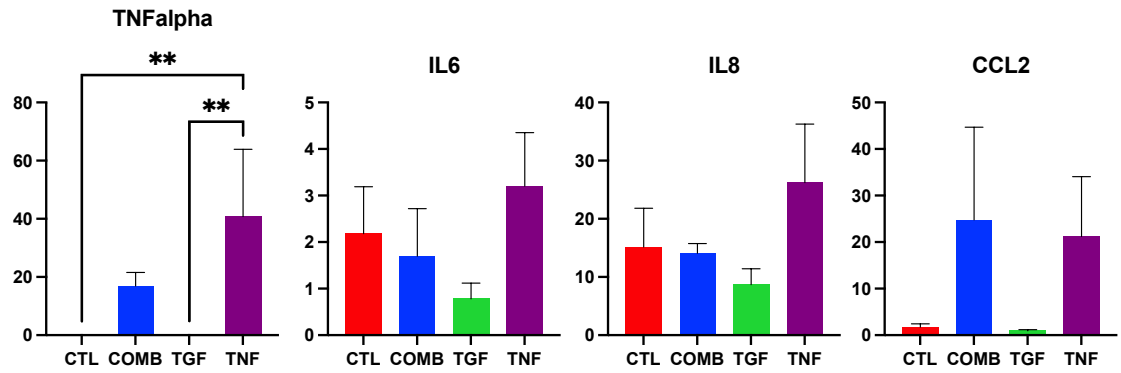

Figure 24 : Exploration of the genes expression and cytokines release involving M1 and M2 states of inflammation. RNA-seq analysis of M1 (a.) and M2 (b.) phenotype marker expression in HTMEx exposed to DMEM/F12 only (CTL) , TGF 5ng/ml 48h (TGF) , TNF-α 40ng/ml 48h (TNF) or both combined for 48h (COMB) c: cytokines levels in supernatants of HTMEx exposed to DMEM/F12 only (CTL) , TGF 5ng/ml 48h (TGF) , TNF-α 40ng/ml 48h (TNF) or both combined for 48h (COMB). *P<0.05, **P< 0.01, ***P<0.001, ****P<0.0001.

Exploration of the gene expression and cytokine release involving ECM turnover

Additionally, we analyzed the turnover of ECM components in the TM. MMPs are responsible for ECM degradation, while TIMPs and ADAMs regulate MMP activity. Gene expression modulation is reported in figure 25 a. To determine the levels of MMP-1, -3, -9, and -12 in the supernatant of HTMEx exposed to TNF-α and TGF-β2, we used a Luminex assay (figure 25b.). TNF-α produced increases in MMP1, MMP-3 and MMP-12 but not in MMP-9 and MMP13. Its presence also decreases TIMP 3 and 4 expressions as well as ADAMTS1, ADAMTS5, ADAMTS15, ADAM23, and ADAM33 expressions. As for TGF-β2, HTMEx treated with TGF-β2 showed reduced expression of MMP1, and MMP3 and upregulation of ADAMTS3. TGF-β2 and TNF-α have an opposite effect on ECM organization in HTMEx. TNF-α promoting its degradation, and TGF-β2 its synthesis.

a.

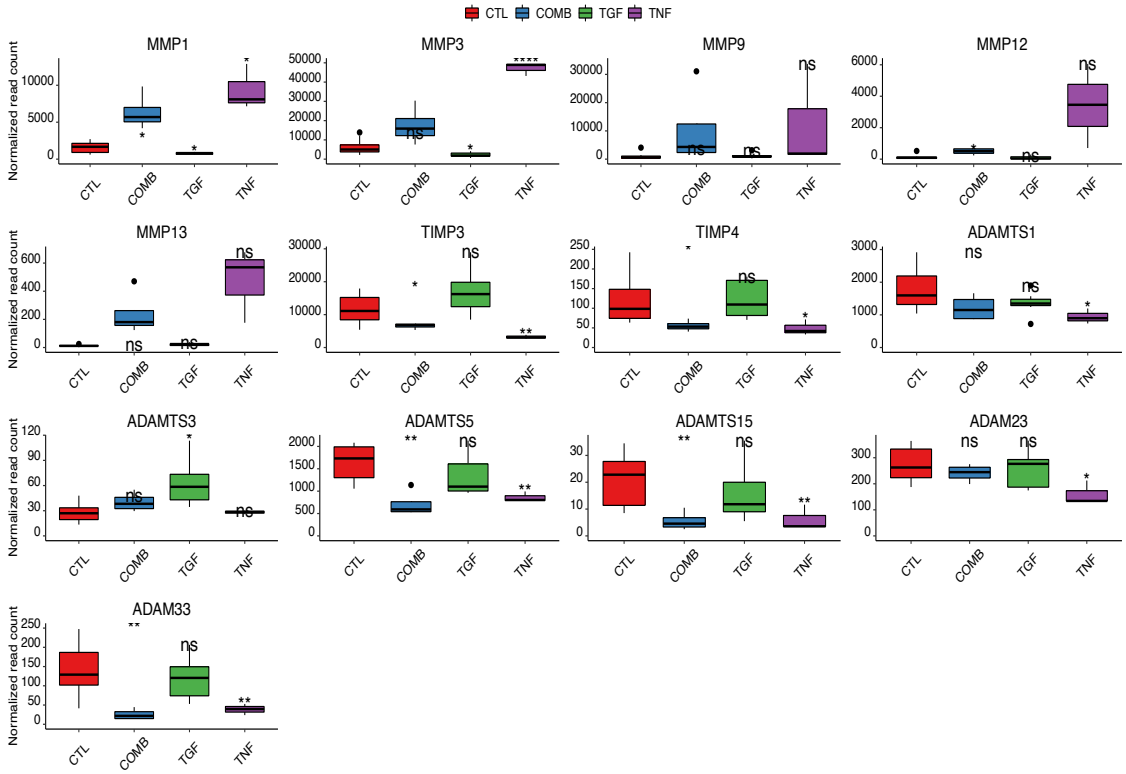

b.

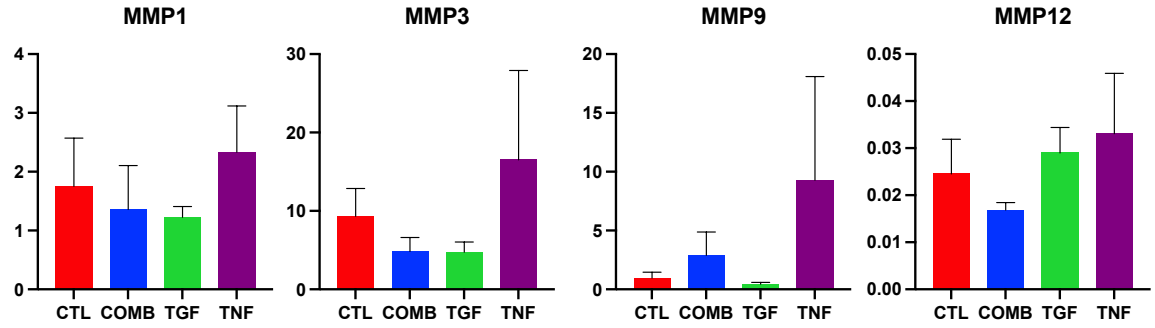

Figure 25 : Exploration of the gene expression and cytokine release involving ECM turnover
a. RNA-seq analysis of ECM organization genes expression in HTMEx exposed to DMEM/F12 only (CTL), TGF-β2 5ng/ml 48h (TGF), TNF-α 40ng/ml 48h (TNF) or both combined for 48h (COMB) b. MMP levels in supernatants of HTMEx exposed to DMEM/F12 only (CTL) , TGF-β2 5ng/ml 48h (TGF) , TNF-α 40ng/ml 48h (TNF) or both combined for 48h (COMB). *P<0.05, **P< 0.01, ***P<0.001, ****P<0.0001.

Role of TNF-α and TGF-β2 in fibrosis

TGF-β triggers NF-κB signaling by a sequential regulation of TAK1 and IKK kinases which leads to the phosphorylation of Iκ-Bα followed by nuclear translocation of RELA (p65). NF-κB signaling induces the expression of SMAD7, which in turn suppresses TGF-β-induced Smad2/3 phosphorylation and activation. Figure 26 summarizes the regulatory effect of TNF-α and TGF-β on different proteins in terms of fibrosis.

a.

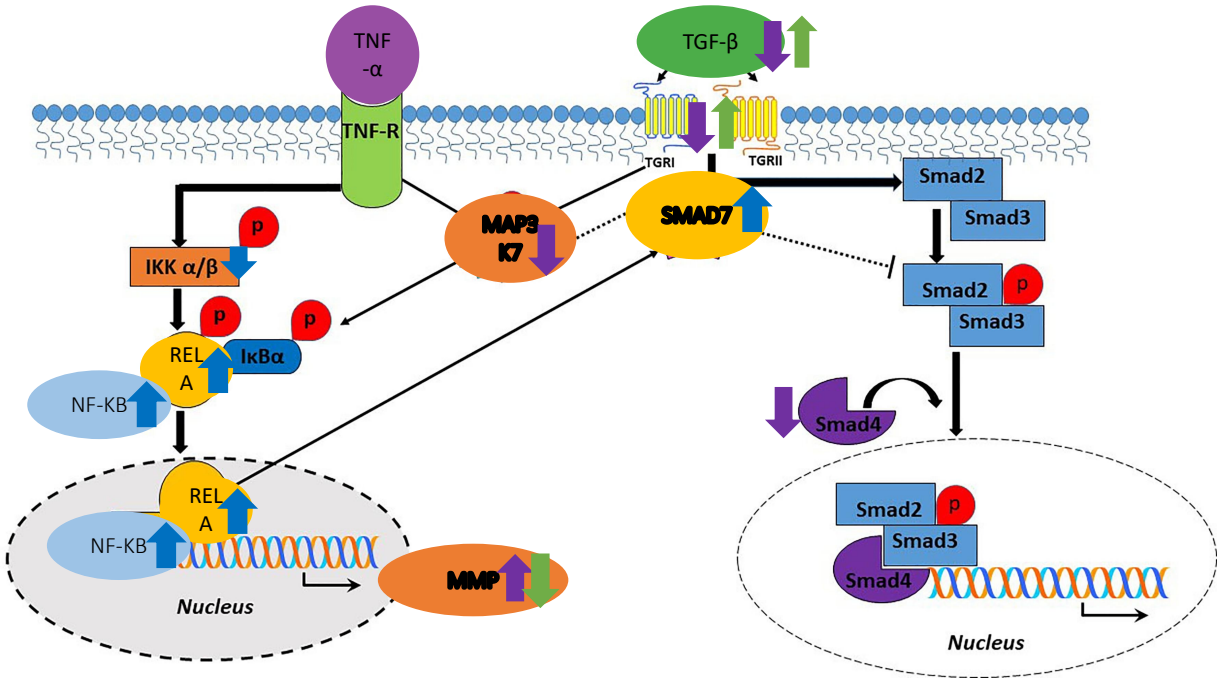
TNF
-α
TNF-R
TGF-β
TGRI
TGRII
MAP3
K7
SMAD7
Smad2
Smad3
Smad2
p
Smad3
IKK α/β
p
p
REL
A
IκBα
NF-KB
Smad4
REL
A
NF-KB
Nucleus
MMP
Smad2
p
Smad3
Smad4
Nucleus

b.

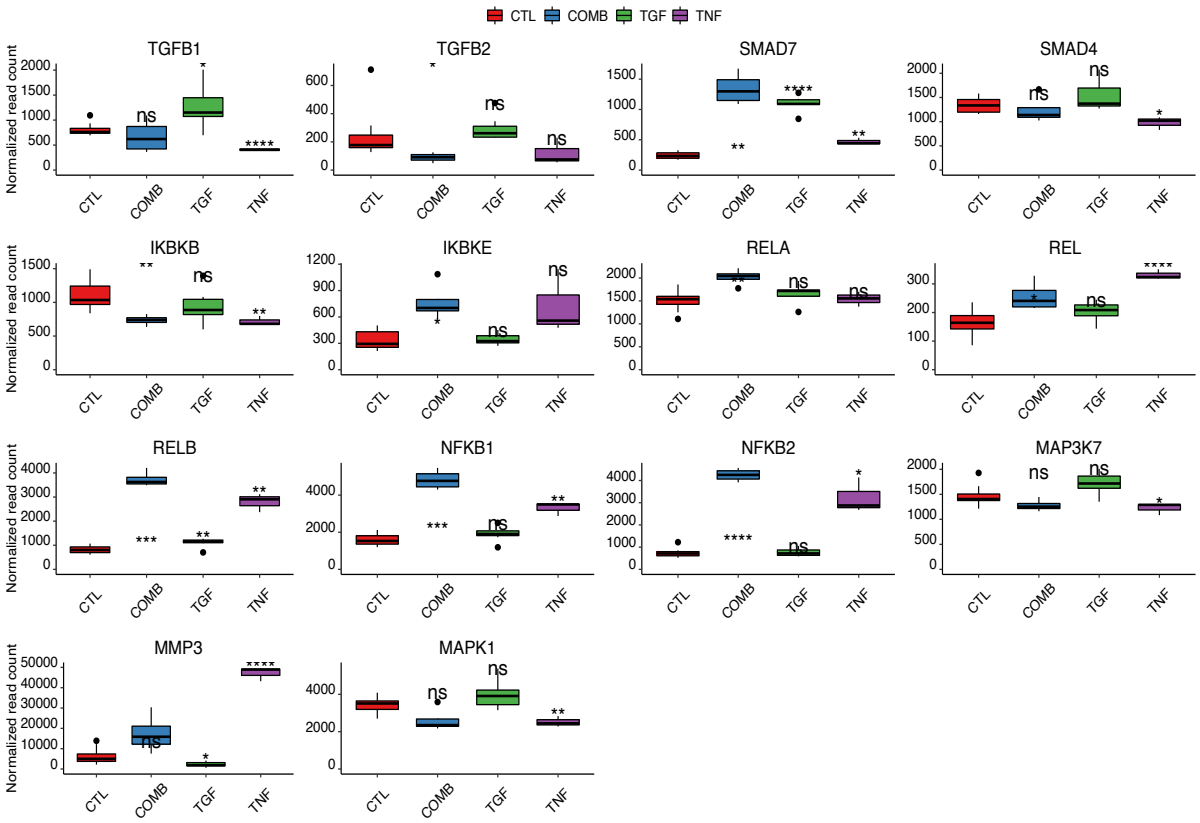

Figure 26 : Role of TNF-α and TGF-β on fibrosis
a. Schematic representation of the regulatory effect of TNF-α and TGF-β on different proteins in fibrosis. Purple arrows represent the effect of TNF-α, green arrows represent the effect of TGF-β2, and blue arrows represent the common regulatory effect of TNF-α and TGF-β combined [332]. b. Normalized read count plots of genes involved fibrosis modulation. Error bars are standard error of the mean, ns: $P > 0.05$, *: $P \leq 0.05$, **: $P \leq 0.01$, ***: $P \leq 0.001$, **** $P \leq 0.0001$.

Role of TNF-α and TGF-β2 in apoptosis

We investigated the modulation of genes implicated in apoptosis in HTMEx treated with TGF-β2 or/and TNF-α (figure 27 and 28). FAS pathway genes (FAS, DAPK2, BID) and TNF pathways genes (TRAF1, TRAF2, TRAF3, NFKB1, NFKB2, REL, RELA, RELB, TNFAIP3, TNFSF15, RIPK2) were logically up regulated in presence of TNF-alpha alone or combined with TGF-β2. However, TGF-β2 did not affect the modulation of these apoptosis genes. TNF-α also showed an antiapoptotic effect with upregulation of gene involved in BCL2 family pathway (BCL2A1, BIRC1, BIRC3, NFKBIB, NFKBIA, IKBKE). TGF-β2 treatment increases the expression of apoptosis genes of the MAPK pathway (MAP3K7, ATF2, MAPK9, MAPK14), this upregulation was not found when TGF-β2 was combined with TNF-α. For its part, TNF-α significantly decreased the expression of ELK1, FOS, JUN, MAP3K7, MAPK9, MAPK14 compared to the control. TGF-β2 and TNF-α have an opposite effect on apoptosis modulation in HTMEx.

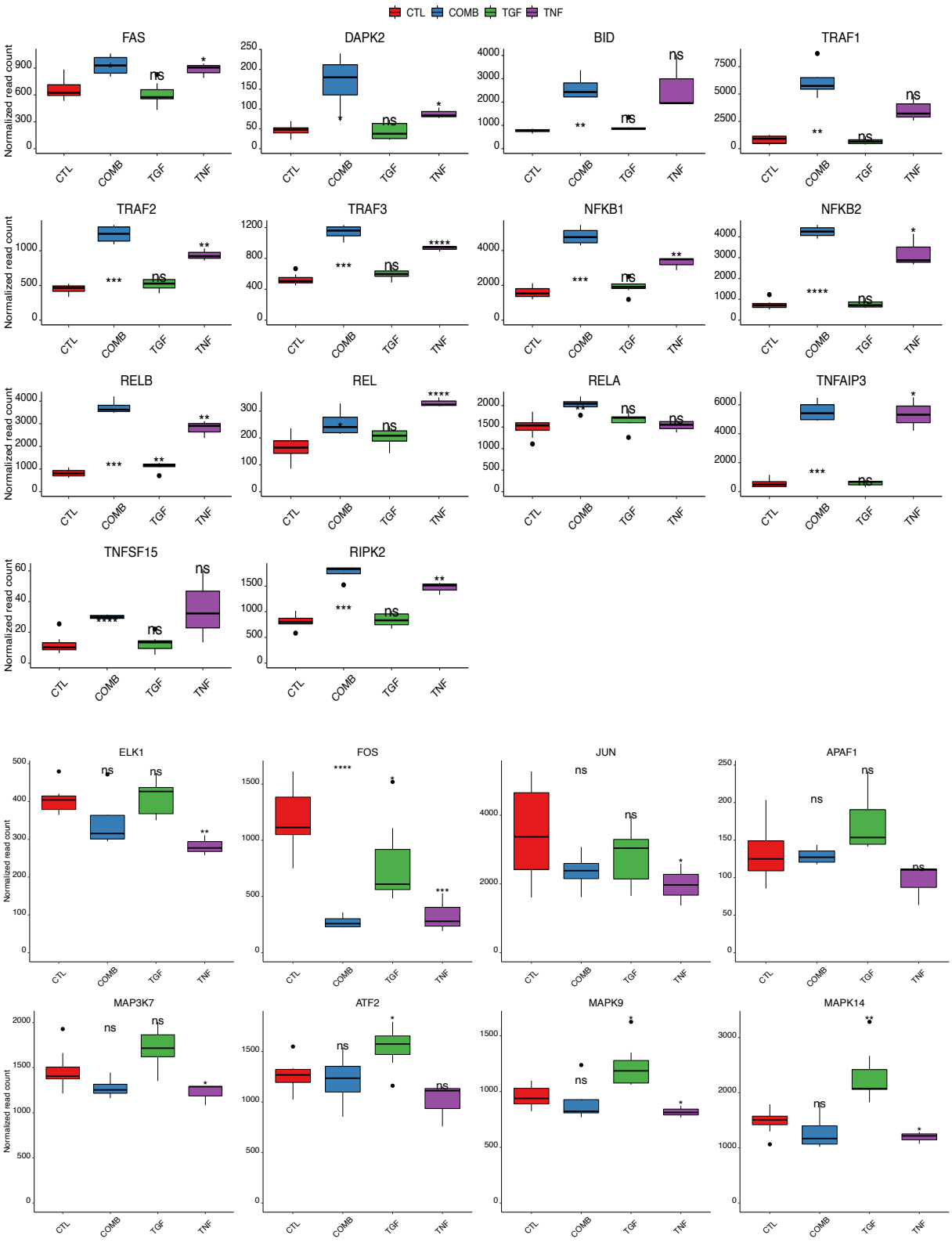

Figure 27 Modulation of expression of pro apoptotic genes
Modulation of expression of pro apoptotic genes in HTMEx exposed to DMEM/F12 only (CTL), TGF-β2 5ng/ml 48h (TGF), TNF-α 40ng/ml 48h (TNF) or both combined for 48h (COMB). Error bars are standard error of the mean, ns: $P > 0.05$, *: $P \leq 0.05$, **: $P \leq 0.01$, ***: $P \leq 0.001$, **** $P \leq 0.0001$.

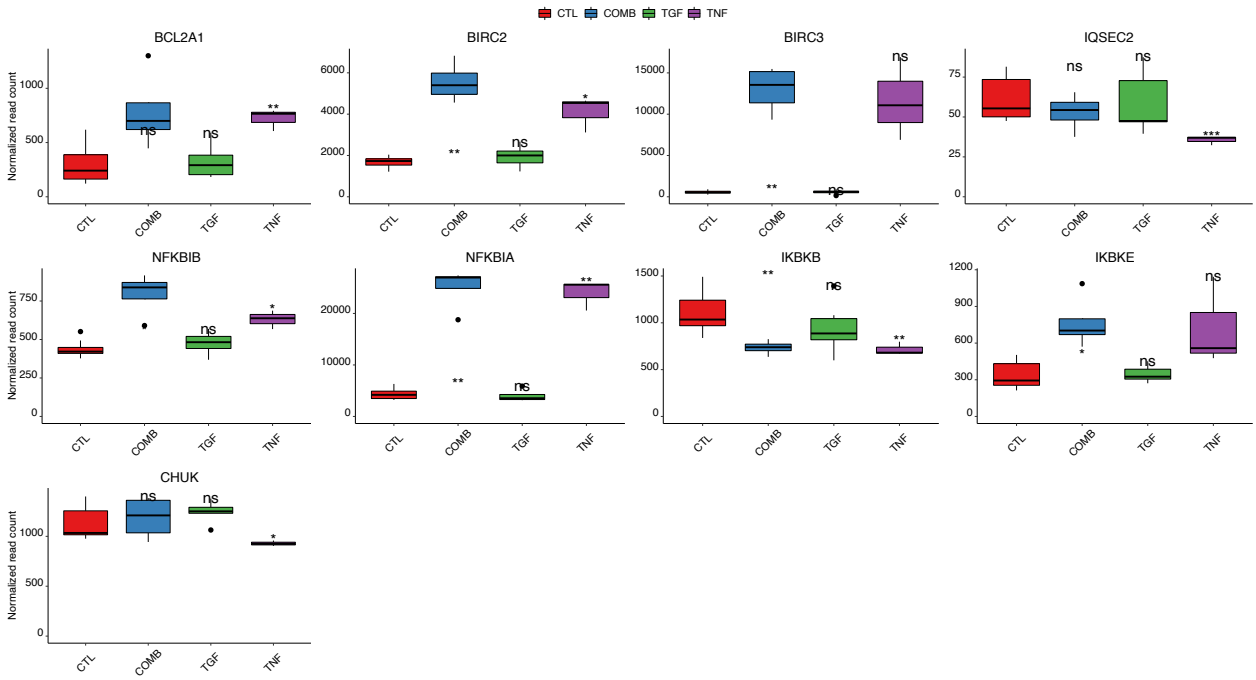

Figure 28 : Modulation of expression of anti-apoptotic genes
Modulation of expression of anti-apoptotic genes in HTMEx exposed to DMEM/F12 only (CTL), TGF-β2 5ng/ml 48h (TGF), TNF-α 40ng/ml 48h (TNF) or both combined for 48h (COMB). Error bars are standard error of the mean, ns: $P > 0.05$, *: $P \leq 0.05$, **: $P \leq 0.01$, ***: $P \leq 0.001$, **** $P \leq 0.0001$.

Role of TNF-α and TGF-β in oxidative stress response

As shown in figure 29, TGF-β2 and TNF-α have an opposite effect in expression of genes involved in the response to oxidative stress. When both TGF-β2 and TNF-α were applied together, we observed that TNF-α counteracted the effects of TGF-β2. Interestingly TNF-α decreased the expression of the prooxidant genes NOX4, NOX5, and FOS and enhanced the expression of the antioxidant genes SOD2 and the transcription factors NFKB1, and NFKB2. However, TGF-β2 did not affect the modulation of these genes except for a significant upregulation of NOX4 and downregulation of FOS.

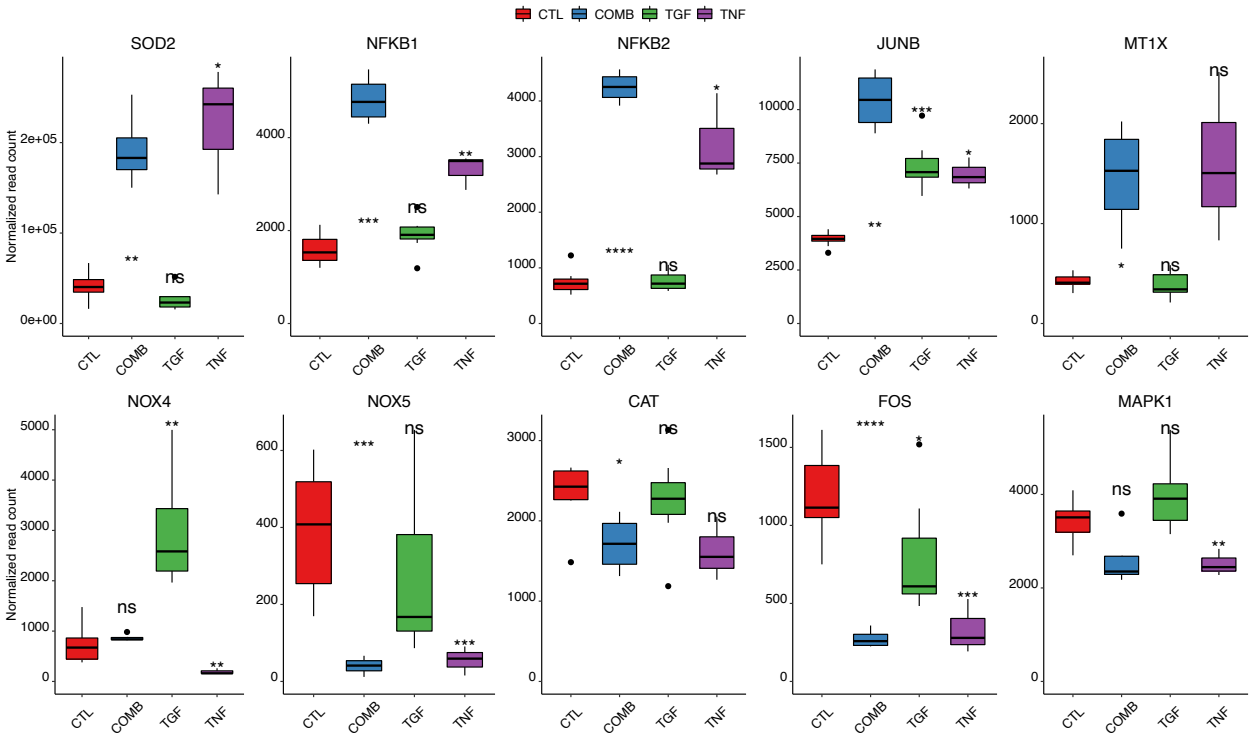

Figure 29 Modulation of expression of genes involved in oxidative stress response
Modulation of expression of genes involved in oxidative stress response in HTMEx exposed to DMEM/F12 only (CTL), TGF-β2 5ng/ml 48h (TGF), TNF-α 40ng/ml 48h (TNF) or both combined for 48h (COMB). Error bars are standard error of the mean, ns: $P > 0.05$, *: $P \leq 0.05$, **: $P \leq 0.01$, ***: $P \leq 0.001$, **** $P \leq 0.0001$.

Discussion

The present study aimed to investigate the effect of TGF-β2 and TNF-α, both individually and combined, on the regulation of ECM, inflammation, apoptosis, and oxidative stress responses in HTMEx. By conducting these comprehensive analyses, our aim was to enhance our understanding of the intricate inflammatory response and ECM remodeling processes within the TM.

Our results demonstrated that TNF-α induced a pro-inflammatory response, which was associated with an increase in the expression of pro-inflammatory cytokines and chemokines (CXCL10, CXCL11, IL1B, CCL20, CCL5, CXCL8, CCL2, IL32, CXCL1, CXCL5, and CXCL6). TNF-α also induced an apoptotic response in TM cells, as evidenced by the upregulation of apoptotic markers.

In contrast, TGF-β2 induced a remodeling response in TM cells, characterized by the upregulation of genes involved in ECM synthesis and cytoskeletal reorganization. TGF-β2 also suppressed the proinflammatory response, as evidenced by a decrease in the expression of proinflammatory cytokines and chemokines.

Additionally, TNF-α and TGF-β2 led to contrasting oxidative stress responses in HTMEx. TNF-α resulted in a reduction in the expression of prooxidant genes NOX4, NOX5, and FOS, while increasing the expression of antioxidant genes such as SOD2 and transcription factors NFKB1 and NFKB2. On the other hand, TGF-β2 did not impact the regulation of these genes except for a notable upregulation of NOX4 and downregulation of FOS.

When both TGF-β2 and TNF-α were applied together, we observed that TNF-α counteracted the profibrotic effects of TGF-β2. The study suggested that dysregulation of SMAD 7, a key mediator in the cross-talk between the TNF and TGF-β2 signaling pathways, could potentially contribute to the imbalance between TNF-α and TGF-β2 in the TM. SMAD 7 is an intracellular protein that plays an important role in regulating the balance between TNF pathway and TGF signaling pathway [311]. Specifically, SMAD 7 acts as an inhibitor of TGF-β signaling by binding to the TGF-β receptor and preventing the recruitment of downstream SMAD proteins. On the other hand, SMAD 7 also inhibits TNF-α -induced signaling by blocking the activation of the NF-κB pathway. Thus, SMAD 7 is thought to play an important role in maintaining the balance between these two pathways in various physiological processes. Dysregulation of SMAD 7 has been implicated in various diseases, including cancer and fibrosis [332]. In the context of glaucoma, dysregulation of SMAD 7 could potentially contribute to the imbalance between TNF-α and TGF-β2 in the TM and lead to the development and progression of the disease.

It seems that inflammation plays a major role in glaucomatous disease and specifically in trabecular dysfunction [32]. Increased protein levels of pro-inflammatory cytokines (TNF-α, IL-1β, IL-6, IL-8, and IFN-γ in human glaucomatous retinal tissue have been reported [32] . IL-6, IL-1β and TNF-α were found in TM specimens of POAG patients with high IOP. TM cells secrete various growth factors and cytokines in response to mechanical stretching, including IL-1, IL-6, IL-8, and TNF-α [340,341]. Birke et al. demonstrated increased TM outflow in response to perfusion of IL-1α and Il-1β in human TM. This was partly mediated by the induction of the expression of MMPs (MMP-3 and MMP-9) [342]. Pro-inflammatory cytokines (IL-1, IL-8, and TNF-α) are known to upregulate MMP expression, resulting in elastin and collagen deposition in the surrounding tissues. Hence, changes in MMPs and TIMPs appear to be closely related to the inflammatory responses.

Another inflammatory cytokine, IL-6, partially increased outflow facility in perfused human organ cultures, through modulation of endothelial permeability and induction of MMPs, resulting in ECM degradation [343]. Blondin et al. have reported that human TM cells secrete CCL2/MCP-1 in a constitutive manner, whereas the secretion of IL-8 occurs only after the cells were exposed to stimuli such as TNF-α [344].

These findings suggest that TNF-α and TGF-β2 play opposite roles in regulating the function of the HTMEx. Moreover, TNF-α can counteract the effects of TGF-β2 when both cytokines are present. These results suggest that targeting the TNF-α/TGF-β2 balance may be a promising therapeutic approach. By enhancing the production of TNF-α, it may be possible to promote ECM degradation and reduce TM resistance hence IOP.

Développement d'un modèle ex vivo de neurorétine glaucomateuse permettant l'étude de composés thérapeutiques neuroprotecteurs.

Contexte et objectifs

Enfin, nous avons étendu notre exploration vers la neurorétine, l'autre versant de la dégénérescence du glaucome. En effet, le glaucome est une neuropathie optique dégénérative cécitante dans laquelle la perte des cellules ganglionnaires rétiniennes (CGR) entraîne une altération progressive du champ visuel [345]. Actuellement, la seule stratégie thérapeutique démontrée pour ralentir la progression de la neuropathie optique glaucomateuse est de réduire la PIO. La prévention de la mort des CGR par des stratégies neuroprotectrices pourrait modifier complètement le pronostic visuel des patients atteints de glaucome.

Dans le même esprit que l'explant trabéculaire, nous avons utilisé un explant de neurorétine pour créer un modèle de neurorétine glaucomateuse par axotomie *ex vivo* afin d'évaluer des composés thérapeutiques à visée neuroprotectrice. Dans ce modèle, la section du nerf optique entraine une dégénérescence rapide des CGR, une gliose et une perturbation du transport axonal.

Après avoir exposé à un agent thérapeutique des explants de rétines de rat prélevées après axotomie du nerf optique, nous pouvons analyser la survie des cellules ganglionnaires rétiniennes en utilisant des immunomarquages en fluorescence, une quantification en western blot des protéines RBPMS, Brn3a et NeuN, utilisées comme marqueurs de CGR [346,347]. L'activation des cellules gliales et de la microglie rétinienne est mesurée à l'aide de la quantification en RT-qPCR des ARNm *GFAP*, *CD68* et *ITGAM* et des marquages en immunofluorescence de GFAP, CD68 et Iba1. Nous pouvons également analyser l'expression de l'ARNm des cytokines inflammatoires utilisées comme marqueurs de l'état M1, classique ou pro-inflammatoire (*TNF-α, IL1β* et *IL6*) et de l'état M2, alternatif ou anti-inflammatoire (*Arginase 1, IL10, CD163* et *TNFAIP6*).

Nous disposons donc d'un modèle plus économe en animaux pour pouvoir cribler de potentielles molécules ou approches thérapeutiques neuroprotectrices dans le glaucome. Un animal peut ainsi fournir huit explants, tandis qu'un modèle *in vivo* de glaucome exige un animal pour obtenir un œil glaucomateux, et souvent davantage compte-tenu de la faible reproductibilité des modèles de glaucomes chez l'animal. Le modèle d'explant rétinien offre l'avantage par rapport aux lignées cellulaires ou aux cultures dissociées, de maintenir une architecture de type *in vivo* avec toutes les couches neurorétiniennes et conservant les interactions intercellulaires. Il permet aussi un accès direct à la couche des CGR. La section du nerf optique entraîne la mort par apoptose de 90 % des CGR lésées dans les 14 jours suivant l'axotomie [27–29]. Ainsi, ce modèle comble le fossé entre les modèles précliniques pertinents mais chronophages, coûteux, et utilisant des animaux, et les modèles de culture cellulaire

rapides/haut débit, souvent basés sur un seul type de cellule, qui ne peuvent pas remplacer la complexité d'un tissu entier.

La neuroinflammation semble être un élément clé dans la progression et la propagation de cette neuropthie. Ainsi, l'immunomodulation microgliale représente une approche thérapeutique intéressante dans laquelle les cellules souches mésenchymateuses (CSM) pourraient jouer un rôle [340,348–350]. Leurs potentiels neuroprotecteur et régénérateur ont déjà suscité l'espoir dans les modèles animaux [351,352] [353–355]. Pourtant, aucun traitement définitif n'a été développé et des problèmes de sécurité ont été signalés dans des essais sur l'homme [356].

Nous avons étudié les propriétés neuroprotectrices et immunomodulatrices ainsi que l'innocuité des CSM dans un modèle d'explant de neurorétine *ex vivo*.

La description de ce modèle et l'évaluation des effets neuroprotecteurs et d'immunomodulation des CSM sont présentées dans l'article suivant, publié en 2021 dans *Journal of Neuroinflammation.*

Article 5 : Evaluation of neuroprotective and immunomodulatory properties of mesenchymal stem cells in an ex vivo retinal explant model

Reboussin *et al.*
Journal of Neuroinflammation (2022) 19:63
https://doi.org/10.1186/s12974-022-02418-w

Journal of Neuroinflammation

RESEARCH Open Access

Evaluation of neuroprotective and immunomodulatory properties of mesenchymal stem cells in an ex vivo retinal explant model

Élodie Reboussin[1†], Juliette Buffault[1,2*†], Françoise Brignole-Baudouin[1,3], Annabelle Réaux-Le Goazigo[1], Luisa Riancho[1], Céline Olmiere[4], José-Alain Sahel[1,2,5], Stéphane Mélik Parsadaniantz[1] and Christophe Baudouin[1,2]

† Co-first authors

Abstract

Background: Glaucoma is a blinding degenerative neuropathy in which the death of retinal ganglion cells (RGCs) causes progressive loss of visual field and eventually vision. Neuroinflammation appears to be a key event in the progression and spread of this disease. Thus, microglial immunomodulation represents a promising therapeutic approach in which mesenchymal stem cells (MSCs) might play a crucial role. Their neuroprotective and regenerative potentials have already raised hope in animal models. Yet no definitive treatment has been developed, and some safety concerns have been reported in human trials. In the present study, we investigated the neuroprotective and immunomodulatory properties as well as the safety of MSCs in an *ex vivo* neuroretina explant model.

Methods: Labeled rat bone marrow MSCs were placed in coculture with rat retinal explants after optic nerve axotomy. We analyzed the neuroprotective effect of MSCs on RGC survival by immunofluorescence using RBPMS, Brn3a, and NeuN markers. Gliosis and retinal microglial activation were measured by using GFAP, CD68, and ITGAM mRNA quantification and GFAP, CD68, and Iba1 immunofluorescence stainings. We also analyzed the mRNA expression of both 'M1' or *classically activated* state inflammatory cytokines (TNFα, IL1β, and IL6), and 'M2' or *alternatively activated* state microglial markers (Arginase 1, IL10, CD163, and TNFAIP6).

Results: The number of RGCs was significantly higher in retinal explants cultured with MSCs compared to the control group at Day 7 following the optic nerve axotomy. Retinal explants cultured with MSCs showed a decrease in mRNA markers of gliosis and microglial activations, and immunostainings revealed that GFAP, Iba1, and CD68 were limited to the inner layers of the retina compared to controls in which microglial activation was observed throughout the retina. In addition, MSCs inhibited the M1 phenotype of the microglia. However, edema of the explants was observed in presence of MSCs, with an increase in fibronectin labeling at the surface of the explant corresponding to an epiretinal membrane-like phenotype.

Conclusion: Using an *ex vivo* neuroretina model, we demonstrated a neuroprotective and immunomodulatory effect of MSCs on RGCs. Unfortunately, the presence of MSCs also led to explant edema and epiretinal membrane formation, as described in human trials. Using the MSC secretome might offer the beneficial effects of MSCs without their potential adverse effects, through paracrine signaling.

Keywords: glaucoma; neuroprotection; immunomodulation; cellular therapy; mesenchymal stem cell; microglia; retinal ganglion cell.

Background

Glaucoma is a blinding degenerative neuropathy in which retinal ganglion cell (RGC) death leads to a progressive loss of visual field and eventually vision [345]. Preventing RGC death through neuroprotective strategies could completely modify the visual prognosis of patients with glaucoma. In the last few decades, MSCs and their neuroprotective and regenerative properties have raised considerable hope in glaucoma therapy. However, no protocol has yet been validated in humans [356].

MSCs are multipotent cells found in many adult tissues, able to proliferate, self-renew and differentiate into many types of specialized cells, including osteocytes, adipocytes, or chondrocytes. Moreover, MSCs produce numerous growth or neurotrophic factors, leading to the hypothesis that they could play a major role in stimulating the survival and growth of RGCs [353,355,356]. MSC-based therapies in retinal diseases have been explored in order to prevent or delay RGCs death and even to regenerate RGCs [351,352]. Intravitreal transplantation of bone marrow MSCs (BMMSCs) in rat ocular hypertension models has been shown to be highly neuroprotective by reducing RGCs death [353–355]. Anterior chamber transplantation of rat BMMSCs in a rat ocular hypertension model also demonstrated neuroprotective effects as measured by peripheral RGC density and a significant but transient reduction in IOP [357].

In glaucoma patients as well as in rodent preclinical models of glaucoma, higher expression of glial fibrillary acidic protein (GFAP) was found to be associated with the degeneration of the optic nerve fibers [340]. So, glial immunomodulation represents a promising therapeutic approach in which MSCs might play a crucial role. Indeed, in glaucoma, RGC loss is associated with an inflammatory process caused by activation of resident glial cells, *e.g* microglial cells, Müller cells, and astrocytes [32,340,358–360]. Once activated, these cells release a cocktail of cytokines, chemokines, and reactive oxygen species (ROS) and consequently contribute to RGCs loss. Among these cells, microglial cells, also called sentinel immune cells, exist in two dynamic and opposite activated states with neurotoxic or neuroprotective effects [337,361,362]. During retinal degeneration, microglia are activated and particularly polarized to a pro-inflammatory M1 phenotype [363]. The “classical activation state” or “M1 state” is characterized by the production of ROS and secretion of numerous pro-inflammatory molecules such as TNFα, IL-1β, and IL-6. The second state, also known as the “alternatively activated state” or “M2 state,” is induced by IL-4 or IL-13. It allows clearance of debris, restores tissue homeostasis, and promotes tissue repair by inhibiting inflammation through the production of anti-inflammatory, neurotrophic factors, and chemokine receptors [337,361,362,364]. Several M2 phenotype markers characterize this M2 state, *e.g* the enzyme Arginase 1 (ARG1), a marker of microglia involved in tissue repair and phagocytosis, the receptor CD163, a marker of microglia implicated in the anti-inflammatory process and healing, IL-10, an anti-inflammatory cytokine used by the M2 subtype to antagonize the pro-inflammatory phase and healing, and TNFα-stimulated gene-6 (TSG-6/TNFAIP6), which is a key anti-inflammatory factor produced by MSCs [338,365–367]. Reducing the pro-

inflammatory M1 phenotype or inducing M2 microglial polarization might represent a potential and promising therapeutic option to treat neuroinflammatory degenerative diseases such as glaucoma [340,348–350]. Among potent immunomodulators of microglial polarization, MSCs possess potent immunoregulatory properties and might inhibit a harmful inflammatory reaction in the diseased retina [350,356,368].

Obtaining a model of RGC loss to reproduce the degenerative process observed in glaucoma is a challenge. Indeed, many animal models have been developed but have encountered reproducibility issues in the rate of RGC loss [356]. The retinal explant model offers the advantage compared to cell lines or dissociated cultures, to maintain an *in-vivo* like architecture with all neuroretina layers retaining intercellular interactions; it allows direct access to the RGC layer; it limits the number of animals used and is less time-consuming than the classical use of animal models, considering the degeneration rate of RGCs. Optic nerve transection leads to the death by apoptosis of 90% of injured RGCs within 14 days post axotomy [369–371]. Thus, this model fills the gap between relevant but time/cost/animal-consuming preclinical models and rapid/high-throughput cell culture models often based on one single cell type, which cannot substitute for the complexity of an entire tissue.

Considering the promising MSC neuroprotective results previously demonstrated in animal models, our objective was to evaluate the effects of MSCs use as a neuroprotective and immunomodulatory therapy in a neuroretina explant model of RGC degeneration, with a particular attention to immuno-inflammatory patterns and potential safety issues.

Materials and Methods

Animals

Adult (6 to 8 weeks old) male Long Evans rats weighing 250-300 g were purchased from Janvier Laboratories and used for harvesting fresh BMMSCs and retinal explants to proceed to coculture. Animals were kept in pathogen-free conditions with food and water *ad libitum* and housed in a 12-h light/12-h dark cycle. All experiments were conducted after evaluation and approval by the Institutional Animal Care and Use Committee following the guidelines from Directive 2010/63/EU of the European Parliament on the protection of animals used for scientific purposes. All experimental procedures were approved by the local animal care ethics committee C2EA-05—Charles Darwin.

MSC isolation and culture

Fresh BMMSCs were harvested from femurs of 6-week-old Long Evans rats (Janvier Laboratories). Briefly, femurs were isolated, and the cavities were flushed with 5 ml of expansion medium composed of αMEM (Thermo Fisher Scientific, ref. 31095029), 10% heat-inactivated Fetal Calf Serum (Thermo Fisher Scientific, ref. 10499044), and 1% Penicillin-Streptomycin 10,000 U/mL (Thermo Fisher

Scientific, ref. 15140122), through a 21G needle. Cells were incubated in 75 cm^2 flasks (200,000 cells/cm^2) at 37 °C in 5 % CO_2 humidified air for 72 hours. Three days later, nonadherent cells were washed away with DPBS (Thermo Fisher Scientific, ref. 14190169), and fresh medium was added and kept until the first passage. MSCs were cultured with a weekly passage at a seeding rate of 100,000 cells/ml and characterized using flow cytometry (FCM) until cocultured with retinal explants.

Flow Cytometry

BMMSCs were cultured in 75 cm2 flasks until near confluence, in standard culture conditions (5% CO2, 37°C, and saturated humidity atmosphere). Then, MSCs were harvested using Trypsin 0.05% EDTA (Thermo Fisher Scientific, ref. 25300054), washed twice with DPBS, and suspended in DPBS at 500,000 cells/ml after numeration using Flow-Count fluorospheres (Beckman Coulter, ref. 7547053). The suspension of live MSCs was characterized using flow cytometry (Cytomics FC 500 flow cytometer, Beckman Coulter, Miami, FL, USA) and positive (CD29, CD90, CD73) and negative (CD11b/c, CD45, CD68, MHC class II (Ia)) antigens were analyzed. The antibodies used for this characterization are presented in table 21. Incubations for direct fluorochrome-conjugated antibodies and for non-conjugated primary antibodies were performed in 50µl DPBS for 30mn in the dark. For indirect immunostaining, another 30mn-incubation was carried out with the secondary antibody. After immunostaining, cells were washed once in DPBS and finally suspended in 300µl of DPBS for flow cytometric acquisition.

Tableau 21 : Antibodies used for the MSC characterization using flow cytometry

Antibody	Host	Supplier	Reference
Positive markers			
CD29	Armenian hamster	eBioscience	11-0291-80
CD73	Mouse	BD Biosciences	551123
CD90	Mouse	eBioscience	45-0900-80
Negative markers			
CD11b/c	Rabbit	BD Pharmingen	554862
CD45	Mouse	Serotec	MCA43PE
CD68	Mouse	Serotec	MCA341R
Ia	Mouse	Bio-Rad	MCA46G
Isotype control FITC	Armenian hamster	eBioscience	11-4888-81
IgG2a kappa Isotype control	Mouse	eBioscience	45-4724-80
IgG1, κ	Mouse	BD Pharmingen	554680
IgG-UNLB	Mouse	SouthernBiotech	0107-01

Retinal explant cultures

8-week-old Long Evans rats (Janvier Laboratories) were used to collect retinal explants for culture, as previously described [372,373]. Rats were euthanized, and the eyes were excised, then quickly placed in an ice-cold CO_2 independent medium (Thermo Fisher Scientific, ref. 18045-054). Under sterile

conditions at 4°C in a CO_2 independent medium, the anterior chamber, lens, and vitreous body were removed, and the retina was separated from the surrounding ocular tissues by dissection with curved microforceps. Retinas were then cut into four equal quarters and flat-mounted with the RGC layer up on Millicell-Polytetrafluoroethylene (PTFE) 0.4µm culture plate inserts (Merck Millipore, ref. PICM01250), in culture medium composed of Neurobasal A (Thermo Fisher Scientific, ref. 10888022), 2% B27 supplement (Thermo Fisher Scientific, ref. 0080085-SA), 1% N2 supplement (Thermo Fisher Scientific, ref. 17502048), L-glutamine (Thermo Fisher Scientific, ref. 25030032), and 1% Penicillin-Streptomycin 10,000 U/mL, at 37 °C in 5 % CO_2 humidified air. The next day, half of the medium was changed, which was then changed every 48 hours thereafter.

Pharmacologic agents

Brain Derived Neurotrophic Factor (BDNF) (Sigma–Aldrich, ref. SRP3014) or N-Methyl-D-Aspartate (NMDA) (Sigma–Aldrich, ref. M3262) were diluted daily in retinal culture medium and added in direct contact with the RGCs at a concentration of 200 ng/ml or 50 µM respectively, in a 3 µl droplet carefully dispensed onto the surface of the explant [372]. Also, half of the retinal culture medium containing BDNF or NMDA was changed at Day 1 and every 48 hours thereafter.

Retinal explant-MSC coculture

MSCs from passages 5 to 7 were used for this experiment. Before coculture, MSCs were trypsinized, washed in DPBS, and suspended in retinal explant culture medium at 5,000 cells/µl [372,373]. MSCs were labeled with Vybrant™ DiO Cell-Labeling Solution (Invitrogen, V22886) before the coculture to track them within the coculture system. Once the retinal explants were flat-mounted with the RGC layer up, 2 µl of this MSC suspension was gently dispensed onto the surface of the retinal explants.

Immunohistochemistry

Tissue preparation

For cryosections, retinal explants were fixed in PFA 4% for 24 h at 4°C, then dehydrated in sucrose 30% (DPBS; pH 7.4) overnight at 4°C, before being embedded in OCT (Tissue-Tek® O.C.T. Compound, Sakura® Finetek) and frozen. Cryosections of retinal explants 12 µm in thickness were performed using a Leica cryostat CM 3050S and stored at -20°C until use. For wholemount counting, retinal explants were fixed in PFA at 4°C overnight and rinsed in DPBS before the immunofluorescence step.

Dual immunofluorescence labeling in whole flat-mounted retinal explants or cryosections

Retinal explant wholemounts or cryosections were incubated for 2 h at room temperature (RT) in a blocking buffer (5% BSA, 2% Triton X-100, and 0.5% Tween20, in DPBS) and left to incubate overnight at 4°C in the incubation buffer (2.5% BSA, 1% Triton X-100 and 0.25% Tween20, in DPBS) with polyclonal rabbit anti-RBPMS (1/200, Merck Millipore, ref. ABN 1362), monoclonal mouse anti-Brn-3a (1/100, Merck Millipore, ref. MAB1585), monoclonal mouse anti-NeuN (1/500, Merck Millipore, ref. MAB377), monoclonal mouse anti-CD68 (1/400, AbD Serotec, ref. MCA341R), polyclonal rabbit anti-GFAP (1/500, Dako, Agilent, ref. Z033429-2), polyclonal rabbit anti-Iba1 (1/500, Wako, ref. W1W019-19741), polyclonal rabbit anti-fibronectin (1/250, Abcam, ref. ab2413), and polyclonal goat anti-choline acetyltransferase (1/200, Merck Millipore, ref. AB144P). Explant wholemounts or cryosections were washed in DPBS and incubated with an Alexa Fluor 594-conjugated donkey anti-mouse immunoglobulin (1/500, Thermo Fisher Scientific, ref. A21203), an Alexa Fluor 488- conjugated donkey anti-rabbit immunoglobulin (1/500, Thermo Fisher Scientific, ref. A21206), or an Alexa Fluor 594-conjugated donkey anti-goat immunoglobulin (1/500, Thermo Fisher Scientific, ref. A11058) as secondary antibodies (Thermo Fisher Scientific), and the nuclei were stained with Dapi (1/500) for 1 hour, at RT. Then, retinal explants, wholemounts or cryosections, were washed and mounted in Fluoromount (Sigma Aldrich, ref. F4680-25ML).

Histopathological analysis of retinal explants

Retinal explant cryosections 12 µm in thickness were stained with hematoxylin and eosin (H&E). Stained cryosections were scanned at 100x and 200x magnifications with the digital whole-slide scanner NanoZoomer 2.0 HT scanner (Hamamatsu Photonics), using the NanoZoomer's 3-CCD TDI camera. NDP viewer software (Hamamatsu Photonics) was used to measure the thickness of the retinal explants and analyze their histology.

Immunohistological quantification

For RGC quantification in wholemount retinas, imaging was performed at 200x magnification (306 μm^2) using an epifluorescence microscope (Zeiss AX-10). RGCs were identified based on Brn3a and RBPMS markers. Images were taken at four locations from the optic nerve to the peripheral retina for each explant. Cell counts were performed manually using image analysis software (ImageJ, United States National Institutes of Health (NIH)) and *cell counter plugin* and expressed as RGC/306 μm^2 or percentage of cells compared to Days *Ex Vivo* (DEV) 0. Concerning quantification in transverse sections, sections were taken throughout the whole explant, with approximately 18 slides/explants, allowing placement of different areas of the explant on the same slide. Three images were acquired per section, in 5 different sections on a slide. RGC or displaced amacrine cells (DAC) quantification was expressed

as RGC/mm or DAC/mm. For GFAP, Iba1 and CD68 immunostaining quantification, explant cryosections were taken using an epifluorescence microscope (Zeiss AX-10). Three images were acquired for each explant using a x10 or x20 objective and the same parameters of time exposure for each explant. NIH Image J software was then used to quantify the Raw Integrated Density of each section, allowing us to obtain the sum of pixels values. For all images, Background values have been subtracted of Raw Integrated Density and the same area was selected. Sections were analyzed in a blinded manner; the experimenter was blinded to the treatment.

Quantitative RT-PCR

Total RNA of 6 to 16 retinal explants per group (3 mg/explant) was purified using the NucleoSpin RNA XS kit (Macherey-Nagel, ref. 740902.50) according to protocol. Total RNA was reverse-transcribed into cDNA a High Capacity RNA to cDNA kit (Life Technologies, ref. 4368814) according to the manufacturer's instructions. Real-time PCR was performed using the TaqMan Gene Expression PCR Master mix (Applied Biosystems, ref. 4324020) and the Applied Biosystem Fast 7500 (Applied Biosystems). The delta-delta Ct method (ddCt) was used to analyze the relative gene expression; that is, the fold change of mRNA upon downregulation of various target genes was determined. Rps18 was used as a housekeeping gene.

Statistical Analysis

Statistical analyses were performed using GraphPad Prism 7. Data are presented as mean ± SEM. Student's t-test or Mann-Whitney was performed for unpaired comparisons between RGC viabilities after counting with Brn3a and RBPMS staining and relative mRNA levels. Unpaired t-test was used to quantify neurons after exposure to pharmacological agents (BDNF and NMDA), and two-way ANOVA or Mann Whitney was used for retinal explant cocultures with MSCs. RT-qPCR data were analyzed using One-Way ANOVA, Student's t-test, or Mann-Whitney for unpaired comparisons. One-way ANOVA was used to quantify GFAP, Iba1 and CD68 immunostaining.

Results

Isolation and characterization of rat bone marrow mesenchymal stem cells

Rat BMMSCs from three different production batches were characterized using FCM analysis. The data showed that MSCs highly expressed positive MSC markers CD29, CD73, and CD90 and did not express CD11b/c, CD45, CD68, and the MHC Class II (Ia) antigen in accordance with the International Society for Cellular Therapy [32]. Overlaid fluorescence histograms of specific markers (in black line *vs*

negative control in grey), percentages of positive cells and mean fluorescence intensities are presented in the Additional file 1.

RGC degeneration in a retinal explant culture model

The best therapeutic window to assess neuroprotection was determined by evaluation of RGCs degeneration following optic nerve axotomy in the retinal explant culture model, which can vary between laboratories, handlers, or culture conditions. Brn3a and RBPMS specific RGCs markers were used for RGCs counting from 'Day *ex vivo*' (DEV) 0 to 7 (Figure 30 A, B, C, and D) [374,375]. Loss of RGCs occurred with both markers after 24 hours of culture but without significance. The number of RGCs was statistically different at DEV 3 and later compared to DEV 0 for Brn3a quantification (44% RGCs death at DEV 3 from DEV 0, $P<0.0001$) or DEV 5 for RBPMS quantification (36% RGCs death compared DEV 0, $P<0.0001$) (figure 30). From DEV 5 to DEV 7, a plateau of the RGCs loss curves for Brn3a and RBPMS quantification was obtained. From these results, we determined an optimal therapeutic window from DEV 5 to 7 of culture for testing neuroprotective agents or MSCs.

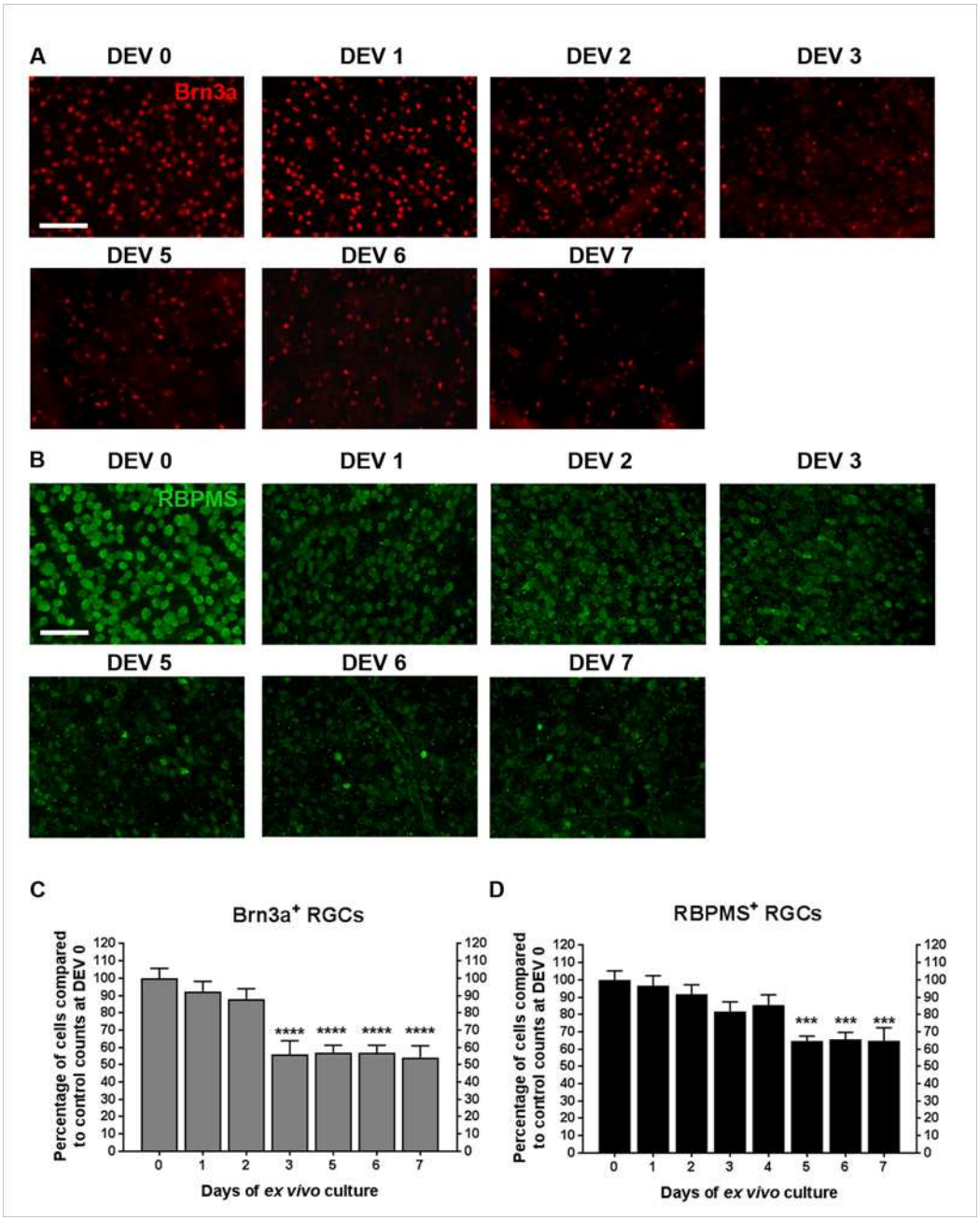

Figure 30 : RGC degeneration in a retinal explant culture model
Representative images of wholemount retinal explants (n=8 per day) in culture from DEV0 to DEV7 immunolabeled with Brn3 (A) and RBPMS (B) at 200x magnification (scale bar = 100 µm). Quantification of Brn3a+ RGCs (C) and RBPMS+ RGCs (D) from wholemount retinal explants was expressed as percentage of DEV 0 (defined as 100%). Error bars are standard error of the mean. ***P<0.001, ****P<0.0001.

Retinal explant responses to neuroprotective or excitotoxic stimuli

To evaluate the ability of the retinal explant model to respond to neuroprotective agents, we exposed explants for 5 days to BDNF [376,377]. At DEV 5 with Brn3a and RBPMS markers, quantification of RGCs on wholemount retinas confirmed the neuroprotective effect of BDNF, with a significant increase in the percentage of Brn3a+ RGCs survival at DEV 5 in treated group compared to control group

(76.38%±7.08% vs. 45.47%±1.55%, P=0.0053) and RBPMS+ RGCs survival at DEV 5 in treated group compared to control group (72.81%±6.16% vs. 50.06%±1.37%, P=0.0113) (figure 31). Retinal explants significantly respond to a neuroprotective stimulus.

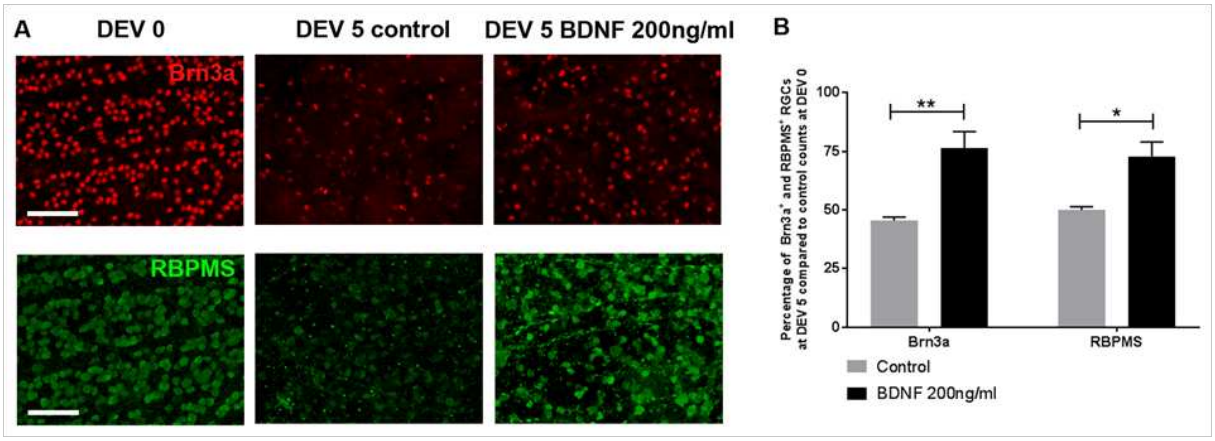

Figure 31 : Retinal explant responses to neuroprotective stimuli
A. Representative images of wholemount retinal explants (n=4/day) in culture at DEV 0 and DEV 5, immunolabeled with Brn3a (red) and RBPMS (green) at 200x magnification (scale bar = 100 µm) treated daily with BNDF (200 ng/ml). **B.** Quantification of Brn3a+ or RBPMS+ RGCs in control group (grey bar) and Brn3a+ or RBPMS+ RGCs in BDNF-treated group (black bar) at DEV 5 from wholemount retinal explants was expressed as percentage of DEV 0 (defined as 100%). Error bars are standard error of the mean. *P<0.05, **P<0.01.

To evaluate the ability of the retinal explant model to respond to excitotoxic agents, we exposed explants for 5 days to NMDA [376,377]. At DEV 5 NMDA exposure at 50 µM caused significant decrease in RGCs survival compared to controls with both markers Brn3a (0.65%±0.33% vs. 39.73%±3.98%, P<0.0001) and RBPMS (17.46%±2.91% vs. 47.75%±4.53%, P=0.0014) (figure 32). Retinal explants significantly respond to an excitotoxic stimulus.

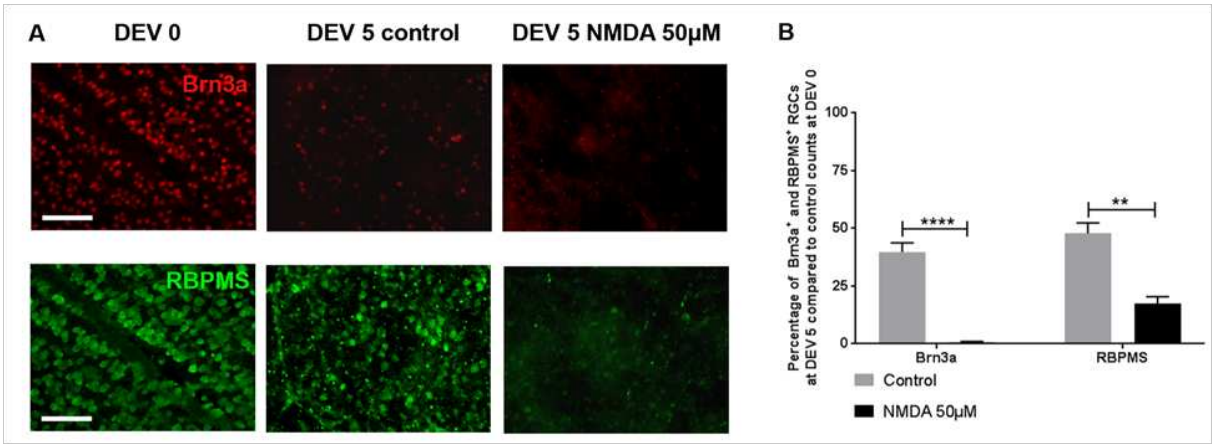

Figure 32 : Retinal explant responses to excitotoxic stimuli
A. Representative images of wholemount retinal explants (n=4/day) in culture at DEV 0 and DEV 5, immunolabeled with Brn3a (red) and RBPMS (green) at 200x magnification (scale bar = 100 µm) treated daily with NMDA (50 µM). **B.** Quantification of Brn3a+ or RBPMS+ RGCs in control group (grey bar) and Brn3a+ or RBPMS+ RGCs in NMDA-treated group (black bar) at DEV 5 from wholemount retinal explants was expressed as percentage of DEV 0 (defined as 100%). Error bars are standard error of the mean. Error bars are standard error of the mean. **P<0.01, ****P<0.0001.

Coculture of MSCs with retinal explants confers RGC neuroprotection

In accordance with the publications of Johnson *et al.*, we investigated whether the presence of MSCs could limit or prevent RGC loss in retinal explants after an even longer duration, namely at DEV 7 [373,378]. At DEV 7, the number of RGCs stained with Brn3a and NeuN was significantly higher in cryosections of retinal explants cocultured with 1.10^4 MSCs compared to the control group (28.13±4.61/mm *vs* 16.16±5.85/mm, P=0.0490 and 62.55±6.92/mm *vs* 44.39±8.26/mm, P=0.0018, respectively). RBPMS quantification did not show statistically significant differences at DEV 7 between control and MSC coculture groups. No significant difference in RGC numbers was found between DEV 0 and DEV 7 with 10^4 MSCs for RBPMS, Brn3a, or NeuN staining (figure 33). However, NeuN being a neuronal marker expressed by both RGCs and DACs, we specifically quantified DACs in RGC layer using an anti-choline acetyltransferase (ChAT) antibody in order to avoid a bias in RGCs survival counting using this marker. We found no significant difference in ChAT+ DACs between group at DEV 0 and DEV 7 (Additional file 2). Thus, RGCs survival estimated with NeuN is not influenced by potential NeuN+ DACs in the RGC layer. MSCs reduced RGC loss in retinal explants at DEV 7.

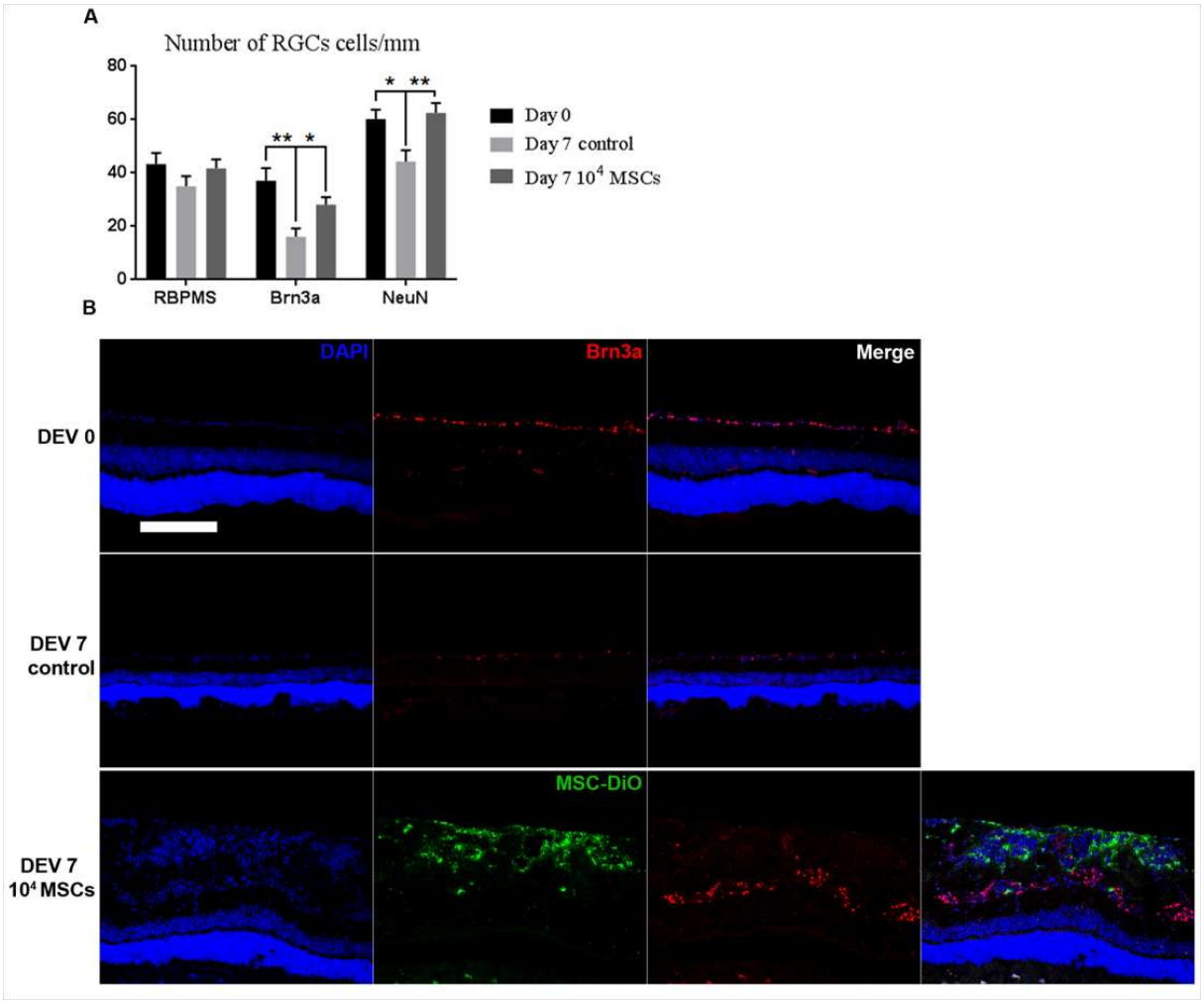

Figure 33 : Neuroprotection evaluation of RGCs on retinal explant responses to cocultured MSCs
A. Quantification of RBPMS+, NeuN+ and Brn3a+ RGCs from retinal explants (n=6/day) cocultured with 1.10^4 MSCs for 7 days. RGC counts on cryosections are expressed as RGCs/mm. *P<0.05, **P< 0.001. **B.** Representative images of retinal

explant cryosections cocultured with 1.10^4 MSCs for 7 days at DEV 0 and DEV 7, immunolabeled with Brn3a (red) and DiO labeled MSCs (green) at 200x magnification (scale bar = 100 µm).

MSCs decrease gliosis in retinal explants

To determine the inflammatory response following MSCs implantation, we analyzed GFAP immunostaining and GFAP mRNA expression in retinal explants at DEV 0 and DEV 7. GFAP immunoreactivity in astrocytes and Müller cells was upregulated in all retinal layers at DEV 7 in the control group compared to DEV 0, where GFAP was limited to the nerve fiber layer (NFL) and outer plexiform layer (OPL). In contrast, at DEV 7 in the MSC coculture group, GFAP immunostaining was limited to the NFL and to a lesser extent to the OPL (figure 34A). Moreover, we measured the Raw Integrated Density at DEV 0 and DEV 7 in the control group and the MSCs coculture group. This semi-quantitative analysis clearly demonstrated the significant upregulation of GFAP staining at DEV 7 in both groups confirming the glial activation ($P=0.0015$ and $P=0.0361$ respectively) compared to DEV 0 (figure 34B). Nonetheless, no significant difference was observed between the control and the MSC coculture group at DEV 7. GFAP mRNA was significantly higher at DEV 7 in the control and MSC coculture groups (38.5-fold, $P<0.0001$ and 11.4-fold, $P<0.0001$ respectively) compared to DEV 0. However, GFAP mRNA was significantly lower at DEV 7 in the MSC coculture group compared to the control group ($P<0.0001$) (figure 34C). These data demonstrate that MSC coculture conferred limited glial activation in retinal explants at DEV 7 compared to the control group. However, GFAP activation was limited but still robust in the NFL and OPL layer in the MSC coculture group, proving a significant, localized reactive gliosis following MSC implantation.

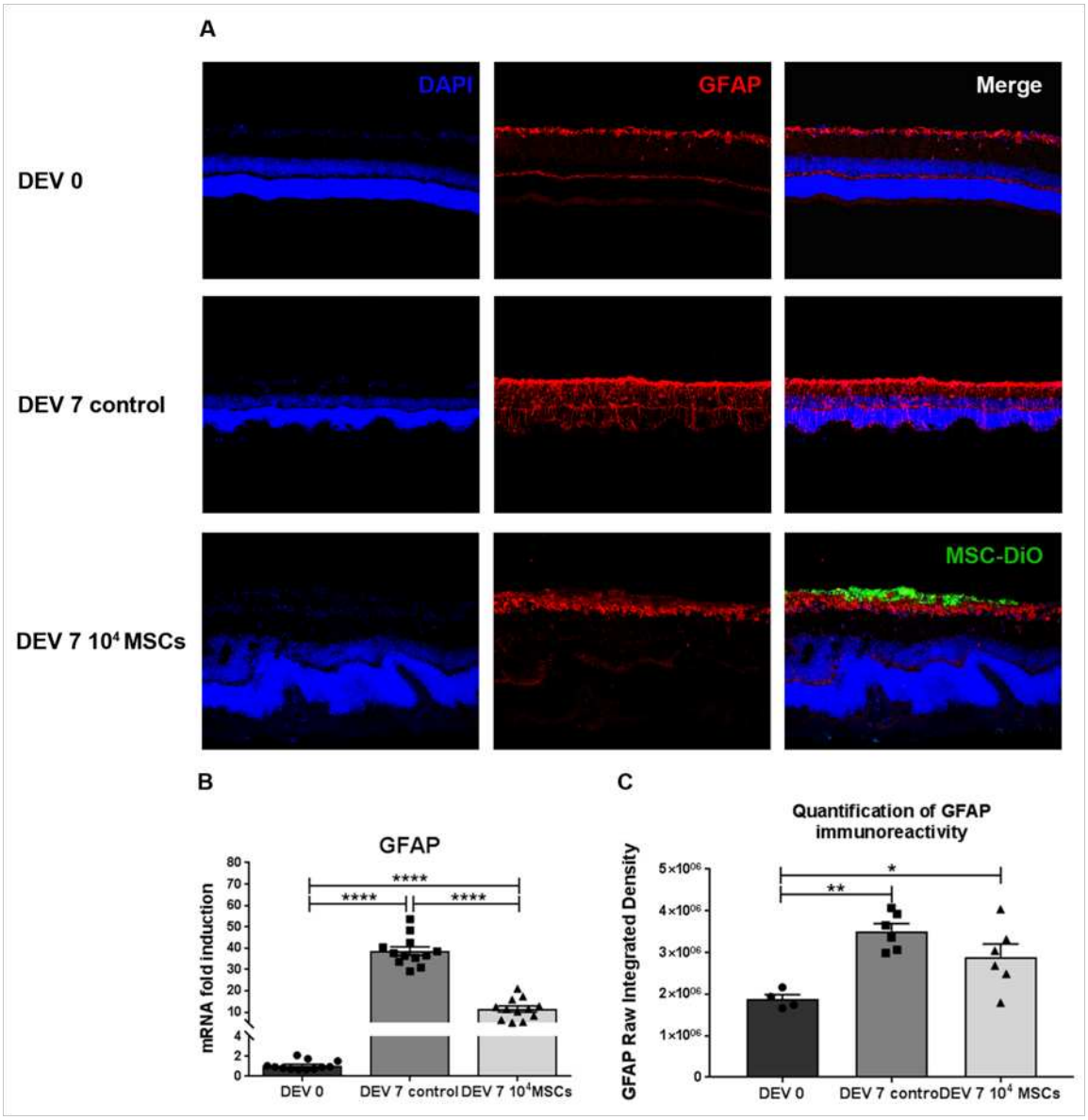

Figure 34 : Gliosis evaluation on retinal explants cocultured with MSCs
A. Representative images of retinal explant cryosections cocultured with 1.104 MSCs for 7 days at DEV 0 and DEV 7, immunolabeled with GFAP (red) and DiO labeled MSCs (green) at 200x magnification (scale bar = 100 µm). B. Quantification of GFAP immunoreactivity (expressed as Raw Integrated Density). N=4-6 animals/group. Ordinary one-way ANOVA was performed. *P<0.05, **P<0.01. C. RT-qPCR analysis of GFAP expression in retinal explants at DEV 0 and DEV 7. mRNA levels are presented after normalization with the housekeeping gene Rps18. N=12 animals/group. Unpaired t-test was performed for unpaired comparisons. ****P< 0.0001.

MSCs reduce microglial activation

To determine the microglial cell response following coculture with MSCs, we analyzed ionized calcium binding adaptor molecule 1 (Iba1) and CD68 immunostaining and ITGAM and CD68 mRNA expressions in retinal explants at DEV 0 and DEV 7. At DEV 0, Iba1+ microglial cells were located in the inner plexiform layer (IPL) and ganglion cell layer (GCL), and no CD68+ cells were found in retinal layers. At DEV 7 in the control group, Iba1+ and CD68+ cells were found in all retinal layers, contrary to the MSC group, where Iba1+ and CD68+ cells were limited to the inner retinal layers (GCL, IPL and

inner nuclear layer (INL)). Moreover, at DEV 7 in the MSC group, microglial cells were present mainly at the interface between the GCL and MSCs (figure 35 A, B). Then, we quantified Iba1 and CD68 Raw Integrated Density at DEV 0 and DEV 7 in the control and MSC coculture groups. It demonstrates the significant upregulation of Iba1 staining at DEV 7 in MSC coculture group compared to DEV 0 ($P=0.0235$). Moreover, no significant difference was observed between control group at DEV 7 and MSC coculture or DEV 0 groups (figure 35 C). Concerning CD68 staining, no significant difference was observed in all groups, despite a slight tendency to fluorescence increase at DEV 7 for both groups (figure 35 D). RT-qPCR analysis showed that ITGAM and CD68 mRNA fold inductions were significantly lower in the MSC group compared to the control group (respectively 17.3 vs. 33.1 and 83.4 vs. 169, $p<0.0001$) (figures 35 E, F). These data demonstrate that microglial cells were distributed differently throughout the retina at DEV 7 in the control and MSC groups, with a limited but strong distribution of microglial cells to the internal retinal layers in the MSC group. In the control group at DEV 7, Iba1+ microglial cells migrated and proliferated toward the outers layers of the retina. Furthermore, microglial activation and proliferation were higher at DEV 7 in the control group compared to the MSC coculture group. However, in the MSC coculture group, this microglial activation was concentrated at the RGC/MSC interface. MSC limited the microglial activation in retinal explants.

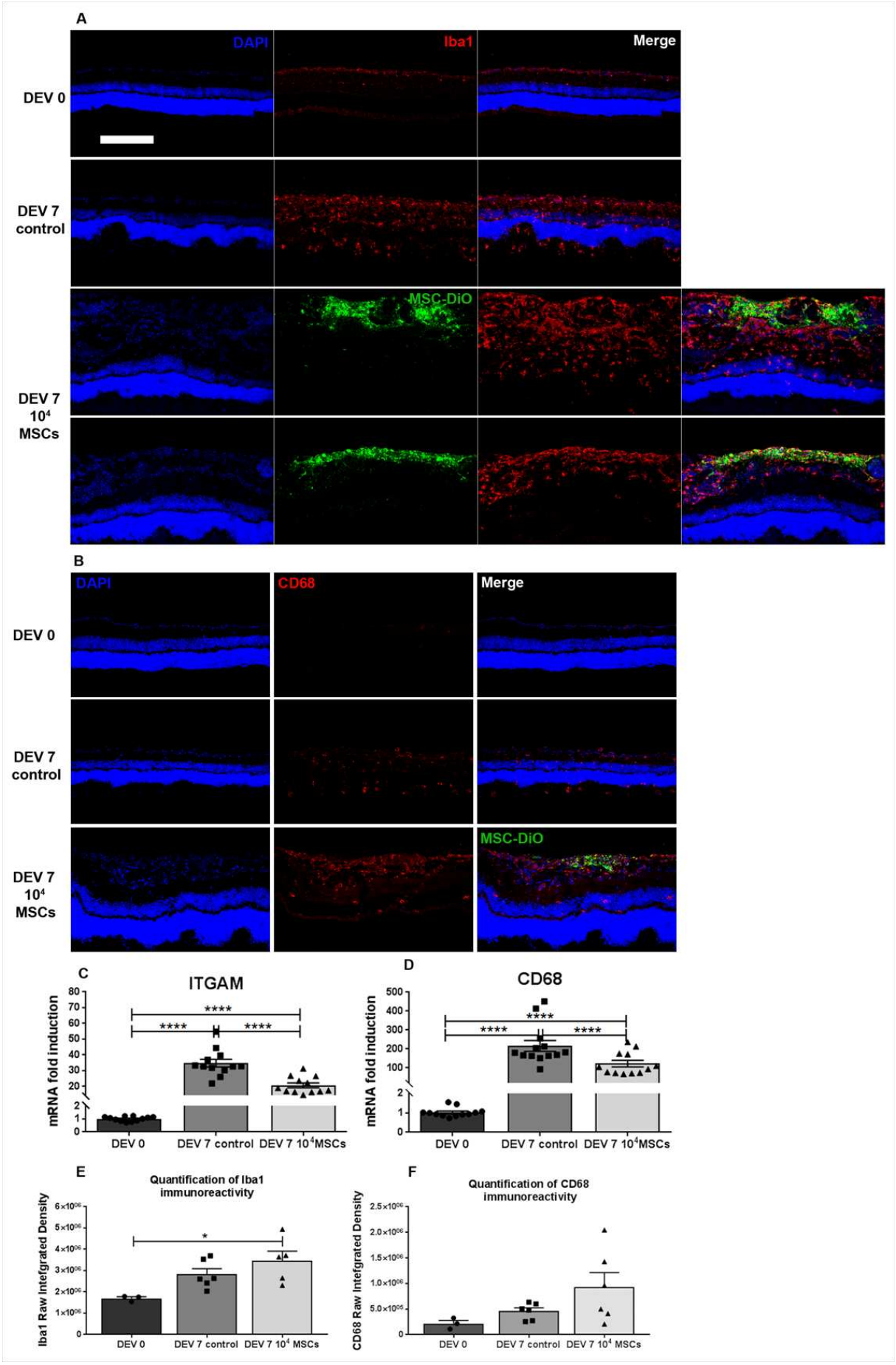
A
DAPI
Iba1
Merge
DEV 0
DEV 7 control
MSC-DiO
DEV 7 10⁴ MSCs
B
DAPI
CD68
Merge
DEV 0
DEV 7 control
MSC-DiO
DEV 7 10⁴ MSCs
C
ITGAM
mRNA fold induction
****
****
****
DEV 0
DEV 7 control
DEV 7 10⁴MSCs
D
CD68
mRNA fold induction
****
****
****
DEV 0
DEV 7 control
DEV 7 10⁴MSCs
E
Quantification of Iba1 immunoreactivity
Iba1 Raw Intefgrated Density
*
DEV 0
DEV 7 control
DEV 7 10⁴ MSCs
F
Quantification of CD68 immunoreactivity
CD68 Raw Intefgrated Density
DEV 0
DEV 7 control
DEV 7 10⁴ MSCs

Figure 35 : Evaluation of microglial activation on retinal explants cocultured with MSCs
Representative images of retinal explant cryosections cocultured with 1.10^4 MSCs at DEV 0 and DEV 7 immunolabeled with Iba1 (red) **(A.)**, CD68 (red) **(B.)** and DiO labeled MSCs (green) at 200x magnification (scale bar = 100 µm). **C.** Quantification of Iba1 immunoreactivity (expressed as Raw Integrated Density). N=4-6 animals/group. Ordinary one-way ANOVA was performed. *P<0.05. **D.** Quantification of CD68 immunoreactivity (expressed as Raw Integrated Density). N=4-6 animals/group. Ordinary one-way ANOVA was performed. **E and F.** RT-qPCR analysis of ITGAM and CD68 expression in retinal explants at DEV 0 and DEV 7. mRNA levels are presented after normalization with the housekeeping gene Rps18. N=12-13 animals/group. Unpaired t-test was performed for unpaired comparisons. ****P< 0.0001.

MSCs have an immunomodulatory effect on retinal explants

To investigate whether the presence of MSCs in the retinal explant coculture model could exert immunomodulatory properties and influence on microglial phenotypes, we analyzed microglial polarization markers through the mRNA expression of type M1 *classically activated*, namely TNFα, IL1β and IL6, and M2 *alternatively activated*, namely Arginase 1, IL10, CD163 and TNFAIP6 [337,338]. Our data showed that mRNA expression of M1 phenotype markers TNFα, and IL1β levels were significantly lower at DEV 7 in the MSC group compared to the control group ($p=0.0143$ and $p<0.001$ respectively) (figure 36 A). There was a significant increase in the level of IL6 mRNA expression at DEV 7 but no significant difference between the control group and the MSC coculture group. The mRNA expression levels of the markers of M2-polarized microglia, Arginase 1, IL10, and TNFAIP6 were significantly lower in the MSCs coculture group at DEV 7 compared to the control group ($p<0.0001$, $p=0.071$, and $p<0.0001$, respectively) (figure 36 B). Only mRNA expression of the M2 marker CD163 was significantly lower in the control group compared to DEV 0, with no significant difference between the MSC coculture group and the control group at DEV 7. However, there were no significant difference between the DEV 7 MSC group and DEV 0 for IL10, CD163 or TNFAIP6 mRNA expression levels. MSCs reduced the expression of M1 inflammatory markers.

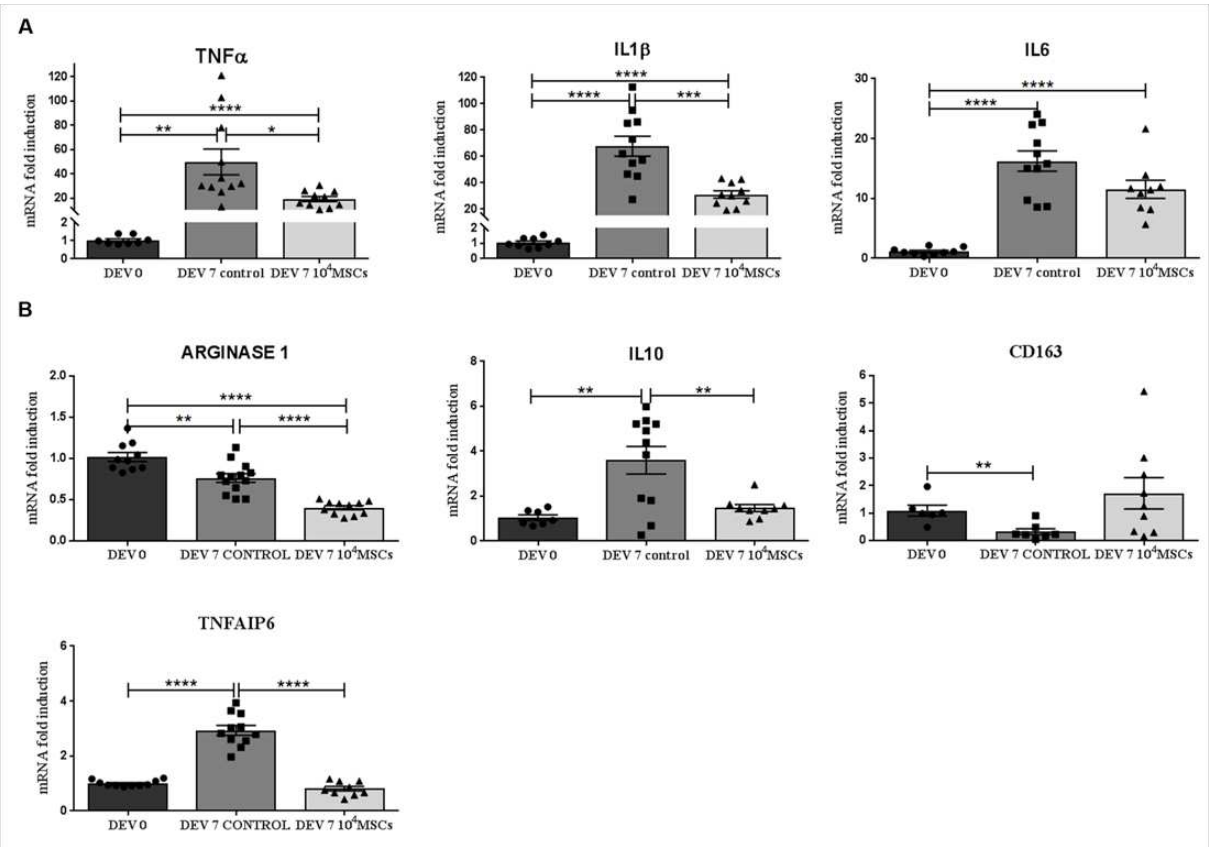

Figure 36 : RT-qPCR analysis of M1 (A.) and M2 (B.) phenotype marker expression in retinal explants at DEV 0 and DEV 7

mRNA levels are presented after normalization with the housekeeping gene Rps18. N=6-16 explants/group. Unpaired t-test or Mann-Whitney test were performed for unpaired or nonparametric comparisons. *P<0.05, **P< 0.01, ***P<0.001, ****P<0.0001.

MSCs affect retinal architecture and induce an ERM-like phenotype

Before the coculture, DiO labeling of MSCs allowed tracking of the MSCs to determine their ability to graft into the retinal explant. At DEV 7, a few MSCs were found in the retinal explants at the GCL level. Most MSCs did not penetrate the retina and remained at the surface of the explant, probably where the 2 µl of MSC suspension was deposited (figure 32B).

Explant "swelling" was observed in all explants in the MSC cocultured group, with increased explant thickness and retinal folding, compared to DEV 0 and to DEV 7 controls. MSCs also induced the appearance of an epiretinal membrane at the surface of the retinal explants. In order to investigate whether this distortion was associated with an epiretinal membrane phenotype, we used an anti-fibronectin antibody, since this protein is known to be upregulated in idiopathic epiretinal membranes [379]. Figure 37 shows the increase in fibronectin labelling at the surface of the explant cocultured with MSCs. This fibronectin expression was higher on the apical side of the explant, at the contact area between the MSCs and GCL. Likewise, H&E staining was performed to assess retinal micro-architectural organization and to quantify explant swelling in presence of MSCs. The laminar structure

of the retinal explants at DEV 7 in the control group showed a folded appearance to the outer segments (OS) and outer nuclear layer (ONL) compared to DEV 0 (figure 38). Explants in the coculture group exhibited a thicker internal retinal layer. Figure 38C shows a significant increase in retinal explant thickness, which was found in all the explants in the MSCs cocultured group compared to the DEV 7 control and DEV 0 groups (405±30 µm vs 218±20 µm and 220±28 µm respectively, P<0.0001). MSCs induced thickening of the explants and disorganization of the retinal architecture with a formation of an epiretinal membrane.

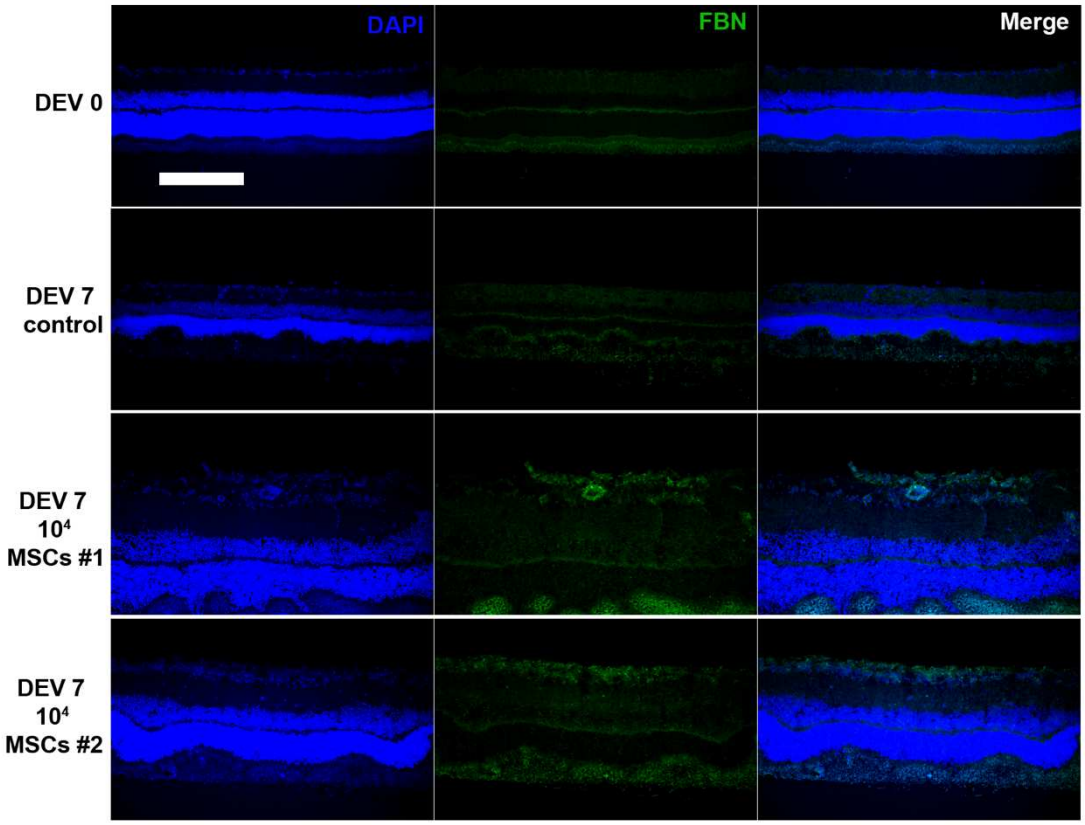

Figure 37 : Representative cryosections of retinal explants cocultured with 104 MSCs at DEV 0 and DEV 7, immunolabeled with fibronectin (green)
at 200x magnification (scale bar = 100 µm) (n=3-5/group).

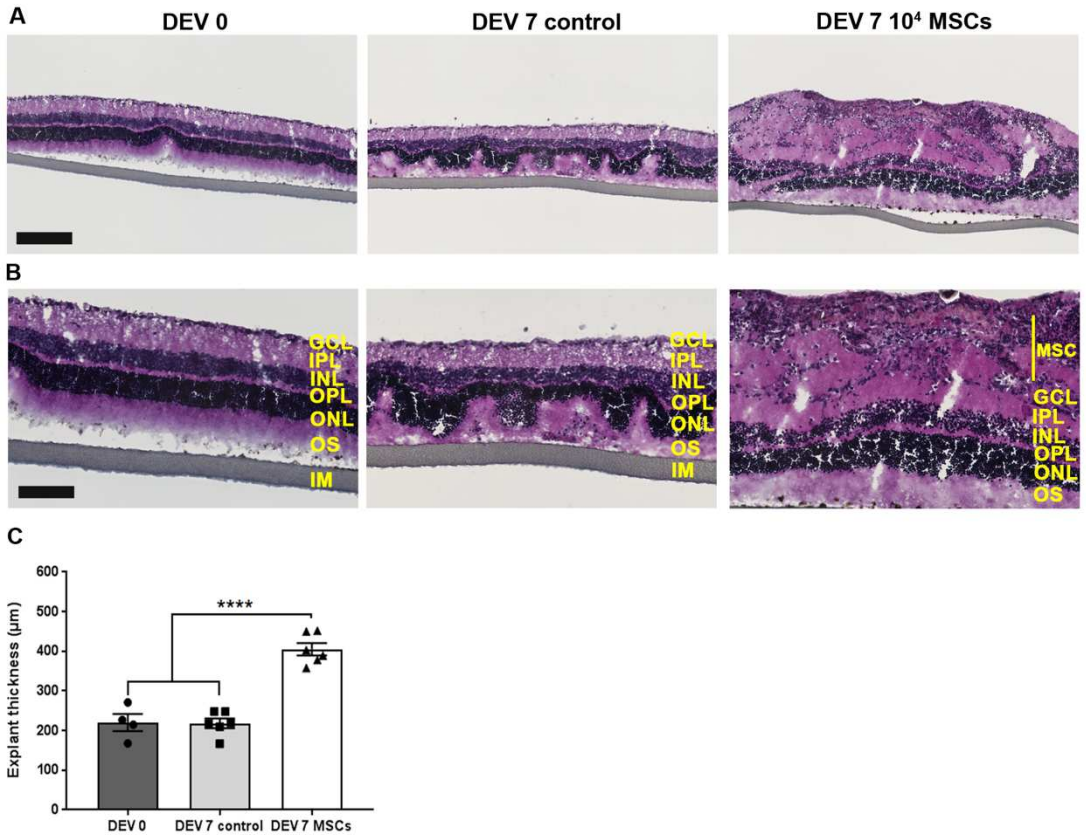

Figure 38 : Representative hematoxylin and eosin (H&E) staining of retinal explant cryosections cocultured with MSCs (A) Representative hematoxylin and eosin (H&E) staining of retinal explant cryosections cocultured with 10^4 MSCs at Days Ex Vivo 0 and Ex Vivo 7 at 100x magnification (scale bar = 200 µm) and (**B.**) at 200x magnification (scale bar = 100µm). Abbreviations: MSC: mesenchymal stem cell, GCL: ganglion cell layer, IPL: inner plexiform layer, INL: inner nuclear layer, OPL: outer plexiform layer, ONL: outer nuclear layer, OS: outer segments, IM: insert membrane. (**C.**) Retinal explant thickness measurement. Each bar is the mean ± SEM. n=4-6/group. Ordinary one-way ANOVA was performed. ****P<0.0001.

Discussion

Over the last decade, there has been increasing interest in the use of stem cells, including retinal progenitor cells (RPCs), embryonic stem cells (ESCs), induced pluripotent stem cells (iPSCs) and MSCs to regenerate RGCs in glaucoma [380]. MSCs have also shown neuroprotective and immunomodulatory properties. They have the advantages of demonstrating immunosuppressive effects and are less immunogenic and tumorigenic than ESCs. Compared with harvesting RPCs, it is relatively easy to obtain MSCs, and they possess a higher proliferative capacity [356]. The iPSCs strategy is also interesting, as these cells have the potential for reducing immunogenicity through autologous transplantation, but iPSCs have a lower variable differentiation efficiency and a relatively high risk of gene mutation [381].

Despite promising results in animals, clinical trials of intravitreal injections of BMMSCs have raised some safety concerns, which require further studies and the development of additional experimental models mimicking retinal degeneration in glaucoma [356].

In the present study, we showed that our *ex-vivo* axotomy model results in rapid RGC degeneration and gliosis caused by optic nerve transection and disruption of axonal transport, enabling investigation of neuroprotective or anti-inflammatory therapeutic compounds or stem cell transplantation therapies in human or rodent tissues [382,383]. This retinal explant model has the advantage of maintaining an *in-vivo* type architecture with all the neuroretina layers retaining intercellular interactions. It also limits the number of animals sacrificed, since one animal provides eight explants. Thus, this model fills the gap between relevant but time/cost/animal-consuming preclinical models and cell culture models which cannot substitute for the complexity of an entire tissue.

Advances in glaucoma research increasingly suggest that this degenerative optic nerve disease is linked to neuroinflammation [32]. The activation of microglia seems to play an important role in glaucoma pathogenesis, and strategies aiming to modulate reactive microglia are explored to slow down the progression of glaucoma and improve RGC survival [340]. In this study, we show that the MSCs have immunomodulatory properties and could be able to block RGC death in the retinal explant axotomy model by modifying the inflammatory state.

Although MSCs allowed us to observe neuroprotection, reduced gliosis, and modulation of inflammation in our *ex vivo* retinal explant model, we noticed edema and folding of the retinal explants.

This swelling of the explants may correspond to the adverse effects reported in clinical trials in humans. Indeed, despite promising results in animals with good efficacy and good safety profiles, the translation to humans in clinical trials was more than disappointing [350]. Several studies and trials have warned of serious ocular adverse effects following MSC transplantation, questioning the safety of using MSCs in retinal disease [384–386]. Among the complications reported, retinal detachments, retinal folds, subretinal exudative fluid, vitreous hemorrhage, vitreoretinal proliferation, proinflammatory vitreous clumping, thick epiretinal membrane formation as well as ocular hypertension and microcystic corneal edema have been described [385,387–389]. Surprisingly, these effects were not found in a phase 1 trial studying the safety of intravitreal autologous MSC transplantation in 14 patients with retinitis pigmentosa [390]. This could be due to the atrophic status of the retina in such severe degenerations. In a clinical phase I study, Satarian *et al.* described severe fibrous tissue proliferation in the BMMSC-injected eye of one patient, which was reproduced in a mouse vitreous cavity injected with the same MSCs [389]. MSCs of the other two patients did not generate fibrosis in the animal vitreous. Considering the heterogeneity of individual MSC samples, they thus proposed evaluation of the cells in animals prior to their intravitreal injection in patients.

Possible explanations for the disorganization found in our explants following coculture with MSCs could include differentiation of MSCs into myofibroblasts, promoting retinal fibrosis [391]. We noticed an increase of gliosis and microglial activation at the junction between the explants and MSCs. Tassoni *et al.* also demonstrated in both *in vivo* and *ex vivo* mice retina that intravitreal BMMSC transplantation

was associated with gliosis-mediated retinal folding, upregulation of intermediate filaments, and recruitment of macrophages. They described a JAK/STAT3 and MAPK (ERK1/2 and JNK) cascade activation in retinal Müller glia [392].

The question, therefore, arises of finding a method allowing preservation of the beneficial effects of MSCs while avoiding the undesirable effects and disadvantages of using MSCs, such as potential tumorigenicity, need for autologous collection, and variability.

It was initially hypothesized that cell replacement was an important mechanism of action of MSCs. However, considering the poor ability to graft MSCs into the retina [353,373], the beneficial effects of MSCs are now believed to be mediated mostly by their paracrine ability to release multiple factors such as neurotrophins, growth factors (BDNF, NGF, PDGF), chemokines, immunomodulators (IDO, PGE2, TSG-6) and extracellular vesicles [368,393,394]. This broad range of released factors with diverse functions, including anti-inflammatory potential, neuroprotection, and immunomodulation, is known as the secretome or conditioned medium (CM). Concerning the immunomodulatory effects of MSCs, we were able to show in our model that MSCs reduced the expression of M1 state as well as M2 state cytokine mRNAs. Therefore, MSCs induced an immunosuppressant effect, but failed to promote M2 subtype polarization. Such properties of MSCs have been found in several studies [338,395]. Holan *et al.* demonstrated that the cytokine environment of MSCs influences the spectrum of cytokines they produce, and thus, their immunoregulatory potential [396]. To enhance the efficiency of such CM, several priming methods, such as culture duration, O_2 level, addition of growth factors or anti/pro-inflammatory cytokines, or three-dimensional culture methods, could allow switching the factors produced by MSCs towards an anti-inflammatory profile [397–400].

More recently, other stem cell-free approaches using extracellular vesicles (exosomes and microvesicles), have been under investigation. These vesicles are considered to be responsible for the paracrine effects of MSCs, promoting immunomodulation, tissue repair, and regeneration, with a lower risk of oncogenic transformation and immune reactions than injections of whole MSCs [350,401–403].

Conclusion

Using an *ex vivo* retinal explant model, we demonstrated a neuroprotective and immunomodulatory effect of MSCs on RGCs. Since this model allowed us to reproduce the expected but also undesirable effects of injections of MSCs, it appears suitable for screening efficacy and safety of potential candidates for retinal therapy and should be useful for future assessment of cell-based or alternative methods of neuroprotection and neuroregeneration.

Acknowledgements: We thank the Cytometry Core Facility ‘Phénotypage Cellulaire et Tissulaire de l'Institut de la Vision’, Sorbonne Université, Institut de la Vision, Paris, France. We thank Stéphane Fouquet and Marie-Laure Niepon from the Image platform at Sorbonne Université, Institut de la Vision, Paris, France. We thank Claire Poilane and Didier Gleize from the Pathological department, Centre Hospitalier National d'Ophtalmologie des Quinze-Vingts, Paris, France.

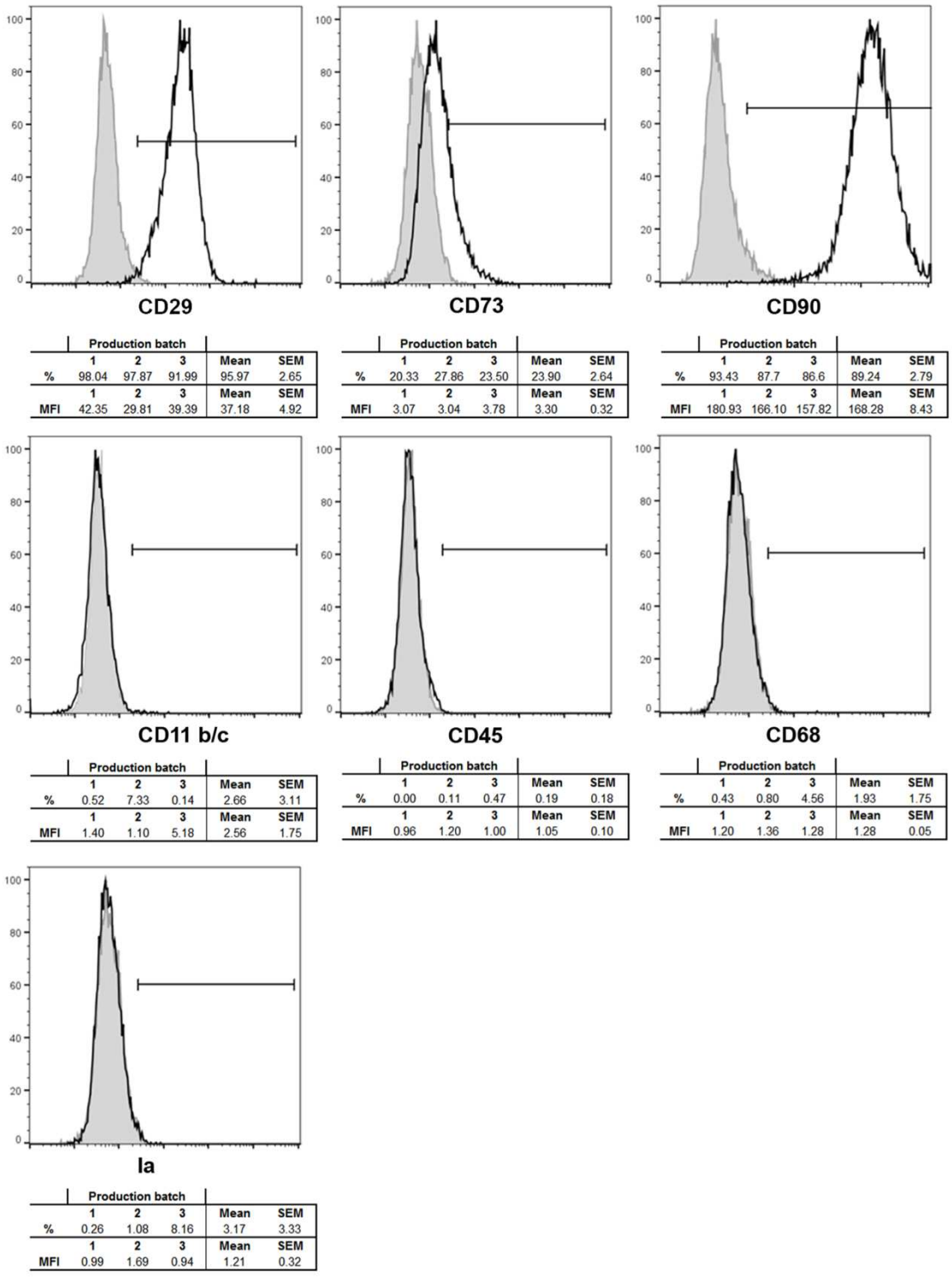

CD29	Production batch				
	1	2	3	Mean	SEM
%	98.04	97.87	91.99	95.97	2.65
	1	2	3	Mean	SEM
MFI	42.35	29.81	39.39	37.18	4.92

CD73	Production batch				
	1	2	3	Mean	SEM
%	20.33	27.86	23.50	23.90	2.64
	1	2	3	Mean	SEM
MFI	3.07	3.04	3.78	3.30	0.32

CD90	Production batch				
	1	2	3	Mean	SEM
%	93.43	87.7	86.6	89.24	2.79
	1	2	3	Mean	SEM
MFI	180.93	166.10	157.82	168.28	8.43

CD11 b/c	Production batch				
	1	2	3	Mean	SEM
%	0.52	7.33	0.14	2.66	3.11
	1	2	3	Mean	SEM
MFI	1.40	1.10	5.18	2.56	1.75

CD45	Production batch				
	1	2	3	Mean	SEM
%	0.00	0.11	0.47	0.19	0.18
	1	2	3	Mean	SEM
MFI	0.96	1.20	1.00	1.05	0.10

CD68	Production batch				
	1	2	3	Mean	SEM
%	0.43	0.80	4.56	1.93	1.75
	1	2	3	Mean	SEM
MFI	1.20	1.36	1.28	1.28	0.05

Ia	Production batch				
	1	2	3	Mean	SEM
%	0.26	1.08	8.16	3.17	3.33
	1	2	3	Mean	SEM
MFI	0.99	1.69	0.94	1.21	0.32

Additional File 1. Flow cytometric images showing the histogram overlays of specific antibodies vs isotypic-matched immunoglobulins for each marker from one BMMSC production batch with table presenting the percentages of positive cells and means of fluorescence intensities (MFI) for each marker and each production, with their means, and standard error of the means (SEM).

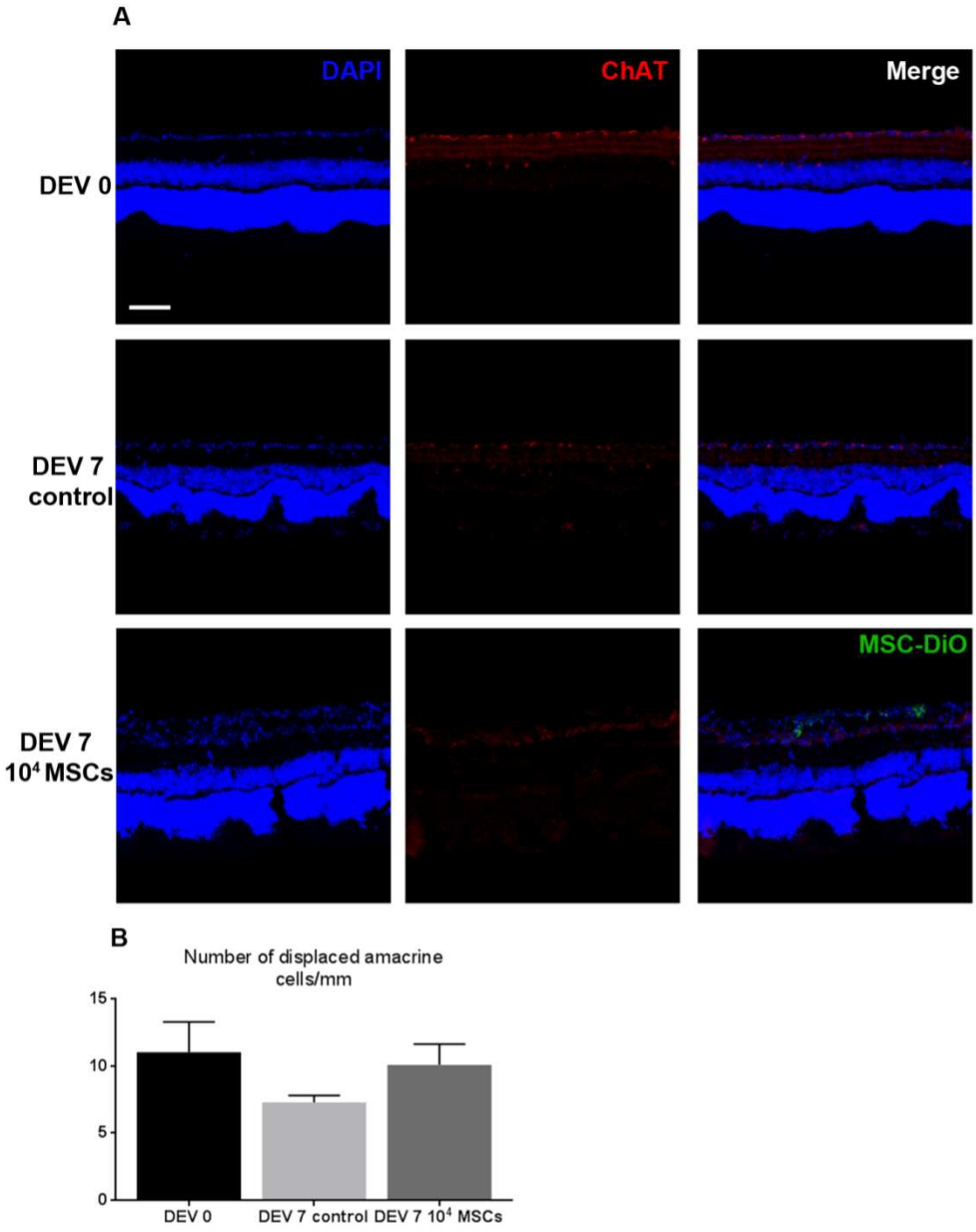

Additional File 2. A. Representative images of retinal explant cryosections cocultured with 1.104 MSCs for 7 days at DEV 0 and DEV 7, immunolabeled with ChAT (red) and DiO labeled MSCs (green) at 200x magnification (scale bar = 100 µm). B. Quantification of ChAT+ DACs from retinal explants (n=4-6/day) co-cultured with 1.104 MSCs for 7 days. DACs counts on cryosections are expressed as DACs/mm.

Évaluation des effets neuroprotecteurs et immunomodulateurs des inhibiteurs de la Rho-kinase dans un modèle ex vivo neurorétinien de rat après axotomie

É. Reboussin, P. Bastelica, I. Benmessabih, A. Réaux-Le Goazigo, C. Olmière, F. Brignole-Baudouin, C. Baudouin, J. Buffault*, S. Mélik-Parsadaniantz*

*Co-last authors

Les inhibiteurs des rho-kinases (ROCK-i) ont été reconnus comme agents antiglaucomateux [404]. Comme nous l'avons vu dans la première partie de cette thèse, ces inhibiteurs diminuent la PIO en augmentant le débit d'évacuation de l'humeur aqueuse au niveau du trabéculum. Leur rôle dans la neuroprotection et la régénération neuronale a été suggéré comme étant utile dans le traitement de maladies neurologiques, telles que les lésions de la moelle épinière, la maladie d'Alzheimer et la sclérose en plaques [405,406]. Au niveau de l'œil, des études chez le rat ont montré que l'instillation topique d'un ROCK-i pourrait promouvoir la survie des CGR et la régénération du nerf optique après son écrasement [407,408]. En agissant directement sur les neurones et en interrompant l'apoptose des CGR, ils pourraient constituer une nouvelle approche pharmacologique pour la neuroprotection du glaucome. La réduction conjointe de la PIO avec des effets neuroprotecteurs ou régénératifs par une même molécule susciterait beaucoup d'espoir dans le traitement des patients atteints de glaucome.

L'utilisation de notre modèle d'explant rétinien pour évaluer l'effet neuroprotecteur et immunomodulateur des ROCK-i a fait l'objet d'un travail de recherche d'un étudiant de master 2 au sein de notre laboratoire (I. Benmessabih, co-encadré par E. Reboussin et moi-même) avec des résultats préliminaires prometteurs.

Introduction

Les rho-kinases, ou ROCK, sont des protéines kinases découvertes en 1995 par Leung *et al.* Elles possèdent une structure *coiled-coil* formant des hélices enroulées abritant le site de liaison des protéines Rho [409,410]. Elles possèdent deux isoformes, ROCK1 et ROCK2. Les ROCK sont des protéines ubiquitaires jouant un rôle dans divers processus cellulaires tels que la stabilisation du cytosquelette d'actine, la régulation de la production de cytokines et chimiokines, la régulation de la mort cellulaire et la rétractation des neurites dans les neurones [269,410]. Il est à noter que l'expression des isoformes ROCK1 et ROCK2 varie selon les régions de l'organisme. Dans l'œil, ROCK2 est fortement exprimé par rapport à ROCK1[411].

Elles sont devenues des cibles d'intérêt pour des traitements neuroprotecteurs et immunomodulateurs [405,406].

Les inhibiteurs des ROCK (ROCK-i) sont des inhibiteurs compétitifs et présentent donc une inhibition réversible. Ils se fixent dans le domaine kinase des ROCK et empêchent les protéines cibles de se fixer et d'être phosphorylées. Certains d'entre eux sont spécifiques d'une des isoformes de ROCK, d'autres inhibent les deux isoformes, avec une action égale pour les deux ou non.

Les ROCK-i ont trouvé des applications diverses, de la différenciation de cellules souches en culture à la recherche sur le cancer et le traitement du glaucome. Ils ont démontré des effets bénéfiques sur la PIO en favorisant l'évacuation de l'humeur aqueuse [407,412]. En effet, les ROCK-i ont démontré leurs effets sur l'HTO grâce à leurs effets sur le cytosquelette des cellules du TM et leur MEC [14,413,414], permettant ainsi une meilleure évacuation de l'humeur aqueuse et une baisse de la PIO. Des études suggèrent un effet neuroprotecteur indépendant de la PIO associé des ROCK-i [407,408,415]. Cet effet serait mixte par amélioration du flux sanguin vers le nerf optique mais aussi par un effet direct sur la neurorétine en augmentant la survie des cellules ganglionnaires et en favorisant la régénération axonale [412,416].

Dans cette étude, nous avons évalué trois ROCK-i distincts, à savoir Y-27632, Y-33075 (également connu sous le nom de Y-39983), et H-1152, pour étudier leurs effets sur la survie des CGR et sur l'inflammation rétinienne dans un modèle d'explant rétinien après axotomie. Ces trois ROCK-i présentent des caractéristiques spécifiques qui les distinguent les uns des autres, ce qui permet une comparaison approfondie de leurs effets neuroprotecteurs et immunomodulateurs.

Y-27632 est l'un des premiers ROCK-i développés (1997) et c'est une des molécules classiquement utilisées dans les études sur le glaucome et les cellules souches, notamment dans notre équipe où il a été utilisé dans un modèle de glaucome TGF-β2-induit sur culture primaire de cellules de TM humaines. Sur ce modèle il a démontré un effet de détente du cytosquelette des cellules et de la MEC [14]. Y-27632 est non-spécifique d'une isoforme mais a une affinité légèrement plus importante pour ROCK1 que pour ROCK2. Cette molécule a été testée *in vivo* en instillation topique chez le lapin et a démontré son effet hypotenseur, tandis qu'en injection intravitréenne chez le rat, dans un modèle d'ischémie rétinienne transitoire, une diminution de la mort des CGR dans la rétine a été observée [414,417,418].

Y-33075 est un ROCK-i développé plus récemment (2005) possédant deux particularités le différenciant d'Y-27632 : un pouvoir inhibiteur 30 fois plus important et l'absence d'affinité spécifique pour une isoforme de ROCK [419,420]. *In vivo*, Y-33075 a été testé en injection intravitréenne dans un modèle d'encéphalomyélite auto-immune chez la souris et a démontré une diminution de la démyélinisation des axones du nerf optique [421].

H-1152 a pour particularité d'être spécifique de ROCK2 et d'avoir une affinité six fois plus importante pour ce dernier qu'Y-27632. *In vitro*, la molécule a été testée sur un modèle d'hypoxie rétinienne transitoire dans une rétine bovine isolée, ainsi que sur une rétine organotypique isolée soumise à des

conditions de stress où H-1152 a démontré un effet neuroprotecteur et un effet d'inhibition de l'activité gliale [346,422].

Matériel & Méthodes

Animaux

Pour la production des explants de neurorétine, nous avons utilisé des rats Long Evans mâles adultes (8-10 semaines) pesant 250-300g, fournis par Janvier Labs (Le Genest-Saint-Isle, France). Les animaux ont été hébergés dans des conditions dites « *pathogen-free* » avec nourriture et eau *ad libitum* et sous un cycle 12h lumière/12h obscurité. Toutes les expérimentations ont été conduites après évaluation et approbation de *l'Institutional Animal Care* and *Use Committee* suivant les lignes directrices de la Directive 2010/63/EU du Parlement européen concernant la protection des animaux utilisés à des fins scientifiques. Toutes les procédures expérimentales ont été approuvées par le comité local d'éthique sur l'expérimentation animale C2EA-05-Charles Darwin. Les animaux ont été euthanasiés par asphyxie en caisson CO2 puis dislocation cervicale.

Culture d'explants de rétine et exposition aux agents pharmacologiques

Les yeux ont été prélevés après section du nerf optique et ont été rapidement placés dans un milieu CO2-indépendant (Thermo Fisher Scientific, Réf : 18045-054). La chambre antérieure a été séparée du reste de l'œil, le vitré extrait du globe oculaire, puis la rétine a été séparée des tissus oculaires périphériques par dissection. La rétine a été ensuite coupée en quatre explants de taille égale montés à plat, couche des CGR vers le haut, sur membrane Millicell-Polytetrafluoroethylene (PTFE) de 0, 4µm dans un insert de culture. Les explants ont ensuite été placés dans un milieu composé de milieu Neurobasal-A, 2% de supplément B27, 1% de supplément N2, 0, 4% L-glutamine, 1% de Pénicilline-Streptomycine 10 000U/mL (tableau 22) et des différents traitements ROCK-i et leur contrôles (DEV4 CTL). Les solutions contrôles ont été obtenues en diluant le véhicule (eau *RNase free*) à la même concentration que les solutions de ROCK-i (tableau 23). Les explants ont ensuite été mis en culture à 37°C à 5% de CO2 dans un air humidifié. Le milieu de culture était ensuite changé pour moitié le lendemain, puis toutes les 48h. Trois microlitres de solution de ROCK-i ou contrôle ont été déposés quotidiennement à la surface de chaque explant. La culture des explants était arrêtée après 4 jours (DEV4).

Tableau 22 : Fournisseurs et références du matériel et réactifs utilisés pour la culture d'explants

Désignation	Fournisseur	Référence
Insert de culture	Merck Millipore	PICM01250
Milieu Neurobasal-A	Thermo Fisher	10888022
Supplément B27	Thermo Fisher	0080085-SA
Supplément N2	Thermo Fisher	17502048
L-glutamine	Thermo Fisher	25030032
Milieu CO2-indépendant	Thermo Fisher	18045-054

Tableau 23 : Détails des ROCK-i utilisés

Type	Désignation	Fournisseur	Référence	Concentration solution stock (H_2O)	Dilution dans le milieu de culture
ROCK inhibiteurs	Y-27632	MedChemExpress	HY-10583	100mM	1/1000, 1/500 et 1/200
	Y39983	MedChemExpress	HY-10069	10mM	
	H-1552	MedChemExpress	HY-15720A	20mM	

Immunohistochimie sur explants entiers et coupes d'explants

A DEV0 et DEV4, les explants ont été fixés dans du PFA 4% (Merck Millipore, Réf : 1.00496.5000) pendant 2h à 4°C.

Pour l'immunohistochimie sur explants entiers, les explants ont ensuite été incubés dans la solution de saturation (5% BSA, 2% Triton, 0, 5% Tween 20) durant 3 heures, puis dans la solution d'anticorps primaires toute la nuit sous agitation à 4°c (cf. tableau 24) (2, 5% BSA, 1% Triton, 0, 25% Tween 20). Le lendemain, après 3 rinçages de 10 minutes au PBS, les explants ont été incubés en présence des anticorps secondaires et de DAPI (2, 5% BSA, 1% Triton, 0, 25% Tween 20 + anticorps anti-souris/anti-lapin/DAPI) durant 2 heures, à l'obscurité, sous agitation et à température ambiante. Après 3 lavages de 10 minutes au PBS, les explants ont été montés entre lames et lamelles et conservés dans l'obscurité à 4°C.

Pour l'immunohistochimie sur les coupes d'explants, après fixation au PFA 4%, les explants ont été déshydratés dans une solution de sucrose 30% pendant 24h à 4°C. Après déshydratation, les explants ont été rincés puis inclus en OCT avant d'être stockés à -20°C. Les explants ont ensuite été coupés au cryostat (12µm d'épaisseur) avant d'être placés sur lame et stockés à -20°C en attendant le marquage. Les coupes sont ensuite réhydratées puis soumises à un double immunomarquage Iba1/ki67 (marqueur de prolifération microgliale), Iba1/CD68 ou GFAP/S100β. Les images ont été réalisées au microscope confocal inversé (Olympus, FV10) au grossissement x40.

Tableau 24 : Anticorps et marqueurs utilisés pour les marquages d'immunofluorescence

Type	**Désignation**	**Fournisseur**	**Référence**
Anticorps primaires	Mouse monoclonal anti-3A3A	Merck Laboratories	MAB1585
	Rabbit polyclonal anti-GFAP	Wako	Z0334
	Rabbit polyclonal anti-Iba1	FUJIFILM Wako Pure Chemical Corporation	W1W019-19741
	Mouse monoclonal anti-CD68	Bio Rad Laboratories	MCA341R
	Goat polyclonal anti-Iba1	Abcam	Ab5076
	Rabbit monoclonal anti-Ki67	Abcam	Ab16667
	Mouse monoclonal anti-S100β	Sigma	S2532
	Rabbit polyclonal anti-GFAP	Agilent	Z033429-2

Anticorps secondaires	Donkey anti-mouse IgG (Alexa Fluor® 594 conjugate)	Thermo Fisher Laboratories	A21203
	Donkey anti-rabbit IgG (Alexa Fluor® 488 conjugate)	Thermo Fisher Laboratories	A21206
	Donkey anti-goat IgG (Alexa Fluor® 594 conjugate)	Thermo Fisher Laboratories	A11058
Autres	DAPI		

Analyse immunohistologique

Quantification des CGR

Les images ont été réalisées au microscope à épifluorescence (Zeiss AX-10) au grossissement x200 avec 4 images par explant (1 image en rétine centrale proche du nerf optique, 1 en périphérie de la rétine et 2 en moyenne périphérie. Le comptage a été réalisé grâce au marqueur Brn3A, marquant en moyenne 83% des CGR [346], *via* le logiciel ImageJ (United States National Institutes of Health (NIH)) et le plugin *Cell counter*. La moyenne du nombre de CGR par champ a été calculée pour chaque explant puis pour chaque traitement. Les moyennes de chaque traitement ont été comparées avec les moyennes des autres traitements ROCK-i, la moyenne des explants DEV4 CTL et la moyenne des explants DEV0.

Analyse de la réaction inflammatoire

L'analyse de la réaction inflammatoire a été réalisée par un marquage des protéines Iba1 et/ou CD68, respectivement marqueur de la microglie et marqueur de l'activation microgliale. L'astrogliose a été quant à elle étudiée par un marquage des protéines GFAP et S100β, respectivement marqueurs des filaments intermédiaires des astrocytes et marqueur de la prolifération et de la migration des astrocytes matures. Les images ont été réalisées au microscope confocal inversé (Olympus, FV10) au grossissement x200 ou x400.

RT-PCR quantitative

Les ARN totaux de tous les explants ont été purifiés grâce au kit d'extraction *NucleoSpin RNA* (Macherey–Nagel, Réf : 740955.250) selon le protocole du fabricant et conservés à -80°C. Les ARN totaux ont ensuite été rétrotranscrits en ADN complémentaire avec le kit *High Capacity RNA to cDNA* (Life Technologies, réf. 4368814) selon les instructions du fabricant. Une PCR en temps réel a été réalisée grâce au mélange *Master Mix TaqMan™ Fast Advanced* (Applied Biosystems, Réf. 4444557) et la machine *QuantStudio™ 5 Real-Time PCR System for Human Identification* (Applied Biosystems, Réf. A34322). La méthode delta-delta Ct (ddCt) a été utilisée pour analyser les variations de l'expression relative des différents gènes étudiés. L'expression relative des différents marqueurs (GFAP, CD11B, CD68, TNF-α, IL1-β, IL6, Arginase 1, CD163 et IL10) a été comparée à l'expression basale des explants DEV0 normalisée à 1.

Analyse statistique

Les analyses statistiques ont été réalisées grâce au logiciel GraphPad Prism 7. Les données sont présentées sous la forme de moyenne ± SEM. Pour la quantification des CGR et les analyses RT-qPCR, des T-tests ou tests de Mann-Whitney ont été réalisés.

Résultats

Y-33075 a une action neuroprotectrice sur les CGR

Pour le contrôle, il existe une baisse significative du nombre de CGR entre DEV0 et DEV4 (674 ± 21 cellules par image versus 354 ± 30, respectivement) représentant 52, 5 % de cellules restantes (T-test, p<0, 0001) (figure 39).

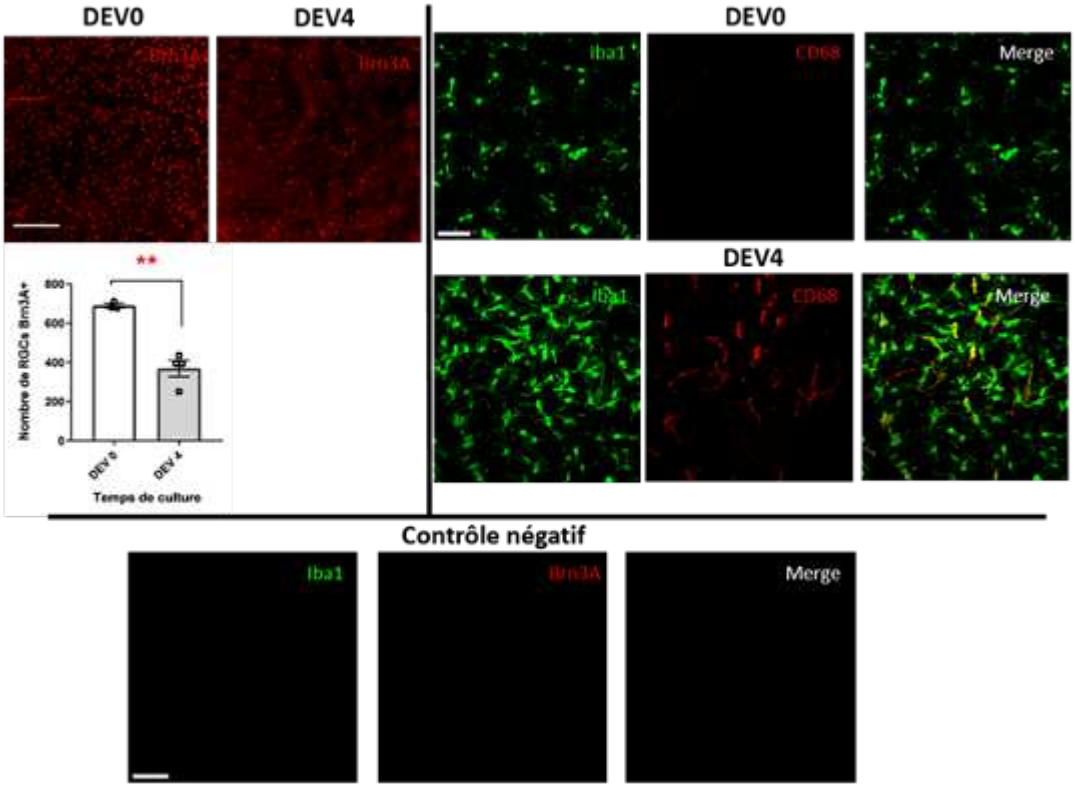

Figure 39 : Explants rétiniens à DEV0 et DEV4
A. Images de microscopie confocale (x20) d'explants de rétine marqués Brn3A après dissection (DEV0) et après 4 jours de culture (DEV4) (barre d'échelle = 150µm) B. Quantification des CGR Brn3A+ (n=4). Les barres d'erreur correspondent à l'erreur standard moyenne (**p = 0,0019) C. Images de microscopie confocale (x40, barre d'échelle : 50µm) d'explants de rétines marqués Iba1 (vert) et CD68 (rouge) après dissection (DEV0) et après 4 jours de culture (DEV4).

Avec les ROCK-i Y-27632 et H-1152, il n'y avait pas de différence significative par rapport au CTL DEV4 pour les trois concentrations étudiées. Respectivement 444 ± 68, 335 ± 63 et 338 ± 32 cellules par image pour les concentrations de 100µM, 200µM et 500µM de Y-27632 et 518 ± 53, 407 ± 5 et 411 ± 40 cellules/image pour les concentrations 20 µM, 40 µM et 100 µM de H-1152. Cependant, pour Y-27632 et H-1152, nous pouvons remarquer une diminution des moyennes entre les premières concentrations (respectivement 100µM et 20µM) et les concentrations suivantes. Malgré une absence

de différence significative entre les groupes de chaque molécule, nous pouvons envisager un dépassement du seuil de toxicité pour ces deux molécules qui pourrait expliquer une absence d'effet neuroprotecteur (figure 40).

Pour le ROCK-i Y-33075, on observe une différence significative par rapport au CTL DEV4 en moyenne 508 ± 32, 467 ± 28 et 560 ± 23 cellules/image pour les concentrations 10 µM, 20 µM et 50 µM respectivement (Mann-Whitney, p = 0,0140; p = 0, 0286; Unpaired t-test, p =0,0140) (figure 40). Le ROCK-i Y-33075 semble donc avoir une efficacité dans la neuroprotection des CGR.

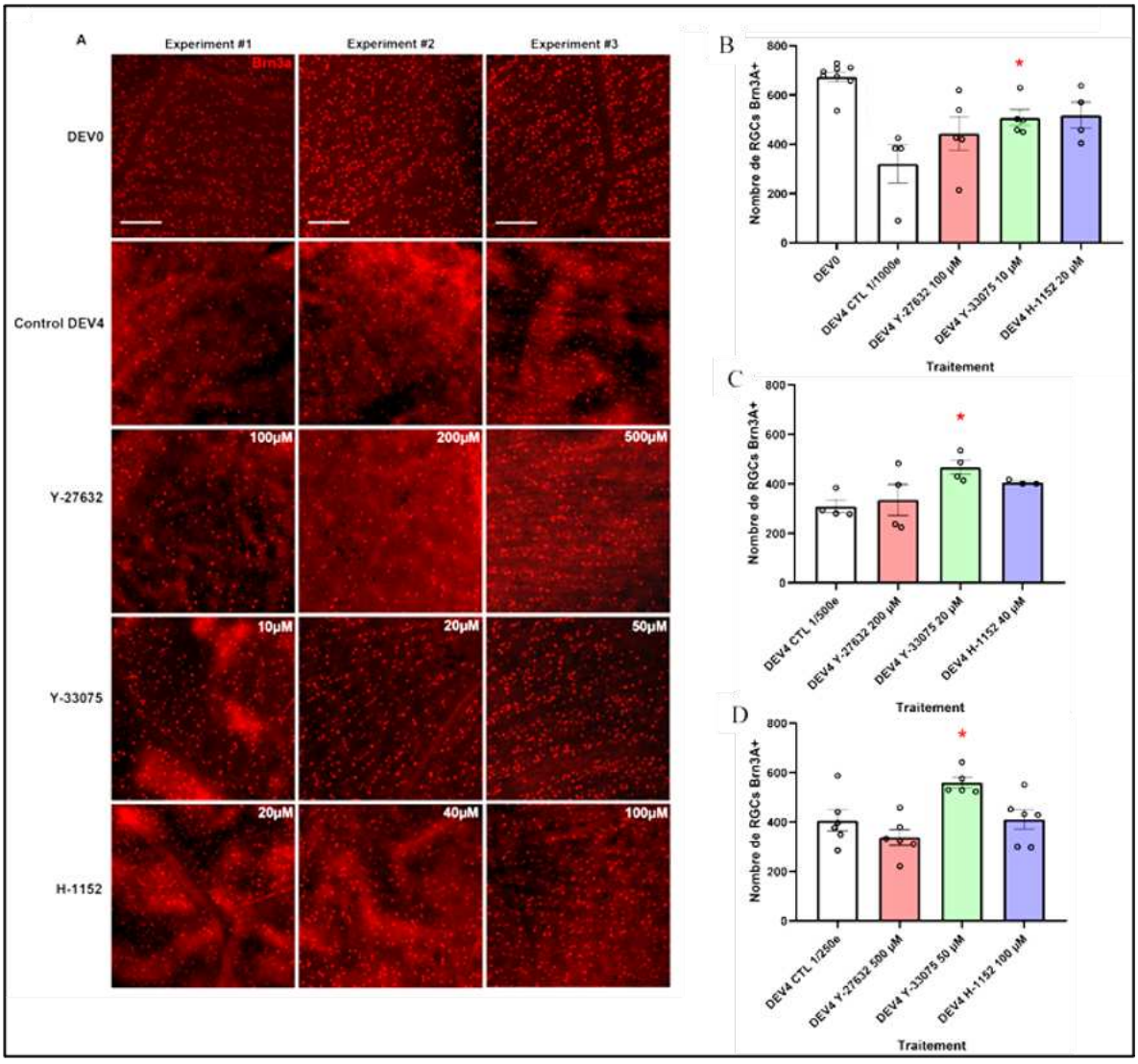

Figure 40 : Évaluation de l'effet neuroprotecteurs des différents ROCK-i
Images d'immunomarquage Brn3A représentatives d'explants rétiniens entiers en culture des groupes DEV0, DEV4 CTL ou des groupes traités DEV4 (y-27632 100µM, Y-33075 10µM, H-1152 20µM) (grossissement x200 : barre d'échelle=150µm). A. Comptages de cellules Brn3A+ (n=3-6 par groupe) pour les différents traitements comparés au groupe DEV4 CTL. B. Faibles concentrations C. Concentrations moyennes. D. Fortes concentrations (*p<0,05, barres d'erreur standard moyenn

Y-27632, Y-33075 et H-1152 réduisent l'inflammation dans la rétine

Tout d'abord, entre les groupes DEV0 et DEV4 CTL, nous constatons une augmentation qualitative de la taille des corps cellulaires des cellules microgliales grâce au marquage Iba1, ainsi qu'une augmentation du marquage CD68 à DEV4 (Figure 41 et 42). Ces différences de marquages témoignent d'une inflammation et d'une activation de la microglie rétinienne au cours du temps après axotomie du nerf optique.

Lorsque l'on compare les groupes DEV4 CTL aux groupes traités, on note chez ces derniers, une diminution qualitative de la taille des corps cellulaires, et une morphologie cellulaire se rapprochant de celle de la microglie des explants à DEV0 (Figure 41).

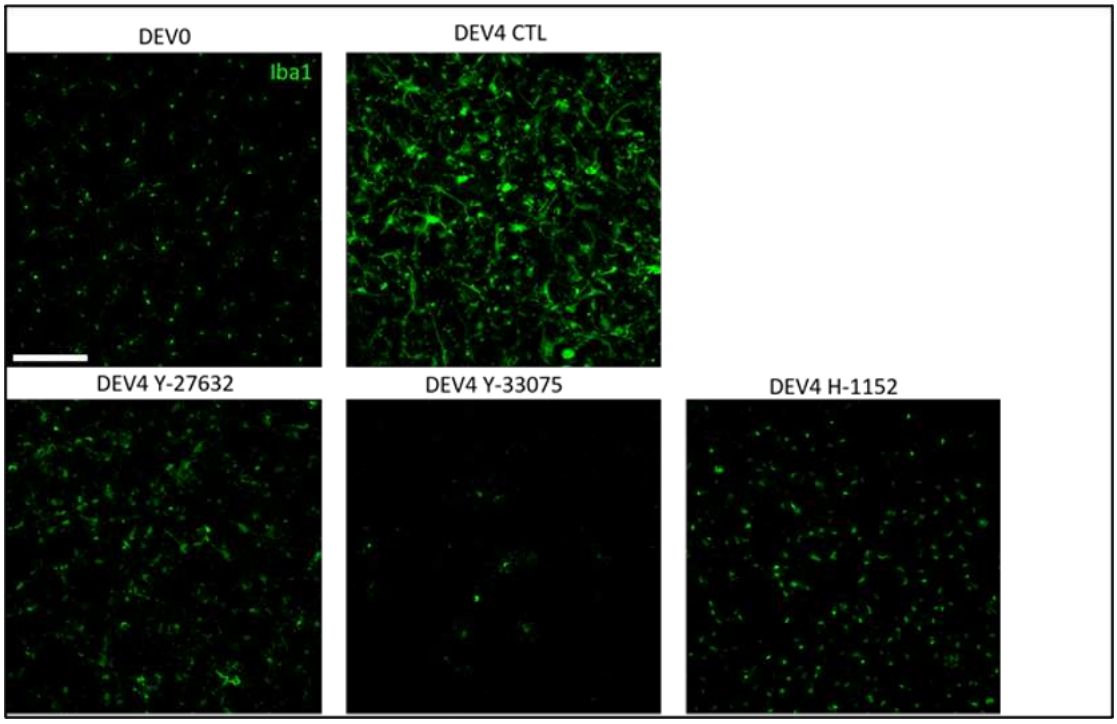

Figure 41 : Évaluation de l'effet des différents ROCK-i sur l'inflammation sur des explants rétiniens à plat
Images en microscopie confocale (x200, barre d'échelle : 150µm) représentant les explants de rétine marqués Iba1 (vert) après dissection (DEV0), après 4 jours de culture sans traitement (DEV4 CTL) et après 4 jours de traitement par ROCK-i (Y-27632 500µM, Y-33075 50µM et H-1152 100µM).

Ces différences, notamment concernant le marquage CD68, sont confirmées par l'étude des marquages réalisés sur les cryosections transversales d'explants qui montrent également une augmentation d'Iba1 et de CD68, témoins de l'activation de la microglie, entre les groupes DEV0 et DEV4 CTL. Au contraire, nous remarquons un niveau similaire de marquage entre les groupes DEV0 et DEV4 traités. Nous remarquons également une réduction du marquage Iba1 dans les groupes DEV4 Y-27632 et Y-33075

comparés au groupe DEV0 et un marquage équivalent entre le groupe DEV4 H-1152 et le groupe DEV0 (Figure 42).

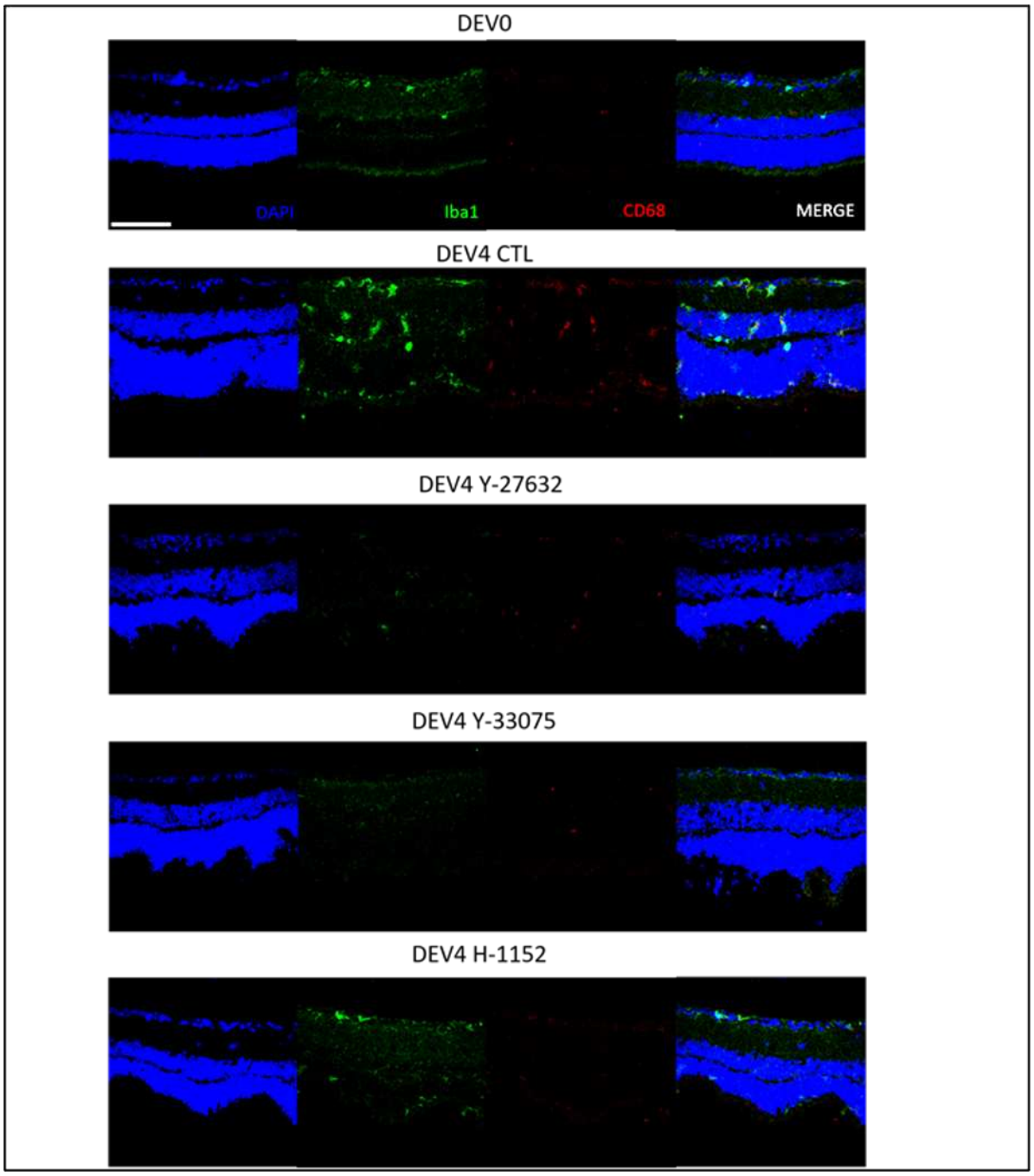

Figure 42 : Évaluation de l'effet des différents ROCK-i sur l'inflammation sur des explants rétiniens en coupe
Images en microscopie confocale (x400, barre d'échelle : 100µm) de cryosection marquées DAPI (bleu), Iba1 (vert) et CD68 (rouge) après dissection (DEV0), après 4 jours de culture sans traitement (DEV4 CTL) et après 4 jours de traitement ROCK-i (Y-27632 500µM, Y-33075 50µM et H-1152 100µM)

De plus, le double marquage KI67/Iba1 révèle une augmentation du nombre de cellules microgliales en prolifération (cellules Iba1/KI67 double positives) dans le groupe DEV4 CTL comparé au groupe DEV0 ce qui témoigne d'une activité de prolifération de la microglie en réaction à l'inflammation importante présente dans le groupe DEV4 CTL. Cette prolifération semble inhibée en présence des ROCK-i. En effet, nous observons une diminution des cellules microgliales marquées par Iba1 et KI67 (Figure 43).

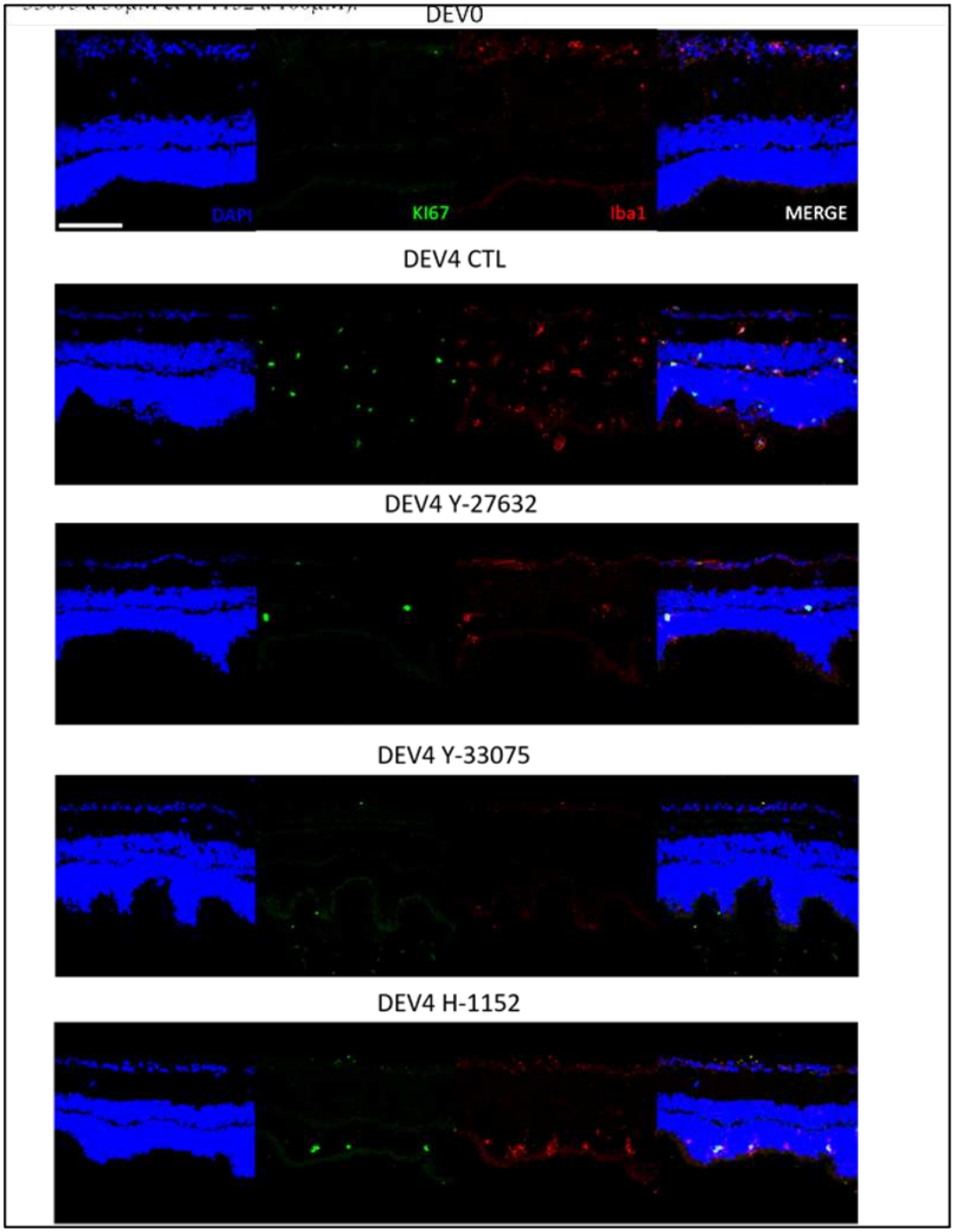

Figure 43 : Évaluation du nombre de cellules microgliales en prolifération sur des coups d'explants rétiniens traités par les différents ROCK-i
Images en microscopie confocale (x400, barre d'échelle : 100µm) de cryosections marquées DAPI (bleu), Ki67 (vert) et IbA1 (rouge) après dissection (DEV0), après 4 jours de culture sans traitement (DEV4 CTL) et après 4 jours de traitement ROCK-i (Y-27632 500µM, Y-33075 50µM, et H-1152 100µM)

Concernant l'activité astrocytaire, nous remarquons une forte augmentation du marquage GFAP (marquage des astrocytes et des cellules de Müller) et du marquage S100β (marqueur de l'astrogliose) qui passe d'un marquage quasi-exclusif de la couche des CGR et de la couche plexiforme interne pour le groupe DEV0 à un marquage étendu à toutes les couches de la rétine, plus intense dans la couche plexiforme interne dans le groupe DEV4 CTL. Cette observation témoigne d'une modification importante de la morphologie et de l'activité des astrocytes dans des conditions inflammatoires (Figure 44). Pour les groupes traités, nous obtenons des résultats différents pour chaque ROCK-i. Pour Y-27632, nous n'observons pas de baisse du marquage GFAP et S100β par rapport au groupe DEV4 CTL. En revanche, Y-33075 réduit fortement le marquage GFAP pour revenir au niveau de DEV0 sans réduction du marquage S100β. Enfin, H-1152 réduit les deux marquages GFAP et S100β. Y-33075 et H-1152 inhibent donc bien l'astrogliose dans la rétine et H-1152 inhibe même la prolifération des astrocytes (marqueur de prolifération S100β réduit). Ces observations en immunomarquages ont ensuite été confirmées par l'analyse de l'expression génique des marqueurs de l'astrogliose et de l'activation microgliale décrite ci-après.

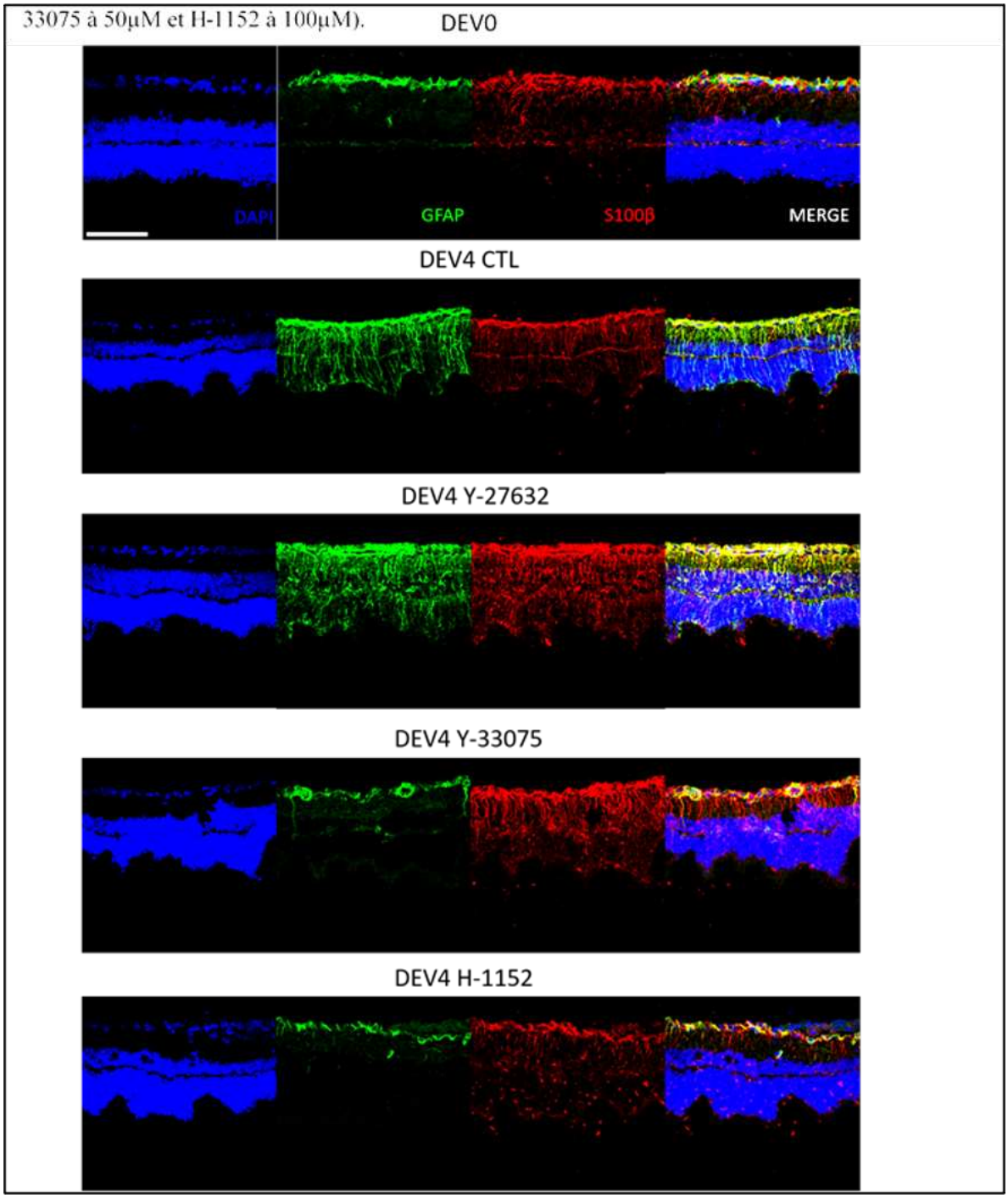

Figure 44 : Évaluation de l'astrogliose sur coupes d'explants exposés aux différents ROCK-i
Images en microscopie confocale (x400, barre d'échelle : 100µm) de cryosections marquées au DAPI (bleu), GFAP (marquage des astrocytes et des cellules de Müller, vert) et S100β (marqueur de l'astrogliose, rouge) après dissection (DEV0), après 4 jours de culture sans traitement (DEV4 CTL) et après 4 jours de traitement ROCK-i (Y-27632 500µM, Y-33075 50µM et H-1152 100µM)

Les ROCK-i diminuent l'expression des marqueurs de l'inflammation

Pour le contrôle, nous avons remarqué une augmentation significative de l'expression génique de tous les marqueurs étudiés, à l'exception des marqueurs de la polarisation M2, dans le groupe DEV4 CTL comparé au groupe DEV0, de l'ordre de 10 fois pour GFAP et 200 fois pour IL-1β (Figure 45). Concernant la polarisation M1 des cellules microgliales, TNF-α et IL-1β étaient significativement réduits avec les trois ROCK-i aux concentrations les plus importantes testées par rapport au groupe contrôle (TNF-α : Y-27632 500µM $p<0.03$; Y-33075 50µM $p< 0.003$; H-1152 100µM $p<0,005$; IL-1β : Y-27632 500µM $p<0.03$; Y-33075 50µM $p<0,003$; H-1152 100µM $p = 0.02$). Nous avons également observé, par rapport à DEV4, une réduction de l'expression de CD11b significative avec les traitements Y-27632 500µM et Y-33075 50µM ($p<0.003$ pour les deux traitements) ainsi que pour le marqueur CD68 pour le traitement Y-33075 50µM ($p = 0.003$). Enfin, pour les marqueurs de l'état d'activation M2 de la microglie, nous n'avons pas retrouvé de différence significative entre les groupes DEV0 et DEV4 CTL mais nous observons une baisse significative de l'expression de l'*Arginase 1* et d'*IL10* pour le groupe H-1152 100µM et de CD163 dans le groupe Y-27632 500µM ainsi qu'une tendance à la baisse mais non significative dans le groupe H-1152 100µM (résultat indéterminé pour Y-33075 50µM nous empêchant de conclure pour ce groupe). Nous pouvons ainsi conclure quant aux résultats de RT-qPCR à une baisse significative de l'expression d'une majorité des marqueurs de l'inflammation et de l'activation microgliale étudiés pour les 3 ROCK-i aux plus fortes concentrations testées.

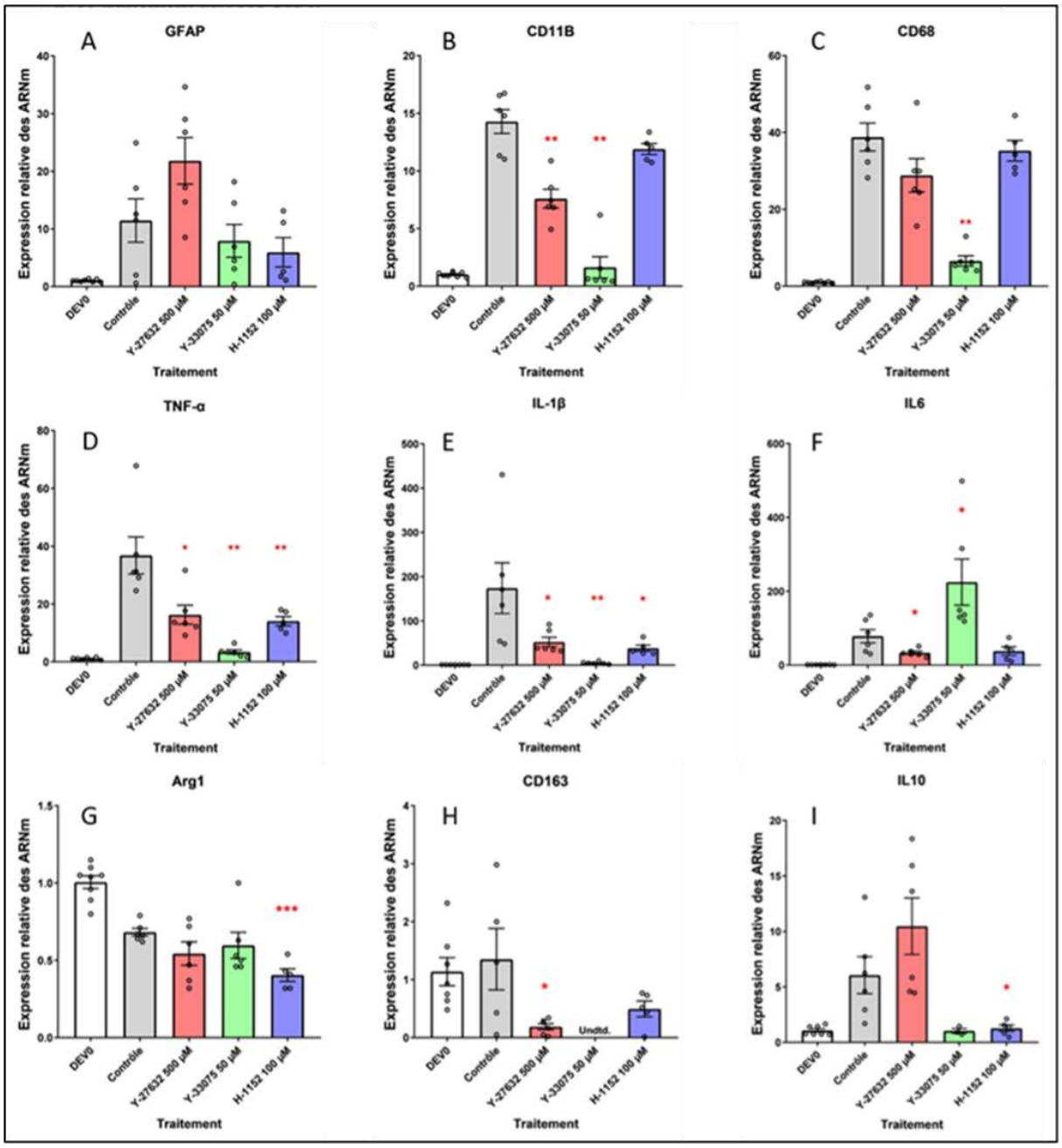

Figure 45 : Quantification de l'expression génique des marqueurs de l'inflammation après traitement par différents ROCK-i par RT-PCR.
Graphiques représentant l'expression génique relatives des marqueurs A. GFAP, B. CD11B, C. CD68, D. TNF-alpha, E IL1-β, F. IL6, G. Arginase 1, H. CD163 et IL10 dans les explants de rétine à DEV0, DEV4 CTL et DEV4 après traitement par les différents ROCK-i.

Discussion

Notre étude sur ce modèle d'explant rétinien de rat après axotomie a révélé des résultats prometteurs quant au rôle immunomodulateur et neuroprotecteur des ROCK-i. Ces résultats sont encourageants pour la recherche sur le glaucome, une maladie neurodégénérative inflammatoire. Au quatrième jour après l'axotomie, nous avons constaté une diminution significative de la perte des CGR dans les explants

traités avec le Y-33075 par rapport aux explants non traités (DEV4 CTL), suggérant un effet neuroprotecteur.

En outre, nous avons observé que les trois ROCK-i testés, à des concentrations élevées, exerçaient un effet anti-inflammatoire en réduisant l'expression des marqueurs d'activation des cellules de Müller, d'astrogliose et d'activation des cellules microgliales. Il convient de noter que ce modèle d'explant est indépendant du flux sanguin, ce qui renforce l'idée que les effets observés sont dus à l'action directe des ROCK-i sur la neurorétine. Cette modulation anti-inflammatoire se révèle être une stratégie thérapeutique intéressante pour le traitement de cette maladie neurodégénérative et neuroinflammatoire [32]. On sait en effet que dans les yeux des patients atteints de glaucome, la production gliale de TNF-α est augmentée et que le récepteur de celui-ci est régulé positivement sur les CGR et leurs axones [334]. Plusieurs modèles animaux de glaucome ont fourni des preuves de l'activation des cellules microgliales et des astrocytes précédant la perte des CGR [32]. De plus, les gènes de la cascade de signalisation RhoA/ROCK sont fortement régulés à la hausse dans la microglie neurodégénérative [423].

Grâce à la phosphorylation de différents substrats moléculaires, l'activité ROCK affecte une multitude de fonctions cellulaires, par exemple l'organisation du cytosquelette, la synthèse des protéines, la fonction des cellules gliales, l'autophagie, l'apoptose, l'activation microgliale et la fonction synaptique. Dans le contexte de la neurodégénérescence, une activité ROCK élevée dans le système nerveux central a été associée à des effets néfastes, alors que l'inhibition de l'activité ROCK entrainerait neuroprotection, stabilité axonale, survie des CGR et même régénération axonale [424]. L'inhibition de cette voie peut ainsi diminuer l'inflammation en inhibant la migration des cellules inflammatoires, en diminuant la production des médiateurs inflammatoires tels que le TNF-alpha, en réduisant l'activation des cellules gliales et en supprimant la production de cytokines pro-inflammatoires, et ainsi éviter la perte des CGR (figure 46).

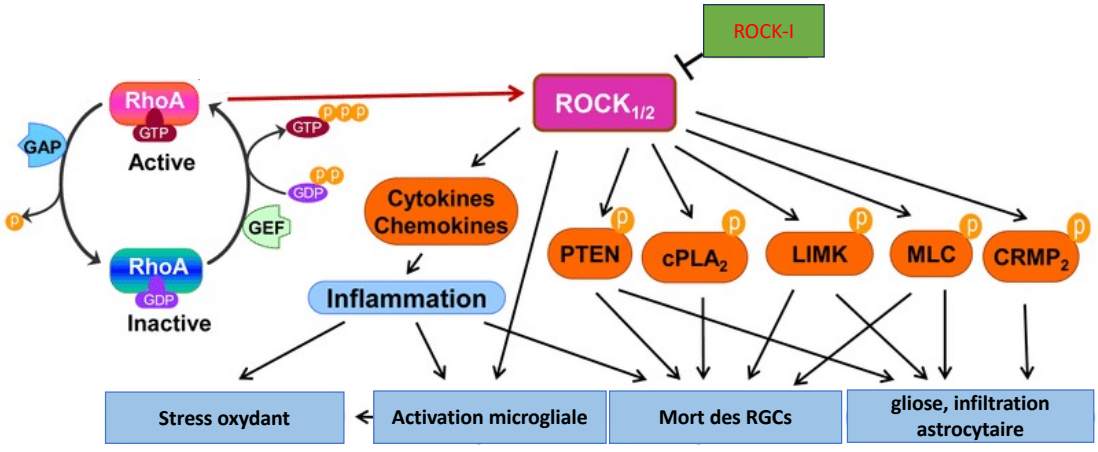

Figure 46 : Représentation schématique de la voie RhoA/Rho kinase dans la pathogenèse de la neuroinflammation
La voie RhoA/Rho kinase déclenche une série d'événements, notamment l'inflammation, l'activation microgliale, la mort des RGC, et l'astrogliose ; ROCK : Rho Kinase ; GTP : guanosine triphosphate ; GDP: guanosine diphosphate ; GAP : protéine

activatrice de la GTPase PTEN : homologue de la phosphatase et de la tensine ; cPLA2 : phospholipase cytosolique A2 ; LIMK : LIM kinase ; MLC : chaîne légère de myosine ; CRMP2 : *collapsin response mediator protein 2*

Ces résultats sont en accord avec d'autres résultats encourageants de la littérature concernant l'activité neuroprotectrice des ROCK-i. Le ROCK-i Y-27632 a ainsi été testé en injection intravitréenne chez le rat, dans un modèle d'ischémie rétinienne transitoire où une diminution de la mort des CGR a été observée [418]. Y-33075 a été testé en injection intravitréenne dans un modèle d'encéphalomyélite auto-immune chez la souris et a conduit à une diminution de la démyélinisation des axones du nerf optique [419]. H-1152 a été testé *in vitro* sur un modèle d'hypoxie rétinienne transitoire dans une rétine bovine isolée, ainsi que sur modèle organotypique de rétine isolée soumise à des conditions de stress et a pu révéler un effet à la fois neuroprotecteur et inhibiteur de l'activité gliale [346,422].

Notre étude met en lumière le potentiel du Y-33075, notamment à la concentration la plus élevée étudiée (50 µM), comme la seule molécule à avoir simultanément démontré un effet neuroprotecteur et immunomodulateur. Ces propriétés en font un bon candidat pour des études futures *in vivo* et éventuellement pour le développement d'un traitement complet, capable de réduire la PIO, de protéger les cellules nerveuses rétiniennes et de moduler la réponse inflammatoire dans le glaucome.

Ces résultats soulignent une fois de plus l'utilité de notre modèle d'explant rétinien pour le criblage de molécules à visée neuroprotectrice dans le glaucome. Ce modèle permet de préserver l'architecture complexe et multicellulaire de la rétine, se rapprochant ainsi des conditions in vivo. En outre, l'utilisation d'explants de rétine permet d'étudier plusieurs molécules simultanément tout en réduisant le nombre d'animaux sacrifiés, en accord avec les principes des 3R (Remplacement, Réduction et Raffinement) en recherche animale.

Discussion

De la modélisation *in vitro* d'un trabéculum en trois dimensions à l'exploration des explants de trabéculum et de rétine, ce travail cherche à décrire et comprendre les mécanismes d'action du TGF-β2, et ses relations avec le TNF-α. Cette thèse appréhende la physiopathologie du glaucome de manière holistique et souligne l'importance de la régulation de la voie ROCK et de la modulation de l'inflammation dans la trabéculoprotection et la neuroprotection.

Dans le cadre de cette thèse, nous avons, dans un premier temps, cherché à mettre au point un modèle de trabéculum en 3D respectant son architecture complexe. Cette approche nous permettrait de mieux comprendre le fonctionnement physiologique de cette structure anatomique fondamentale dans la régulation de la pression intraoculaire, ses réactions en situation de stress ou de toxicité, ainsi que l'impact et les mécanismes potentiels de nouvelles molécules thérapeutiques.

Nos premiers travaux nous ont permis d'abord d'obtenir des modèles en 2D, puis en 3D à partir de cultures primaires de cellules trabéculaires humaines. En effet, dans notre équipe, la collaboration entre l'Institut de la Vision et l'Hôpital des 15-20 nous permet de bénéficier de cellules trabéculaires humaines de donneurs sains, à partir de collerettes de greffons cornéens préparés pour kératoplastie. Pour simuler le dysfonctionnement observé dans le glaucome, nous avons utilisé le TGF-β2. La famille des cytokines TGF-β est connue pour être associée à des altérations de plusieurs fonctions cellulaires, notamment la différenciation, la prolifération et l'accumulation de la MEC. Le TGF-β2 a un effet profibrotique et des taux élevés de cette cytokine ont été trouvés dans l'humeur aqueuse de patients atteints de glaucome, ce qui suggère qu'il pourrait jouer un rôle dans la pathogenèse de l'hypertension oculaire en altérant la fonction de la matrice trabéculaire [207]. Nos résultats ont démontré que l'utilisation du TGF-β2 dans nos modèles *in vitro* reproduisait avec succès les altérations du cytosquelette et l'accumulation de protéines matricielles observées dans la trabéculopathie glaucomateuse. La culture cellulaire en 3D en Matrigel™ nous a permis d'obtenir une organisation en maille de cellules trabéculaires avec des interconnexions et la formation d'espaces intercellulaires variables selon les traitements. Cette organisation qui reflète mieux l'anatomie réelle du trabéculum n'était pas retrouvée en 2D. La culture en 3D recrée les conditions du microenvironnement rencontrées *in vivo* et offre aux cellules un environnement leur permettant d'interagir entre elles et avec la MEC [13,254]. Cela aiderait également à mieux étudier le fonctionnement physiologique du trabéculum mais aussi les modifications qui ont lieu dans des conditions de stress ou de toxicité, ainsi que l'effet des médicaments [42]. Ce modèle de trabéculum en 3D a été utilisé pour la première fois dans notre équipe par Bouchemi et al. pour étudier l'effet du chlorure de benzalkonium (BAK), un conservateur couramment utilisé en collyre [29]. Il avait montré que BAK induisait l'expression génique de chimiokines inflammatoires IL-6 et IL-8 et tendait à moduler celle des MMP, qui jouent un rôle crucial dans la dégradation de la MEC et donc l'augmentation de l'évacuation d'HA hors de l'œil. Nous avons, pour notre part, étudié l'effet de molécules

thérapeutiques tels que le latanoprost et les ROCK-i sur l'organisation de la MEC et la régulation du cytosquelette. Nos travaux ont mis en évidence d'une part, un effet significatif d'un ROCK-i (Y-27632) sur la dégradation de la MEC et la relaxation du cytosquelette et en parallèle, une action du latanoprost sur les dépôt de fibronectine sans action sur le cytosquelette [14]. Néanmoins, pour l'instant, les résultats fournis sont uniquement qualitatifs, ce qui constitue une limite de l'étude. Des recherches supplémentaires seront nécessaires pour mieux exploiter toutes les informations fournies par ce modèle. En effet, les principaux signaux biomécaniques auxquels sont soumises les cellules trabéculaires ne sont pas étudiés dans ce travail. Par exemple, les cellules trabéculaires *in vivo* sont soumises à un changement significatif de pression, à une contrainte de cisaillement et à un étirement mécanique. Des systèmes de mesure de la rigidité et de l'écoulement utilisant ce modèle pourraient également être mis en œuvre pour améliorer la pertinence du modèle.

Nous avons eu ensuite pour objectif d'enrichir notre modèle en travaillant directement sur des tissus. À partir d'explants trabéculaires prélevés sur des collerettes de greffons, nous avons à notre disposition un modèle *ex vivo* à la fois de trabéculum normal et de trabéculum glaucomateux sous l'effet du TGF-β2. En effet, le TGF-β2 induisait un réarrangement du cytosquelette d'actine et une accumulation de MEC qui modifiait bien l'architecture filtrante du trabéculum que nous avons pu objectiver en microscopie confocale. Nous avons réalisé une caractérisation transcriptomique globale (RNA-Seq), en parallèle avec des analyses immunohistologiques, afin de corréler les signatures géniques avec les altérations morphologiques observées. Cette approche nous a permis d'identifier des gènes différentiellement régulés, principalement impliqués dans la régulation de la MEC et des voies de signalisation profibrotiques du TGF-β mais aussi des voies de BMP et de Wnt. Le TGF-β2 a été utilisé dans plusieurs études pour reproduire les changements observés dans le trabéculum des patients atteints de glaucome, car il modifie simultanément le cytosquelette et la MEC [14,200,262]. Dans notre étude, nous avons confirmé que le TGF-β2 induit l'expression de protéines de la MEC, telles que les collagènes, la fibronectine, l'élastine, des inhibiteurs de la dégradation de la MEC tels que SERPINE-1, et des enzymes de réticulation telles que les lysyl oxydases (LOX).

L'utilisation d'explants trabéculaires humains (HTMEx) représente un moyen simple et efficace d'obtenir un modèle 3D de trabéculum permettant d'étudier l'effet de molécules thérapeutiques, de facteurs de croissance et d'autres composés sur la fonction trabéculaire. De plus, nous avons pu subdiviser le trabéculum d'une seule collerette et ainsi étudier les modifications d'un même tissu dans différentes conditions. Cependant, l'utilisation de ces explants comporte des limites, telles que la difficulté d'obtenir des tissus frais, la variabilité entre les donneurs et la disponibilité limitée de tissus provenant de patients atteints de glaucome. La possibilité de disposer de collerettes cornéosclérales après transplantation cornéenne reste une source précieuse de tissu trabéculaire entier. Étant donné que les trabéculums provenant de patients atteints de glaucome ont souvent un faible nombre de cellules, l'ajout de TGF-β2 à un trabéculum sain permet la reproduction des modifications de l'organisation

cytosquelettique et de la MEC, tout en fournissant suffisamment de matériel pour une étude transcriptomique [12,239]

D'autres molécules pourraient être utilisées pour développer des modèles de glaucomes secondaires. Par exemple, l'exposition des HTMEx à la dexaméthasone peut constituer une méthode efficace pour étudier le glaucome cortico-induit, et l'utilisation du TGF-β1 peut donner un aperçu du glaucome pseudoexfoliatif [196,199]. L'utilisation de chlorure de benzalkonium ou de peroxyde d'hydrogène serait également intéressante pour étudier les effets du stress oxydant sur les HTMEx [222,316].

Grâce à la caractérisation précise de notre modèle d'explants trabéculaires pathologiques induits par le TGF-β2, nous avons choisi d'explorer l'effet d'une cytokine antagoniste, le TNF-α, dans le contexte du glaucome. Cette balance TGF-β2/TNF-α si importante dans toute pathologie inflammatoire chronique nous semblait logiquement intéressante à étudier dans le glaucome [332,333]. Nos résultats ont, comme nous l'attendions, démontré que le TNF-α induisait une réponse pro-inflammatoire, avec l'augmentation de l'expression de cytokines et de chimiokines pro-inflammatoires en même temps qu'une réponse apoptotique dans les cellules trabéculaires. En revanche, le TGF-β2 induisait un remodelage matriciel au sein des HTMEx, caractérisé par l'augmentation de l'expression de gènes impliqués dans la synthèse de la MEC et la réorganisation du cytosquelette. Lorsque le TGF-β2 et le TNF-α étaient appliqués en même temps, nous avons observé que le TNF-α neutralisait les effets profibrotiques du TGF-β2. Inversement, le TGF-β2 supprimait la réponse pro-inflammatoire avec une diminution de l'expression des cytokines et des chimiokines proinflammatoires. Ces résultats suggèrent que le TNF-α et le TGF-β2 jouent des rôles opposés dans la régulation de la fonction trabéculaire et donc que le TNF-α peut contrecarrer les effets du TGF-β2. SMAD7, un médiateur clé dans les interactions entre les voies de signalisation du TNF et du TGF-β2 (figure 26a), semble jouer un rôle important dans l'homéostasie du trabéculum [311]. Une mauvaise régulation de SMAD7 a été impliquée dans diverses maladies, notamment les cancers et la fibrose et une modulation thérapeutique de SMAD7 pourrait représenter une approche prometteuse pour limiter l'accumulation de la MEC dans le trabéculum [332].

En parallèle, nous avons développé un modèle d'explant rétinien de rat, économe en termes d'utilisation des animaux, puisqu'un seul rat nous permet d'obtenir huit explants pouvant être soumis à divers traitements. Ce modèle s'est révélé efficace pour le criblage de molécules à visée neuroprotectrice, car la perte des CGR est reproductible d'un explant à l'autre. Nous avons exploré l'effet de facteurs de croissance tels que le BDNF, les cellules souches mésenchymateuses et un ROCK-i sur la neuroprotection et l'immunomodulation, deux aspects importants dans la pathologie neuro-inflammatoire qu'est le glaucome à angle ouvert [32].

Synthèse et perspectives

La thèse présentée ici se distingue par l'utilisation de modèles réduisant le recours aux modèles animaux ou le nombre d'animaux utilisés, tels que des explants de trabéculums humains et des modèles *ex vivo* de neurorétine de rat, pour étudier les mécanismes impliqués dans la pathologie du glaucome.

Deux voies interdépendantes prédominantes semblent être impliquées à la fois dans la dysfonction de la matrice trabéculaire et la dégénérescence neurorétinienne du glaucome : le TGF-β2 et ses voies de signalisation conventionnelles (Smad) et non conventionnelles (MAPK, Rho GTPase) impliquées dans la fibrose et le remaniement du cytosquelette des cellules ; les voies de l'inflammation avec notamment le TNF-α, régulant l'apoptose et les protéines de la MEC en activant métalloprotéases et collagènes.

L'analyse transcriptomique menée dans cette étude a permis de caractériser les modifications induites par le TGF-β2, en identifiant les principales cytokines impliquées dans le glaucome et en identifiant des cibles thérapeutiques potentielles. Parmi ces cibles, l'inhibition de la voie Rho/ROCK a été étudiée en détail, montrant un effet double à la fois sur la MEC et sur le cytosquelette des cellules trabéculaires. Il est intéressant de noter que cette même cible pourrait également avoir un effet neuroprotecteur sur les cellules trabéculaires humaines. Enfin, l'étude menée sur le TNF-α a permis de mettre en évidence l'implication de l'inflammation dans le remodelage trabéculaire et la pathologie du glaucome. Ces résultats soulignent l'importance de prendre en compte les aspects inflammatoires dans les recherches futures sur le glaucome.

Ces premiers travaux ouvrent la voie à de nombreuses perspectives de recherche. Les résultats obtenus ont permis d'identifier plusieurs cibles thérapeutiques potentielles pour le traitement du glaucome, cibles qui restent à valider mais qui offrent de nombreux espoirs pour le développement de nouveaux traitements. De plus, les modèles alternatifs notamment tissulaires utilisés dans cette étude, tels que les explants trabéculaires et rétiniens, sont des outils précieux pour le criblage de molécules thérapeutiques. En effet, ces modèles permettent de mieux simuler les conditions physiologiques *in vivo*, offrant ainsi une approche plus pertinente pour l'étude des mécanismes impliqués dans la pathologie du glaucome.

Références

[1] Tham Y-C, Li X, Wong TY, Quigley HA, Aung T, Cheng C-Y. Global prevalence of glaucoma and projections of glaucoma burden through 2040: a systematic review and meta-analysis. Ophthalmology 2014;121:2081–90. https://doi.org/10.1016/j.ophtha.2014.05.013.

[2] Kass MA, Heuer DK, Higginbotham EJ, Johnson CA, Keltner JL, Miller JP, et al. The Ocular Hypertension Treatment Study: a randomized trial determines that topical ocular hypotensive medication delays or prevents the onset of primary open-angle glaucoma. Arch Ophthalmol 2002;120:701–13; discussion 829-830.

[3] Stamer WD, Clark AF. The many faces of the trabecular meshwork cell. Exp Eye Res 2017;158:112–23. https://doi.org/10.1016/j.exer.2016.07.009.

[4] Tektas O-Y, Lütjen-Drecoll E. Structural changes of the trabecular meshwork in different kinds of glaucoma. Exp Eye Res 2009;88:769–75. https://doi.org/10.1016/j.exer.2008.11.025.

[5] Keller KE, Aga M, Bradley JM, Kelley MJ, Acott TS. Extracellular matrix turnover and outflow resistance. Exp Eye Res 2009;88:676–82. https://doi.org/10.1016/j.exer.2008.11.023.

[6] Tamm ER. The trabecular meshwork outflow pathways: structural and functional aspects. Exp Eye Res 2009;88:648–55. https://doi.org/10.1016/j.exer.2009.02.007.

[7] Rossi C, Cicalini I, Cufaro MC, Agnifili L, Mastropasqua L, Lanuti P, et al. Multi-Omics Approach for Studying Tears in Treatment-Naïve Glaucoma Patients. Int J Mol Sci 2019;20:4029. https://doi.org/10.3390/ijms20164029.

[8] Khanna RK, Catanese S, Emond P, Corcia P, Blasco H, Pisella P-J. Metabolomics and lipidomics approaches in human tears: A systematic review. Surv Ophthalmol 2022;67:1229–43. https://doi.org/10.1016/j.survophthal.2022.01.010.

[9] Gilhooley MJ, Owen N, Moosajee M, Yu Wai Man P. From Transcriptomics to Treatment in Inherited Optic Neuropathies. Genes (Basel) 2021;12:147. https://doi.org/10.3390/genes12020147.

[10] Winiarczyk M, Biela K, Michalak K, Winiarczyk D, Mackiewicz J. Changes in Tear Proteomic Profile in Ocular Diseases. Int J Environ Res Public Health 2022;19:13341. https://doi.org/10.3390/ijerph192013341.

[11] Hubrecht RC, Carter E. The 3Rs and Humane Experimental Technique: Implementing Change. Animals (Basel) 2019;9:754. https://doi.org/10.3390/ani9100754.

[12] Buffault J, Labbé A, Hamard P, Brignole-Baudouin F, Baudouin C. The trabecular meshwork: Structure, function and clinical implications. A review of the literature. J Fr Ophtalmol 2020;43:e217–30. https://doi.org/10.1016/j.jfo.2020.05.002.

[13] Buffault J, Brignole-Baudouin F, Labbé A, Baudouin C. An Overview of Current Glaucomatous Trabecular Meshwork Models. Curr Eye Res 2023:1–11. https://doi.org/10.1080/02713683.2023.2253378.

[14] Buffault J, Brignole-Baudouin F, Reboussin É, Kessal K, Labbé A, Mélik Parsadaniantz S, et al. The Dual Effect of Rho-Kinase Inhibition on Trabecular Meshwork Cells Cytoskeleton and Extracellular Matrix in an In Vitro Model of Glaucoma. J Clin Med 2022;11:1001. https://doi.org/10.3390/jcm11041001.

[15] Wang Z, Gerstein M, Snyder M. RNA-Seq: a revolutionary tool for transcriptomics. Nat Rev Genet 2009;10:57–63. https://doi.org/10.1038/nrg2484.

[16] Reboussin É, Buffault J, Brignole-Baudouin F, Réaux-Le Goazigo A, Riancho L, Olmiere C, et al. Evaluation of neuroprotective and immunomodulatory properties of mesenchymal stem cells in an ex vivo retinal explant model. J Neuroinflammation 2022;19:63. https://doi.org/10.1186/s12974-022-02418-w.

[17] Gordon MO, Kass MA. The Ocular Hypertension Treatment Study: design and baseline description of the participants. Arch Ophthalmol 1999;117:573–83.

[18] Kwon YH, Fingert JH, Kuehn MH, Alward WLM. Primary open-angle glaucoma. N Engl J Med 2009;360:1113–24. https://doi.org/10.1056/NEJMra0804630.

[19] The Advanced Glaucoma Intervention Study (AGIS): 7. The relationship between control of intraocular pressure and visual field deterioration.The AGIS Investigators. Am J Ophthalmol 2000;130:429–40.

[20] Heijl A, Leske MC, Bengtsson B, Hyman L, Bengtsson B, Hussein M, et al. Reduction of intraocular pressure and glaucoma progression: results from the Early Manifest Glaucoma Trial. Arch Ophthalmol 2002;120:1268–79.

[21] Latina MA, de Leon JMS. Selective laser trabeculoplasty. Ophthalmol Clin North Am 2005;18:409–19, vi. https://doi.org/10.1016/j.ohc.2005.05.005.

[22] Fernández-Vega Cueto A, Álvarez L, García M, Álvarez-Barrios A, Artime E, Fernández-Vega Cueto L, et al. Candidate Glaucoma Biomarkers: From Proteins to Metabolites, and the Pitfalls to Clinical Applications. Biology (Basel) 2021;10:763. https://doi.org/10.3390/biology10080763.

[23] Fea AM, Ricardi F, Novarese C, Cimorosi F, Vallino V, Boscia G. Precision Medicine in Glaucoma: Artificial Intelligence, Biomarkers, Genetics and Redox State. Int J Mol Sci 2023;24:2814. https://doi.org/10.3390/ijms24032814.

[24] Shalaby WS, Ahmed OM, Waisbourd M, Katz LJ. A review of potential novel glaucoma therapeutic options independent of intraocular pressure. Surv Ophthalmol 2022;67:1062–80. https://doi.org/10.1016/j.survophthal.2021.12.003.

[25] Hurley DJ, Normile C, Irnaten M, O'Brien C. The Intertwined Roles of Oxidative Stress and Endoplasmic Reticulum Stress in Glaucoma. Antioxidants (Basel) 2022;11:886. https://doi.org/10.3390/antiox11050886.

[26] Lin C, Wu X. Curcumin Protects Trabecular Meshwork Cells From Oxidative Stress. Invest Ophthalmol Vis Sci 2016;57:4327–32. https://doi.org/10.1167/iovs.16-19883.

[27] Liao J, Lai Z, Huang G, Lin J, Huang W, Qin Y, et al. Setanaxib mitigates oxidative damage following retinal ischemia-reperfusion via NOX1 and NOX4 inhibition in retinal ganglion cells. Biomed Pharmacother 2023;170:116042. https://doi.org/10.1016/j.biopha.2023.116042.

[28] Gupta A, Galletti JG, Yu Z, Burgess K, de Paiva CS. A, B, C's of Trk Receptors and Their Ligands in Ocular Repair. Int J Mol Sci 2022;23:14069. https://doi.org/10.3390/ijms232214069.

[29] Wang R, Wang Y, Qin Y, Wei H. Antioxidative effects of ghrelin on human trabecular meshwork cells. J Fr Ophtalmol 2023:S0181-5512(23)00144-4. https://doi.org/10.1016/j.jfo.2022.11.023.

[30] Zhang Y, Wu N, Li Q, Hu X, Wang L, Sun J-G, et al. Neuroprotective effect of the somatostatin receptor 5 agonist L-817,818 on retinal ganglion cells in experimental glaucoma. Exp Eye Res 2021;204:108449. https://doi.org/10.1016/j.exer.2021.108449.

[31] Ye D, Xu Y, Shi Y, Fan M, Lu P, Bai X, et al. Anti-PANoptosis is involved in neuroprotective effects of melatonin in acute ocular hypertension model. J Pineal Res 2022;73:e12828. https://doi.org/10.1111/jpi.12828.

[32] Baudouin C, Kolko M, Melik-Parsadaniantz S, Messmer EM. Inflammation in Glaucoma: From the back to the front of the eye, and beyond. Prog Retin Eye Res 2020:100916. https://doi.org/10.1016/j.preteyeres.2020.100916.

[33] Lambuk L, Ahmad S, Sadikan MZ, Nordin NA, Kadir R, Nasir NAA, et al. Targeting Differential Roles of Tumor Necrosis Factor Receptors as a Therapeutic Strategy for Glaucoma. Front Immunol 2022;13:857812. https://doi.org/10.3389/fimmu.2022.857812.

[34] Izumi Y, Ishikawa M, Nakazawa T, Kunikata H, Sato K, Covey DF, et al. Neurosteroids as stress modulators and neurotherapeutics: lessons from the retina. Neural Regen Res 2023;18:1004–8. https://doi.org/10.4103/1673-5374.355752.

[35] Kasindi A, Fuchs D-T, Koronyo Y, Rentsendorj A, Black KL, Koronyo-Hamaoui M. Glatiramer Acetate Immunomodulation: Evidence of Neuroprotection and Cognitive Preservation. Cells 2022;11:1578. https://doi.org/10.3390/cells11091578.

[36] Xu K, Yu L, Wang Z, Lin P, Zhang N, Xing Y, et al. Use of gene therapy for optic nerve protection: Current concepts. Front Neurosci 2023;17:1158030. https://doi.org/10.3389/fnins.2023.1158030.

[37] Rhee J, Shih KC. Use of Gene Therapy in Retinal Ganglion Cell Neuroprotection: Current Concepts and Future Directions. Biomolecules 2021;11:581. https://doi.org/10.3390/biom11040581.

[38] Patel C, Pande S, Sagathia V, Ranch K, Beladiya J, Boddu SHS, et al. Nanocarriers for the Delivery of Neuroprotective Agents in the Treatment of Ocular Neurodegenerative Diseases. Pharmaceutics 2023;15:837. https://doi.org/10.3390/pharmaceutics15030837.

[39] Shen Y, Sun J, Sun X. Intraocular nano-microscale drug delivery systems for glaucoma treatment: design strategies and recent progress. J Nanobiotechnology 2023;21:84. https://doi.org/10.1186/s12951-023-01838-x.

[40] Vranka JA, Kelley MJ, Acott TS, Keller KE. Extracellular matrix in the trabecular meshwork: intraocular pressure regulation and dysregulation in glaucoma. Exp Eye Res 2015;133:112–25. https://doi.org/10.1016/j.exer.2014.07.014.

[41] Cvekl A, Tamm ER. Anterior eye development and ocular mesenchyme. Bioessays 2004;26:374–86. https://doi.org/10.1002/bies.20009.

[42] Renard J-P, Sellem E. Le GPAO, Rapport 2014 de la Société française d'ophtalmologie. n.d.

[43] Lütjen-Drecoll E. Functional morphology of the trabecular meshwork in primate eyes. Prog Retin Eye Res 1999;18:91–119. https://doi.org/10.1016/s1350-9462(98)00011-1.

[44] Gong H, Tripathi RC, Tripathi BJ. Morphology of the aqueous outflow pathway. Microsc Res Tech 1996;33:336–67. https://doi.org/10.1002/(SICI)1097-0029(19960301)33:4<336::AID-JEMT4>3.0.CO;2-N.

[45] Buller C, Johnson D. Segmental variability of the trabecular meshwork in normal and glaucomatous eyes. Invest Ophthalmol Vis Sci 1994;35:3841–51.

[46] Johnson DH, Johnson M. How does nonpenetrating glaucoma surgery work? Aqueous outflow resistance and glaucoma surgery. J Glaucoma 2001;10:55–67. https://doi.org/10.1097/00061198-200102000-00011.

[47] Renard J-P, Sellem E, Aptel F. Mécanismes de l'écoulement de l'humeur aqueuse. Glaucome primitif à angle ouvert. Elsevier Masson, 2014.

[48] Sugita A, Nishida H, Yoshioka H. Innervation of trabecular meshwork. Jpn J Ophthalmol 1986;30:257–65.

[49] McDougal DH, Gamlin PD. Autonomic control of the eye. Compr Physiol 2015;5:439–73. https://doi.org/10.1002/cphy.c140014.

[50] Nomura T, Smelser GK. The identification of adrenergic and cholinergic nerve endings in the trabecular meshwork. Invest Ophthalmol 1974;13:525–32.

[51] Shuman MA, Polansky JR, Merkel C, Alvarado JA. Tissue plasminogen activator in cultured human trabecular meshwork cells. Predominance of enzyme over plasminogen activator inhibitor. Invest Ophthalmol Vis Sci 1988;29:401–5.

[52] Lynch MG, Peeler JS, Brown RH, Niederkorn JY. Expression of HLA class I and II antigens on cells of the human trabecular meshwork. Ophthalmology 1987;94:851–7. https://doi.org/10.1016/s0161-6420(87)33539-0.

[53] Latina M, Flotte T, Crean E, Sherwood ME, Granstein RD. Immunohistochemical staining of the human anterior segment. Evidence that resident cells play a role in immunologic responses. Arch Ophthalmol 1988;106:95–9. https://doi.org/10.1001/archopht.1988.01060130101037.

[54] Coupland SE, Penfold P, Billson F, Hoffmann F. Immunohistochemistry study of the glaucomatous and normal human trabecular meshwork. Ger J Ophthalmol 1994;3:168–74.

[55] Tripathi BJ, Tripathi RC, Wong P, Raja S. Expression of HLA by the human trabecular meshwork and corneal endothelium. Exp Eye Res 1990;51:269–76. https://doi.org/10.1016/0014-4835(90)90023-n.

[56] Shifera AS, Trivedi S, Chau P, Bonnemaison LH, Iguchi R, Alvarado JA. Constitutive secretion of chemokines by cultured human trabecular meshwork cells. Exp Eye Res 2010;91:42–7. https://doi.org/10.1016/j.exer.2010.04.001.

[57] Alvarado JA, Katz LJ, Trivedi S, Shifera AS. Monocyte modulation of aqueous outflow and recruitment to the trabecular meshwork following selective laser trabeculoplasty. Arch Ophthalmol 2010;128:731–7. https://doi.org/10.1001/archophthalmol.2010.85.

[58] Li X, Nagy JI, Li D, Acott TS, Kelley MJ. Gap junction connexin43 is a key element in mediating phagocytosis activity in human trabecular meshwork cells. Int J Physiol Pathophysiol Pharmacol 2020;12:25–31.

[59] Peotter JL, Phillips J, Tong T, Dimeo K, Gonzalez JM, Peters DM. Involvement of Tiam1, RhoG and ELMO2/ILK in Rac1-mediated phagocytosis in human trabecular meshwork cells. Exp Cell Res 2016;347:301–11. https://doi.org/10.1016/j.yexcr.2016.08.009.

[60] Weinreb RN, Robinson MR, Dibas M, Stamer WD. Matrix Metalloproteinases and Glaucoma Treatment. J Ocul Pharmacol Ther 2020. https://doi.org/10.1089/jop.2019.0146.

[61] Yun H, Zhou Y, Wills A, Du Y. Stem Cells in the Trabecular Meshwork for Regulating Intraocular Pressure. J Ocul Pharmacol Ther 2016;32:253–60. https://doi.org/10.1089/jop.2016.0005.

[62] Du Y, Roh DS, Mann MM, Funderburgh ML, Funderburgh JL, Schuman JS. Multipotent stem cells from trabecular meshwork become phagocytic TM cells. Invest Ophthalmol Vis Sci 2012;53:1566–75. https://doi.org/10.1167/iovs.11-9134.

[63] Tamm ER, Braunger BM, Fuchshofer R. Chapter Eighteen - Intraocular Pressure and the Mechanisms Involved in Resistance of the Aqueous Humor Flow in the Trabecular Meshwork Outflow Pathways. In: Hejtmancik JF, Nickerson JM, editors. Progress in Molecular Biology and Translational Science, vol. 134, Academic Press; 2015, p. 301–14. https://doi.org/10.1016/bs.pmbts.2015.06.007.

[64] Knepper PA, Yue BY. Chapter 22 - Abnormal trabecular meshwork outflow. In: Levin LA, Albert DM, editors. Ocular Disease, Edinburgh: W.B. Saunders; 2010, p. 171–7. https://doi.org/10.1016/B978-0-7020-2983-7.00022-X.

[65] Keller KE, Acott TS. The Juxtacanalicular Region of Ocular Trabecular Meshwork: A Tissue with a Unique Extracellular Matrix and Specialized Function. J Ocul Biol 2013;1:3.

[66] Ueda J, Wentz-Hunter K, Yue BYJT. Distribution of myocilin and extracellular matrix components in the juxtacanalicular tissue of human eyes. Invest Ophthalmol Vis Sci 2002;43:1068–76.

[67] Fautsch MP, Johnson DH. Aqueous humor outflow: what do we know? Where will it lead us? Invest Ophthalmol Vis Sci 2006;47:4181–7. https://doi.org/10.1167/iovs.06-0830.

[68] Winkler NS, Fautsch MP. Effects of prostaglandin analogues on aqueous humor outflow pathways. J Ocul Pharmacol Ther 2014;30:102–9. https://doi.org/10.1089/jop.2013.0179.

[69] Grant WM. Further studies on facility of flow through the trabecular meshwork. AMA Arch Ophthalmol 1958;60:523–33.

[70] Rohen JW, Futa R, Lütjen-Drecoll E. The fine structure of the cribriform meshwork in normal and glaucomatous eyes as seen in tangential sections. Invest Ophthalmol Vis Sci 1981;21:574–85.

[71] Wang K, Read AT, Sulchek T, Ethier CR. Trabecular meshwork stiffness in glaucoma. Exp Eye Res 2017;158:3–12. https://doi.org/10.1016/j.exer.2016.07.011.

[72] Liton PB, Challa P, Stinnett S, Luna C, Epstein DL, Gonzalez P. Cellular senescence in the glaucomatous outflow pathway. Exp Gerontol 2005;40:745–8. https://doi.org/10.1016/j.exger.2005.06.005.

[73] Liu B, McNally S, Kilpatrick JI, Jarvis SP, O'Brien CJ. Aging and ocular tissue stiffness in glaucoma. Surv Ophthalmol 2018;63:56–74. https://doi.org/10.1016/j.survophthal.2017.06.007.

[74] Hamard P, Valtot F, Sourdille P, Bourles-Dagonet F, Baudouin C. Confocal microscopic examination of trabecular meshwork removed during ab externo trabeculectomy. Br J Ophthalmol 2002;86:1046–52. https://doi.org/10.1136/bjo.86.9.1046.

[75] Tian B, Gabelt BT, Geiger B, Kaufman PL. The role of the actomyosin system in regulating trabecular fluid outflow. Exp Eye Res 2009;88:713–7. https://doi.org/10.1016/j.exer.2008.08.008.

[76] Prendes MA, Harris A, Wirostko BM, Gerber AL, Siesky B. The role of transforming growth factor β in glaucoma and the therapeutic implications. Br J Ophthalmol 2013;97:680–6. https://doi.org/10.1136/bjophthalmol-2011-301132.

[77] Webber HC, Bermudez JY, Sethi A, Clark AF, Mao W. Crosstalk between TGFβ and Wnt signaling pathways in the human trabecular meshwork. Exp Eye Res 2016;148:97–102. https://doi.org/10.1016/j.exer.2016.04.007.

[78] Pervan CL. Smad-independent TGF-β2 signaling pathways in human trabecular meshwork cells. Exp Eye Res 2017;158:137–45. https://doi.org/10.1016/j.exer.2016.07.012.

[79] Tripathi RC. Pathologic anatomy in the outflow pathway of aqueous humour in chronic simple glaucoma. Exp Eye Res 1977;25 Suppl:403–7.

[80] Picht G, Welge-Luessen U, Grehn F, Lütjen-Drecoll E. Transforming growth factor beta 2 levels in the aqueous humor in different types of glaucoma and the relation to filtering bleb development. Graefes Arch Clin Exp Ophthalmol 2001;239:199–207.

[81] Lu P, Takai K, Weaver VM, Werb Z. Extracellular Matrix Degradation and Remodeling in Development and Disease. Cold Spring Harb Perspect Biol 2011;3:a005058. https://doi.org/10.1101/cshperspect.a005058.

[82] Tovar-Vidales T, Fitzgerald AM, Clark AF. Human trabecular meshwork cells express BMP antagonist mRNAs and proteins. Exp Eye Res 2016;147:156–60. https://doi.org/10.1016/j.exer.2016.05.004.

[83] Hernandez H, Millar JC, Curry SM, Clark AF, McDowell CM. BMP and Activin Membrane Bound Inhibitor Regulates the Extracellular Matrix in the Trabecular Meshwork. Invest Ophthalmol Vis Sci 2018;59:2154–66. https://doi.org/10.1167/iovs.17-23282.

[84] Wordinger RJ, Fleenor DL, Hellberg PE, Pang I-H, Tovar TO, Zode GS, et al. Effects of TGF-beta2, BMP-4, and gremlin in the trabecular meshwork: implications for glaucoma. Invest Ophthalmol Vis Sci 2007;48:1191–200. https://doi.org/10.1167/iovs.06-0296.

[85] McDowell CM, Hernandez H, Mao W, Clark AF. Gremlin Induces Ocular Hypertension in Mice Through Smad3-Dependent Signaling. Invest Ophthalmol Vis Sci 2015;56:5485–92. https://doi.org/10.1167/iovs.15-16993.

[86] Mody AA, Wordinger RJ, Clark AF. Role of ID Proteins in BMP4 Inhibition of Profibrotic Effects of TGF-β2 in Human TM Cells. Invest Ophthalmol Vis Sci 2017;58:849–59. https://doi.org/10.1167/iovs.16-20472.

[87] Benoist d'Azy C, Pereira B, Chiambaretta F, Dutheil F. Oxidative and Anti-Oxidative Stress Markers in Chronic Glaucoma: A Systematic Review and Meta-Analysis. PLoS ONE 2016;11:e0166915. https://doi.org/10.1371/journal.pone.0166915.

[88] Zhao J, Wang S, Zhong W, Yang B, Sun L, Zheng Y. Oxidative stress in the trabecular meshwork (Review). Int J Mol Med 2016;38:995–1002. https://doi.org/10.3892/ijmm.2016.2714.

[89] Nita M, Grzybowski A. The Role of the Reactive Oxygen Species and Oxidative Stress in the Pathomechanism of the Age-Related Ocular Diseases and Other Pathologies of the Anterior and Posterior Eye Segments in Adults. Oxid Med Cell Longev 2016;2016:3164734. https://doi.org/10.1155/2016/3164734.

[90] Rao VR, Lautz JD, Kaja S, Foecking EM, Lukács E, Stubbs EB. Mitochondrial-Targeted Antioxidants Attenuate TGF-β2 Signaling in Human Trabecular Meshwork Cells. Invest Ophthalmol Vis Sci 2019;60:3613–24. https://doi.org/10.1167/iovs.19-27542.

[91] Hamanaka T, Kasahara K, Takemura T. Histopathology of the trabecular meshwork and Schlemm's canal in primary angle-closure glaucoma. Invest Ophthalmol Vis Sci 2011;52:8849–61. https://doi.org/10.1167/iovs.11-7591.

[92] Sihota R, Goyal A, Kaur J, Gupta V, Nag TC. Scanning electron microscopy of the trabecular meshwork: understanding the pathogenesis of primary angle closure glaucoma. Indian J Ophthalmol 2012;60:183–8. https://doi.org/10.4103/0301-4738.95868.

[93] Tawara A, Tou N, Kubota T, Harada Y, Yokota K. Immunohistochemical evaluation of the extracellular matrix in trabecular meshwork in steroid-induced glaucoma. Graefes Arch Clin Exp Ophthalmol 2008;246:1021–8. https://doi.org/10.1007/s00417-008-0800-0.

[94] Clark AF, Brotchie D, Read AT, Hellberg P, English-Wright S, Pang I-H, et al. Dexamethasone alters F-actin architecture and promotes cross-linked actin network formation in human trabecular meshwork tissue. Cell Motil Cytoskeleton 2005;60:83–95. https://doi.org/10.1002/cm.20049.

[95] Raghunathan VK, Morgan JT, Park SA, Weber D, Phinney BS, Murphy CJ, et al. Dexamethasone Stiffens Trabecular Meshwork, Trabecular Meshwork Cells, and Matrix. Invest Ophthalmol Vis Sci 2015;56:4447–59. https://doi.org/10.1167/iovs.15-16739.

[96] Polansky JR, Fauss DJ, Zimmerman CC. Regulation of TIGR/MYOC gene expression in human trabecular meshwork cells. Eye (Lond) 2000;14 (Pt 3B):503–14. https://doi.org/10.1038/eye.2000.137.

[97] Filla MS, Liu X, Nguyen TD, Polansky JR, Brandt CR, Kaufman PL, et al. In Vitro Localization of TIGR/MYOC in Trabecular Meshwork Extracellular Matrix and Binding to Fibronectin. Invest Ophthalmol Vis Sci 2002;43:151–61.

[98] Sakai H, Shen X, Koga T, Park B-C, Noskina Y, Tibudan M, et al. Mitochondrial association of myocilin, product of a glaucoma gene, in human trabecular meshwork cells. J Cell Physiol 2007;213:775–84. https://doi.org/10.1002/jcp.21147.

[99] Yam GH-F, Gaplovska-Kysela K, Zuber C, Roth J. Aggregated myocilin induces russell bodies and causes apoptosis: implications for the pathogenesis of myocilin-caused primary open-angle glaucoma. Am J Pathol 2007;170:100–9. https://doi.org/10.2353/ajpath.2007.060806.

[100] Campbell DG. Pigmentary dispersion and glaucoma. A new theory. Arch Ophthalmol 1979;97:1667–72.

[101] Scott A, Kotecha A, Bunce C, Balidis M, Garway-Heath DF, Miller MH, et al. YAG laser peripheral iridotomy for the prevention of pigment dispersion glaucoma a prospective, randomized, controlled trial. Ophthalmology 2011;118:468–73. https://doi.org/10.1016/j.ophtha.2010.07.026.

[102] Wang C, Dang Y, Loewen RT, Waxman S, Shah P, Xia X, et al. Impact of pigment dispersion on trabecular meshwork cells. Graefes Arch Clin Exp Ophthalmol 2019;257:1217–30. https://doi.org/10.1007/s00417-019-04300-7.

[103] Dang Y, Waxman S, Wang C, Loewen RT, Sun M, Loewen NA. A porcine ex vivo model of pigmentary glaucoma. Sci Rep 2018;8:5468. https://doi.org/10.1038/s41598-018-23861-x.

[104] Wang J, Liu X, Zhong Y. Rho/Rho-associated kinase pathway in glaucoma (Review). Int J Oncol 2013;43:1357–67. https://doi.org/10.3892/ijo.2013.2100.

[105] Dang Y, Wang C, Shah P, Waxman S, Loewen RT, Loewen NA. RKI-1447, a Rho kinase inhibitor, causes ocular hypotension, actin stress fiber disruption, and increased phagocytosis. Graefes Arch Clin Exp Ophthalmol 2019;257:101–9. https://doi.org/10.1007/s00417-018-4175-6.

[106] Schweitzer C. [Pseudoexfoliation syndrome and pseudoexfoliation glaucoma]. J Fr Ophtalmol 2018;41:78–90. https://doi.org/10.1016/j.jfo.2017.09.003.

[107] Challa P, Johnson WM. Composition of Exfoliation Material. J Glaucoma 2018;27 Suppl 1:S29–31. https://doi.org/10.1097/IJG.0000000000000917.

[108] Sharon Y, Friling R, Luski M, Campoverde BQ, Amer R, Kramer M. Uveitic Glaucoma: Long-term Clinical Outcome and Risk Factors for Progression. Ocul Immunol Inflamm 2017;25:740–7. https://doi.org/10.1080/09273948.2016.1255341.

[109] Baneke AJ, Lim KS, Stanford M. The Pathogenesis of Raised Intraocular Pressure in Uveitis. Current Eye Research 2016;41:137–49. https://doi.org/10.3109/02713683.2015.1017650.

[110] Tektas O-Y, Heinz C, Heiligenhaus A, Hammer CM, Luetjen-Drecoll E. Morphological changes of trabeculectomy specimens in different kinds of uveitic glaucoma. Curr Eye Res 2011;36:442–8. https://doi.org/10.3109/02713683.2011.566409.

[111] Souissi K, Afrit MAE, Trojet S, Kraiem A. Étiopathogénie des modifications de la pression intraoculaire au cours des uvéites. /data/revues/01815512/00290004/456/ 2008.

[112] Baudouin C, Pisella PJ, Fillacier K, Goldschild M, Becquet F, De Saint Jean M, et al. Ocular surface inflammatory changes induced by topical antiglaucoma drugs: human and animal studies. Ophthalmology 1999;106:556–63. https://doi.org/10.1016/S0161-6420(99)90116-1.

[113] Brignole-Baudouin F, Desbenoit N, Hamm G, Liang H, Both J-P, Brunelle A, et al. A new safety concern for glaucoma treatment demonstrated by mass spectrometry imaging of benzalkonium chloride distribution in the eye, an experimental study in rabbits. PLoS ONE 2012;7:e50180. https://doi.org/10.1371/journal.pone.0050180.

[114] Hamard P, Blondin C, Debbasch C, Warnet J-M, Baudouin C, Brignole F. In vitro effects of preserved and unpreserved antiglaucoma drugs on apoptotic marker expression by human trabecular cells. Graefes Arch Clin Exp Ophthalmol 2003;241:1037–43. https://doi.org/10.1007/s00417-003-0777-7.

[115] Baudouin C, Denoyer A, Desbenoit N, Hamm G, Grise A. In vitro and in vivo experimental studies on trabecular meshwork degeneration induced by benzalkonium chloride (an American Ophthalmological Society thesis). Trans Am Ophthalmol Soc 2012;110:40–63.

[116] Denoyer A, Godefroy D, Célérier I, Frugier J, Degardin J, Harrison JK, et al. CXCR3 antagonism of SDF-1(5-67) restores trabecular function and prevents retinal neurodegeneration in a rat model of ocular hypertension. PLoS ONE 2012;7:e37873. https://doi.org/10.1371/journal.pone.0037873.

[117] Bouchemi M, Roubeix C, Kessal K, Riancho L, Raveu A-L, Soualmia H, et al. Effect of benzalkonium chloride on trabecular meshwork cells in a new in vitro 3D trabecular meshwork model for glaucoma. Toxicol In Vitro 2017;41:21–9. https://doi.org/10.1016/j.tiv.2017.02.006.

[118] The Advanced Glaucoma Intervention Study (AGIS): 7. The relationship between control of intraocular pressure and visual field deterioration.The AGIS Investigators. Am J Ophthalmol 2000;130:429–40.

[119] Bahler CK, Howell KG, Hann CR, Fautsch MP, Johnson DH. Prostaglandins Increase Trabecular Meshwork Outflow Facility in Cultured Human Anterior Segments. Am J Ophthalmol 2008;145:114–9. https://doi.org/10.1016/j.ajo.2007.09.001.

[120] Kalouche G, Beguier F, Bakria M, Melik-Parsadaniantz S, Leriche C, Debeir T, et al. Activation of Prostaglandin FP and EP2 Receptors Differently Modulates Myofibroblast Transition in a Model of Adult Primary Human Trabecular Meshwork Cells. Invest Ophthalmol Vis Sci 2016;57:1816–25. https://doi.org/10.1167/iovs.15-17693.

[121] Amano M, Nakayama M, Kaibuchi K. Rho-kinase/ROCK: A key regulator of the cytoskeleton and cell polarity. Cytoskeleton (Hoboken) 2010;67:545–54. https://doi.org/10.1002/cm.20472.

[122] Pattabiraman PP, Rao PV. Mechanistic basis of Rho GTPase-induced extracellular matrix synthesis in trabecular meshwork cells. Am J Physiol, Cell Physiol 2010;298:C749-763. https://doi.org/10.1152/ajpcell.00317.2009.

[123] Torrejon KY, Papke EL, Halman JR, Bergkvist M, Danias J, Sharfstein ST, et al. TGFβ2-induced outflow alterations in a bioengineered trabecular meshwork are offset by a rho-associated kinase inhibitor. Sci Rep 2016;6. https://doi.org/10.1038/srep38319.

[124] Maruyama Y, Ikeda Y, Mori K, Yoshii K, Ueno M, Sotozono C, et al. Safety and Efficacy of Long-Term Ripasudil 0.4% Instillation for the Reduction of Intraocular Pressure in Japanese Open-Angle Glaucoma Patients. J Ocul Pharmacol Ther 2020. https://doi.org/10.1089/jop.2019.0125.

[125] US Department of Health and Human Services, Food and Drug Administration. Rhopressa approcal letter 208254. 2017.

[126] Kopczynski CC, Heah T. Netarsudil ophthalmic solution 0.02% for the treatment of patients with open-angle glaucoma or ocular hypertension. Drugs Today 2018;54:467–78. https://doi.org/10.1358/dot.2018.54.8.2849627.

[127] Serle JB, Katz LJ, McLaurin E, Heah T, Ramirez-Davis N, Usner DW, et al. Two Phase 3 Clinical Trials Comparing the Safety and Efficacy of Netarsudil to Timolol in Patients With Elevated Intraocular Pressure: Rho Kinase Elevated IOP Treatment Trial 1 and 2 (ROCKET-1 and ROCKET-2). Am J Ophthalmol 2018;186:116–27. https://doi.org/10.1016/j.ajo.2017.11.019.

[128] Sakamoto E, Ishida W, Sumi T, Kishimoto T, Tada K, Fukuda K, et al. Evaluation of offset of conjunctival hyperemia induced by a Rho-kinase inhibitor; 0.4% Ripasudil ophthalmic solution clinical trial. Sci Rep 2019;9:3755. https://doi.org/10.1038/s41598-019-40255-9.

[129] Asrani S, Bacharach J, Holland E, McKee H, Sheng H, Lewis RA, et al. Fixed-Dose Combination of Netarsudil and Latanoprost in Ocular Hypertension and Open-Angle Glaucoma: Pooled Efficacy/Safety Analysis of Phase 3 MERCURY-1 and -2. Adv Ther 2020. https://doi.org/10.1007/s12325-020-01277-2.

[130] Radell JE, Serle JB. Netarsudil/latanoprost fixed-dose combination for the treatment of open-angle glaucoma or ocular hypertension. Drugs Today 2019;55:563–74. https://doi.org/10.1358/dot.2019.55.9.3039670.

[131] Latina MA, Park C. Selective targeting of trabecular meshwork cells: in vitro studies of pulsed and CW laser interactions. Exp Eye Res 1995;60:359–71. https://doi.org/10.1016/s0014-4835(05)80093-4.

[132] Alvarado JA, Alvarado RG, Yeh RF, Franse-Carman L, Marcellino GR, Brownstein MJ. A new insight into the cellular regulation of aqueous outflow: how trabecular meshwork endothelial cells drive a mechanism that regulates the permeability of Schlemm's canal endothelial cells. Br J Ophthalmol 2005;89:1500–5. https://doi.org/10.1136/bjo.2005.081307.

[133] Kramer TR, Noecker RJ. Comparison of the morphologic changes after selective laser trabeculoplasty and argon laser trabeculoplasty in human eye bank eyes. Ophthalmology 2001;108:773–9. https://doi.org/10.1016/s0161-6420(00)00660-6.

[134] Landers J, Martin K, Sarkies N, Bourne R, Watson P. A twenty-year follow-up study of trabeculectomy: risk factors and outcomes. Ophthalmology 2012;119:694–702. https://doi.org/10.1016/j.ophtha.2011.09.043.

[135] Hamard P, Lachkar Y. [Non penetrating filtering surgery, evolution and results]. J Fr Ophtalmol 2002;25:527–36.

[136] Kirwan JF, Lockwood AJ, Shah P, Macleod A, Broadway DC, King AJ, et al. Trabeculectomy in the 21st Century: A Multicenter Analysis. Ophthalmology 2013;120:2532–9. https://doi.org/10.1016/j.ophtha.2013.07.049.

[137] Gedde SJ, Feuer WJ, Shi W, Lim KS, Barton K, Goyal S, et al. Treatment Outcomes in the Primary Tube Versus Trabeculectomy Study after 1 Year of Follow-up. Ophthalmology 2018;125:650–63. https://doi.org/10.1016/j.ophtha.2018.02.003.

[138] Cillino S, Di Pace F, Casuccio A, Cillino G, Lodato G. Deep sclerectomy versus trabeculectomy with low-dosage mitomycin C: four-year follow-up. Ophthalmologica 2008;222:81–7. https://doi.org/10.1159/000112623.

[139] Andrew NH, Akkach S, Casson RJ. A review of aqueous outflow resistance and its relevance to microinvasive glaucoma surgery. Surv Ophthalmol 2019. https://doi.org/10.1016/j.survophthal.2019.08.002.

[140] Lavia C, Dallorto L, Maule M, Ceccarelli M, Fea AM. Minimally-invasive glaucoma surgeries (MIGS) for open angle glaucoma: A systematic review and meta-analysis. PLoS ONE 2017;12:e0183142. https://doi.org/10.1371/journal.pone.0183142.

[141] Wellik SR, Dale EA. A review of the iStent(®) trabecular micro-bypass stent: safety and efficacy. Clin Ophthalmol 2015;9:677–84. https://doi.org/10.2147/OPTH.S57217.

[142] Pfeiffer N, Garcia-Feijoo J, Martinez-de-la-Casa JM, Larrosa JM, Fea A, Lemij H, et al. A Randomized Trial of a Schlemm's Canal Microstent with Phacoemulsification for Reducing Intraocular Pressure in Open-Angle Glaucoma. Ophthalmology 2015;122:1283–93. https://doi.org/10.1016/j.ophtha.2015.03.031.

[143] Dorairaj SK, Kahook MY, Williamson BK, Seibold LK, ElMallah MK, Singh IP. A multicenter retrospective comparison of goniotomy versus trabecular bypass device implantation in glaucoma patients undergoing cataract extraction. Clin Ophthalmol 2018;12:791–7. https://doi.org/10.2147/OPTH.S158403.

[144] Körber N. [Canaloplasty ab interno - a Minimally Invasive Alternative]. Klin Monbl Augenheilkd 2017;234:991–5. https://doi.org/10.1055/s-0042-123829.

[145] Grover DS, Godfrey DG, Smith O, Feuer WJ, Montes de Oca I, Fellman RL. Gonioscopy-assisted transluminal trabeculotomy, ab interno trabeculotomy: technique report and preliminary results. Ophthalmology 2014;121:855–61. https://doi.org/10.1016/j.ophtha.2013.11.001.

[146] Richter GM, Coleman AL. Minimally invasive glaucoma surgery: current status and future prospects. Clin Ophthalmol 2016;10:189–206. https://doi.org/10.2147/OPTH.S80490.

[147] Perinchery SM, Shinde A, Fu CY, Jeesmond Hong XJ, Baskaran M, Aung T, et al. High resolution iridocorneal angle imaging system by axicon lens assisted gonioscopy. Sci Rep 2016;6:30844. https://doi.org/10.1038/srep30844.

[148] Yasuno Y, Yamanari M, Kawana K, Miura M, Fukuda S, Makita S, et al. Visibility of trabecular meshwork by standard and polarization-sensitive optical coherence tomography. J Biomed Opt 2010;15:061705. https://doi.org/10.1117/1.3499421.

[149] King BJ, Burns SA, Sapoznik KA, Luo T, Gast TJ. High-Resolution, Adaptive Optics Imaging of the Human Trabecular Meshwork In Vivo. Transl Vis Sci Technol 2019;8:5. https://doi.org/10.1167/tvst.8.5.5.

[150] Lin C, Wu X. Curcumin Protects Trabecular Meshwork Cells From Oxidative Stress. Invest Ophthalmol Vis Sci 2016;57:4327–32. https://doi.org/10.1167/iovs.16-19883.

[151] Kalouche G, Boucher C, Coste A, Debussche L, Orsini C, Baudouin C, et al. Prostaglandin EP2 receptor signaling protects human trabecular meshwork cells from apoptosis induced by ER stress through down-regulation of p53. Biochim Biophys Acta 2016;1863:2322–32. https://doi.org/10.1016/j.bbamcr.2016.06.008.

[152] Wang EX, Jiang X. Stem cells from trabecular meshwork cells can secrete extracellular matrix. Biochem Biophys Res Commun 2020;523:522–6. https://doi.org/10.1016/j.bbrc.2019.12.080.

[153] Coulon SJ, Schuman JS, Du Y, Bahrani Fard MR, Ethier CR, Stamer WD. A novel glaucoma approach: Stem cell regeneration of the trabecular meshwork. Prog Retin Eye Res 2022;90:101063. https://doi.org/10.1016/j.preteyeres.2022.101063.

[154] Kelley MJ, Rose AY, Keller KE, Hessle H, Samples JR, Acott TS. Stem cells in the trabecular meshwork: present and future promises. Exp Eye Res 2009;88:747–51. https://doi.org/10.1016/j.exer.2008.10.024.

[155] Roubeix C, Godefroy D, Mias C, Sapienza A, Riancho L, Degardin J, et al. Intraocular pressure reduction and neuroprotection conferred by bone marrow-derived mesenchymal stem cells in an animal model of glaucoma. Stem Cell Res Ther 2015;6:177. https://doi.org/10.1186/s13287-015-0168-0.

[156] Ding QJ, Zhu W, Cook AC, Anfinson KR, Tucker BA, Kuehn MH. Induction of Trabecular Meshwork Cells From Induced Pluripotent Stem Cells. Invest Ophthalmol Vis Sci 2014;55:7065–72. https://doi.org/10.1167/iovs.14-14800.

[157] Zhu W, Godwin CR, Cheng L, Scheetz TE, Kuehn MH. Transplantation of iPSC-TM stimulates division of trabecular meshwork cells in human eyes. Sci Rep 2020;10:2905. https://doi.org/10.1038/s41598-020-59941-0.

[158] Zhu W, Jain A, Gramlich OW, Tucker BA, Sheffield VC, Kuehn MH. Restoration of Aqueous Humor Outflow Following Transplantation of iPSC-Derived Trabecular Meshwork Cells in a Transgenic Mouse Model of Glaucoma. Invest Ophthalmol Vis Sci 2017;58:2054–62. https://doi.org/10.1167/iovs.16-20672.

[159] Castro A, Du Y. Trabecular Meshwork Regeneration - A Potential Treatment for Glaucoma. Curr Ophthalmol Rep 2019;7:80–8. https://doi.org/10.1007/s40135-019-00203-2.

[160] A. Bouhenni R, Dunmire J, Sewell A, Edward DP. Animal Models of Glaucoma. J Biomed Biotechnol 2012;2012:692609. https://doi.org/10.1155/2012/692609.

[161] Biswas S, Wan KH. Review of rodent hypertensive glaucoma models. Acta Ophthalmol 2019;97:e331–40. https://doi.org/10.1111/aos.13983.

[162] McDowell CM, Kizhatil K, Elliott MH, Overby DR, van Batenburg-Sherwood J, Millar JC, et al. Consensus Recommendation for Mouse Models of Ocular Hypertension to Study Aqueous Humor Outflow and Its Mechanisms. Invest Ophthalmol Vis Sci 2022;63:12. https://doi.org/10.1167/iovs.63.2.12.

[163] Zode GS, Kuehn MH, Nishimura DY, Searby CC, Mohan K, Grozdanic SD, et al. Reduction of ER stress via a chemical chaperone prevents disease phenotypes in a mouse model of primary open angle glaucoma. J Clin Invest 2011;121:3542–53. https://doi.org/10.1172/JCI58183.

[164] Tham Y-C, Li X, Wong TY, Quigley HA, Aung T, Cheng C-Y. Global prevalence of glaucoma and projections of glaucoma burden through 2040: a systematic review and meta-analysis. Ophthalmology 2014;121:2081–90. https://doi.org/10.1016/j.ophtha.2014.05.013.

[165] Stamer WD, Clark AF. The many faces of the trabecular meshwork cell. Exp Eye Res 2017;158:112–23. https://doi.org/10.1016/j.exer.2016.07.009.

[166] Safa BN, Wong CA, Ha J, Ethier CR. Glaucoma and biomechanics. Curr Opin Ophthalmol 2022;33:80–90. https://doi.org/10.1097/ICU.0000000000000829.

[167] Johnson M. "What controls aqueous humour outflow resistance?" Exp Eye Res 2006;82:545–57. https://doi.org/10.1016/j.exer.2005.10.011.

[168] Ueda J, Wentz-Hunter K, Yue BYJT. Distribution of myocilin and extracellular matrix components in the juxtacanalicular tissue of human eyes. Invest Ophthalmol Vis Sci 2002;43:1068–76.

[169] Vranka JA, Kelley MJ, Acott TS, Keller KE. Extracellular matrix in the trabecular meshwork: intraocular pressure regulation and dysregulation in glaucoma. Exp Eye Res 2015;133:112–25. https://doi.org/10.1016/j.exer.2014.07.014.

[170] Schlunck G, Han H, Wecker T, Kampik D, Meyer-ter-Vehn T, Grehn F. Substrate rigidity modulates cell matrix interactions and protein expression in human trabecular meshwork cells. Invest Ophthalmol Vis Sci 2008;49:262–9. https://doi.org/10.1167/iovs.07-0956.

[171] Pouw AE, Greiner MA, Coussa RG, Jiao C, Han IC, Skeie JM, et al. Cell–Matrix Interactions in the Eye: From Cornea to Choroid. Cells 2021;10. https://doi.org/10.3390/cells10030687.

[172] Stamer WD, Roberts BC, Howell DN, Epstein DL. Isolation, culture, and characterization of endothelial cells from Schlemm's canal. Invest Ophthalmol Vis Sci 1998;39:1804–12.

[173] Camras LJ, Yuan F, Fan S, Samuelson TW, Ahmed IK, Schieber AT, et al. A novel Schlemm's Canal scaffold increases outflow facility in a human anterior segment perfusion model. Invest Ophthalmol Vis Sci 2012;53:6115–21. https://doi.org/10.1167/iovs.12-9570.

[174] Cassidy PS, Kelly RA, Reina-Torres E, Sherwood JM, Humphries MM, Kiang A-S, et al. siRNA targeting Schlemm's canal endothelial tight junctions enhances outflow facility and reduces IOP in a steroid-induced

OHT rodent model. Mol Ther Methods Clin Dev 2021;20:86–94. https://doi.org/10.1016/j.omtm.2020.10.022.

[175] Bill A, Phillips CI. Uveoscleral drainage of aqueous humour in human eyes. Exp Eye Res 1971;12:275–81. https://doi.org/10.1016/0014-4835(71)90149-7.

[176] Ergorul C, Levin LA. Solving the Lost in Translation Problem: Improving the Effectiveness of Translational Research. Curr Opin Pharmacol 2013;13:108–14. https://doi.org/10.1016/j.coph.2012.08.005.

[177] Pang I-H, Millar JC, Clark AF. Elevation of intraocular pressure in rodents using viral vectors targeting the trabecular meshwork. Exp Eye Res 2015;141:33–41. https://doi.org/10.1016/j.exer.2015.04.003.

[178] Senatorov V, Malyukova I, Fariss R, Wawrousek EF, Swaminathan S, Sharan SK, et al. Expression of mutated mouse myocilin induces open-angle glaucoma in transgenic mice. J Neurosci 2006;26:11903–14. https://doi.org/10.1523/JNEUROSCI.3020-06.2006.

[179] Zhou Y, Grinchuk O, Tomarev SI. Transgenic mice expressing the Tyr437His mutant of human myocilin protein develop glaucoma. Invest Ophthalmol Vis Sci 2008;49:1932–9. https://doi.org/10.1167/iovs.07-1339.

[180] Flügel-Koch C, Ohlmann A, Piatigorsky J, Tamm ER. Disruption of anterior segment development by TGF-beta1 overexpression in the eyes of transgenic mice. Dev Dyn 2002;225:111–25. https://doi.org/10.1002/dvdy.10144.

[181] Kroeber M, Ohlmann A, Russell P, Tamm ER. Transgenic studies on the role of optineurin in the mouse eye. Experimental Eye Research 2006;82:1075–85. https://doi.org/10.1016/j.exer.2005.11.004.

[182] Shepard AR, Millar JC, Pang I-H, Jacobson N, Wang W-H, Clark AF. Adenoviral gene transfer of active human transforming growth factor-{beta}2 elevates intraocular pressure and reduces outflow facility in rodent eyes. Invest Ophthalmol Vis Sci 2010;51:2067–76. https://doi.org/10.1167/iovs.09-4567.

[183] McDowell CM, Hernandez H, Mao W, Clark AF. Gremlin Induces Ocular Hypertension in Mice Through Smad3-Dependent Signaling. Invest Ophthalmol Vis Sci 2015;56:5485–92. https://doi.org/10.1167/iovs.15-16993.

[184] Dillinger AE, Kuespert S, Seleem AA, Neuendorf J, Schneider M, Fuchshofer R. CCN2/CTGF tip the balance of growth factors towards TGF-β2 in primary open-angle glaucoma. Front Mol Biosci 2023;10:1045411. https://doi.org/10.3389/fmolb.2023.1045411.

[185] Mao W, Millar JC, Wang W-H, Silverman SM, Liu Y, Wordinger RJ, et al. Existence of the Canonical Wnt Signaling Pathway in the Human Trabecular Meshwork. Invest Ophthalmol Vis Sci 2012;53:7043–51. https://doi.org/10.1167/iovs.12-9664.

[186] Wang W-H, McNatt LG, Pang I-H, Millar JC, Hellberg PE, Hellberg MH, et al. Increased expression of the WNT antagonist sFRP-1 in glaucoma elevates intraocular pressure. J Clin Invest 2008;118:1056–64. https://doi.org/10.1172/JCI33871.

[187] Giovingo M, Nolan M, McCarty R, Pang I-H, Clark AF, Beverley RM, et al. sCD44 overexpression increases intraocular pressure and aqueous outflow resistance. Mol Vis 2013;19:2151–64.

[188] McDowell CM, Luan T, Zhang Z, Putliwala T, Wordinger RJ, Millar JC, et al. Mutant Human Myocilin Induces Strain Specific Differences in Ocular Hypertension and Optic Nerve Damage in Mice. Exp Eye Res 2012;100:65–72. https://doi.org/10.1016/j.exer.2012.04.016.

[189] Bonneau N, Baudouin C, Réaux-Le Goazigo A, Brignole-Baudouin F. An overview of current alternative models in the context of ocular surface toxicity. J Appl Toxicol 2022;42:718–37. https://doi.org/10.1002/jat.4246.

[190] Keller KE, Bhattacharya SK, Borrás T, Brunner TM, Chansangpetch S, Clark AF, et al. Consensus recommendations for trabecular meshwork cell isolation, characterization and culture. Exp Eye Res 2018. https://doi.org/10.1016/j.exer.2018.03.001.

[191] Vernazza S, Tirendi S, Scarfì S, Passalacqua M, Oddone F, Traverso CE, et al. 2D- and 3D-cultures of human trabecular meshwork cells: A preliminary assessment of an in vitro model for glaucoma study. PLoS One 2019;14:e0221942. https://doi.org/10.1371/journal.pone.0221942.

[192] Wang K, Read AT, Sulchek T, Ethier CR. Trabecular meshwork stiffness in glaucoma. Exp Eye Res 2017;158:3–12. https://doi.org/10.1016/j.exer.2016.07.011.

[193] Kasetti RB, Patel PD, Maddineni P, Zode GS. Ex-vivo cultured human corneoscleral segment model to study the effects of glaucoma factors on trabecular meshwork. PLoS One 2020;15:e0232111. https://doi.org/10.1371/journal.pone.0232111.

[194] Norte-Muñoz M, Botelho MF, Schoeberlein A, Chaves J, Neto Murta J, Ponsaerts P, et al. Insights and future directions for the application of perinatal derivatives in eye diseases: A critical review of preclinical and clinical studies. Front Bioeng Biotechnol 2022;10:969927. https://doi.org/10.3389/fbioe.2022.969927.

[195] Hongisto V, Jernström S, Fey V, Mpindi J-P, Kleivi Sahlberg K, Kallioniemi O, et al. High-throughput 3D screening reveals differences in drug sensitivities between culture models of JIMT1 breast cancer cells. PLoS ONE 2013;8:e77232. https://doi.org/10.1371/journal.pone.0077232.

[196] Roodnat AW, Callaghan B, Doyle C, Henry M, Goljanek-Whysall K, Simpson DA, et al. Genome-Wide RNA Sequencing of Human Trabecular Meshwork Cells Treated with TGF-β1: Relevance to Pseudoexfoliation Glaucoma. Biomolecules 2022;12:1693. https://doi.org/10.3390/biom12111693.

[197] Waduthanthri KD, Montemagno C, Çetinel S. Establishment of human trabecular meshwork cell cultures using nontransplantable corneoscleral rims. Turk J Biol 2019;43:89–98. https://doi.org/10.3906/biy-1810-69.

[198] Stamer DW, Roberts BC, Epstein DL, Allingham RR. Isolation of primary open-angle glaucomatous trabecular meshwork cells from whole eye tissue. Curr Eye Res 2000;20:347–50.

[199] Watanabe M, Ida Y, Ohguro H, Ota C, Hikage F. Establishment of appropriate glaucoma models using dexamethasone or TGFβ2 treated three-dimension (3D) cultured human trabecular meshwork (HTM) cells. Sci Rep 2021;11:19369. https://doi.org/10.1038/s41598-021-98766-3.

[200] Ota C, Ida Y, Ohguro H, Hikage F. ROCK inhibitors beneficially alter the spatial configuration of TGFβ2-treated 3D organoids from a human trabecular meshwork (HTM). Sci Rep 2020;10:20292. https://doi.org/10.1038/s41598-020-77302-9.

[201] Abu-Hassan DW, Li X, Ryan EI, Acott TS, Kelley MJ. Induced pluripotent stem cells restore function in a human cell loss model of open-angle glaucoma. Stem Cells 2015;33:751–61. https://doi.org/10.1002/stem.1885.

[202] Wang W, Miao Y, Sui S, Wang Y, Wu S, Cao Q, et al. Xeno- and Feeder-Free Differentiation of Human iPSCs to Trabecular Meshwork-Like Cells by Recombinant Cytokines. Transl Vis Sci Technol 2021;10:27. https://doi.org/10.1167/tvst.10.6.27.

[203] Zhu W, Jain A, Gramlich OW, Tucker BA, Sheffield VC, Kuehn MH. Restoration of Aqueous Humor Outflow Following Transplantation of iPSC-Derived Trabecular Meshwork Cells in a Transgenic Mouse Model of Glaucoma. Invest Ophthalmol Vis Sci 2017;58:2054–62. https://doi.org/10.1167/iovs.16-20672.

[204] Zhu W, Godwin CR, Cheng L, Scheetz TE, Kuehn MH. Transplantation of iPSC-TM stimulates division of trabecular meshwork cells in human eyes. Sci Rep 2020;10:2905. https://doi.org/10.1038/s41598-020-59941-0.

[205] Yu WY, Sheridan C, Grierson I, Mason S, Kearns V, Lo ACY, et al. Progenitors for the corneal endothelium and trabecular meshwork: a potential source for personalized stem cell therapy in corneal endothelial diseases and glaucoma. J Biomed Biotechnol 2011;2011:412743. https://doi.org/10.1155/2011/412743.

[206] Zhang Y, Cai S, Tseng SCG, Zhu Y-T. Isolation and Expansion of Multipotent Progenitors from Human Trabecular Meshwork. Sci Rep 2018;8:2814. https://doi.org/10.1038/s41598-018-21098-2.

[207] Tripathi RC, Li J, Chan WF, Tripathi BJ. Aqueous humor in glaucomatous eyes contains an increased level of TGF-beta 2. Exp Eye Res 1994;59:723–7.

[208] Guo T, Guo L, Fan Y, Fang L, Wei J, Tan Y, et al. Aqueous humor levels of TGFβ2 and SFRP1 in different types of glaucoma. BMC Ophthalmol 2019;19:170. https://doi.org/10.1186/s12886-019-1183-1.

[209] Gottanka J, Chan D, Eichhorn M, Lütjen-Drecoll E, Ethier CR. Effects of TGF-β2 in Perfused Human Eyes. Investigative Ophthalmology & Visual Science 2004;45:153–8. https://doi.org/10.1167/iovs.03-0796.

[210] Torrejon KY, Papke EL, Halman JR, Bergkvist M, Danias J, Sharfstein ST, et al. TGFβ2-induced outflow alterations in a bioengineered trabecular meshwork are offset by a rho-associated kinase inhibitor. Sci Rep 2016;6. https://doi.org/10.1038/srep38319.

[211] Fleenor DL, Shepard AR, Hellberg PE, Jacobson N, Pang I-H, Clark AF. TGFbeta2-induced changes in human trabecular meshwork: implications for intraocular pressure. Invest Ophthalmol Vis Sci 2006;47:226–34. https://doi.org/10.1167/iovs.05-1060.

[212] Lv Y, Zhang Z, Xing X, Liu A. lncRNA TGFβ2-AS1 promotes ECM production via TGF-β2 in human trabecular meshwork cells. Biochem Biophys Res Commun 2020;527:881–8. https://doi.org/10.1016/j.bbrc.2020.05.003.

[213] Bermudez JY, Montecchi-Palmer M, Mao W, Clark AF. Cross-linked actin networks (CLANs) in glaucoma. Exp Eye Res 2017;159:16–22. https://doi.org/10.1016/j.exer.2017.02.010.

[214] Tirendi S, Saccà SC, Vernazza S, Traverso C, Bassi AM, Izzotti A. A 3D Model of Human Trabecular Meshwork for the Research Study of Glaucoma. Front Neurol 2020;11:591776. https://doi.org/10.3389/fneur.2020.591776.

[215] Reinehr S, Mueller-Buehl AM, Tsai T, Joachim SC. Specific Biomarkers in the Aqueous Humour of Glaucoma Patients. Klin Monbl Augenheilkd 2022;239:169–76. https://doi.org/10.1055/a-1690-7468.

[216] Choritz L, Machert M, Thieme H. Correlation of endothelin-1 concentration in aqueous humor with intraocular pressure in primary open angle and pseudoexfoliation glaucoma. Invest Ophthalmol Vis Sci 2012;53:7336–42. https://doi.org/10.1167/iovs.12-10216.

[217] Shoshani YZ, Harris A, Shoja MM, Rusia D, Siesky B, Arieli Y, et al. Endothelin and its suspected role in the pathogenesis and possible treatment of glaucoma. Curr Eye Res 2012;37:1–11. https://doi.org/10.3109/02713683.2011.622849.

[218] Dismuke WM, Liang J, Overby DR, Stamer WD. Concentration-related effects of nitric oxide and endothelin-1 on human trabecular meshwork cell contractility. Exp Eye Res 2014;120:28–35. https://doi.org/10.1016/j.exer.2013.12.012.

[219] Wang J, Rong Y, Liu Y, Zhu M, Chen W, Chen Z, et al. The effect of ET1-CTGF mediated pathway on the accumulation of extracellular matrix in the trabecular meshwork and its contribution to the increase in IOP. Int Ophthalmol 2023. https://doi.org/10.1007/s10792-023-02733-y.

[220] Zhou EH, Paolucci M, Dryja TP, Manley T, Xiang C, Rice DS, et al. A Compact Whole-Eye Perfusion System to Evaluate Pharmacologic Responses of Outflow Facility. Invest Ophthalmol Vis Sci 2017;58:2991–3003. https://doi.org/10.1167/iovs.16-20974.

[221] Baudouin C, Denoyer A, Desbenoit N, Hamm G, Grise A. In vitro and in vivo experimental studies on trabecular meshwork degeneration induced by benzalkonium chloride (an American Ophthalmological Society thesis). Trans Am Ophthalmol Soc 2012;110:40–63.

[222] Bouchemi M, Roubeix C, Kessal K, Riancho L, Raveu A-L, Soualmia H, et al. Effect of benzalkonium chloride on trabecular meshwork cells in a new in vitro 3D trabecular meshwork model for glaucoma. Toxicol In Vitro 2017;41:21–9. https://doi.org/10.1016/j.tiv.2017.02.006.

[223] Torrejon KY, Pu D, Bergkvist M, Danias J, Sharfstein ST, Xie Y. Recreating a human trabecular meshwork outflow system on microfabricated porous structures. Biotechnol Bioeng 2013;110:3205–18. https://doi.org/10.1002/bit.24977.

[224] Torrejon KY, Papke EL, Halman JR, Stolwijk J, Dautriche CN, Bergkvist M, et al. Bioengineered glaucomatous 3D human trabecular meshwork as an in vitro disease model. Biotechnol Bioeng 2016;113:1357–68. https://doi.org/10.1002/bit.25899.

[225] Włodarczyk-Biegun MK, Villiou M, Koch M, Muth C, Wang P, Ott J, et al. Melt Electrowriting of Graded Porous Scaffolds to Mimic the Matrix Structure of the Human Trabecular Meshwork. ACS Biomater Sci Eng 2022;8:3899–911. https://doi.org/10.1021/acsbiomaterials.2c00623.

[226] Lu R, Soden PA, Lee E. Tissue-Engineered Models for Glaucoma Research. Micromachines (Basel) 2020;11:612. https://doi.org/10.3390/mi11060612.

[227] Bikuna-Izagirre M, Aldazabal J, Extramiana L, Moreno-Montañés J, Carnero E, Paredes J. Technological advances in ocular trabecular meshwork in vitro models for glaucoma research. Biotechnol Bioeng 2022;119:2698–714. https://doi.org/10.1002/bit.28182.

[228] Tie J, Chen D, Guo J, Liao S, Luo X, Zhang Y, et al. Transcriptome-wide study of the response of human trabecular meshwork cells to the substrate stiffness increase. J Cell Biochem 2020;121:3112–23. https://doi.org/10.1002/jcb.29578.

[229] Lee KY, Mooney DJ. Hydrogels for tissue engineering. Chem Rev 2001;101:1869–79. https://doi.org/10.1021/cr000108x.

[230] Kleinman HK, Martin GR. Matrigel: basement membrane matrix with biological activity. Semin Cancer Biol 2005;15:378–86. https://doi.org/10.1016/j.semcancer.2005.05.004.

[231] Benton G, Arnaoutova I, George J, Kleinman HK, Koblinski J. Matrigel: from discovery and ECM mimicry to assays and models for cancer research. Adv Drug Deliv Rev 2014;79–80:3–18. https://doi.org/10.1016/j.addr.2014.06.005.

[232] Cheng K, Lai Y, Kisaalita WS. Three-dimensional polymer scaffolds for high throughput cell-based assay systems. Biomaterials 2008;29:2802–12. https://doi.org/10.1016/j.biomaterials.2008.03.015.

[233] Hernandez M, Gong H, Ritch R, Shields MB, Krupin T. Extracellular matrix of the trabecular meshwork and optic nerve head. The glaucomas: basic sciences. Mosby, St Louis, Missouri: 1996.

[234] Keller KE, Aga M, Bradley JM, Kelley MJ, Acott TS. Extracellular matrix turnover and outflow resistance. Exp Eye Res 2009;88:676–82. https://doi.org/10.1016/j.exer.2008.11.023.

[235] Vranka JA, Kelley MJ, Acott TS, Keller KE. Extracellular matrix in the trabecular meshwork: intraocular pressure regulation and dysregulation in glaucoma. Exp Eye Res 2015;133:112–25. https://doi.org/10.1016/j.exer.2014.07.014.

[236] Osmond MJ, Krebs MD, Pantcheva MB. Human trabecular meshwork cell behavior is influenced by collagen scaffold pore architecture and glycosaminoglycan composition. Biotechnol Bioeng 2020;117:3150–9. https://doi.org/10.1002/bit.27477.

[237] Adhikari B, Osmond MJ, Pantcheva MB, Krebs MD. Glycosaminoglycans Influence Extracellular Matrix of Human Trabecular Meshwork Cells Cultured on 3D Scaffolds. ACS Biomater Sci Eng 2022;8:5221–32. https://doi.org/10.1021/acsbiomaterials.2c00457.

[238] Osmond M, Bernier SM, Pantcheva MB, Krebs MD. Collagen and collagen-chondroitin sulfate scaffolds with uniaxially aligned pores for the biomimetic, three dimensional culture of trabecular meshwork cells. Biotechnol Bioeng 2017;114:915–23. https://doi.org/10.1002/bit.26206.

[239] Liton PB, Challa P, Stinnett S, Luna C, Epstein DL, Gonzalez P. Cellular senescence in the glaucomatous outflow pathway. Exp Gerontol 2005;40:745–8. https://doi.org/10.1016/j.exger.2005.06.005.

[240] Li H, Bagué T, Kirschner A, Strat AN, Roberts H, Weisenthal RW, et al. A tissue-engineered human trabecular meshwork hydrogel for advanced glaucoma disease modeling. Exp Eye Res 2021;205:108472. https://doi.org/10.1016/j.exer.2021.108472.

[241] Waduthanthri KD, He Y, Montemagno C, Cetinel S. An injectable peptide hydrogel for reconstruction of the human trabecular meshwork. Acta Biomater 2019;100:244–54. https://doi.org/10.1016/j.actbio.2019.09.032.

[242] Watanabe M, Sato T, Tsugeno Y, Umetsu A, Suzuki S, Furuhashi M, et al. Human Trabecular Meshwork (HTM) Cells Treated with TGF-β2 or Dexamethasone Respond to Compression Stress in Different Manners. Biomedicines 2022;10:1338. https://doi.org/10.3390/biomedicines10061338.

[243] Watanabe M, Ida Y, Ohguro H, Ota C, Hikage F. Diverse effects of pan-ROCK and ROCK2 inhibitors on 2 D and 3D cultured human trabecular meshwork (HTM) cells treated with TGFβ2. Sci Rep 2021;11:15286. https://doi.org/10.1038/s41598-021-94791-4.

[244] Perkins TW, Alvarado JA, Polansky JR, Stilwell L, Maglio M, Juster R. Trabecular meshwork cells grown on filters. Conductivity and cytochalasin effects. Invest Ophthalmol Vis Sci 1988;29:1836–46.

[245] Overby D, Gong H, Qiu G, Freddo TF, Johnson M. The mechanism of increasing outflow facility during washout in the bovine eye. Invest Ophthalmol Vis Sci 2002;43:3455–64.

[246] Mao W, Tovar-Vidales T, Yorio T, Wordinger RJ, Clark AF. Perfusion-cultured bovine anterior segments as an ex vivo model for studying glucocorticoid-induced ocular hypertension and glaucoma. Invest Ophthalmol Vis Sci 2011;52:8068–75. https://doi.org/10.1167/iovs.11-8133.

[247] Van Buskirk EM, Grant WM. Lens depression and aqueous outflow in enucleated primate eyes. Am J Ophthalmol 1973;76:632–40. https://doi.org/10.1016/0002-9394(73)90555-2.

[248] Dang Y, Waxman S, Wang C, Loewen RT, Sun M, Loewen NA. A porcine ex vivo model of pigmentary glaucoma. Sci Rep 2018;8:5468. https://doi.org/10.1038/s41598-018-23861-x.

[249] Grant WM. Experimental aqueous perfusion in enucleated human eyes. Arch Ophthalmol 1963;69:783–801. https://doi.org/10.1001/archopht.1963.00960040789022.

[250] Bahler CK, Howell KG, Hann CR, Fautsch MP, Johnson DH. Prostaglandins Increase Trabecular Meshwork Outflow Facility in Cultured Human Anterior Segments. Am J Ophthalmol 2008;145:114–9. https://doi.org/10.1016/j.ajo.2007.09.001.

[251] Kasetti RB, Patel PD, Maddineni P, Zode GS. Ex-vivo cultured human corneoscleral segment model to study the effects of glaucoma factors on trabecular meshwork. PLoS One 2020;15:e0232111. https://doi.org/10.1371/journal.pone.0232111.

[252] Peng M, Margetts TJ, Sugali CK, Rayana NP, Dai J, Sharma TP, et al. An ex vivo model of human corneal rim perfusion organ culture. Exp Eye Res 2022;214:108891. https://doi.org/10.1016/j.exer.2021.108891.

[253] Buffault J, Reboussin É, Kessal K, Akkurt Arslan M, Blond F, Guillonneau X, et al. RNA-Seq Transcriptomic Analysis of Human Trabecular Meshwork Explants Exposed to TGF-β2: A Novel Approach Beyond Traditional Cell Culture Models. Ahead of Pub 2023.

[254] Vernazza S, Tirendi S, Scarfì S, Passalacqua M, Oddone F, Traverso CE, et al. 2D- and 3D-cultures of human trabecular meshwork cells: A preliminary assessment of an in vitro model for glaucoma study. PLoS One 2019;14:e0221942. https://doi.org/10.1371/journal.pone.0221942.

[255] Saccà SC, Tirendi S, Scarfì S, Passalacqua M, Oddone F, Traverso CE, et al. An advanced in vitro model to assess glaucoma onset. ALTEX 2020;37:265–74. https://doi.org/10.14573/altex.1909262.

[256] Crouch DJ, Sheridan CM, D'Sa RA, Willoughby CE, Bosworth LA. Exploiting biomaterial approaches to manufacture an artificial trabecular meshwork: A progress report. Biomater Biosyst 2021;1:100011. https://doi.org/10.1016/j.bbiosy.2021.100011.

[257] Yun H, Zhou Y, Wills A, Du Y. Stem Cells in the Trabecular Meshwork for Regulating Intraocular Pressure. J Ocul Pharmacol Ther 2016;32:253–60. https://doi.org/10.1089/jop.2016.0005.

[258] Fan X, Bilir EK, Kingston OA, Oldershaw RA, Kearns VR, Willoughby CE, et al. Replacement of the Trabecular Meshwork Cells-A Way Ahead in IOP Control? Biomolecules 2021;11:1371. https://doi.org/10.3390/biom11091371.

[259] Jang H-K, Kim B-S. Modulation of stem cell differentiation with biomaterials. Int J Stem Cells 2010;3:80–4. https://doi.org/10.15283/ijsc.2010.3.2.80.

[260] Schlunck G, Han H, Wecker T, Kampik D, Meyer-ter-Vehn T, Grehn F. Substrate rigidity modulates cell matrix interactions and protein expression in human trabecular meshwork cells. Invest Ophthalmol Vis Sci 2008;49:262–9. https://doi.org/10.1167/iovs.07-0956.

[261] Kim B, Roberts CJ, Mahmoud AM, Grzybowski DM, Weber PA, Yi Z. Topographic Effect of Micro/Nanoengineered Polymer Substrates on Cultured Trabecular Meshwork Cells. Investigative Ophthalmology & Visual Science 2011;52:4666.

[262] Torrejon KY, Papke EL, Halman JR, Bergkvist M, Danias J, Sharfstein ST, et al. TGFβ2-induced outflow alterations in a bioengineered trabecular meshwork are offset by a rho-associated kinase inhibitor. Sci Rep 2016;6. https://doi.org/10.1038/srep38319.

[263] Tian YI, Zhang X, Torrejon K, Danias J, Du Y, Xie Y. A Biomimetic, Stem Cell-derived in vitro Ocular Outflow Model. Adv Biosyst 2020;4:e2000004. https://doi.org/10.1002/adbi.202000004.

[264] Vernazza S, Tirendi S, Passalacqua M, Piacente F, Scarfì S, Oddone F, et al. An Innovative In Vitro Open-Angle Glaucoma Model (IVOM) Shows Changes Induced by Increased Ocular Pressure and Oxidative Stress. Int J Mol Sci 2021;22:12129. https://doi.org/10.3390/ijms222212129.

[265] Vernazza S, Passalacqua M, Tirendi S, Marengo B, Domenicotti C, Sbardella D, et al. Citicoline Eye Drops Protect Trabecular Meshwork Cells from Oxidative Stress Injury in a 3D In Vitro Glaucoma Model. Int J Mol Sci 2022;23:11375. https://doi.org/10.3390/ijms231911375.

[266] Aires ID, Ambrósio AF, Santiago AR. Modeling Human Glaucoma: Lessons from the in vitro Models. Ophthalmic Res 2017;57:77–86. https://doi.org/10.1159/000448480.

[267] Wang J, Liu X, Zhong Y. Rho/Rho-associated kinase pathway in glaucoma (Review). Int J Oncol 2013;43:1357–67. https://doi.org/10.3892/ijo.2013.2100.

[268] Winkler NS, Fautsch MP. Effects of prostaglandin analogues on aqueous humor outflow pathways. J Ocul Pharmacol Ther 2014;30:102–9. https://doi.org/10.1089/jop.2013.0179.

[269] Amano M, Nakayama M, Kaibuchi K. Rho-kinase/ROCK: A key regulator of the cytoskeleton and cell polarity. Cytoskeleton (Hoboken) 2010;67:545–54. https://doi.org/10.1002/cm.20472.

[270] Zhang N, Wang J, Li Y, Jiang B. Prevalence of primary open angle glaucoma in the last 20 years: a meta-analysis and systematic review. Sci Rep 2021;11:13762. https://doi.org/10.1038/s41598-021-92971-w.

[271] Tripathi RC, Li J, Chan WF, Tripathi BJ. Aqueous humor in glaucomatous eyes contains an increased level of TGF-beta 2. Exp Eye Res 1994;59:723–7.

[272] Kasetti RB, Maddineni P, Kodati B, Nagarajan B, Yacoub S. Astragaloside IV Attenuates Ocular Hypertension in a Mouse Model of TGFβ2 Induced Primary Open Angle Glaucoma. Int J Mol Sci 2021;22:12508. https://doi.org/10.3390/ijms222212508.

[273] Wang J, Harris A, Prendes MA, Alshawa L, Gross JC, Wentz SM, et al. Targeting Transforming Growth Factor-β Signaling in Primary Open-Angle Glaucoma. J Glaucoma 2017;26:390–5. https://doi.org/10.1097/IJG.0000000000000627.

[274] Rao PV, Pattabiraman PP, Kopczynski C. Role of the Rho GTPase/Rho kinase signaling pathway in pathogenesis and treatment of glaucoma: Bench to bedside research. Exp Eye Res 2017;158:23–32. https://doi.org/10.1016/j.exer.2016.08.023.

[275] Prunier C, Prudent R, Kapur R, Sadoul K, Lafanechère L. LIM kinases: cofilin and beyond. Oncotarget 2017;8:41749. https://doi.org/10.18632/oncotarget.16978.

[276] Liao JK, Seto M, Noma K. Rho kinase (ROCK) inhibitors. J Cardiovasc Pharmacol 2007;50:17–24. https://doi.org/10.1097/FJC.0b013e318070d1bd.

[277] Tanihara H, Inoue T, Yamamoto T, Kuwayama Y, Abe H, Araie M, et al. Phase 1 clinical trials of a selective Rho kinase inhibitor, K-115. JAMA Ophthalmol 2013;131:1288–95. https://doi.org/10.1001/jamaophthalmol.2013.323.

[278] Tanihara H, Inoue T, Yamamoto T, Kuwayama Y, Abe H, Suganami H, et al. Intra-ocular pressure-lowering effects of a Rho kinase inhibitor, ripasudil (K-115), over 24 hours in primary open-angle glaucoma and ocular hypertension: a randomized, open-label, crossover study. Acta Ophthalmol 2015;93:e254-260. https://doi.org/10.1111/aos.12599.

[279] Tanihara H, Inoue T, Yamamoto T, Kuwayama Y, Abe H, Araie M, et al. Phase 2 randomized clinical study of a Rho kinase inhibitor, K-115, in primary open-angle glaucoma and ocular hypertension. Am J Ophthalmol 2013;156:731–6. https://doi.org/10.1016/j.ajo.2013.05.016.

[280] Bacharach J, Dubiner HB, Levy B, Kopczynski CC, Novack GD, AR-13324-CS202 Study Group. Double-masked, randomized, dose-response study of AR-13324 versus latanoprost in patients with elevated intraocular pressure. Ophthalmology 2015;122:302–7. https://doi.org/10.1016/j.ophtha.2014.08.022.

[281] Tanihara H, Inoue T, Yamamoto T, Kuwayama Y, Abe H, Fukushima A, et al. One-year clinical evaluation of 0.4% ripasudil (K-115) in patients with open-angle glaucoma and ocular hypertension. Acta Ophthalmol 2016;94:e26-34. https://doi.org/10.1111/aos.12829.

[282] Wang SK, Chang RT. An emerging treatment option for glaucoma: Rho kinase inhibitors. Clin Ophthalmol 2014;8:883–90. https://doi.org/10.2147/OPTH.S41000.

[283] Fujimoto T, Inoue T, Inoue-Mochita M, Tanihara H. Live cell imaging of actin dynamics in dexamethasone-treated porcine trabecular meshwork cells. Experimental Eye Research 2016;145:393–400. https://doi.org/10.1016/j.exer.2016.02.007.

[284] Hamard P, Blondin C, Debbasch C, Warnet J-M, Baudouin C, Brignole F. In vitro effects of preserved and unpreserved antiglaucoma drugs on apoptotic marker expression by human trabecular cells. Graefes Arch Clin Exp Ophthalmol 2003;241:1037–43. https://doi.org/10.1007/s00417-003-0777-7.

[285] Benton G, Arnaoutova I, George J, Kleinman HK, Koblinski J. Matrigel: from discovery and ECM mimicry to assays and models for cancer research. Adv Drug Deliv Rev 2014;79–80:3–18. https://doi.org/10.1016/j.addr.2014.06.005.

[286] Hughes CS, Postovit LM, Lajoie GA. Matrigel: a complex protein mixture required for optimal growth of cell culture. Proteomics 2010;10:1886–90. https://doi.org/10.1002/pmic.200900758.

[287] Di Rosa M, Tibullo D, Saccone S, Distefano G, Basile MS, Di Raimondo F, et al. CHI3L1 nuclear localization in monocyte derived dendritic cells. Immunobiology 2016;221:347–56. https://doi.org/10.1016/j.imbio.2015.09.023.

[288] Kottler UB, Jünemann AGM, Aigner T, Zenkel M, Rummelt C, Schlötzer-Schrehardt U. Comparative effects of TGF-beta 1 and TGF-beta 2 on extracellular matrix production, proliferation, migration, and collagen contraction of human Tenon's capsule fibroblasts in pseudoexfoliation and primary open-angle glaucoma. Exp Eye Res 2005;80:121–34. https://doi.org/10.1016/j.exer.2004.08.018.

[289] Connor TB, Roberts AB, Sporn MB, Danielpour D, Dart LL, Michels RG, et al. Correlation of fibrosis and transforming growth factor-beta type 2 levels in the eye. J Clin Invest 1989;83:1661–6. https://doi.org/10.1172/JCI114065.

[290] Li G, Lee C, Read AT, Wang K, Ha J, Kuhn M, et al. Anti-fibrotic activity of a rho-kinase inhibitor restores outflow function and intraocular pressure homeostasis. Elife 2021;10. https://doi.org/10.7554/eLife.60831.

[291] Hongisto V, Jernström S, Fey V, Mpindi J-P, Kleivi Sahlberg K, Kallioniemi O, et al. High-throughput 3D screening reveals differences in drug sensitivities between culture models of JIMT1 breast cancer cells. PLoS ONE 2013;8:e77232. https://doi.org/10.1371/journal.pone.0077232.

[292] Rao PV, Deng PF, Kumar J, Epstein DL. Modulation of aqueous humor outflow facility by the Rho kinase-specific inhibitor Y-27632. Invest Ophthalmol Vis Sci 2001;42:1029–37.

[293] Murphy KC, Morgan JT, Wood JA, Sadeli A, Murphy CJ, Russell P. The formation of cortical actin arrays in human trabecular meshwork cells in response to cytoskeletal disruption. Exp Cell Res 2014;328:164–71. https://doi.org/10.1016/j.yexcr.2014.06.014.

[294] Heo JY, Ooi YH, Rhee DJ. Effect of prostaglandin analogs: Latanoprost, bimatoprost, and unoprostone on matrix metalloproteinases and their inhibitors in human trabecular meshwork endothelial cells. Exp Eye Res 2020;194:108019. https://doi.org/10.1016/j.exer.2020.108019.

[295] Tanna AP, Johnson M. Rho Kinase Inhibitors as a Novel Treatment for Glaucoma and Ocular Hypertension. Ophthalmology 2018;125:1741–56. https://doi.org/10.1016/j.ophtha.2018.04.040.

[296] Lewis RA, Levy B, Ramirez N, Kopczynski CC, Usner DW, Novack GD, et al. Fixed-dose combination of AR-13324 and latanoprost: a double-masked, 28-day, randomised, controlled study in patients with open-angle glaucoma or ocular hypertension. Br J Ophthalmol 2016;100:339–44. https://doi.org/10.1136/bjophthalmol-2015-306778.

[297] Tanihara H, Inoue T, Yamamoto T, Kuwayama Y, Abe H, Suganami H, et al. Additive Intraocular Pressure-Lowering Effects of the Rho Kinase Inhibitor Ripasudil (K-115) Combined With Timolol or Latanoprost: A Report of 2 Randomized Clinical Trials. JAMA Ophthalmol 2015;133:755–61. https://doi.org/10.1001/jamaophthalmol.2015.0525.

[298] Kass MA, Heuer DK, Higginbotham EJ, Johnson CA, Keltner JL, Miller JP, et al. The Ocular Hypertension Treatment Study: a randomized trial determines that topical ocular hypotensive medication delays or prevents the onset of primary open-angle glaucoma. Arch Ophthalmol 2002;120:701–13; discussion 829-830.

[299] Pattabiraman PP, Maddala R, Rao PV. Regulation of plasticity and fibrogenic activity of trabecular meshwork cells by Rho GTPase signaling. J Cell Physiol 2014;229:927–42. https://doi.org/10.1002/jcp.24524.

[300] Wormald R, Virgili G, Azuara-Blanco A. Systematic reviews and randomised controlled trials on open angle glaucoma. Eye (Lond) 2020;34:161–7. https://doi.org/10.1038/s41433-019-0687-5.

[301] Callaghan B, Lester K, Lane B, Fan X, Goljanek-Whysall K, Simpson DA, et al. Genome-wide transcriptome profiling of human trabecular meshwork cells treated with TGF-β2. Sci Rep 2022;12:9564. https://doi.org/10.1038/s41598-022-13573-8.

[302] Fuellen G, Jünemann A. Gene Expression Data for Investigating Glaucoma Treatment Options and Pharmacology in the Anterior Segment, State-of-the-Art and Future Directions. Front Neurosci 2022;16:912043. https://doi.org/10.3389/fnins.2022.912043.

[303] Wolf J, Lapp T, Reinhard T, Agostini H, Schlunck G, Lange C. Web-based gene expression analysis-paving the way to decode healthy and diseased ocular tissue. Ophthalmologie 2023;120:59–65. https://doi.org/10.1007/s00347-022-01721-4.

[304] Stamer WD, Seftor RE, Williams SK, Samaha HA, Snyder RW. Isolation and culture of human trabecular meshwork cells by extracellular matrix digestion. Curr Eye Res 1995;14:611–7.

[305] Carnes MU, Allingham RR, Ashley-Koch A, Hauser MA. Transcriptome analysis of adult and fetal trabecular meshwork, cornea, and ciliary body tissues by RNA sequencing. Exp Eye Res 2018;167:91–9. https://doi.org/10.1016/j.exer.2016.11.021.

[306] van Zyl T, Yan W, McAdams AM, Monavarfeshani A, Hageman GS, Sanes JR. Cell atlas of the human ocular anterior segment: Tissue-specific and shared cell types. Proc Natl Acad Sci U S A 2022;119:e2200914119. https://doi.org/10.1073/pnas.2200914119.

[307] van Zyl T, Yan W, McAdams A, Peng Y-R, Shekhar K, Regev A, et al. Cell atlas of aqueous humor outflow pathways in eyes of humans and four model species provides insight into glaucoma pathogenesis. Proc Natl Acad Sci U S A 2020;117:10339–49. https://doi.org/10.1073/pnas.2001250117.

[308] Shannon P, Markiel A, Ozier O, Baliga NS, Wang JT, Ramage D, et al. Cytoscape: A Software Environment for Integrated Models of Biomolecular Interaction Networks. Genome Res 2003;13:2498–504. https://doi.org/10.1101/gr.1239303.

[309] Dituri F, Cossu C, Mancarella S, Giannelli G. The Interactivity between TGFβ and BMP Signaling in Organogenesis, Fibrosis, and Cancer. Cells 2019;8:1130. https://doi.org/10.3390/cells8101130.

[310] Miyazono K, Kamiya Y, Morikawa M. Bone morphogenetic protein receptors and signal transduction. The Journal of Biochemistry 2010;147:35–51. https://doi.org/10.1093/jb/mvp148.

[311] Fuchshofer R, Stephan DA, Russell P, Tamm ER. Gene expression profiling of TGFbeta2- and/or BMP7-treated trabecular meshwork cells: Identification of Smad7 as a critical inhibitor of TGF-beta2 signaling. Exp Eye Res 2009;88:1020–32. https://doi.org/10.1016/j.exer.2009.01.002.

[312] Webber HC, Bermudez JY, Sethi A, Clark AF, Mao W. Crosstalk between TGFβ and Wnt signaling pathways in the human trabecular meshwork. Exp Eye Res 2016;148:97–102. https://doi.org/10.1016/j.exer.2016.04.007.

[313] Wordinger RJ, Sharma T, Clark AF. The role of TGF-β2 and bone morphogenetic proteins in the trabecular meshwork and glaucoma. J Ocul Pharmacol Ther 2014;30:154–62. https://doi.org/10.1089/jop.2013.0220.

[314] Yu R, Wu Y, He P, Bai Y, Zhang Y, Bian X, et al. LIM and Cysteine-Rich Domains 1 Promotes Transforming Growth Factor β1–Induced Epithelial–Mesenchymal Transition in Human Kidney 2 Cells. Laboratory Investigation 2023;103:100016. https://doi.org/10.1016/j.labinv.2022.100016.

[315] Patel G, Fury W, Yang H, Gomez-Caraballo M, Bai Y, Yang T, et al. Molecular taxonomy of human ocular outflow tissues defined by single-cell transcriptomics. Proc Natl Acad Sci U S A 2020;117:12856–67. https://doi.org/10.1073/pnas.2001896117.

[316] Saccà SC, Izzotti A, Rossi P, Traverso C. Glaucomatous outflow pathway and oxidative stress. Exp Eye Res 2007;84:389–99. https://doi.org/10.1016/j.exer.2006.10.008.

[317] Mody AA, Wordinger RJ, Clark AF. Role of ID Proteins in BMP4 Inhibition of Profibrotic Effects of TGF-β2 in Human TM Cells. Invest Ophthalmol Vis Sci 2017;58:849–59. https://doi.org/10.1167/iovs.16-20472.

[318] Wordinger RJ, Fleenor DL, Hellberg PE, Pang I-H, Tovar TO, Zode GS, et al. Effects of TGF-beta2, BMP-4, and gremlin in the trabecular meshwork: implications for glaucoma. Invest Ophthalmol Vis Sci 2007;48:1191–200. https://doi.org/10.1167/iovs.06-0296.

[319] Nettesheim A, Shim MS, Hirt J, Liton PB. Transcriptome analysis reveals autophagy as regulator of TGFβ/Smad-induced fibrogenesis in trabecular meshwork cells. Sci Rep 2019;9:16092. https://doi.org/10.1038/s41598-019-52627-2.

[320] Webber HC, Bermudez JY, Millar JC, Mao W, Clark AF. The Role of Wnt/β-Catenin Signaling and K-Cadherin in the Regulation of Intraocular Pressure. Invest Ophthalmol Vis Sci 2018;59:1454–66. https://doi.org/10.1167/iovs.17-21964.

[321] Liu L, He J, Liu C, Yang M, Fu J, Yi J, et al. Cartilage intermediate layer protein affects the progression of intervertebral disc degeneration by regulating the extracellular microenvironment (Review). Int J Mol Med 2021;47:475–84. https://doi.org/10.3892/ijmm.2020.4832.

[322] Jia S, Chen F, Wang H, Kesavamoorthy G, Lai JS-M, Wong IY-H, et al. Effect of Vitamin D3 on Regulating Human Tenon's Fibroblasts Activity. Transl Vis Sci Technol 2021;10:7. https://doi.org/10.1167/tvst.10.8.7.

[323] Groß S, Thum T. TGF-β Inhibitor CILP as a Novel Biomarker for Cardiac Fibrosis. JACC Basic Transl Sci 2020;5:444–6. https://doi.org/10.1016/j.jacbts.2020.03.013.

[324] Mori M, Nakajima M, Mikami Y, Seki S, Takigawa M, Kubo T, et al. Transcriptional regulation of the cartilage intermediate layer protein (CILP) gene. Biochem Biophys Res Commun 2006;341:121–7. https://doi.org/10.1016/j.bbrc.2005.12.159.

[325] Zhang C-L, Zhao Q, Liang H, Qiao X, Wang J-Y, Wu D, et al. Cartilage intermediate layer protein-1 alleviates pressure overload-induced cardiac fibrosis via interfering TGF-β1 signaling. Journal of Molecular and Cellular Cardiology 2018;116:135–44. https://doi.org/10.1016/j.yjmcc.2018.02.006.

[326] Fu CT, Sretavan D. Involvement of EphB/Ephrin-B Signaling in Axonal Survival in Mouse Experimental Glaucoma. Investigative Ophthalmology & Visual Science 2012;53:76–84. https://doi.org/10.1167/iovs.11-8546.

[327] Colak D, Morales J, Bosley TM, Al-Bakheet A, AlYounes B, Kaya N, et al. Genome-Wide Expression Profiling of Patients with Primary Open Angle Glaucoma. Investigative Ophthalmology & Visual Science 2012;53:5899–904. https://doi.org/10.1167/iovs.12-9634.

[328] Vittal V, Rose A, Gregory KE, Kelley MJ, Acott TS. Changes in Gene Expression by Trabecular Meshwork Cells in Response to Mechanical Stretching. Investigative Ophthalmology & Visual Science 2005;46:2857–68. https://doi.org/10.1167/iovs.05-0075.

[329] Fina D, Franzè E, Rovedatti L, Corazza GR, Biancone L, Sileri PP, et al. Interleukin-25 production is differently regulated by TNF-α and TGF-β1 in the human gut. Mucosal Immunol 2011;4:239–44. https://doi.org/10.1038/mi.2010.68.

[330] Sumiyoshi K, Nakao A, Setoguchi Y, Tsuboi R, Okumura K, Ogawa H. TGF-beta/Smad signaling inhibits IFN-gamma and TNF-alpha-induced TARC (CCL17) production in HaCaT cells. J Dermatol Sci 2003;31:53–8. https://doi.org/10.1016/s0923-1811(02)00141-x.

[331] Louis TJ, Qasem A, Naser SA. Attenuation of Excess TNF-α Release in Crohn's Disease by Silencing of iRHOMs 1/2 and the Restoration of TGF-β Mediated Immunosuppression Through Modulation of TACE Trafficking. Front Immunol 2022;13:887830. https://doi.org/10.3389/fimmu.2022.887830.

[332] Dash S, Sahu AK, Srivastava A, Chowdhury R, Mukherjee S. Exploring the extensive crosstalk between the antagonistic cytokines- TGF-β and TNF-α in regulating cancer pathogenesis. Cytokine 2021;138:155348. https://doi.org/10.1016/j.cyto.2020.155348.

[333] Liu Z-W, Zhang Y-M, Zhang L-Y, Zhou T, Li Y-Y, Zhou G-C, et al. Duality of Interactions Between TGF-β and TNF-α During Tumor Formation. Front Immunol 2021;12:810286. https://doi.org/10.3389/fimmu.2021.810286.

[334] Tezel G. TNF-α Signaling in Glaucomatous Neurodegeneration. Prog Brain Res 2008;173:409–21. https://doi.org/10.1016/S0079-6123(08)01128-X.

[335] Leask A, Abraham DJ. TGF-beta signaling and the fibrotic response. FASEB J 2004;18:816–27. https://doi.org/10.1096/fj.03-1273rev.

[336] Verrecchia F, Mauviel A. TGF-beta and TNF-alpha: antagonistic cytokines controlling type I collagen gene expression. Cell Signal 2004;16:873–80. https://doi.org/10.1016/j.cellsig.2004.02.007.

[337] Tang Y, Le W. Differential Roles of M1 and M2 Microglia in Neurodegenerative Diseases. Mol Neurobiol 2016;53:1181–94. https://doi.org/10.1007/s12035-014-9070-5.

[338] Liu Y, Zeng R, Wang Y, Huang W, Hu B, Zhu G, et al. Mesenchymal stem cells enhance microglia M2 polarization and attenuate neuroinflammation through TSG-6. Brain Res 2019;1724:146422. https://doi.org/10.1016/j.brainres.2019.146422.

[339] Rőszer T. Understanding the Mysterious M2 Macrophage through Activation Markers and Effector Mechanisms. Mediators Inflamm 2015;2015:816460. https://doi.org/10.1155/2015/816460.

[340] Mélik Parsadaniantz S, Réaux-le Goazigo A, Sapienza A, Habas C, Baudouin C. Glaucoma: A Degenerative Optic Neuropathy Related to Neuroinflammation? Cells 2020;9. https://doi.org/10.3390/cells9030535.

[341] Saccà SC, Pulliero A, Izzotti A. The dysfunction of the trabecular meshwork during glaucoma course. J Cell Physiol 2015;230:510–25. https://doi.org/10.1002/jcp.24826.

[342] Birke MT, Birke K, Lütjen-Drecoll E, Schlötzer-Schrehardt U, Hammer CM. Cytokine-dependent ELAM-1 induction and concomitant intraocular pressure regulation in porcine anterior eye perfusion culture. Invest Ophthalmol Vis Sci 2011;52:468–75. https://doi.org/10.1167/iovs.10-5990.

[343] Liton PB, Luna C, Bodman M, Hong A, Epstein DL, Gonzalez P. Induction of IL-6 expression by mechanical stress in the trabecular meshwork. Biochem Biophys Res Commun 2005;337:1229–36. https://doi.org/10.1016/j.bbrc.2005.09.182.

[344] Blondin C, Hamard P, Brignole F, Baudouin C. Human Trabecular Meshwork Cells Produce the Pro-inflammatory Chemokines Interleukin-8 (IL-8) and Monocyte Chemoattractant Protein-1 (MCP-1) in vitro. Investigative Ophthalmology & Visual Science 2003;44:679.

[345] Allison K, Patel D, Alabi O. Epidemiology of Glaucoma: The Past, Present, and Predictions for the Future. Cureus 2020;12:e11686. https://doi.org/10.7759/cureus.11686.

[346] Nadal-Nicolás FM, Jiménez-López M, Sobrado-Calvo P, Nieto-López L, Cánovas-Martínez I, Salinas-Navarro M, et al. Brn3a as a marker of retinal ganglion cells: qualitative and quantitative time course studies in naive and optic nerve-injured retinas. Invest Ophthalmol Vis Sci 2009;50:3860–8. https://doi.org/10.1167/iovs.08-3267.

[347] Nadal-Nicolás FM, Galindo-Romero C, Lucas-Ruiz F, Marsh-Amstrong N, Li W, Vidal-Sanz M, et al. Pan-retinal ganglion cell markers in mice, rats, and rhesus macaques. Zool Res 2023;44:226–48. https://doi.org/10.24272/j.issn.2095-8137.2022.308.

[348] Adornetto A, Russo R, Parisi V. Neuroinflammation as a target for glaucoma therapy. Neural Regen Res 2019;14:391–4. https://doi.org/10.4103/1673-5374.245465.

[349] Mannino G, Russo C, Longo A, Anfuso CD, Lupo G, Lo Furno D, et al. Potential therapeutic applications of mesenchymal stem cells for the treatment of eye diseases. World J Stem Cells 2021;13:632–44. https://doi.org/10.4252/wjsc.v13.i6.632.

[350] Nicoară SD, Brie I, Jurj A, Soriţău O. The Future of Stem Cells and Their Derivates in the Treatment of Glaucoma. A Critical Point of View. Int J Mol Sci 2021;22:11077. https://doi.org/10.3390/ijms222011077.

[351] Harrell CR, Fellabaum C, Arsenijevic A, Markovic BS, Djonov V, Volarevic V. Therapeutic Potential of Mesenchymal Stem Cells and Their Secretome in the Treatment of Glaucoma. Stem Cells Int 2019;2019:7869130. https://doi.org/10.1155/2019/7869130.

[352] Öner A. Stem Cell Treatment in Retinal Diseases: Recent Developments. Turk J Ophthalmol 2018;48:33–8. https://doi.org/10.4274/tjo.89972.

[353] Emre E, Yüksel N, Duruksu G, Pirhan D, Subaşi C, Erman G, et al. Neuroprotective effects of intravitreally transplanted adipose tissue and bone marrow-derived mesenchymal stem cells in an experimental ocular hypertension model. Cytotherapy 2015;17:543–59. https://doi.org/10.1016/j.jcyt.2014.12.005.

[354] Johnson TV, Bull ND, Hunt DP, Marina N, Tomarev SI, Martin KR. Neuroprotective effects of intravitreal mesenchymal stem cell transplantation in experimental glaucoma. Invest Ophthalmol Vis Sci 2010;51:2051–9. https://doi.org/10.1167/iovs.09-4509.

[355] Hu Y, Tan HB, Wang XM, Rong H, Cui HP, Cui H. Bone marrow mesenchymal stem cells protect against retinal ganglion cell loss in aged rats with glaucoma. Clin Interv Aging 2013;8:1467–70. https://doi.org/10.2147/CIA.S47350.

[356] Holan V, Palacka K, Hermankova B. Mesenchymal Stem Cell-Based Therapy for Retinal Degenerative Diseases: Experimental Models and Clinical Trials. Cells 2021;10:588. https://doi.org/10.3390/cells10030588.

[357] Roubeix C, Godefroy D, Mias C, Sapienza A, Riancho L, Degardin J, et al. Intraocular pressure reduction and neuroprotection conferred by bone marrow-derived mesenchymal stem cells in an animal model of glaucoma. Stem Cell Res Ther 2015;6:177. https://doi.org/10.1186/s13287-015-0168-0.

[358] Russo R, Varano GP, Adornetto A, Nucci C, Corasaniti MT, Bagetta G, et al. Retinal ganglion cell death in glaucoma: Exploring the role of neuroinflammation. Eur J Pharmacol 2016;787:134–42. https://doi.org/10.1016/j.ejphar.2016.03.064.

[359] García-Bermúdez MY, Freude KK, Mouhammad ZA, van Wijngaarden P, Martin KK, Kolko M. Glial Cells in Glaucoma: Friends, Foes, and Potential Therapeutic Targets. Front Neurol 2021;12:624983. https://doi.org/10.3389/fneur.2021.624983.

[360] Lazzara F, Amato R, Platania CBM, Conti F, Chou T-H, Porciatti V, et al. 1α,25-dihydroxyvitamin D3 protects retinal ganglion cells in glaucomatous mice. J Neuroinflammation 2021;18:206. https://doi.org/10.1186/s12974-021-02263-3.

[361] Cherry JD, Olschowka JA, O'Banion MK. Neuroinflammation and M2 microglia: the good, the bad, and the inflamed. J Neuroinflammation 2014;11:98. https://doi.org/10.1186/1742-2094-11-98.

[362] Huang Y, Feng Z. The good and bad of microglia/macrophages: new hope in stroke therapeutics. Acta Pharmacol Sin 2013;34:6–7. https://doi.org/10.1038/aps.2012.178.

[363] Zhou T, Huang Z, Sun X, Zhu X, Zhou L, Li M, et al. Microglia Polarization with M1/M2 Phenotype Changes in rd1 Mouse Model of Retinal Degeneration. Front Neuroanat 2017;11:77. https://doi.org/10.3389/fnana.2017.00077.

[364] Mantovani A, Sica A, Sozzani S, Allavena P, Vecchi A, Locati M. The chemokine system in diverse forms of macrophage activation and polarization. Trends Immunol 2004;25:677–86. https://doi.org/10.1016/j.it.2004.09.015.

[365] Mutoji KN, Sun M, Nash A, Puri S, Hascall V, Coulson-Thomas VJ. Anti-inflammatory protein TNFα-stimulated gene-6 (TSG-6) reduces inflammatory response after brain injury in mice. BMC Immunol 2021;22:52. https://doi.org/10.1186/s12865-021-00443-7.

[366] Jha KA, Pentecost M, Lenin R, Klaic L, Elshaer SL, Gentry J, et al. Concentrated Conditioned Media from Adipose Tissue Derived Mesenchymal Stem Cells Mitigates Visual Deficits and Retinal Inflammation Following Mild Traumatic Brain Injury. Int J Mol Sci 2018;19:E2016. https://doi.org/10.3390/ijms19072016.

[367] Hou Y, Luan J, Huang T, Deng T, Li X, Xiao Z, et al. Tauroursodeoxycholic acid alleviates secondary injury in spinal cord injury mice by reducing oxidative stress, apoptosis, and inflammatory response. J Neuroinflammation 2021;18:216. https://doi.org/10.1186/s12974-021-02248-2.

[368] Carty F, Mahon BP, English K. The influence of macrophages on mesenchymal stromal cell therapy: passive or aggressive agents? Clin Exp Immunol 2017;188:1–11. https://doi.org/10.1111/cei.12929.

[369] Magharious MM, D'Onofrio PM, Koeberle PD. Optic nerve transection: a model of adult neuron apoptosis in the central nervous system. J Vis Exp 2011:2241. https://doi.org/10.3791/2241.

[370] Berkelaar M, Clarke D, Wang Y, Bray G, Aguayo A. Axotomy results in delayed death and apoptosis of retinal ganglion cells in adult rats. J Neurosci 1994;14:4368–74. https://doi.org/10.1523/JNEUROSCI.14-07-04368.1994.

[371] Quigley HA, Nickells RW, Kerrigan LA, Pease ME, Thibault DJ, Zack DJ. Retinal ganglion cell death in experimental glaucoma and after axotomy occurs by apoptosis. Invest Ophthalmol Vis Sci 1995;36:774–86.

[372] Bull ND, Johnson TV, Welsapar G, DeKorver NW, Tomarev SI, Martin KR. Use of an adult rat retinal explant model for screening of potential retinal ganglion cell neuroprotective therapies. Invest Ophthalmol Vis Sci 2011;52:3309–20. https://doi.org/10.1167/iovs.10-6873.

[373] Johnson TV, DeKorver NW, Levasseur VA, Osborne A, Tassoni A, Lorber B, et al. Identification of retinal ganglion cell neuroprotection conferred by platelet-derived growth factor through analysis of the mesenchymal stem cell secretome. Brain 2014;137:503–19. https://doi.org/10.1093/brain/awt292.

[374] Rodriguez AR, de Sevilla Müller LP, Brecha NC. The RNA binding protein RBPMS is a selective marker of ganglion cells in the mammalian retina. J Comp Neurol 2014;522:1411–43. https://doi.org/10.1002/cne.23521.

[375] Pereiro X, Ruzafa N, Urcola JH, Sharma SC, Vecino E. Differential Distribution of RBPMS in Pig, Rat, and Human Retina after Damage. Int J Mol Sci 2020;21:9330. https://doi.org/10.3390/ijms21239330.

[376] Bull ND, Chidlow G, Wood JPM, Martin KR, Casson RJ. The mechanism of axonal degeneration after perikaryal excitotoxic injury to the retina. Exp Neurol 2012;236:34–45. https://doi.org/10.1016/j.expneurol.2012.03.021.

[377] Martins J, Elvas F, Brudzewsky D, Martins T, Kolomiets B, Tralhão P, et al. Activation of Neuropeptide Y Receptors Modulates Retinal Ganglion Cell Physiology and Exerts Neuroprotective Actions In Vitro. ASN Neuro 2015;7. https://doi.org/10.1177/1759091415598292.

[378] Johnson TV, Martin KR. Development and characterization of an adult retinal explant organotypic tissue culture system as an in vitro intraocular stem cell transplantation model. Invest Ophthalmol Vis Sci 2008;49:3503–12. https://doi.org/10.1167/iovs.07-1601.

[379] Christakopoulos C, Cehofski LJ, Christensen SR, Vorum H, Honoré B. Proteomics reveals a set of highly enriched proteins in epiretinal membrane compared with inner limiting membrane. Exp Eye Res 2019;186:107722. https://doi.org/10.1016/j.exer.2019.107722.

[380] Hua Z-Q, Liu H, Wang N, Jin Z-B. Towards stem cell-based neuronal regeneration for glaucoma. Prog Brain Res 2020;257:99–118. https://doi.org/10.1016/bs.pbr.2020.05.026.

[381] Wang Y, Tang Z, Gu P. Stem/progenitor cell-based transplantation for retinal degeneration: a review of clinical trials. Cell Death Dis 2020;11:793. https://doi.org/10.1038/s41419-020-02955-3.

[382] Murali A, Ramlogan-Steel CA, Andrzejewski S, Steel JC, Layton CJ. Retinal explant culture: A platform to investigate human neuro-retina. Clin Exp Ophthalmol 2019;47:274–85. https://doi.org/10.1111/ceo.13434.

[383] Rettinger CL, Wang H-C. Current Advancements in the Development and Characterization of Full-Thickness Adult Neuroretina Organotypic Culture Systems. Cells Tissues Organs 2018;206:119–32. https://doi.org/10.1159/000497296.

[384] Turner L. US stem cell clinics, patient safety, and the FDA. Trends Mol Med 2015;21:271–3. https://doi.org/10.1016/j.molmed.2015.02.008.

[385] Vilela CAP, Messias A, Calado RT, Siqueira RC, Silva MJL, Covas DT, et al. Retinal function after intravitreal injection of autologous bone marrow-derived mesenchymal stromal cells in advanced glaucoma. Doc Ophthalmol 2021. https://doi.org/10.1007/s10633-021-09817-z.

[386] Kuriyan AE, Albini TA, Flynn HW. The Growing “Stem Cell Clinic” Problem. Am J Ophthalmol 2017;177:xix–xx. https://doi.org/10.1016/j.ajo.2017.03.030.

[387] Kuriyan AE, Albini TA, Townsend JH, Rodriguez M, Pandya HK, Leonard RE, et al. Vision Loss after Intravitreal Injection of Autologous “Stem Cells” for AMD. N Engl J Med 2017;376:1047–53. https://doi.org/10.1056/NEJMoa1609583.

[388] Kim JY, You YS, Kim SH, Kwon OW. Epiretinal Membrane Formation after Intravitreal Autologous Stem Cell Implantation in a Retinitis Pigmentosa Patient. Retin Cases Brief Rep 2017;11:227–31. https://doi.org/10.1097/ICB.0000000000000327.

[389] Satarian L, Nourinia R, Safi S, Kanavi MR, Jarughi N, Daftarian N, et al. Intravitreal Injection of Bone Marrow Mesenchymal Stem Cells in Patients with Advanced Retinitis Pigmentosa; a Safety Study. J Ophthalmic Vis Res 2017;12:58–64. https://doi.org/10.4103/2008-322X.200164.

[390] Tuekprakhon A, Sangkitporn S, Trinavarat A, Pawestri AR, Vamvanij V, Ruangchainikom M, et al. Intravitreal autologous mesenchymal stem cell transplantation: a non-randomized phase I clinical trial in patients with retinitis pigmentosa. Stem Cell Res Ther 2021;12:52. https://doi.org/10.1186/s13287-020-02122-7.

[391] Ray HC, Corliss BA, Bruce AC, Kesting S, Dey P, Mansour J, et al. Myh11+ microvascular mural cells and derived mesenchymal stem cells promote retinal fibrosis. Sci Rep 2020;10:15808. https://doi.org/10.1038/s41598-020-72875-x.

[392] Tassoni A, Gutteridge A, Barber AC, Osborne A, Martin KR. Molecular Mechanisms Mediating Retinal Reactive Gliosis Following Bone Marrow Mesenchymal Stem Cell Transplantation. Stem Cells 2015;33:3006–16. https://doi.org/10.1002/stem.2095.

[393] Konala VBR, Mamidi MK, Bhonde R, Das AK, Pochampally R, Pal R. The current landscape of the mesenchymal stromal cell secretome: A new paradigm for cell-free regeneration. Cytotherapy 2016;18:13–24. https://doi.org/10.1016/j.jcyt.2015.10.008.

[394] Teixeira FG, Carvalho MM, Sousa N, Salgado AJ. Mesenchymal stem cells secretome: a new paradigm for central nervous system regeneration? Cell Mol Life Sci 2013;70:3871–82. https://doi.org/10.1007/s00018-013-1290-8.

[395] Di Nicola M, Carlo-Stella C, Magni M, Milanesi M, Longoni PD, Matteucci P, et al. Human bone marrow stromal cells suppress T-lymphocyte proliferation induced by cellular or nonspecific mitogenic stimuli. Blood 2002;99:3838–43. https://doi.org/10.1182/blood.v99.10.3838.

[396] Holan V, Hermankova B, Bohacova P, Kossl J, Chudickova M, Hajkova M, et al. Distinct Immunoregulatory Mechanisms in Mesenchymal Stem Cells: Role of the Cytokine Environment. Stem Cell Rev Rep 2016;12:654–63. https://doi.org/10.1007/s12015-016-9688-y.

[397] Cunningham CJ, Redondo-Castro E, Allan SM. The therapeutic potential of the mesenchymal stem cell secretome in ischaemic stroke. J Cereb Blood Flow Metab 2018;38:1276–92. https://doi.org/10.1177/0271678X18776802.

[398] Kusuma GD, Carthew J, Lim R, Frith JE. Effect of the Microenvironment on Mesenchymal Stem Cell Paracrine Signaling: Opportunities to Engineer the Therapeutic Effect. Stem Cells Dev 2017;26:617–31. https://doi.org/10.1089/scd.2016.0349.

[399] Madrigal M, Rao KS, Riordan NH. A review of therapeutic effects of mesenchymal stem cell secretions and induction of secretory modification by different culture methods. J Transl Med 2014;12:260. https://doi.org/10.1186/s12967-014-0260-8.

[400] Miceli V, Bulati M, Iannolo G, Zito G, Gallo A, Conaldi PG. Therapeutic Properties of Mesenchymal Stromal/Stem Cells: The Need of Cell Priming for Cell-Free Therapies in Regenerative Medicine. Int J Mol Sci 2021;22:E763. https://doi.org/10.3390/ijms22020763.

[401] Harrell CR, Simovic Markovic B, Fellabaum C, Arsenijevic A, Djonov V, Arsenijevic N, et al. Therapeutic Potential of Mesenchymal Stem Cell-Derived Exosomes in the Treatment of Eye Diseases. Adv Exp Med Biol 2018;1089:47–57. https://doi.org/10.1007/5584_2018_219.

[402] Mead B, Tomarev S. Bone Marrow-Derived Mesenchymal Stem Cells-Derived Exosomes Promote Survival of Retinal Ganglion Cells Through miRNA-Dependent Mechanisms. Stem Cells Transl Med 2017;6:1273–85. https://doi.org/10.1002/sctm.16-0428.

[403] Mathew B, Torres LA, Gamboa Acha L, Tran S, Liu A, Patel R, et al. Uptake and Distribution of Administered Bone Marrow Mesenchymal Stem Cell Extracellular Vesicles in Retina. Cells 2021;10:730. https://doi.org/10.3390/cells10040730.

[404] Serle JB, Katz LJ, McLaurin E, Heah T, Ramirez-Davis N, Usner DW, et al. Two Phase 3 Clinical Trials Comparing the Safety and Efficacy of Netarsudil to Timolol in Patients With Elevated Intraocular Pressure: Rho Kinase Elevated IOP Treatment Trial 1 and 2 (ROCKET-1 and ROCKET-2). Am J Ophthalmol 2018;186:116–27. https://doi.org/10.1016/j.ajo.2017.11.019.

[405] Mani S, Jindal D, Chopra H, Jha SK, Singh SK, Ashraf GM, et al. ROCK2 inhibition: A futuristic approach for the management of Alzheimer's disease. Neurosci Biobehav Rev 2022;142:104871. https://doi.org/10.1016/j.neubiorev.2022.104871.

[406] Wei W, Wang Y, Zhang J, Gu Q, Liu X, Song L, et al. Fasudil ameliorates cognitive deficits, oxidative stress and neuronal apoptosis via inhibiting ROCK/MAPK and activating Nrf2 signalling pathways in APP/PS1 mice. Folia Neuropathol 2021;59:32–49. https://doi.org/10.5114/fn.2021.105130.

[407] Abbhi V, Piplani P. Rho-kinase (ROCK) Inhibitors - A Neuroprotective Therapeutic Paradigm with a Focus on Ocular Utility. Curr Med Chem 2020;27:2222–56. https://doi.org/10.2174/0929867325666181031102829.

[408] Shaw PX, Sang A, Wang Y, Ho D, Douglas C, Dia L, et al. Topical administration of a Rock/Net inhibitor promotes retinal ganglion cell survival and axon regeneration after optic nerve injury. Exp Eye Res 2017;158:33–42. https://doi.org/10.1016/j.exer.2016.07.006.

[409] Lim L, Manser E, Leung T, Hall C. Regulation of phosphorylation pathways by p21 GTPases. The p21 Ras-related Rho subfamily and its role in phosphorylation signalling pathways. Eur J Biochem 1996;242:171–85. https://doi.org/10.1111/j.1432-1033.1996.0171r.x.

[410] Julian L, Olson MF. Rho-associated coiled-coil containing kinases (ROCK): structure, regulation, and functions. Small GTPases 2014;5:e29846. https://doi.org/10.4161/sgtp.29846.

[411] Nourinia R, Nakao S, Zandi S, Safi S, Hafezi-Moghadam A, Ahmadieh H. ROCK inhibitors for the treatment of ocular diseases. Br J Ophthalmol 2017. https://doi.org/10.1136/bjophthalmol-2017-310378.

[412] Saha BC, Kumari R, Kushumesh R, Ambasta A, Sinha BP. Status of Rho kinase inhibitors in glaucoma therapeutics-an overview. Int Ophthalmol 2021. https://doi.org/10.1007/s10792-021-02002-w.

[413] Ramachandran C, Patil RV, Combrink K, Sharif NA, Srinivas SP. Rho-Rho kinase pathway in the actomyosin contraction and cell-matrix adhesion in immortalized human trabecular meshwork cells. Mol Vis 2011;17:1877–90.

[414] Honjo M, Tanihara H, Inatani M, Kido N, Sawamura T, Yue BY, et al. Effects of rho-associated protein kinase inhibitor Y-27632 on intraocular pressure and outflow facility. Invest Ophthalmol Vis Sci 2001;42:137–44.

[415] Van de Velde S, De Groef L, Stalmans I, Moons L, Van Hove I. Towards axonal regeneration and neuroprotection in glaucoma: Rho kinase inhibitors as promising therapeutics. Prog Neurobiol 2015;131:105–19. https://doi.org/10.1016/j.pneurobio.2015.06.002.

[416] Al-Humimat G, Marashdeh I, Daradkeh D, Kooner K. Investigational Rho Kinase Inhibitors for the Treatment of Glaucoma. J Exp Pharmacol 2021;13:197–212. https://doi.org/10.2147/JEP.S259297.

[417] Dang Y, Wang C, Shah P, Waxman S, Loewen RT, Loewen NA. RKI-1447, a Rho kinase inhibitor, causes ocular hypotension, actin stress fiber disruption, and increased phagocytosis. Graefes Arch Clin Exp Ophthalmol 2019;257:101–9. https://doi.org/10.1007/s00417-018-4175-6.

[418] Hirata A, Inatani M, Inomata Y, Yonemura N, Kawaji T, Honjo M, et al. Y-27632, a Rho-associated protein kinase inhibitor, attenuates neuronal cell death after transient retinal ischemia. Graefes Arch Clin Exp Ophthalmol 2008;246:51–9. https://doi.org/10.1007/s00417-007-0666-6.

[419] Gao C, Huang L, Long Y, Zheng J, Yang J, Pu S, et al. Y-39983, a selective Rho-kinase inhibitor, attenuates experimental autoimmune encephalomyelitis via inhibition of demyelination. Neuroimmunomodulation 2013;20:334–40. https://doi.org/10.1159/000353568.

[420] Nakajima E, Nakajima T, Minagawa Y, Shearer TR, Azuma M. Contribution of ROCK in contraction of trabecular meshwork: proposed mechanism for regulating aqueous outflow in monkey and human eyes. J Pharm Sci 2005;94:701–8. https://doi.org/10.1002/jps.20285.

[421] Tokushige H, Waki M, Takayama Y, Tanihara H. Effects of Y-39983, a selective Rho-associated protein kinase inhibitor, on blood flow in optic nerve head in rabbits and axonal regeneration of retinal ganglion cells in rats. Curr Eye Res 2011;36:964–70. https://doi.org/10.3109/02713683.2011.599106.

[422] Tura A, Schuettauf F, Monnier PP, Bartz-Schmidt KU, Henke-Fahle S. Efficacy of Rho-kinase inhibition in promoting cell survival and reducing reactive gliosis in the rodent retina. Invest Ophthalmol Vis Sci 2009;50:452–61. https://doi.org/10.1167/iovs.08-1973.

[423] Glotfelty EJ, Tovar-Y-Romo LB, Hsueh S-C, Tweedie D, Li Y, Harvey BK, et al. The RhoA-ROCK1/ROCK2 Pathway Exacerbates Inflammatory Signaling in Immortalized and Primary Microglia. Cells 2023;12:1367. https://doi.org/10.3390/cells12101367.

[424] Koch JC, Tatenhorst L, Roser A-E, Saal K-A, Tönges L, Lingor P. ROCK inhibition in models of neurodegeneration and its potential for clinical translation. Pharmacology & Therapeutics 2018;189:1–21. https://doi.org/10.1016/j.pharmthera.2018.03.008.